STUDIES ON OLIGONUCLEOTIDES AND ANALOGUES: FROM DRUG CANDIDATES TO COMPONENTS FOR HIGH-ORDERED SUPRAMOLECULAR STRUCTURES

Fabrizia Nici

Dottorato in Scienze Biotecnologiche - XXVIII ciclo
Indirizzo Biotecnologie Industriali e Molecolari
Università di Napoli Federico II

Dottorato in Scienze Biotecnologiche XXVIII ciclo
Indirizzo Biotecnologie Industriali e Molecolari
Università di Napoli Federico II

STUDIES ON OLIGONUCLEOTIDES AND ANALOGUES: FROM DRUG CANDIDATES TO COMPONENTS FOR HIGH-ORDERED SUPRAMOLECULAR STRUCTURES

Fabrizia Nici

Dottorando:	Fabrizia Nici
Relatore:	Prof. Giorgia Oliviero
Coordinatore:	Prof. Giovanni Sannia

A mia madre e mio padre

INDEX

Short abstract

Last century advances in molecular biology and biotechnologies enabled us to understand the exceptionally broad repertoire of nucleic acids functions. For a long time DNA was regarded as a rigid molecule with the sole purpose to store and transmit genetic information. However, this idea has been completely overtaken with the discovery of the catalytic activity of specific RNA molecules. In effect, the early 1970s and the embryonic works on antisense oligonucleotides paved the way for our current understanding and use of oligonucleotides (ONs) and their analogues in numerous and very different application fields, such as gene modulation, i.e. the antisense and antigene strategies, new generation drugs, i.e. the aptamers, but also nanotechnologies. My research activity is included in this general context and, in particular, has been devoted to unravelling ON uses in a broad range of fields, which goes from the development of novel drug candidates to gene regulation and implementation of new approaches for the simple construction of biosensors. Specifically, my search has been focused on:

- Realization of novel antiviral aptamers and consolidation of a new, cost effective and quick binding assay for the optimization of already reported aptamers, not achievable through the universally accepted method for the individuation of selective and efficient aptamers, the SELEX method.
- Studies on already reported protocols for the functionalization of Porous Silicon (PSi) matrices, in view of the development of optical DNA-based biosensor and discovery of a new efficient protocol for the PSi-friendly *in situ* oligonucleotide synthesis.
- Chemical synthesis and structural and biological characterization of PNA sequences for the inhibition of a miRNA, designated as responsible for the down-regulation of the Cystic Fibrosis disease-gene.

The achievement of these goals required a combination of chemical synthesis, with the optimization of existing protocols, and techniques for the biophysical and biological characterization of our biomolecules.

Long Abstract

I progressi degli ultimi decenni nella biologia molecolare e nelle biotecnologie hanno consentito di riconoscere l'incredibile repertorio funzionale degli acidi nucleici. Per molto tempo gli acidi nucleici sono stati visti unicamente come molecole rigide, la cui sola funzione fosse quella di conservare e trasmettere l'informazione genetica. Tuttavia tale idea è stata definitivamente superata con la scoperta dell'attività catalitica di specifiche molecole di RNA. [1] In effetti, data la specificità dell'appaiamento di tipo Watson-Crick e la plasticità di tali molecole, esse sono ormai universalmente riconosciute quali strumenti di eccezionale versatilità in svariati ambiti, tra cui quello nanotecnologico, biosensoristico, farmacologico. In questo contesto, con il loro pionieristico lavoro sull'inibizione del genoma del virus del sarcoma di Rous mediante impiego di oligonucleotidi antisenso, Zamecnick e Stephenson hanno dato inizio nel 1978 a quella che è stata successivamente definita "la nuova grande ondata della rivoluzione biotecnologica".[2,3] Gli oligonucleotidi (ON) sono brevi sequenze sintetiche di acido deossiribonucleico o ribonucleico, con un notevole repertorio di applicazioni, che spaziano dalla modulazione delle funzioni geniche alla costruzione di biosensori allo sviluppo di nanomateriali. [4,5] Negli ultimi anni il notevole potenziale degli ON come strumenti terapeutici nella modulazione genica è stato ampiamente esplorato. In questo ambito, gli ON trovano principalmente applicazione nella strategia antisenso, nella strategia antigene e come *aptameri*.

Il silenziamento dell'espressione genica avviene nella strategia antisenso mediante impiego di sequenze oligonucleotidiche complementari a molecole di mRNA; esse una volta legato specificamente il bersaglio ne impediscono il riconoscimento da parte dell'apparato proteico deputato alla decodifica dell'informazione e la traduzione. [6] In generale, il blocco sterico della traduzione si ottiene quando l'ON antisenso è diretto contro l'estremità 5' del target, inibendone così l'interazione con il macchinario della traduzione; il secondo meccanismo attraverso il quale essi agiscono è rappresentato dalla degradazione mediata da RNasi-H, che avviene quando l'ON antisenso lega il bersaglio in un qualsiasi sito, formando così una eteroduplex RNA/DNA. [7] L'interesse rivolto verso questa strategia è testimoniato dall'approvazione per uso clinico dell'analogo oligonucleotidico, Fomivirsen, contro retiniti indotte da citomegolvirus e dagli studi su molti altri ON antisenso, già in fase 1 o 2 di sperimentazione clinica. Nella strategia antigene l'inibizione dell'espressione genica avviene mediante l'impiego di ON che riconoscono specificamente sequenze situate nel solco maggiore della doppia elica di DNA, instaurando legami ad idrogeno di tipo Hoogsteen con le basi puriniche ed originando così una tripla elica. [8] L'approccio antigene rimane uno degli ambiti più affascinanti di applicazione degli ON, consentendo, in linea teorica, interventi di mutagenesi sito diretta e di terapia genica. Sebbene si tratti teoricamente di una strategia ristretta a tratti polipurinici•polipirimidinici, grandi sforzi sono stati e sono, tuttora, condotti per estendere il repertorio di sequenze bersaglio, tramite il disegno razionale di opportuni derivati. Infatti, sebbene il principio su cui si basano strategia antisenso ed antigene possa sembrare semplice e gli approcci stessi facilmente attuabili, nella pratica l'impiego di ON per la modulazione dell'espressione genica trova importanti ostacoli, tra cui si annoverano principalmente il raggiungimento del sito nel quale essi devono funzionare, che richiede il passaggio attraverso membrane cellulari idrofobiche e la suscettibilità degli ON alla degradazione enzimatica operata da endo- ed esonucleasi.

In virtù di tali considerazioni, negli ultimi decenni la ricerca di ON strutturalmente modificati, che potessero sopperire alle limitazioni delle controparti naturali e, pertanto, funzionare quali strumenti terapeutici, ha ottenuto notevole slancio e condotto ad analoghi dotati di affascinanti proprietà. [9] In generale si distinguono tre tipi di modifiche: modifiche al gruppo fosfato, modifiche allo zucchero e modifiche all'intero scheletro. [10] Alla terza generazione di analoghi, più correttamente noti come ON mimici, appartiene l'Acido Peptido Nucleico (PNA), ormai universalmente riconosciuto come mimico di notevole rilevanza biotecnologica. [11]
Il PNA è un analogo in cui lo scheletro zucchero-fosfato è completamente sostituito da uno scheletro di natura poliammidica, dato dalla ripetizione di unità di N-(2-amminoetil)-glicina, a cui le basi azotate del DNA sono legate mediante un linker metilen carbonilico. Data la presenza delle stesse basi azotate del DNA, situate ad una distanza che mima la distanza nell'acido nucleico, il PNA è in grado di riconoscere ed ibridizzare con sequenze complementari di DNA o RNA ed, in effetti, la mancanza di cariche nello scheletro rende gli ibridi PNA/DNA e PNA/RNA notevolmente più stabili rispetto alle duplex naturali. Un'ulteriore conseguenza della natura poliammidica dello scheletro è che la formazione degli ibridi è indipendente dalla concentrazione salina [11-14]. In virtù della estrema specificità del PNA e della stabilità delle eteroduplex risultanti, l'ibridazione PNA-acido nucleico è particolarmente sensibile ai *mismatch*, come evidenziato dal fatto che i PNA legano con elevata affinità sequenze complementari, più debolmente sequenze recanti un *mismatch*, mentre l'appaiamento non ha luogo per le sequenze recanti due *mismatch*, e questo fenomeno è stato ampiamente sfruttato per la costruzione di dispositivi basati sul PNA ad uso diagnostico. [15] Il PNA presenta, inoltre, elevata stabilità biologica; esso risulta essere, infatti, resistente alla degradazione operata da nucleasi e proteasi, ne consegue un tempo di vita più esteso sia *in vitro* che *in vivo*. Alla resistenza alla degradazione enzimatica si accompagna una maggiore stabilità chimica, le molecole di PNA sono, infatti, stabili in ambiente fortemente acido e, contrariamente a quanto osservato per il DNA, non mostrano fenomeni di depurinazione a seguito del trattamento in condizioni acide drastiche. L'elevata stabilità *in vivo*, la specifica ibridazione con gli acidi nucleici e la mancanza di tossicità, anche a concentrazioni relativamente elevate, hanno reso i PNA molecole promettenti in ambito terapeutico. In virtù della loro abilità nel legarsi a molecole di DNA e di RNA, i PNA hanno trovato anzitutto possibilità di utilizzo quali agenti antisenso ed antigene. In particolare, essi sono stati ampiamente studiati per la loro capacità di modulare l'espressione genica attraverso inibizione della trascrizione mediata dal legame al DNA ed attraverso inibizione della traduzione mediata dal legame all' mRNA. Numerose evidenze sperimentali, inoltre, testimoniano che molecole di PNA sono inibitori dei microRNA (miRNA) più efficienti rispetto agli inibitori oligonucleotidici.[16] Tuttavia, sebbene inizialmente siano stati utilizzati in ambito terapeutico, essi hanno recentemente trovato applicazione in ambito diagnostico e di biologia molecolare. Tra le applicazioni maggiormente esplorate si possono annoverare: inibizione di determinati enzimi, quali telomerasi, elicasi, trascrittasi inversa; mutagenesi sito-diretta; attivazione dell'espressione di geni endogeni; amplificazione mediante PCR; tecnica PARC (*PNA Assisted Rare Cleavage*); impiego come sonda di biosensori per acidi nucleici. [17] Sin da quando il PNA è stato proposto nel 1991, sono state riconosciute le sue proprietà simili, ed in alcuni casi superiori, al DNA ed all'RNA, con le promettenti applicazioni che ne derivano, tuttavia, di recente, sono state descritte anche applicazioni delle molecole di PNA come aptameri. [18]

In effetti, un'altra intrigante applicazione di ON ed analoghi è rappresentata dagli *aptameri*, brevi sequenze di acido nucleico in grado di riconoscere e legare con estrema affinità target molecolari, tra cui proteine, acidi nucleici, piccole molecole organiche. [19] Il principale metodo di selezione di frammenti oligonucleotidici dotati di alta affinità e specificità è stato per la prima volta proposto nel 1990 da Tuerk e Gold e consiste nella Evoluzione Sistematica dei Ligandi realizzata attraverso una Tecnologia di Arricchimento Sequenziale (SELEX). [20] La tecnica consente di selezionare *in vitro* gli aptameri a partire da una libreria combinatoriale contenente un numero molto elevato di sequenze e consiste nella iterazione di due passaggi fondamentali: selezione di sequenze aventi affinità per il target e amplificazione degli aptameri con le proprietà di legame desiderate. Date le loro proprietà, gli aptameri, sin dalla loro introduzione, sono stati ampiamente studiati per le loro applicazioni in ambito terapeutico e biosensoristico. L'impiego di tali molecole nel primo ambito è subordinato all'esistenza di determinate caratteristiche. Anzitutto, le elevate dimensioni e quindi l'ampia superficie di contatto degli acidi nucleici garantiscono maggiori interazioni con i bersagli terapeutici rispetto alle molecole più piccole, conseguentemente sono richieste concentrazioni inferiori per un'efficiente inibizione rispetto ai farmaci tradizionali. Inoltre, l'estensione superficiale permette loro di discriminare tra proteine strettamente correlate tra loro, come, ad esempio, le isoforme della protein-chinasi C (PKC) che posseggono un grado di similitudine del 96%. [21] In secondo luogo, il riconoscimento specifico deve essere accompagnato all'inibizione della funzione biologica della molecola bersaglio, a tal proposito sono stati proposti aptameri ad RNA in grado di riconoscere ed inibire i recettori del fattore di crescita endoteliale vascolare (VEGF) ed, ancora, aptameri formati da oligonucleotidi fosforotioati in grado di inibire la trascrittasi inversa di HIV.[22,23] In questo contesto, particolarmente fervida è stata la ricerca di aptameri in grado di interferire con la replicazione virale ed, in tal senso, nel 1994 Hotoda e colleghi, con la scoperta che la sequenza oligonucleotidica $^{5'}$TGGGAG$^{3'}$ se opportunamente modificata alle estremità era in grado di inibire l'entrata di HIV-1 all'interno delle cellule bersaglio, hanno dato inizio ad una lunga fase, ancora non interrotta, di studi approfonditi sulle più opportune e funzionali modifiche da apportare alla sequenza originaria in vista dello sviluppo di potenti agenti terapeutici. [24-26] Gli aptameri esibiscono una notevole propensione ad assumere una varietà di motivi strutturali secondari e terziari e, di fatti, l'assunzione della corretta conformazione è intimamente connessa con il riconoscimento e l'interazione selettivi col target. Tra le varie architetture, la struttura non canonica a quadrupla elica, G-Quadruplex, è stata individuata in svariati aptameri; tra questi possiamo annoverare il primo aptamero per il quale è stata caratterizzata la struttura quadruplex, cioè il TBA, (Thrombin Binding Aptamer), un pentadecamero ricco in guanine che adotta in soluzione una struttura G-quadruplex intramolecolare e che è in grado di legare ed inibire la trombina, proteina farmacologicamente rilevante, uno degli aptameri leganti l'RNasi-H1 ed, ancora, molti degli aptameri proposti come agenti antivirali, tra cui 93del, T30695 e la già accennata sequenza proposta da Hotoda. [24, 25, 27,28]

Le strutture G-Quadruplex sono strutture costituite da quartetti coplanari di guanine, stabilizzati da legami idrogeno di tipo Hoogsteen, emerse negli ultimi decenni per la loro implicazione in processi di rilevanza biologica. [29] Sequenze ricche in guanina in grado di associarsi in strutture a quadrupla elica sono state individuate, infatti, a livello delle regioni telomeriche del genoma umano, nelle regioni di *switch* delle immunoglobuline, nei promotori di diversi oncogeni. [30, 31] A ciò si aggiungono ulteriori motivi di interesse: le G-Q, come già accennato, costituiscono lo scaffold di

numerosi aptameri ed, inoltre, per le loro intrinseche proprietà sono state proposte per la costituzione di nanomateriali. [32, 33] Come mostra l'elevato numero di lavori in questo ambito, l'arrangiamento G-Q presenta un elevato grado di polimorfismo, e dunque dà origine ad un'ampia famiglia di strutture stabili, caratterizzate da un'architettura di base comune, ma elementi di riconoscimento ben definiti e differenziati. La plasticità conformazionale di queste interessanti strutture permette la regolazione fine del riconoscimento del target, ma anche la possibilità di sviluppare strutture molecolari superiori; elementi, questi, estremamente utili in vista dello sviluppo di nuovi aptameri, nonché di strumenti diagnostici e di interesse biosensoristico.

In effetti, un'altra interessante applicazione delle G-Q e degli ON in generale è rappresentata dallo sviluppo di biosensori. [34]

I biosensori sono dispositivi analitici che convertono un evento biologico in un segnale quantificabile e processabile. Tipicamente un biosensore è costituito da tre elementi fondamentali: i) un recettore o sonda che riconosce l'analita, ii) un'interfaccia che trasforma l'evento biologico in un segnale, che viene trasmesso al iii) trasduttore, l'elemento deputato alla conversione del fenomeno in un segnale elettronico amplificabile. [35] La ricerca in questo campo ha vissuto una crescita esponenziale negli ultimi decenni, a causa delle applicazioni di tali dispositivi in settori quali la diagnostica, e quindi il monitoraggio ed il controllo in campioni di diversa natura di sequenze di DNA correlate a virus, malattie genetiche ed altri agenti patogeni, nonché la rilevazione in svariate matrici di inquinanti ed altri contaminanti. Sequenze oligonucleotidiche o analoghe sono particolarmente adatte alla costituzione di biosensori, considerando l'interazione forte e specifica tra le coppie di basi di filamenti complementari. Infatti, il principio su cui si fondano i biosensori a DNA consiste nell'ibridazione, in altri termini essi si basano sull'immobilizzazione di una sequenza oligonucleotidica sintetica ad un idoneo supporto solido, con sequenza complementare al target ricercato. Sensori elettrochimici o piezoelettrici rispondono alla ibridazione con un segnale amplificabile e quantificabile. Una delle problematiche più comuni nella costruzione di un biosensore a DNA è costituita dalla bioconiugazione, il legame, cioè, della sonda organica al supporto inorganico. La strategia più comune e documentata, in tal senso, è rappresentata dalla immobilizzazione della sonda sintetizzata *ex situ* sul supporto solido. In ogni caso, visti i notevoli vantaggi della sintesi di ON *in situ* sul supporto costituente il dispositivo, importanti sforzi sono stati, negli ultimi anni effettuati per sviluppare protocolli che ne garantissero la rapida ed economica sintesi *in situ* su tali matrici. Di recente, la ricerca nell'ambito dei biosensori basati su DNA è andata di pari passo con quella dei dispositivi basati su aptameri, le cui interessanti caratteristiche strutturali e proprietà di riconoscimento li hanno fatti emergere in ambito biosensoristico sui tradizionali anticorpi.

È in questo ampio contesto che si colloca il mio progetto di tesi, volto all'approfondimento delle applicazioni di ON ed analoghi in ambiti cha vanno dalla progettazione di nuovi candidati farmaci allo sviluppo di nano dispositivi. In dettaglio, il mio lavoro si è focalizzato su:

- **Realizzazione di nuovi aptameri anti-HIV basati su TEL-Oligonculeotidi**

  L'obiettivo di questa parte del progetto si è concretizzato nella realizzazione ed ottimizzazione di nuovi putativi aptameri di piccole dimensioni, partendo da aptameri antivirali precedentemente riportati da noi, in modo da migliorarne parametri farmacodinamici e farmacocinetici ed, al contempo, salvaguardarne l'attività

biologica. Questo tipo di ricerca, contestualmente, ci ha consentito di sviluppare un nuovo saggio per lo studio delle affinità di legame tra aptameri e target, la cui principale caratteristica è quella di non richiedere l'intera proteina bersaglio, con notevole risparmio economico e di tempo. Come già ampiamente discusso, gli aptameri esibiscono proprietà tali da renderli estremamente affascinanti nell'ottica dello sviluppo di nuovi agenti terapeutici. In tal senso, la comunità scientifica è stata, sin dalla loro introduzione, profondamente impegnata nella ricerca di aptameri antivirali. Nel 2010 Oliviero *et al*. hanno proposto oligonucleotiditi tetra ramificati (TEL-ON), in grado di assemblarsi in strutture G-Q eccezionalmente stabili, quali potenziali candidati per il potenziamento dell'attività antivirale della sequenza TGGGAG, proposta precedentemente da Hotoda come aptamero antivirale. I risultati estremamente positivi relativamente alla stabilità ed attività di questi analoghi dell'aptamero di Hotoda, hanno indotto lo stesso gruppo ad esplorare ulteriori modifiche sulla sequenza originaria. [36] Nel 2012 D'Atri *et al*. hanno riportato la sintesi e la caratterizzazione strutturale e biologica di una mini-libreria di TEL-ON, opportunamente modificati ad ambedue le estremità, al fine di valutare gli effetti di variazioni alla sequenza nucleotidica originaria sull'attività. [37] Forti dei risultati ottenuti da questi studi, abbiamo deciso successivamente di sfruttare una combinazione di tecniche guidate da simulazioni *in silico* ed un nuovo e rapido saggio di *binding* per ottenere un nuovo approccio per l'ottimizzazione e lo studio delle proprietà di legame di aptameri analoghi agli aptameri precedentemente riportati ma di minori dimensioni. In tal modo, si è voluta individuare la dimensione più piccola dello scaffold tale da migliorare l'intero scale-up del processo produttivo salvaguardando o, se possibile, migliorando le proprietà biologiche.

La seconda parte del presente progetto è stata dedicata al disegno, sintesi e caratterizzazione di nuovi aptameri basati su strutture G-Q sovramolecolari. In lavori precedenti, il nostro gruppo di ricerca ha riportato gli ottimi parametri termodinamici di strutture G-Q di ordine molecolare superiore, aventi sequenza CGGXGGT (con X = A, C, G and T). [38] Le indagini strutturali condotte su tali sequenze hanno mostrato che esse sono in grado di formare dimeri altamente stabili di G-Q, in cui ogni blocco di G-Q tetramolecolare interagisce con il blocco adiacente mediante interazioni idrofobiche tra i residui di dC posti alle estremità. Le strutture in questione hanno stabilità e parametri termodinamici altamente riproducibili, tali da renderli estremamente interessanti nell'ottica dello sviluppo di nuovi aptameri. In questo contesto, abbiamo disegnato ON tetra ramificati, di sequenza analoga alla sequenza CGGXGGT, opportunamente modificati all'estremità 5' e ne abbiamo studiato i parametri termodinamici e biologici.

- **Coniugazione di oligonucleotidi su supporti solidi: studi su biosensori basati su DNA**

  I biosensori basati su DNA, ovvero dispositivi che trasformano eventi di riconoscimento e ibridazione in segnali quantificabili, trovano applicazione nella diagnostica medica, nel monitoraggio di inquinanti ambientali, nella veicolazione di farmaci etc. In questo contesto, la trasduzione ottica ha trovato grande diffusione nella costruzione di tali dispositivi ed, in particolare, uno dei materiali più utilizzati risulta essere il Silicio Poroso (PSi), date le sue interessanti proprietà fisiche e morfologiche. [39] Ciò nonostante, in letteratura solo pochi lavori riportano la sintesi *in situ* di sequenze oligonucleotidiche su tali supporti. In ogni caso, la sintesi di biomolecole *in situ*, su matrici solide da utilizzare per la costruzione di biosensori, mostra svariati vantaggi se paragonata alla immobilizzazione *ex situ*, ovvero la

tecnica più comune di bioconiugazione; tra questi possiamo annoverare la maggiore densità di sonda a DNA, la possibilità di funzionalizzazione locale, la possibilità di automazione dell'intero processo. Pertanto, considerati i notevoli vantaggi dati dalla sintesi di ON *in situ* su supporti di PSi ed, al contempo, le problematiche ad essa connesse, riconducibili alla chimica della sintesi stessa, alquanto aggressiva nei confronti dei silicio poroso, l'obiettivo di questa ricerca è stato quello di individuare ed ottimizzare un nuovo approccio sintetico compatibile con i protocolli e i reattivi standard della sintesi oligonucleotidica, tali da salvaguardare lo scheletro del supporto solido. Questo studio apre, dunque, la strada alla costruzione rapida ed economica di biosensori a DNA.

- **Analoghi oligonucleotidici: il PNA e la sua applicazione quale inibitore di miRNA**

  L'obiettivo di questa parte del progetto si è configurato nel disegno e nella caratterizzazione di sequenze di PNA anti-miRNA, dirette contro il miRNA miR-509-3p, responsabile della down-regolazione del gene malattia della Fibrosi Cistica.
  I microRNA (miRNA) costituiscono una classe di brevi sequenze di RNA non codificanti, espresse in molte specie, tra cui animali, piante e virus. Essi sono coinvolti nella regolazione genica a livello post-trascrizionale e, come mostrato da numerose evidenze sperimentali, sono implicati in processi quali lo sviluppo, il metabolismo, l'apoptosi, nonché nella patogenesi di molte malattie. Di recente, Amato *et al*., a seguito di studi condotti per identificare nuove mutazioni del gene CFTR connesse all'insorgere della Fibrosi Cistica, hanno riportato l'identificazione di tre Polimorfismi del Singolo Nucleotide (SNP), uno dei quali, c.*1043A>C, è localizzato in una regione del gene responsabile del legame al miRNA noto come miR-509-3p. Tale SNP aumenta l'affinità del miRNA in questione per il gene, determinando, come conseguenza, una ridotta espressione della proteina CFTR *in vitro*. [40]
  In considerazione del fatto che il PNA è stato riconosciuto quale migliore inibitore di miRNA rispetto agli ON ma, al contempo, lunghe sequenze di PNA sono difficilmente sintetizzabili e soffrono di ridotta solubilità in acqua, soprattutto se chimicamente funzionalizzate, il nostro gruppo ha progettato brevi sequenze di PNA, di sequenza perfettamente complementare alla *seed region* del miR-509-3p, cioè le sette basi all'estremità 5' deputate all'espletazione della funzione, e studiato, attraverso tecniche di caratterizzazione chimico-fisica e biologica, la capacità di tali sequenze di riconoscere selettivamente, nonostante le ridotte dimensioni, il miRNA bersaglio ed impedirne il legame al gene.

Bibliografia

1. Kruger K, Grabowski PJ, Zaug AJ, Sands J, Gottschling DE, Cech TR, **1982***.Self-splicing RNA: autoexcision and autocyclization of the ribosomal RNA intervening sequence of Tetrahymena*.Cell 31 (1): 147–57.
2. Zamecnik PC, Stephenson ML, **1978**. *Inhibition of Rous sarcoma virus replication and cell transformation by a specific oligodeoxynucleotide*PNAS 75(1): 280-84
3. Nyce W J, **1998**. *Antisense oligonucleotides as emerging drugs.*Emerging Drugs3(1):365-76
4. Crooke S.T, **1992**. *Therapeutic Applications of Oligonucleotides.* Annu. Rev. Pharmacol. Toxicol. 32: 329-76
5. Wenger J, **2004**. *Nucleic acid nanotechnology-towards Angstrom-scale engineering.*Org. Biomol. Chem. 2: 277- 80
6. Kurreck, **2003**. *Antisense technologies. Improvement through novel chemical modification.* Eur. J. Biochem. 270: 1628
7. Crooke ST, **1999**. *Molecular mechanisms of action of antisense drugs*.*Biochim. Biophys.* Acta 1489 (1): 31-44
8. Hanvey JC, Williams EM, Besterman JM, **1991**. *DNA triple-helix formation at physiologic pH and temperature*. Antisense Res. Dev. 1 (4): 307-17
9. Zon G, **1988**. *Oligonucleotide analogues as potential chemotherapeutic agents.* Pharm. Res. 5(9): 539-49
10. Agrawal S, **1999**. *Importance of nucleotide sequence and chemical modifications of antisense oligonucleotides.* Biochim. Biophys. Acta1489 (1): 53-68
11. Nielsen PE, Egholm M, Berg RH, Buchardt O, **1991**. *Sequence-selective recognition of DNA by strand displacement with a thymine-substituted polyamide.* Science254(5037):1497-500
12. Jensen KK, Orum H, NielsenPE, Norden B, **1997**.*Kinetics for Hybridization of Peptide Nucleic Acids (PNA) with DNA and RNA Studied with the BIAcore Technique*. Biochemistry36:5072-76
13. Rasmussen H, Kastrup JS, Nielsen JN, Nielsen JM, Nielsen PE, **1997**. *Crystal structure of a peptide nucleic acid (PNA) duplex at 1.7 Å resolution*. Nature Struct. Biol. 4 (2) 98-101
14. Bastide L, Bohemer PE, Villani G, Lebleu B, **1999**. *Inhibition of a DNA-helicase by peptide nucleic acids*. Nucleic Acids Res. 27 (2):551-54
15. Nielsen PE, **2001**. *Peptide nucleic acid: a versatile tool in genetic diagnostics and molecular biology*. Curr. Opin. Biotech. 12 (1): 16-20
16. Oh SY, Ju Y, Park H, **2009**. *A highly effective and long-lasting inhibition of miRNAs with PNA-based antisense oligonucleotides*.Mol. Cells 28 (4): 341-5
17. Ray A, Bengt N, **2000**. *Peptide nucleic acid (PNA): its medical and biotechnical applications and promise for the future*. FASEB J. 14:1041-1060
18. Lee EJ, Lim HK, Choa YS, Hah SS, **2013***. Peptide Nucleic Acids are an additional class of aptamers.* RSC Adv. 3: 5828-31
19. Jayasena S, **1999**. *Aptamers: an emerging class of molecules that rival antibodies in diagnostics.* Clinical Chemistry.45(9):1628–50
20. Tuerk C, Gold L, **1990**. *Systematic evolution of ligands by exponential enrichment: RNA ligands to bacteriophage T4 DNA polymerase*.*Science.*249(4968):505-10.

21. Conrad R, Ellington AD,**1996**. *Detecting immobilized protein kinase C isozymes with RNA aptamers.* Anal. Biochem. 242 (2): 261-65
22. Ng EWM, Shima DT, Calias P, Cunningham ET, Guye DR, **2006**.*Pegaptanib, a targeted anti-VEGF aptamer for ocular vascular disease.*Nature Reviews Drug Discovery 5:123-32
23. Chou SH, Chin KH, Wang AH, **2005**. *DNA aptamers as potential anti-HIV agents*.Trends Biochem. Sci. 2005. 30(5):231-34.
24. Hotoda H, Koizumi M, Koga R, Kaneko M, Momota K, Ohmine T, Furukawa H, Agatsuma T, Nishigaki T, Sone J, Tsutsumi S, Kosaka T, Abe K, Kimura S, Shimada K, **1998***.Biologically active oligodeoxyribonucleotides. 5. 5'-End-substituted d(TGGGAG) possesses anti-human immunodeficiency virus type 1 activity by forming a G-quadruplex structur.* J Med Chem. 41: 3655-63.
25. Koizumi M, Koga R, Hotoda H, Ohmine T, Furukawa H, Agatsuma T, Nishigaki T, Abe A, Kosaka T, Tsutsumi S, Sone J, Kaneko M, Kimura S, Shimada K, **1998**.*Biologically active oligodeoxyribonucleotides. 5. 5'-End-substituted d(TGGGAG) possesses anti-human immunodeficiency virus type 1 activity by forming a G-quadruplex structure.*Bioorg. Med. Chem.6: 2469–75
26.D'Onofrio J,Petraccone L, Erra E, Martino L, Fabio GD, Napoli LD, Giancola C, Montesarchio D, **2008**.*Synthesis, biophysical characterization, and anti-HIV activity of glyco-conjugated G-quadruplex-forming oligonucleotides*. Bioconjug. Chem. 18: 1194-1204
27. Macaya RF, Schultze P, Smith FW, Roet JA, Feigon J, **1993**. *Thrombin-binding DNA aptamer forms a unimolecular quadruplex structure in solution*. PNAS, 90: 3745-49
28. Do NQ, Lim KW, Teo MH, Heddi B, Phan1 AT, **2011**. *Stacking of G-quadruplexes: NMR structure of a G-rich oligonucleotide with potential anti-HIV and anticancer activity*. *Nucleic Acids Res.39 (21): 9448–57*.
29. Phan AT, Kuryavyi V, and Patel DJ, **2006**. *DNA architecture: from G to Z*.Curr. Opin. Struct.Biol. 16(3): 288–98.
30. Ambrus A, Chen D, Dai J, Jones RA, Yang D, **2005**. *Solution structure of the biologically relevant G-quadruplex element in the human c-MYC promoter. Implications for G-quadruplex stabilization. Biochemistry.* 44 (6): 2048–58.
31. Oganesian L, Bryan TM, **2007**. *Physiological relevance of telomeric G-quadruplex formation: a potential drug target.*Bioessays. 29 (2): 155–65.
32. Gatto B, Palumbo M, Sissi C, **2009**. *Nucleic acid aptamers based on the G-quadruplex structure: therapeutic and diagnostic potential*.Curr. Med. Chem. 16(10):1248-65
33. Yatsunyk LA, Piétrement O, Albrecht D, Thao Tran PL, Renčiuk DL, Sugiyama H, Arbona JM, Aimé JP, MergnyJL, **2013**. *Guided assembly of tetramolecular G-quadruplexes*. ACS Nano. 7 (7): 5701-10
34. J. Wang, **2002**. *Electrochemical nucleic acid biosensors*. Anal. Chim. Acta469: 63–71
35. Grieshaber D, MacKenzie R, Janos Voros J, Reimhult E, **2008**. *Electrochemical Biosensors - Sensor Principles and Architecture*s. Sensors8:1400-58
36. Oliviero G, Amato J, Borbone N, D'Errico S, Galeone A, Mayol L, Haider S, Olubiyi O, Hoorelbeke B, Balzarini J, Piccialli G, **2010**. *Tetra-end-linked oligonucleotides forming DNA G-quadruplexes: a new class of aptamers showing anti-HIV activity*. Chem Comm. 46:8971-73.

37.D'atri V, Oliviero G, Amato J, Borbone N, D'errico S, Mayol L, Piccialli V, Haider S, Hoorelbeke B, Balzarini J,Piccialli G, **2012**.*New anti-HIV aptamers based on tetra-end-linked DNA G-quadruplexes: effect of the base sequence on anti-HIV activity*. Chem. Comm.48: 9516

38. D'Atri V, Borbone N, Amato J, Gabelica V, D'Errico S, Piccialli G, Mayol L, Oliviero G, **2014**. *DNA-based nanostructures: The effect of the base sequence on octamer formation from d(XGGYGGT) tetramolecular G-quadruplexes*. Biochimie 99: 119-28

39. Harraz F, **2014***.Porous silicon chemical sensors and biosensors: A review Sensors and Actuators B*. 202: 897–912.

40. Amato F, Seia M, Giordano S, Elce A, Zarrilli F, Castaldo G, Tomaiuolo R, **2013**. *Gene mutation in microRNA target sites of CFTR gene: a novel pathogenetic mechanism in cystic fibrosis*. *PLoS One*. 8(3): e60448.

Preface

During my PhD project, I worked on the design, synthesis and structural characterization of several biomolecules, with different kinds of applications. First of all, my attention has been focused on the synthesis of novel putative anti-HIV aptamers and, contextually, on the design of a novel and cost-effective binding assay, to study the affinity between aptamers and their target. Secondly, in view of the simple and easy development of DNA-based optical biosensors, we exploited several chemical protocols to achieve the direct ON synthesis on PSi matrices, ultimately succeeding in the identification of a PSi-friendly protocol for the *in situ* synthesis on PSi support. Finally, but not less intriguing, we explored the properties of PNA as efficient inhibitor of miRNA function. To achieve these goals, we exploited a combination of chemical synthesis and structural characterization via spectroscopic techniques, as well as biological assays.
The results of this work, often obtained in collaboration with other research groups, are discussed in the following reports:

- *Analytical Chemistry, (2016); 88, 2327-34*

In this work, by using a platform based on *in silico* driven techniques and fluorescent techniques, we developed new aptamers endowed with significant antiviral properties.

- *Nanoscale Research Letters, (2014); 9, 317*

In this report, we exploited several chemicals procedures to obtain the feasible synthesis of mixed-sequence oligonucleotides on aminosilane-modified porous silicon photonic structures.

- *BioMed Research International, (2014); 2014, 610718-28*

I worked on the synthesis of small anti-miRNA PNA, to be used for the selective inhibition of a miRNA involved in the down-regulation of the CF disease gene.

Finally, during these years, I have been also involved in other works concerning the study of the interaction between nucleic acids and putative ligands and the chemical synthesis and structural characterization of small organic molecules. The findings of these works are reported in:

- European Journal of Organic Chemistry (2015), 2015(34), 7550-7556.
- European Journal of Organic Chemistry (2015), 2015(10), 2244-2249.
- Molecules (2014), 19(7), 9339-9353.

CHAPTER 1

Oligonucleotides and analogues: a 'great wave in the biotechnology revolution'

1.1 Introduction

The idea of nucleic acids as only carriers for the storage and transmission of the genetic information has long been overtaken with the discovery of the catalytic activity that nucleic acid molecules can perform in a variety of organisms. [1] In particular, driven by the progress of the last decades in the acquisition of genetic information and in the manipulation of small quantities of these molecules, a great number of technologies emerged using DNA, RNA and derivatives with diagnostic, research and technological utility. In this sense, nucleic acids are attractive for a number of reasons. First of all, most man-made manipulations require recognition and binding events and in this context, nucleic acids, in contrast with proteins, obey to the relatively simple Watson and Crick rules; secondly, the spatial location of nucleic acids is concentrated, thus allowing the specific targeting of these molecules; finally, in respect to other macromolecules, they are easier to process and modify. As a consequence, it is, by the time, ascertained that nucleic acids and derivatives offer great opportunities and promise for the biotechnologies.
In this wake, with their pioneering work on the theoretical and therapeutic potential of oligonucleotides, Zamecnick and Stephenson started what has been called 'the next great wave of the biotechnology revolution'. [2] Oligonucleotides (ON) are short nucleic acid polymers, with a plethora of applications, ranging from research to nanotechnology. Despite around 40 years have passed since the proposal of oligonucleotides as pharmaceutical and nanotechnological tools, the interest of the scientific community towards them not only has not decreased, but it rather has critically grown. In effect, the fields covered by ON applications are increasingly many and include diagnostic and therapeutic applications, such as DNA microarrays, gene therapy, antisense and antigene approaches for the inhibition of undesired genetic functions; nanotechnological applications, such as biosensing, ribozymes and nanodevices and finally novel therapeutics, such as DNA vaccines and aptamers. [3-6]
During the last decades, in fact, the use of oligonucleotides as agents for gene modulation has been widely investigated. Oligonucleotides and analogues can be used to correct genetic disorders or to silence gene expression and, in this context, the discovery of RNA interference has strengthened the potential of this approach. Moreover, the use of oligonucleotides as therapeutic and diagnostic tools, opened the possibility of elucidating complex gene expression patterns in genomic experiments. In a similar context, clinical trials have tested the ability of oligonucleotide molecules, designated as *aptamers*, to sequestrate and inhibit pathogenic proteins and other relevant biological targets. [7, 9]
Another intriguing application of ONs is connected to the field of nanotechnology. In fact, the use of biomolecules offers great promise in the small scale approaches, and in this context, nucleic acids are particularly fascinating due to their ability of self-organization, selectivity and processability. [10]
Briefly, the issues here presented, as regards the ONs applications, will be: the antisense strategy, the antigene strategy, the use of oligonucleotides as aptamers and the application of ONs in the biosensing context.

1.2 Oligonucleotides in the antisense strategy

The exploitation of exogenous oligonucleotides to block or modulate gene functions was first introduced by Zamecnick and Stephenson in 1978, who inhibited the expression of Rous sarcoma virus by the introduction of antisense oligonucleotides complementary to segments of the 35S RNA of the virus.
Antisense oligodeoxyribonucleotides (ODN) are short synthetic strands of DNA that consist of 15 to 20 nucleotides. Since the affinity and the specificity of the ODNs towards their target results from hybridization interaction and the selectivity of Watson-Crick base pairing, they are able to target their complementary sequences of RNA by duplex formation and inhibit protein biosynthesis (Fig. 1). In principle, they can interfere with each step of nucleic acid metabolism, preferentially with transcription, splicing and translation.

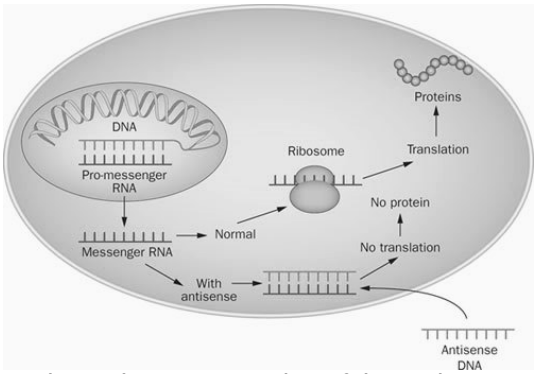

Figure 1.Schematic representation of the antisense approach

The mechanisms by which antisense ODNs may induce biological effects are complex and virtually numerous. In general, the inhibition of translation from mRNA into protein by ODNs may occur via two major mechanisms: an occupancy-only mechanism and the activation of RNase H. [11]
Antisense ODNs are able to block the ribosome translocation sterically by hybridization; more specifically, in this case, the arrest derives from the very high-affinity interaction between the ODN and the targeted mRNA by Watson-Crick base pairing, thus sterically blocking the translation of a transcript into a protein.
A second inhibitory mechanism operates in cells and is mediated by the cellular enzyme RNase H. The precise recognition elements for the enzyme is not known; however, the RNA:DNA heteroduplex is recognized by this enzyme and results in subsequent RNA cleavage.
Since they were first proposed by Zamecnick and Stephenson in 1978 to inhibit viral replication in cell culture, a number of similar applications have been proposed. Antisense therapeutic agents are being investigated *in vitro* and *in vivo* for use in treating human immunodeficiency virus infection, hepatitis B virus infection, herpes simplex virus infection, papillomavirus infection, cancer, restenosis, rheumatoid arthritis, and allergic disorders. Different ODNs are in clinical trials against many diseases such as cytomegalovirus (CMV) ocular infections, as well as in the control of haematological disorders including Crohn's Disease. [12, 13] In addition, there is already one FDA-approved product, formivirsen (Vitravene), for the treatment of human CMV-induced retinitis.

Even if antisense technology is a relatively young field, a high number of current papers and reviews prove the great progress and prospects in the field and numerous companies are working on the development of novel antisense oligonucleotides (Table 1).

Compound	Type of oligo	Disease target	Gene target	Phase
ISIS13312	2′-Modified PS	CMV retinitis	N.A.	I/II
ISIS2302	PS	Crohn's disease	ICAM-1	II/Pivotal
		Psoriasis	ICAM-1	II
		Renal transplant rejection	ICAM-1	II
		Rheumatoid arthritis	ICAM-1	II
		Ulcerative colitis	ICAM-1	II
G3139 (Genta)	N.A.	Cancer	N.A.	I
ISIS2503	PS	Cancer	Ha-ras	I
ISIS3521	PS	Cancer	PKC-α	II
ISIS5132	PS	Cancer	c-raf	II
LR-3001 (Inex)	PS	Chronic myelogenous leukemia	bcr-abl	I

Table 1. trials of antisense therapeutics; PS= phosphorothioate, N.A.= not available

1.3 Oligonucleotides in the antigene strategy

ONs can selectively recognize and bind to double-helical DNA, at the level of specific sequences, by forming Hoogsteen or reverse-Hoogsteen type hydrogen bonds; in this case, modulation of gene expression by ONs may occur via triplex forming oligodeoxynucleotides (TFOs).
TFOs allow the possibility to target the chromosomal DNA, with the resulting inhibition of the transcriptional events as a consequence. In effect, the antigene strategy is one of the most intriguing fields of triplex application to selectively control gene expression.
Conceptually, antigene approaches offer many advantages over antisense: usually two gene copies per cell are available to target rather than multiple copies of mRNA that are continually being transcribed; a persistence block of the transcriptional process; and simultaneous inhibition of all splice variants.
As regards the ways of action, TFOs are, generally, short, synthetic single-stranded DNAs that can inhibit gene transcription by forming DNA triple helices in a sequence specific manner on polypurine-polypyrimidine tracts; in particular, they can bind with a high specificity of recognition the major groove of double helical DNA by forming Hoogsteen type bonds with purine bases of the Watson-Crick base pairs, resulting in triple helix formation. [14] In doing so, triplex-forming oligonucleotides (TFOs) can selectively inhibit gene expression at the transcriptional level or repair genetic defect by direct genome modification in human cells.
A TFO can be classified on purine or pyrimidine motif, on the basis of its composition and its relative binding orientation in respect to the DNA target site.
In the former, the purine TFO binds, in an antiparallel orientation, to purine-rich strands of DNA via reverse Hoogsteen bonds, forming A·A:T, G·G:C or T·A:T base triplets (with the first base of the triplet belonging to the TFO). This kind of binding requires no base protonation and is largely pH independent.

In the latter, a TFO composed of cytosine and thymine binds, in a parallel orientation, to the purine rich strands of DNA via Hoogsteen bonds. Thymines bind to adenine in the A:T base pairs, while protonated cytosines bind to guanines in the G:C base pairs (Fig. 2).

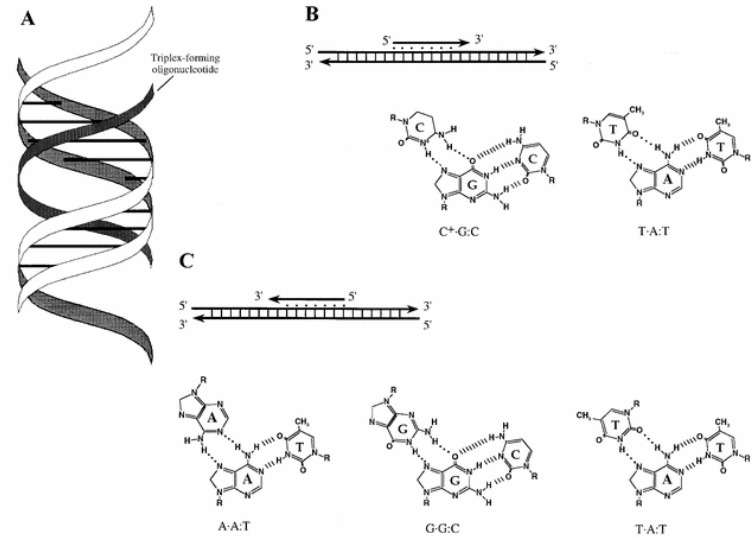

Figure 2. Basic features of a triple helix formation. **A.** Schematic model of the relative orientation of the TFO. **B.** Pyrimidine binding motif: the pyrimidine TFO binds to the polypurine strand of DNA in a parallel orientation. **C.** Purine binding motif: the purine TFO binds to a polypurine strand of DNA in an antiparallel orientation.

However, current strategies for oligonucleotide-directed triple helix formation suffer from important constraints. In particular, given the fact that the binding requires polypurine-polypyrimidine tracts, there are important restrictions on the permitted target sequences, moreover pyrimidine ONs usually do not bind to DNA at physiologically pH without further modifications and, finally, the inefficient way to deliver ONs within the nucleus.
Nevertheless, the antigene strategy continues to draw the scientific interest and great efforts have been doing to overcome its drawbacks. Because of homopurine and homopyrimidine sites are common in gene promoter regions and often overlap binding motifs for transcription-regulatory proteins, TFOs have been shown to inhibit transcription factors binding to purine-rich motifs and have been tested to block transcription of various genes *in vitro* and in intact cells. [15]
One of the most relevant and fascinating application of the antigene strategy is the gene cancer therapy. In 2012, Tonelli and co-workers proposed the exploitation of an ON analogue, *i.e.* the *Peptide Nucleic Acid* (PNA), as antigene tool to correct the expression of MYCN gene in the treatment of aggressive alveolar rhabdomyosarcoma in mice. [16]

1.4 ON analogues

The need for antisense and antigene oligomers with improved features has been widely recognized by the scientific community and has led to the development of chemical modifications to improve the ODN features. For example, given their

susceptibility to nucleases, oligonucleotides have often been found to be unstable in biological fluids, thus limiting their therapeutic applications.
To overcome these problems, various chemically modified oligonucleotides have been synthesized, incorporating modifications to the phosphodiester backbone, sugar or nucleobases portions. In this context, modifications on the backbone, sugar or nucleobases, as well as conjugation, are aimed at improving the classical drawbacks of the natural counterparts, such as nuclease resistance, affinity, bioavailability, biodistribution and immune response.
In general, on the basis of the kind of modification, the ON analogues are distinguished in analogues of the first generation, of the second generation and of the third generation.

1.4.1 First generation analogues

The analogues of the first generation are characterized by the substitution of one of the non-bridging oxygen atoms in the phosphate group. [17] As a consequence, the final compound possesses a chiral phosphodiester much more resistant to the nucleases. This class includes: the phosphorothioates **1**, the methylphosphonates **2**, the phosphoramidates **3**, the phosphorotriesters **4** and the phosphorodithioate **5** (Fig. 3).

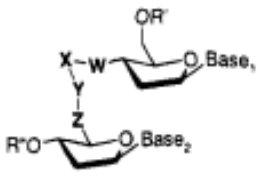

	-W-	-X-	-Y-	-Z-
1	-O-	-P(O)S$^-$-	-O-	-CH_2-
2	-O-	-P(O)CH_3-	-O-	-CH_2-
3	-O-	-P(O)NHR-	-O-	-CH_2-
4	-O-	-P(O)OR-	-O-	-CH_2-
5	-O-	-P(S)S$^-$-	-O-	-CH_2-

Figure 3. Structures of the ON analogues belonging to the first generation of analogues.

Unfortunately, all these derivatives display a lower affinity for the complementary RNA molecules. Moreover, the creation of a new centre of chirality reduce the final synthetic yields, as a result of the preparation of equal amounts of diastereoisomers. Nevertheless, phosphorothioate oligodeoxynucleotides (PS-oligos), thanks to their beneficial properties, including the chemical stability and the favourable pharmacokinetic properties, have been studied intensively in both *in vitro* and *in vivo* models, showing biological activity against a variety of molecular targets and a considerable number of this kind of compounds entered in the clinical trials for the treatment of various diseases, such as cancer, inflammation and viral infection. For example, the very first antisense compound introduced in the market, known as *Vitravene*, is a 2-deoxyphosphorothioate. [18]

1.4.2 Second generation analogues

The second generation of backbone modifications includes analogues characterized by the modification on the sugar moiety, through the introduction of alkyl groups on

the 2' position of the sugar. These modifications were proposed by the medicinal chemists to enhance analogues properties, such as nuclease resistance and cellular absorption and, above all, to reduce the cytotoxicity. The 2'-modifications initially proposed were the 2′-O-alkyls, the 2′-O-alkyls with glycol ether linkages, the 2′-F and 2′-O-aminoalkyls. Among these, taking into account the drawbacks of these analogues in terms of resistance to the nucleases, mainly two kinds of analogues stand out: 2′-O-(methoxyethyl) or 2-O-MOE and 2′-O-(aminopropyl) or 2′-O-AP (Fig. 4). [17]

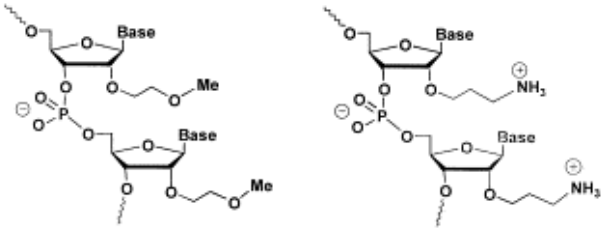

Figure 4. Structures of 2'-O-MOE on the left and 2'-O-AP on the right.

The first one showed +2°C increase in binding affinity compared to the first generation drugs and a nuclease resistance at approximately the same level of the 2′-deoxyphosphorothioate modification. On the other hand, the 2′-O-(aminopropyl) analogues, by virtue of their cationic alkyl chain present at the 2′-position, offered the highest resistance against nucleases.
To further improve the features of these last compounds, the scientific community planned to go beyond the 2'-O-MOE and 2'-O-AP modifications, designing a further class of analogues. The third class of modified oligonucleotides is that in which the sugar-phosphodiester backbone has been replaced entirely. Because of the structural changes on the native backbone, they are better known as *ON mimics*.

1.4.3 ON mimics: the PNA

The third class of ON analogues includes: Locked Nucleic Acids (LNAs), morpholinos and Peptide Nucleic Acids (PNAs). These analogues can form both duplexes and triplexes, are characterized by improved biostability and have been extensively studied both for therapeutic and diagnostic applications.
LNAs were first introduced by Singh *et al.* and represent a novel class of constrained ON analogues in which the ribonucleoside is linked between the 2′-oxygen and the 4′-carbon atom with a methylene unit (Fig. 5).

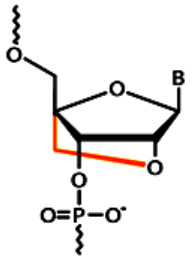

Figure 5. Chemical structure of LNA

The structural features of LNA make it a powerful and versatile tool in terms of affinity toward the complementary DNA and RNA molecules and thermodynamic stability of

the resulting duplexes and triplexes. Thanks to their noteworthy mismatch discrimination, LNAs have been employed for the design of SNP (Single Nucleotide Polymorphisms) assays and, also, for the construction of therapeutic DNAzymes and LNAzymes with intrinsic endonucleolytic activity.
Morpholinos were initially described in 1985 by Summerton. In these molecules, morpholino subunits are easily synthesized starting from the inexpensive ribonucleosides, converted in the morpholinos by the introduction of an amine. They exhibits optimal base-stacking and water solubility (Fig. 6).

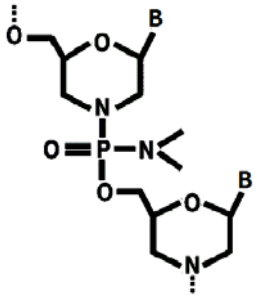

Figure 6. Chemical structure of morpholino analogues

Morpholinos have been experimented as antisense tools and to correct splicing errors in pre-mRNAs. Even more interestingly, some of their most fascinating applications comprehend their use to dissect the temporal progression of embryotic development. [19-21]
Finally, the third mimic is the Peptide Nucleic Acid (PNA), developed by the biochemist Peter Nielsen during the 1980s.[22]
PNA is a powerful biomolecular tool with a variety of important applications in biotechnology.
PNA is a DNA/RNA mimic in which the phosphate deoxyribose backbone is replaced by uncharged *N*-(2-aminoethyl)-glycine linkages (Fig. 7). Nucleobases, attached through methylene carbonyl linkages to the glycine amino group, recognize complementary sequences by standard Watson-Crick pairing. Because PNAs have a neutral backbone, hybridization is not affected by the intrastrand repulsion and occurs with enhanced affinity and rates of association. Moreover PNAs do not appear to be substrates for nucleases or proteases and absence of a repetitive charged backbone also prevents PNAs from binding to proteins that normally recognize polyanions, avoiding a major source of nonspecific interactions.
As regards its production, the key step in the subunits synthesis is represented by the selective alkylation at the N9 position of the purine or the N1 position of the pyrimidines, as showed in figure 7. Due to the peptide nature of its backbone, the PNA subunits are generally assembled through the well-established Solid Phase Peptide Synthesis (SPPS) protocols and the synthesis is suited to automation and, therefore, can be easily performed on automated synthesizers.

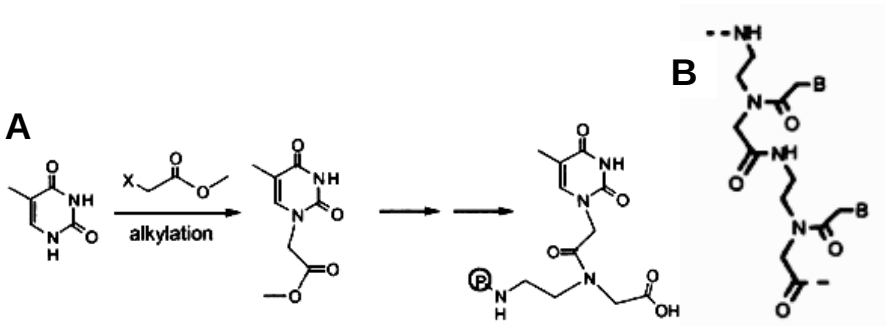

Figure 7. **A** Key steps in PNA subunit synthesis. **B** Chemical structure of PNA

In the last few years PNAs have emerged as promising tool for gene therapeutic drugs design. As ON, in principle, peptide nucleic acids were used to selectively inhibit gene expression at the transcriptional level or at the translational level. But very recently another interesting application has emerged: it has been demonstrated that PNA based ASOs (antisense oligonucleotides) are more effective ASOs of miRNA than DNA ASOs [23].
As regards the antigene strategy, PNAs should be capable of arresting transcriptional processes by virtue of their ability to form a stable triplex structure or a strand-invaded complex with DNA [24]. Such complexes can create a structural hindrance to block the function of RNA polymerase, thus working as antigene agents.
Moreover, antisense peptide nucleic acids offer the promise of therapeutic effect with few or no toxic effects, by virtue of their enhanced selectivity in respect to traditional oligonucleotides. Normally, the PNA antisense effect is based on the steric blocking of either RNA processing, transport into cytoplasm, or translation. Started from the results of *in vitro* translation experiments involving rabbit reticulocyte lysates, it has been concluded that PNAs are capable of inhibiting translation at targets overlapping the AUG start codon [25]. Finally, but not less intriguing, peptide nucleic acids can be used as miRNA inhibitors, thereby open the possibilities of studying the function of genes involved in many pathologies and modulating their expression.
Currently, various technologies to investigate the mechanisms of miRNA function have been well documented. It has been observed that oligonucleotide analogues inhibit microRNA function essentially by a steric block, RNaseH-independent and RISC-independent, through complementary binding of the ON to the microRNA sequence [26]. Chemical modifications of antisense oligonucleotides are important not only to improve their affinity for target miRNAs but also to protect the ON against nuclease degradation. For these reason various modified ONs and analogues have been studied to this purpose. Many studies using PNAs to explore miRNA functionality have been reported: different PNA oligomers have been proven to be effective at blocking miR-122, a miRNA whose function has been linked to lipid metabolism [26], miR-221 involved in the chondrogenic differentiation of chick limb mesenchymal cells [27] and miR-UL148D involved in the human cytomegalovirus infection [28].
In conclusion, PNAs exhibit several notable properties, such as high chemical and thermal stability, resistance to enzymatic degradation and stable binding to their RNA or DNA targets in a sequence-specific manner, for these reasons they have been exploited in a variety of contexts, including the antigene and antisense strategy, diagnostic applications and, more recently, as *aptamers*.

1.5 ONs as *aptamers*

The biotechnological relevance of oligonucleotides and analogues can be expanded due to the emergence of other relevant applications, such as the design of aptamers aimed at binding and inhibiting specific molecular targets.
The word *aptamer* comes from the Latin “aptus”, to fit, and the Greek stem, “meros”, part or region, and is referred to RNA or DNA molecules, generally 25-50 nucleotides in length, endowed with noteworthy affinity and selectivity towards molecular targets, mainly proteins.[29] The basic concept of joining nucleic acids to proteins has naturally emerged with the advent of genetic engineering, which opened the possibility to discover and exploit highly specific interactions between proteins and ON sequences, such as, just to mention a few, the interaction between the restriction enzymes and their target cleavage sequences or transcription factors and their target DNA promoter elements. From the late 1980s the idea of modulating protein function through nucleic acid sequences has been successfully settled in for the development of a new class of therapeutics.
Aptamers are obtained from puzzled pool with several combination of molecules. The process through which they are selected from a randomly synthesized library containing up to 10^{15} different molecules, for their affinity towards their targets, is known as Systematic Evolution of Ligands by Exponential enrichment (SELEX) and was developed in the laboratories of Larry Gold of the University of Colorado during the 1990s. After this iterative process, the resulting nucleic acid molecules can be chemically modified in order to provide them with additional properties and, above all, to extend their half-life in biological fluids. [30]
The broad applications of aptamers range from diagnostics to therapeutics, biosensors and also tools for unravelling fundamental cellular processes. They are often seen as “chemical antibodies”, but, in respect to antibodies, they are relatively small, free from cell-culture contaminants, offer easy chemical synthesis and possibility of conjugation and modification and avoid immune response. For these reasons, enthusiasm in developing therapeutic aptamers is still strong and the scientific community is to date deeply involved in the search of these novel drug candidates, facing at the same time the drawbacks, like the instability in biological media and the low bioavailability.
The developing area of aptamer research has seen in 2004 the FDA approval of *pegaptanib* for the treatment of choroidal neovascularization associated with age-related macular degeneration. The clinical use of pegapatanib can be seen as a milestone in drug development, constituting the first aptamer used for human treatment. Although important challenges remain, this area is in the pipeline, with more than ten candidates undergoing clinical trials, with applications against a variety of diseases, from cancer to diabetes. [31,32] Some of the most extensively studied aptamers have G-rich consensus sequences that allow them to fold into stable four-stranded structures, known as *G-quadruplex.*[33] As for the other biological molecules, also for the aptamers the folding into specific secondary and tertiary structures play a fundamental role in the recognition and binding phenomena. The attempts to enhance target specificity and other aptamers features highlighted the importance of finely predict and know the three-dimensional structures of these novel drug candidates.

1.5.1 G-Quadruplexes: a general overview

G-rich ON sequences have the natural propensity to fold in unusual secondary structure, named G-Quadruplex (G-Q), whose fundamental unit is represented by planar G-quartet assemblies, held together by Hoogsteen hydrogen bonds and stabilized by monovalent cations. Owing to the evidence of G-Q formation within the vertebrate genomes, [34] great interest arose on these non-canonical structures since their discovery, and the scientific community is still deeply involved in disclosing their relation with relevant biological processes. Not less fascinating, due to their architectures and sensitivity to the presence of specific cations and ligands, they have been and are, even now, exploited for the application in nanotechnology and the design of biosensors and DNAzymes. [35]
Although the G-Q core is always the same, G-Quadruplexes are characterized by extremely high variability in regards to the folding topology, loop orientation, molecularity and glycosidic orientation of the sugar bases. [36] To simplify the structural complexity of G-Q, we can carry out a first classification on the basis of the number of strands; in this way we can distinguish between unimolecular G-Q, made up of only one G-rich ON strand and bimolecular and tetramolecular G-Qs, formed from the association of two or four ON strands respectively.
G-Qs can be also classified on the basis of orientation of the strands and the connecting loops. Propeller type loops are those which connect the bottom G-quartet to the top G-quartet of adjacent strands with the same orientation; lateral loops, also known as edge-wise loops, link adjacent strands, while diagonal loops join opposite strands (Fig. 8)

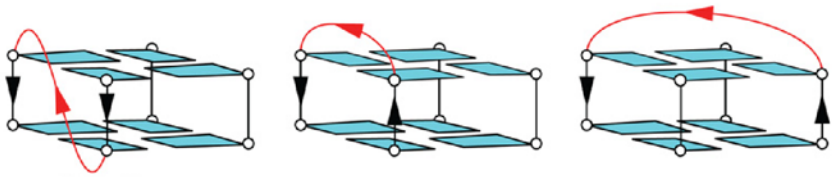

Figure 8. Propeller loops (left), lateral loops (centre) and diagonal loops (right)

The strands orientation generates a further distinction: G-Q structures possessing all the strands in the same orientation are parallel quadruplexes, while opposite orientation of the strands give rise to antiparallel or hybrid quadruplexes. In general, parallel quadruplexes have all the guanosine glycosidic angle sin the *anti*-conformation, while antiparallel quadruplexes show both *anti* and *syn* glycosidic angles.
Moreover, variations on the orientations adopted by the stacked bases lead to different groove dimensions, i.e. the cavities surrounded by the phosphodiester backbone. In general, qudruplexes characterized by lateral or diagonal loops are structurally simple, in contrast grooves in quadruplex with only propeller loops have more complex structures, as shown in figure 9 for the sequence d[AGGG(TTAGGG)$_3$]. [37]

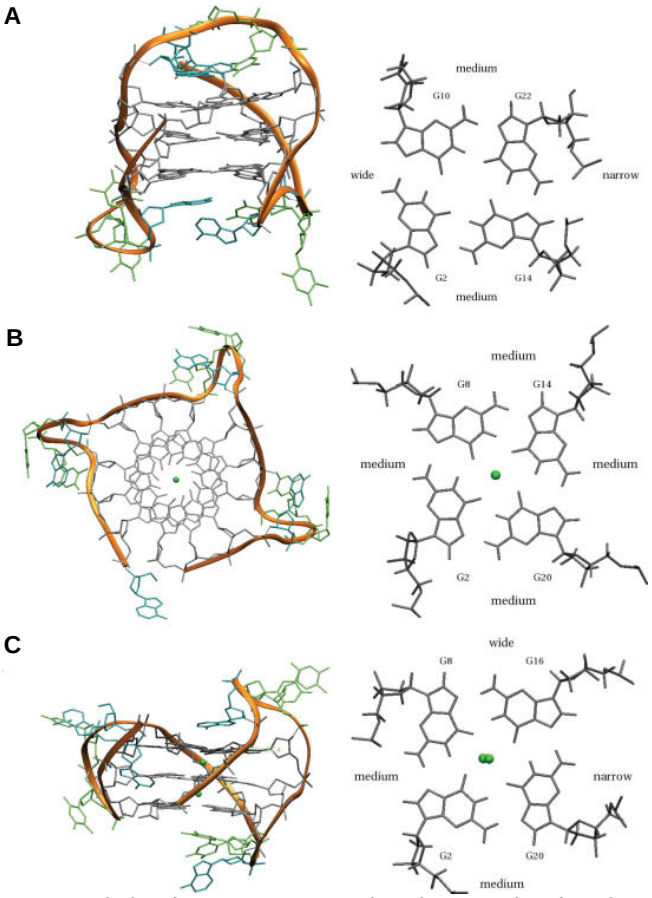

Figure 9. Different structures of the human monomolecular quadruplex formed from the telomeric sequence d[AGGG(TTAGGG)$_3$]. (A) groove structure of a G-Q with a diagonal and two lateral loops, (b) with three propeller loops, (c) with one propeller and two lateral loops.

Finally, a fundamental role is played by monovalent cations on the folding and thermodynamics of G-Qs. In fact, their localization within the G-Q core reduce the strong negative electrostatic potential generated by the guanine O6 oxygen atoms. In this context, the most extensively studied ions are K^+ and Na^+. Their different behaviour as regards their location within the cavity result from their dimension: the smaller sodium cations can reside in plane with the G-quartet, whereas potassium can coordinate between two tetrads. [38]

1.5.2 Biotechnological relevance of G-Quadruplexes

A markedly high number of examples in literature witness the broad range of applications of G-Qs at a biotechnological level.
Owing to the high density of G-quadruplex-forming sequences in genomic regions adjacent to transcriptional start sites, G-Q structures have so far emerged as a new class of molecular targets for gene regulation and anticancer drugs development. In fact, G-rich sequences are broadly distributed in regions of human genome, including telomere ends, immunoglobulin switch regions and regulatory elements of oncogene promoters such as *c-myc*, *k-ras*, *c-kit* and so on. [39-43]
Since a great number of observations come out on the inside of their regulatory role, G-Qs represent a great promise as target in the anticancer treatments. In this sense, one of the first proposed application came from the realization that G-rich sequences

in the telomers, by virtue of their structuration in quadruple helices, can inhibit telomerase activity, thus preventing cell immortalization. A wide number of small molecules have been explored for their capability to interact and stabilize telomeric G-Qs and, among these, for the cyclic polyoxazole natural product telomestatin and the synthetic compounds BRACO19 and RHPS4 evidences of antitumor activity have been reported in xenograft models. Similarly, an inhibition of the transcriptional events of the proto-oncogenes MYC and hTERT has been achieved upon the addition of G-Q ligands TMPyP4 and telomestatin derivative S2T1-6OTD, as reported by Balasubramanian *et al*.[44-47] These and many other observations make G-Q structures one of the most challenging targets in the anti-cancer treatments. Conformational plasticity of G-Qs allows the possibility to exploit them at a diagnostic level, by fine tuning their formation and interaction with their targets. In this context, an exciting trend in biotechnology sees the use of aptamers that selectively recognize targets differentially expressed in diseased cells for bioimaging and for helping the diagnosis of the disease. For example, AS1411 is a multifunctional 26 nt G-rich aptamer, that easily form two G-Q assemblies in presence of potassium cations used, by virtue of its binding to excessively expressed nucleolin on cancer cells, for the diagnosis and treatment of cancer. On the other hand, the sensitivity of G-Qs for metal ions has been exploited for the design of detectors of K^+, Ag^+, Hg^+ etc. In this wake, the exceptionally high stability of G-Qs in organic solvents like ethanol, methanol and other dehydrating agent, in addition to their high conductance, makes them suitable building blocks for the construction of electronic nanodevices. Similarly, catalytically active G-Qs have been exploited for the construction of DNAzymes, as reported by Liu *et al.* that developed a colorimetric sensor for thrombin by incorporating hemin into the complex G-Q TBA aptamer/thrombin. [48] Finally, a variety of reports explored the bioconjugation of G-Qs to magnetic nanoparticles for biosensing applications.

1.6 ONs based biosensors

Research in the field of ON based biosensors has become very popular in the last decades. Biosensors are analytical tools that combine biological materials, such as proteins, DNA/RNA and other selective chemicals and physicochemical signal transducer. In this context, ONs are particularly well suited because they allow the possibility to convert highly selective hybridization phenomena to readable analytical events. Specifically, electrochemical biosensors based on oligonucleotides gained remarkable attention for the task of monitoring and control of specific DNA sequences related to microorganisms, viruses and inherited diseases and, also, for detecting the presence of infectious agents in various environmental matrices. [49]
As regards the first possibility, ON biosensors found application to distinguish genetic materials from infectious organisms and to detect genetic mutations associated to disease phenotypes, such as cancer, neurodegenerative diseases etc. For example, several papers described the design and application of biosensors based on single-stranded ON as probe for the detection of DNA sequence related to Hepatitis B virus. [50] In 2009, Mao *et al.* showed the rapid and sensitive detection of circulating cancer cells, by developing an aptamer-nanoparticle strip biosensor (ANBS), i.e. a biosensor based on the conjugation to gold nanoparticles of ON sequences selectively recognizing receptors on cancer cells in blood. [51] Similarly, a great number of ON biosensors have been designed for the direct and indirect detection of pathogenic

bacteria; in 2012 Zhang *et al.* reported a biosensor, incorporating magnetic nanoparticles and gold nanoparticles as transducer, with target-specific DNA probe for the detection of *Salmonella enterica.*[52] The same principle is used to realize biosensors for food contaminants and environmental pollution monitoring. The need for such biosensors is linked to the increasing exposition to hazardous chemical that provoke excessive immune response, cancer and other diseases. Electrochemical devices incorporating DNA sequences have been proposed for the detection of heavy metals, such as Pb^{2+}, Hg^{2+}, but also antibiotics ant toxins.
These and many other examples highlight the promise and the potential of ON-based biosensors to consolidate a new era of easy, cost-effective and rapid diagnostics.

1.7 Aim of my research work

My research project is set in a wide context aimed at exploiting the several features and applications of oligonucleotides and analogues. In this context, my attention has been focused on the study of G-Q forming aptamers and their potential antiviral activity, the design and resolution of chemical issues linked to the design of novel kinds of ON based biosensors and the exploitation of ON analogues, such as PNA, in the field of gene modulation.
Notably, the project included:

- **The implementation of novel anti-HIV aptamers based on tetra-end-linked DNA**
  The aim of this part of the project was to select very short ON aptamers, starting from previously reported antiviral G-Q forming aptamers, in order to enhance their pharmacodynamic and pharmacokinetic parameters and safeguard their biological activity.
  As already discussed, aptamers offer great promise as novel therapeutics. Among these, particularly fascinating are those endowed with antiviral activity, as witnessed by the huge body of literature on this topic.
  In 2010 Oliviero *et al*. proposed the use of Tetra-End-Linked Oligonucleotides (TEL-ON), which form very stable TEL-quadruplex structures, as promising candidates to improve the antiviral activity against HIV-1 showed by the 6mer G-Q forming sequence TGGGAG, known as Hotoda's aptamer. The promising findings as regards the favorable thermodynamics and activity of these analogues gave confidence about the possibility to further modify the original sequence. In 2012 D'Atri *et al.* reported the synthesis and structural and biological characterization of a mini-library of Hotoda analogues TEL-ONs, modified at both the 3' and 5' ends, in order to assess the effect of different nucleotide sequence on the antiviral activity. [53-54]
  In the wake of these studies, we decided to exploit a combination of *in silico* driven techniques and novel and cost-effective binding assay to consolidate a new approach for the individuation of the smallest and more active analogue of the TEL-aptamer previously designated by us as the best anti-HIV aptamer. The main goal of this search has been to provide a new method for the optimization of therapeutic aptamers, not achievable by the SELEX method.
  The second part of this search has been devoted to the design, synthesis and characterization of new high ordered G-Q aptamers. In previous works, our research group proved the good thermodynamic parameters of G-Q assemblies having the sequences CGGXGGT (with X = A, C, G and T). [55-56] Structural studies on them

showed that these sequences are able to fold into stable dimers of parallel G-Qs, provided with high thermal stability and reproducible folding assembly. These properties make them good candidates for the development of novel putative aptamers. In this frame, we designed novel TEL-analogues of the sequence CGGXGGT, conveniently modified at their 5'-terminus, and studied them for their kinetics and antiviral activity.

- **Conjugation of oligonucleotides onto solid supports: studies on DNA-based biosensors**

  DNA-based biochips, i.e. devices constituted by ONs as molecular recognition element and a transducer element, have interesting applications in nanoelectronics, biomolecular computations, cellular imaging and drug delivery. Optical transduction has been widely exploited for the design of such biosensors and, in this context, porous silicon (PSi) is one of the most used material, owing to its attractive morphological and physical features. Nevertheless, to date only few reports showed the *in situ* synthesis of ON sequences onto PSi matrices. [57]
  However, *in situ* synthesis of ONs onto solid supports presents several advantages in respect to *ex situ* immobilization; for example, increasing of DNA probe density, the process automation, the possibility of surface local functionalization, just to mention a few. Taking into account the advantages of *in situ* synthesis and, at the same time, the hurdles of the entire process, associated to the chemistry used for the ONs growth and the intrinsic properties of the silicon matrix, the aim of this part of the project was to allow the direct synthesis on PSi platforms of mixed ON sequences by standard reagents and protocols, by exploring different chemical protocols. In this way, we ultimately obtained a more convenient production of functionalized biochips.

- **Oligonucleotide analogues: PNA and its use as miRNA inhibitor**

  The aim of this work was to design anti-miRNA PNA sequences for the inhibition of miR-509-3p, a miRNA involved in the down-regulation of cystic fibrosis disease-gene expression.
  The chemical features of the ON mimic PNA have made it an attractive tool in the field of gene regulation. In this context, it has been demonstrated that anti-miRNA ASOs (antisense oligonucleotides) based on PNA are more effective than ASOs based on DNA, thus opening the possibilities of studying the function of genes involved in many pathologies and modulating their expression. Recently, Amato *et al.* proposed specific sequences of peptide nucleic acid as new inhibitors of miR-509-3p. [58] Because of the not trivial synthesis of the tested sequences, my objective has been the optimization of the chemical and physical characteristics of these PNAs. By means of computational simulations, chemical synthesis, biophysical and biological characterization we succeeded in obtaining novel PNAs with enhanced features.

1.8 References

1. Kruger K, Grabowski PJ, Zaug AJ, Sands J, Gottschling DE, Cech TR, **1982**.*Self-splicing RNA: autoexcision and autocyclization of the ribosomal RNA intervening sequence of Tetrahymena.*Cell 31 (1): 147–57.
2. Zamecnik PC, Stephenson ML, **1978**. *Inhibition of Rous sarcoma virus replication and cell transformation by a specific oligodeoxynucleotide.*PNAS75 (1): 280-84
3. Ma DDF, Rede T, Naqvi NA, Cook PD, **2000**. *Synthetic oligonucleotides as therapeutics: The coming of an age*. 5: 156-96
4. Wang DY, Lai BHY, Feldman AR, Sen D, **2002**. *A general approach for the use of oligonucleotide effectors to regulate the catalysis of RNA-cleaving ribozymes and DNAzymes*. Nucl. Acids Res. 30 (8): 1735-1742.
5. Donnelly JJ, Ulmer JB, Shiver JW, Liu MA, **1997**. *DNA Vaccines*. Annual Review of Immunology.15: 617-48
6. Sun H, Zhu X, Lu PY,Rosato RR, Tan W, Zu Y, **2014**. *Oligonucleotide Aptamers: New Tools for Targeted Cancer Therapy.* Molecular Therapy Nucleic Acids 3: 182
7. Kurreck J, **2003**. *Antisense technologies: improvement through novel chemical modifications.* Eur. J. Biochem. 270: 1628-44
8. Crooke ST, **1999**. *Molecular mechanisms action of antisense drugs*. Biochim. Biophys. Acta 1489 (1): 31-44
9. Hanvey JC, Williams EM, Besterman JM, **1991**. *DNA triple-helix formation at physiologic pH and temperature.* Antisense Res. Dev.**1** (4): 307-17
10. Yu W, Lee JS, Johnson C, Kim JW, Deaton R**, 2010***. Independent sets of DNA oligonucleotides for nanotechnology applications.* IEEE Trans Nanobioscience. 9(1):38-43.
11. Dias N Stein CA, **2002**. *Antisense Oligonucleotides: basic concepts and mechanisms.* Mol. Cancer Ther. 1: 347
12. Anderson KP, Fox MC, Brown-Driver V, Martin MJ, Azad RF, **1996**. *Inhibition of human cytomegalovirus immediate-early gene expression by an antisense oligonucleotide complementary to immediate-early RNA.*Antimicrob. Agents Chemother. 40(9):2004-11.
13. Monteleone G, Fantini MC, Onali S, Zorzi F, Sancesario G,Bernardini S, Calabrese E, Viti F, Monteleone I, Biancone L, Pallone F, **2012**. *Phase I Clinical Trial of Smad7 Knockdown Using Antisense Oligonucleotide in Patients With Active Crohn's Disease*. Molecular Therapy 20 (4): 870–76.
14. Helene C, **1991**. *The anti-gene strategy: control of gene expression by triplex-forming-oligonucleotides.* Anticancer Drug Des.6(6):569-84.
15. Maher LJ, **1996**. *Prospects for the therapeutic use of antigene oligonucleotides.* Cancer Invest. 14(1):66-82.
16. Tonelli R, McIntyre A, Camerin C, Walters ZS, Di Leo K, Selfe J, Purgato S, Missiaglia E, Tortori A, Renshaw J, Astolfi A, Taylor KR, Serravalle S, Bishop R, Nanni C, Valentijn LJ, Faccini A, Leuschner I, Formica S, Reis-Filho JS, Ambrosini V, Thway K, Franzoni M, Summersgill B, Marchelli R, Hrelia P, Cantelli-Forti G, Fanti S, Corradini R, Pession A, Shipley J, **2012.** *Antitumor activity of sustained N-myc reduction in rhabdomyosarcomas and transcriptional block by antigene therapy.*Clin. Cancer Res. 18(3):796-807.
17. Verma S, Eckstein F, **1998**. *Modified Oligonucleotides: synthesis and strategy for users.* Annual Review of Biochemistry. 67: 99-134

18. Crooke ST, **2009**. *Vitravene: another piece in the mosaic*. Antisense and Nucleic Acid Drug Development. 8(4): 7-8.
19. Nasevicius A, Ekker SC, **2000**. *Effective targeted gene 'knockdown' in zebrafish*.Nat Genet. 26(2):216-20.
20. Bauer H, Lele Z, Rauch GJ, Geisler R, Hammerschmidt M, **2001**. The type I serine/threonine kinase receptor Alk8/Lost-a-fin is required for Bmp2b/7 signal transduction during dorsoventral patterning of the zebrafish embryo. Development. 128: 849-858.
21. Heasman J, Kofron M, Wyliet C, **2000**. *B-Catenin Signaling Activity Dissected in the Earl Xenopus Embryo: A Novel Antisense Approach*. Developmental Biology 222: 124-134.
22. Nielsen PE, Egholm M, Berg RH, Buchardt O, **1991**. *Sequence-selective recognition of DNA by strand displacement with a thymine-substituted polyamide.*Science. 254(5037):1497-500.
23. Oh SY, Ju YS, Park H,**2009.***A highly effective and long-lasting inhibition of miRNAs with PNA-based antisense oligonucleotides.* Molecules and Cells. 28: 341-345.
24. Knudsen H, and Nielsen PE, **1996**. *Antisense properties of duplex- and triplex-forming PNAs.* Nucleic Acids Res. 24:494–500.
25. Fabani MM, Gait MJ, **2008.** *miR-122 targeting with LNA/29-O-methyl oligonucleotide mixmers, peptide nucleic acids (PNA), and PNA–peptide conjugates*. RNA. 14: 336-346
26. Esau C, Davis S, Murray SF, Yu XX, Pandey SK, Pear M, Watts L, Booten SL, Graham M, McKay R, Subramaniam A, Propp S, Lollo BA, Freier S, Bennett CF, Bhanot S, Monia BP, **2006**. *miR-122 regulation of lipid metabolism revealed by in vivo antisense targeting.*Cell Metab. 3(2):87-98
27. Dongkyun K, Jinsoo S. and Eun-Jung J, **2010**.*MicroRNA-221 regulates chondrogenic differentiation through promoting proteosomal degradation of slug by targeting Mdm2*. J. Biol. Chem. 285: 26900-07.
28. Kim Y, Lee S, Kim S, Kim D, Ahn JH, **2012**. *Human Cytomegalovirus Clinical Strain-Specific microRNA miR-UL148D Targets the Human Chemokine RANTES during Infection*. PLoS Pathog 8(3): e1002577.
29. Proske D, Blank M, Buhmann R, Resch A, **2005***. Aptamers-basic research, drug development, and clinical applications.* Appl. Microbiol. Biotechnol. 69(4):367-74
30. Gopinath SCB, **2007**. *Methods developed for SELEX*. Anal. Bioanal. Chem. 387:171–182
31. Ng EWM, Shima DT, Calias P, Cunningham ET,Guyer JDR, **2006**. *Pegaptanib, a targeted anti-VEGF aptamer for ocular vascular disease.* Nature Reviews Drug Discovery. 5: 123-132.
32. Weinberg MS, **2014**. *Therapeutic Aptamers March On.* Molecular Therapy Nucleic Acids. 3: e194
33. Gatto B, Palumbo M, Sissi C, **2009**.*Nucleic acid aptamers based on the G-quadruplex structure: therapeutic and diagnostic potential.* Curr. Med. Chem. 16(10):1248-65.
34. Biffi G, Tannahill D, McCafferty J, Balasubramanian S, **2013**. *Quantitativevisualization of DNA G-quadruplex structures in human cells.* NatureChemistry. 5: 182-86.

35. Yatsunyk LA, Piétrement O, Albrecht D, Tran PL, Renčiuk D, Sugiyama H, Arbona JM, Aimé JP, Mergny JL, **2013**. *Guided assembly of tetramolecular G-quadruplexes.* ACS Nano. 7(7):5701-10.
36. Simonsson T, **2001**. *G-Quadruplex DNA structures – Variation on a theme*. Biol. Chem. 382: 621 – 628.
37. Wang Y, Patel DJ, **1993**. *Solution structure of the human telomeric repeat d[AG3(T2AG3)3] G-tetraplex*.Structure. 1(4):263-82.
38. Lane AN, Chaires JB, Gray RD, Trent JO,**2008**. *Stability and kineticsof G-quadruplex structures.* Nucleic Acids Res. 36: 5482-15.
39. Gabelica V, E. S. B., M. P. Teulade-Fichou, E. De Pauw, and M. T. Bowers.**2007**. *Stabilization and structure of telomeric and c-myc region intramolecularG-quadruplexes: the role of central cations and small planar ligands.* Journal of the American Chemical Society 129: 895-904.
40. Rankin S, Reszka AP, Huppert J, Zloh M, Parkinson GN, Todd AK, Ladame S, Balasubramanian S, Neidle S, **2005**. *Putative DNA quadruplex formation within the human c-kit oncogene*. J. Am. Chem.Soc. 127: 10584-89.
41. Phan AT, Kuryavyi V, Burge S, Neidle S, Patel DJ,**2007**. *Structure of anunprecedented G-quadruplex scaffold in the human c-kit promoter.*J. Am. Chem. Soc. 129: 4386-92.
42. Dai J, Dexheimer TS, Chen D, Carver M, Ambrus A, Jones RA, Yang D, **2006**. *An intramolecular G-quadruplex structure with mixed parallel/antiparallel G-strands formed in the human BCL-2 promoter region in solution*. J. Am. Chem. Soc. 128: 1096-98.
43. Dexheimer TS, Sun D, Hurley LH, **2006**. *Deconvoluting the structuraland drug-recognition complexity of the G-quadruplex-forming region upstreamof the bcl-2 P1 promoter.* J. Am. Chem. Soc. 128: 5404-5415.
44. Burger AM, Dai F, Schultes CM, Reszka AP, Moore MJ, Double JA, Neidle S, **2005**.*The G-quadruplex-interactive molecule BRACO-19 inhibits tumor growth, consistent with telomere targeting and interference with telomerase function*. Cancer Res. 65: 1489–1496.
45. Phatak P, Cookson JC, Dai F, Smith V, Gartenhaus RB, Stevens MF, Burger AM, **2007**. *Telomere uncapping by the G-quadruplex ligand RHPS4 inhibits clonogenic tumour cell growth in vitro and in vivo consistent with a cancer stem cell targeting mechanism*. Br. J. Cancer. 96: 1223–33.
46. Tauchi T, Shin-Ya K, Sashida G, Sumi M, Okabe S, Ohyashiki JH, Ohyashiki K, **2006**. *Telomerase inhibition with a novel G-quadruplex-interactive agent, telomestatin: in vitro and in vivo studies in acute leukemia*. Oncogene. 25: 5719–25.
47. Kim MY, Gleason-Guzman M, Izbicka E, Nishioka D, Hurley LH, 2003. *The different biological effects of telomestatin and TMPyP4 can be attributed to their selectivity for interaction with intramolecular or intermolecular G-quadruplex structures*. Cancer Res. 63(12):3247-56.
48. Zhang Y, Li B, Jin Y, **2011**. *Label-free fluorescent detection of thrombin using G-quadruplex-based DNAzyme as sensing platform*. Analyst. 136(16):3268-73.
49. Wanga J, **2000**. *From DNA biosensors to gene chips.* Nucleic Acids Res. 28(16): 3011–3016.
50. Shakoori Z, Salimian S, Kharrazi S, Adabi M, Saber R, **2015**. *Electrochemical DNA biosensor based on gold nanorods for detecting hepatitis B virus*. Anal Bioanal Chem. 407(2):455-6.

51. Mao X, Phillips JA, Xu H, Tan W, Zeng L, Liu G, **2009**. *Aptamer-Nanoparticle Strip Biosensor for Rapid and Sensitive Detection of Cancer Cells*. Analytical chemistry. 81(24):10013.

52. Zhang D, Yan Y, Li Q, Yu T, Cheng W, Wang L, Ju H, Ding S, **2012**. *Label-free and high-sensitive detection of Salmonella using a surface plasmon resonance DNA-based biosensor.* J. Biotechnol. 160(3-4):123-8.

53. Oliviero G, Amato J, Borbone N, D'Errico S, Galeone A, Mayol L, Haider S, Olubiyi O, Hoorelbeke B, Balzarini J, Piccialli G, **2010**. *Tetra-end-linked oligonucleotides forming DNA G-quadruplexes: a new class of aptamers showing anti-HIV activity.* Chem. Commun. 46: 8971-73.

54. D'Atri V, Oliviero G, Amato J, Borbone N, D'Errico S, Mayol L, Piccialli V, Haider S, Hoorelbeke B, Balzarini J, Piccialli G, **2012**. *New anti-HIV aptamers based on tetra-end-linked DNA G-quadruplexes: effect of the base sequence on anti-HIV activity*. Chem Commun. 48(76):9516-8.

55. Borbone N, Amato J, Oliviero G, D'Atri V, Gabelica V, De Pauw E, Piccialli G, Mayol L, **2011**. *d(CGGTGGT) forms an octameric parallel G-quadruplex via stacking of unusual G(:C):G(:C):G(:C):G(:C) octads.* Nucleic Acids Res. 39(17):7848-57.

56. D'Atri V, Borbone N, Amato J, Gabelica V, D'Errico S, Piccialli G, Mayol L, Oliviero G, **2014**. *DNA-based nanostructures: The effect of the base sequence on octamer formation from d(XGGYGGT) tetramolecular G-quadruplexes*. Biochimie. 99:119-28.

57. De Stefano L, Oliviero G, Amato J, Borbone N, Piccialli G, Mayol L, Rendina I, Terracciano M, Rea I, **2013**. *Aminosilane functionalizations of mesoporous oxidized silicon for oligonucleotide synthesis and detection.* J. R. Soc. Interface. 10(83):20130160.

58. Amato F, Tomaiuolo R, Borbone N, Elce A, Amato J, D'Errico S, De Rosa G, Mayol L, Piccialli G, Oliviero G, Castaldo G, **2014**. *Design, synthesis and biochemical investigation, by in vitro luciferase reporter system, of peptide nucleic acids as new inhibitors of miR-509-3p involved in the regulation of cystic fibrosis disease-gene expression.* Med. Chem. Commun. 5: 68-71.

CHAPTER 2

Oligonucleotides as aptamers: the implementation of novel anti-HIV aptamers based on tetra-end-linked DNA

2.1 Introduction

Since the last century the global epidemic diffusion of HIV infection required the urgent development of antiviral therapeutics. The story of anti-HIV aptamers is studded with examples of DNA or RNA species tested for their activity against the virus and the exceptionally high number of reports in this field confirms the considerable promise of this strategy. [1-7]
The event that triggers the entry of HIV-1 into the host cell, the T-lymphocytes, is represented by the recognition and binding of an envelope glycoprotein on the surface of the virus, gp120, to the CD4 glycoprotein and a chemokine receptor expressed on the surface of the host cells. [8] Since this event initiates cell fusion, it has been universally validate as a relevant target for drug discovery. Nevertheless, some of the most studied anti-HIV aptamers are those inhibiting other targets. The G-Q forming aptamers *93del*, first published by Patel's group, is probably the subject of the most deep research. [9] 93del and the structural analogue T30695 are potent inhibitor of HIV-1 integrase, the viral enzyme responsible of the integration of the retro-transcribed viral genome into the nuclear host genome, and exhibit anti-integrase activity in the nanomolar range. However, due to their mechanism of action, this kind of aptamers require an efficient delivery system into the infected cells. For this reason, one of the most challenging approach is to achieve the inhibition of the entry of the virus into the host cell, in order to avoid the realization of suitable ON delivery system.
In 1998 Hotoda and co-workers first reported that conjugation with aromatic groups at the 5'-end of the G-Q forming hexadeoxyribonucleotides $^{5'}$TGGGAG$^{3'}$ dramatically provided them with anti-HIV activity. [10, 11] These molecules were shown to be able to bind the third variable region of gp120, the *V3 loop*, thus preventing the entry of the virus into the target cells. Since that, an incredible number of modifications were reported to enhance the antiviral activity of the Hotoda aptamer. Indeed, the most interesting feature of this sequence is represented by its intrinsic mechanism of action that, unlike other reported aptamers, do not require an efficient ON delivery system into the cells. In 2010 Oliviero *et al.* proposed some tetra-end-linked oligonucleotides (TEL-ODNs) containing the sequence TGGGAG, as new modified aptamers with noteworthy anti-HIV activity. [12] In fact, the comparison between the proposed analogue, modified at both the 5' and 3' termini with the tertz-butyldiphenyl groups and the tetra-end-linker moieties respectively, and the same sequence lacking of the TEL moiety showed the better thermodynamic parameters and the enhanced biological activity of the proposed aptamer. In 2012 the same research group designed a mini-library of analogues, having TGGGXG (where X = G, C or T) sequences, bearing the same modifications of the previously reported analogue, in order to probe the influence of the different nucleotides on the structural and biological properties of such quadruplexes. [13] The structural and biological investigations on these sequences identified TEL-[^{TBDPS}TGGGGG]$_4$, **4**, as the best candidate for further SAR studies.

In this frame, we decided to go beyond these promising results by designing new shorter analogues of **4** with the final aim of optimizing their pharmacodynamics and pharmacokinetics and the scale-up of the process. In the novel sequences the TGGGG strands were shortened by one, two and three G-quartet arrays (Fig. 1). The sequences were synthesised and tested for their antiviral activity. At the same time, a novel and cost-effective binding assay was set up to avoid the manipulation of the whole viral glycoprotein.

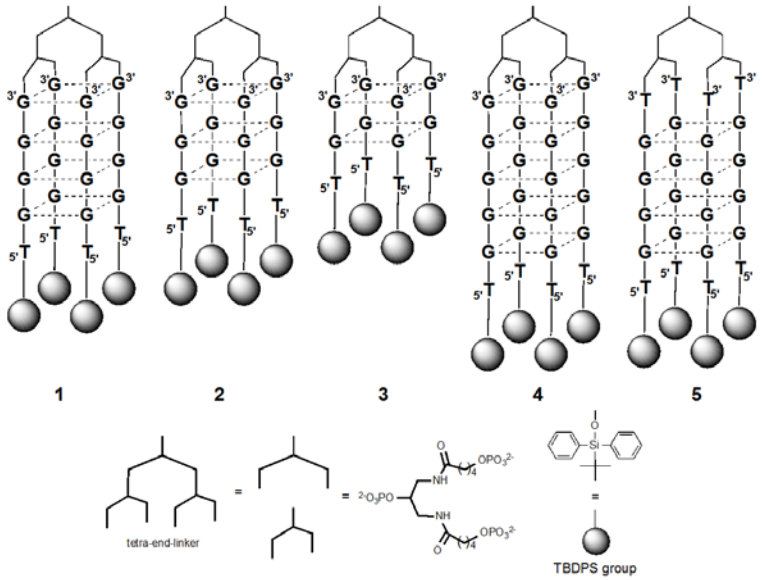

Figure 1. Schematic representation of the investigated TEL-ODNs

Contextually, our attention was attracted by the development of new putative aptamers endowed with a similar TEL-based structure, but able to form high ordered species, in order to investigate the promising structural features of our high ordered G-Q complexes in the context of the design of novel aptamers. Specifically, in previously reported works, our research group showed that particular ON sequences, by virtue of their 5' sticky ends, are able to form stable G-Q dimers, also called *octamers*. [14, 15] The biophysical characterization of these assemblies highlighted that the octamers were formed by two adjacent G-Q building blocks held together by 5' *π-π* stacking interactions. In this frame, we decided to design new putative aptamers, characterized by a dC residue at the 5'-termini, required for the interactions between two adjacent G-Q building blocks, and study their propensity to form high ordered assemblies. Moreover, the importance of the terminal residues at the 5'-ends was analyzed by designing two analogues with the final dC residues capped with an hydrophilic and an hydrophobic group respectively. The resolution of the chemical issues associated to the development of these molecules and their biophysical characterization, in association with their biological activity studies, were an important part of my final research activity.

2.2 Results and discussion

In 1998 the X-ray crystal structure HIV-1 gp120 core complexed with a two-domain fragment of human CD4 and an antigen-binding fragment of a neutralizing antibody was reported, showing the importance of the V3 loop for the binding with the co-receptor on the surface of the host cell. [16] These findings, in addition to the

proposed mechanism of action for Hotoda sequence and their analogues, led us to perform preliminary *in silico* docking simulations in order to assess the capability of the new analogues to fold in the correct secondary structure, retaining at the same time the affinity for the target.
The results showed that **1**-**3**, despite the smaller size, can indeed bind the V3 loop by direct interaction of the phosphate backbone atoms and the hetero-atoms of guanines (Fig. 2). In particular, the phosphate backbone atoms of three different strands interact with the side chains of Glu197, Thr195, Thr194 and Tyr193 of the V3 loop in all the complexes, defining a common binding site.

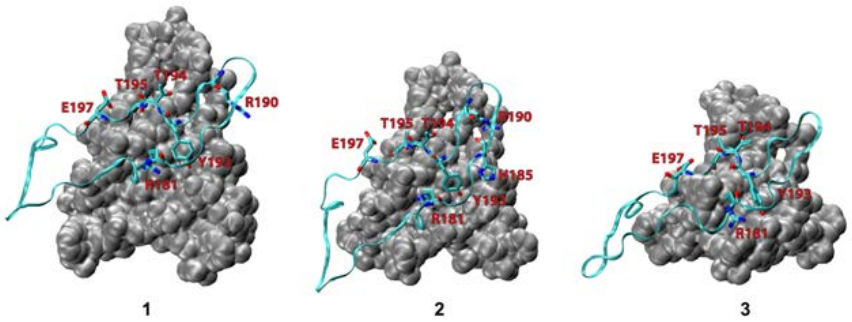

Figure 2. Molecular models showing the interactions between aptamers **1**-**3** and the V3 loop of gp120

These encouraging results led us to proceed with the synthesis and biophysical characterization of **1**-**3**.TEL-ODNs have been prepared according to the previously reported protocol: DNA solid phase synthesis was performed on an automated synthesizer following the phosphoramidite chemistry. Once synthesised, CD measurements have been performed in order to verify that the absence of an increasing number of G-quartets, compared to the reference sequence, did not affect the original parallel arrangement (Fig. 3).

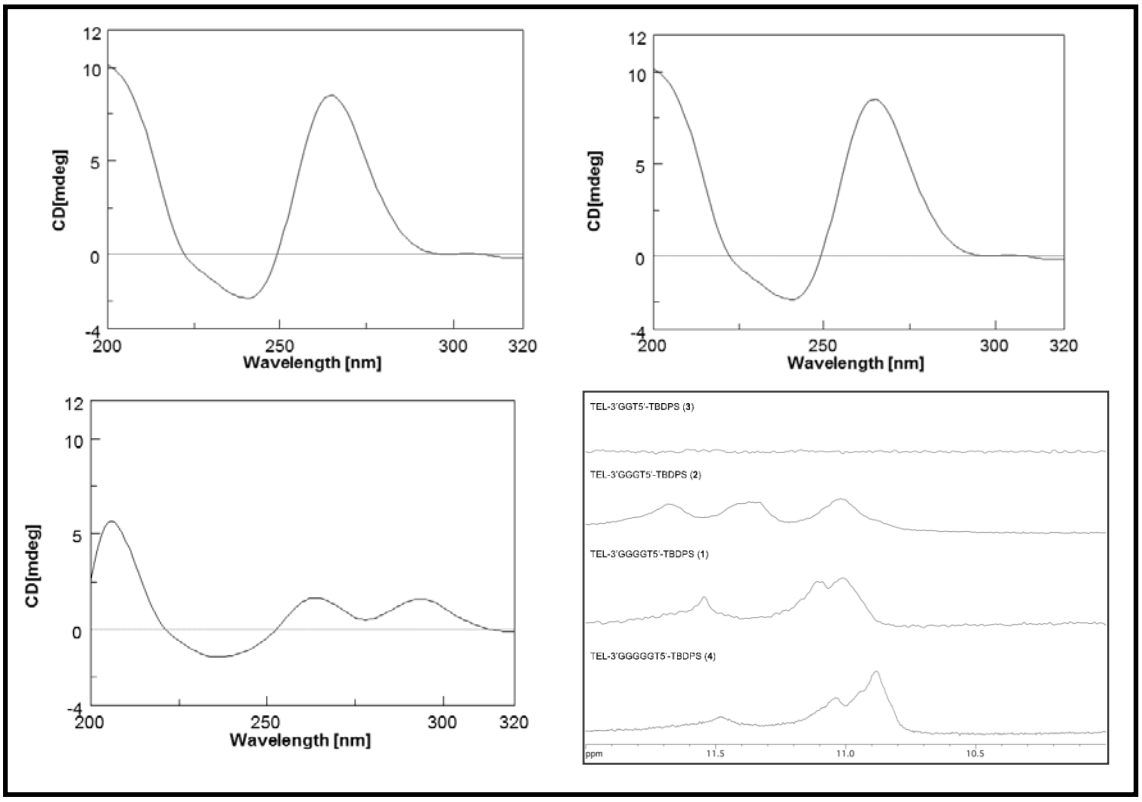

Figure 3. Dichroic profiles of **1**-**3** in 100 mM K^+ buffer at 25°C and, in the box, G-tetrad-specific imino proton region (10-12 ppm) of ^{1}H NMR spectra of TEL-ODNs **1**-**4** acquired at 25 °C in 100 mM K+ buffer (D2O/H2O 9:1).

The overall CD spectra were recorded in 100 mM K^+ buffer. As we can see from figure 3, the profiles of **1** and **2** are in agreement with the formation of quadruplex assembly, showing a positive maximum at about 260 nm and a negative minimum close to 240 nm, which are characteristics of parallel G-quadruplexes. [17, 18] On the other hand, CD spectrum of **3** does not appear to be superimposable to that of a typical G-quadruplex structure. This result can be ascribed to the difficult arrangement of the sequence, probably due to the absence of a favourable number of G-quartets.
The formation of the desired G-Q structures was also proved by means of ^{1}H-NMR experiments. NMR analysis confirmed for **1**-**3** the presence of G-Qs in solution as well, whereas, as expected, **3** did not show the ability to form quadruplex assemblies.
Once performed the structural characterization, we exploit a fluorescence quenching assay to assess the capability of the analogues to bind their natural target, the V3 loop. In drug discovery, the occurrence of false positives is one of the major obstacle in the search for lead compounds that can be developed into drugs. This new method, based on the use of a EnVision plate reader, has recently been reported as a high-speed, low cost and quantitative assay to measure affinity constants and kinetic parameters of binding events. One of its major advantage is that nonspecifically binding compounds did not quench the fluorescence of the target. [19] In fact, this methodology is based on the quenching of the fluorescence following the interaction between a fluorescently labelled target and its specific ligand, or viceversa. For this purpose, we previously synthesize the 35 aminoacids V35 peptide, whose sequence matches the V3 loop used for the previous docking simulations, bearing a Fluorescein Isothiocyanate (FITC) residue at the N-terminus,

as the target of the tested aptamers. In this way, we avoided the manipulation of the entire, more expensive viral glycoprotein. In particular, V35-Fluo and V-35 were manually synthesized according to Fmoc protocols and purified by RP-μHPLC (see fig. 4 for the sequence of V35-Fluo peptide).

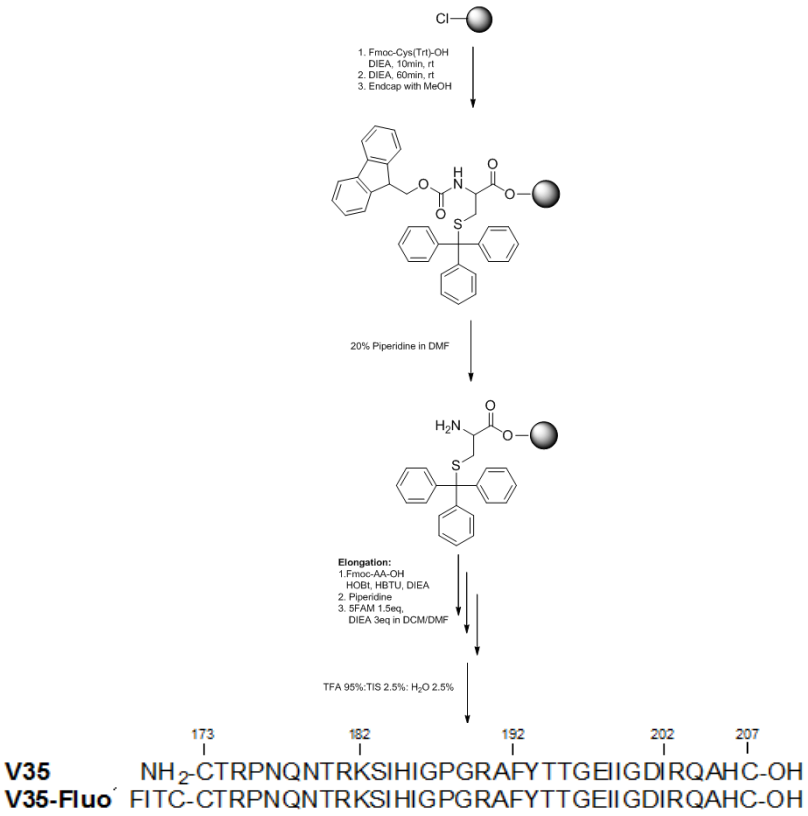

Figure 4. Synthetic scheme of the manual synthesis of V35 and V35-Fluo.

Binding experiments were initially performed on **4**, whose binding affinity was already estimated by SPR, by incubating 50 nM of V35-Fluo with 10 μM of **4**. In the presence of **4** the fluorescence signal of V35-Fluo decreased compared to the fluorescence of the same amount of peptide dissolved in buffer. Then, to monitor changes in fluorescence unrelated to the binding of V35-Fluo to the aptamer, the measurements were carried out by incubating V35-Fluo and **4** in the presence of the unlabeled V35 peptide at the concentration of 25μM (Fig. 14, panel a). In the presence of V35 the fluorescence signal of V35-Fluo was not affected by the presence of the aptamer, thus indicating that the decrease of V35-Fluo fluorescence was due to the aptamer binding. The binding of **4** for V35-Fluo was also measured for several dilutions of **4**, in order to calculate the K_d value (Fig. 5 panel b) and in a time course experiment. The addition of **4**, at t=0, provoke the quenching of the fluorescence of V35-Fluo, then V35 was added to displace **4** specifically bound to V35-Fluo. As already seen, after the addiction of V35, a restoration of the fluorescence of V35-Fluo is observed.

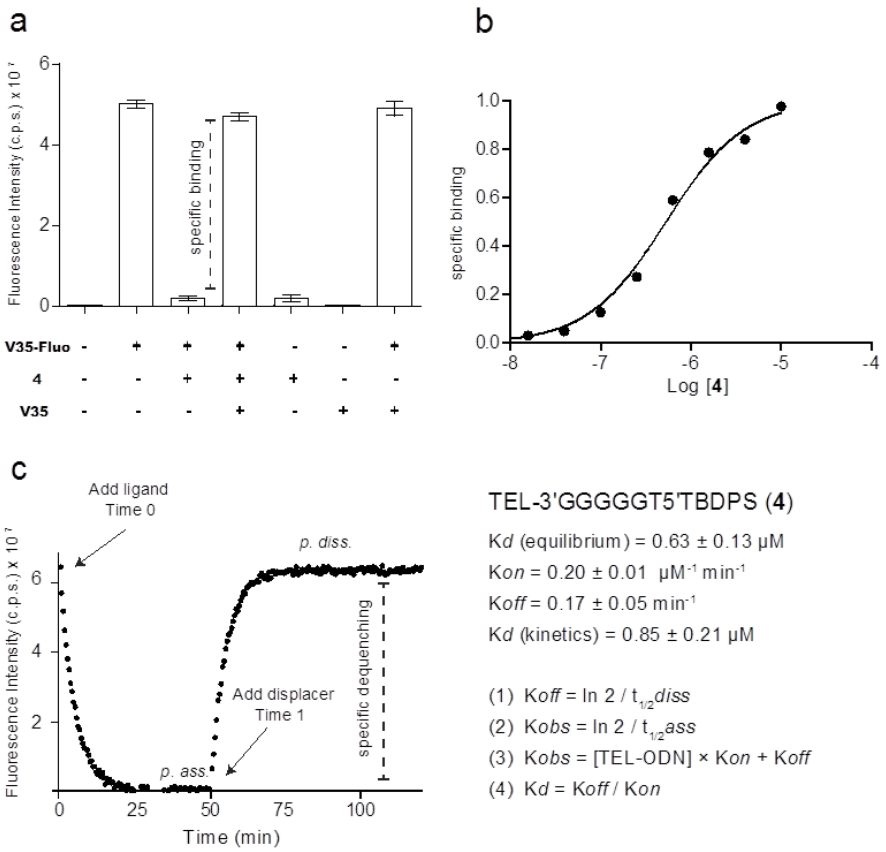

Figure 5. Binding experiments of V35-Fluo and **4**

The positive outcomes of the pilot experiment gave us confidence to perform the same experiments on **1**-**3**. The fluorescence assays were carried out on **1**-**3** and **5**, a TEL-ON analogue lacking of anti-HIV activity, and allowed us to quantify the K_d for all the putative aptamers. However, despite the good results on these last compounds, the K_d measured for **4** resulted somehow higher than that obtained by the SPR experiments. The possible reason of this behaviour could be ascribed to the actual interaction of the aptamer with the target, that in the whole protein acquire a well-defined three dimensional structure. In fact, the crystal structure of the V3 loop shows that it acquires an hairpin conformation stabilized by a disulfide bridge. On the basis of this observation, we decided to repeat the same experiments using a folded version of the peptide, obtained by an appropriate oxidation treatment. The affinity was measured for **1**-**5**; while the value obtained for 5 remains low, the last measures for **1**-**3**return values significantly higher than the previous ones, and in particular close to that obtained for the parent aptamer**4** by SPR (Fig. 6).

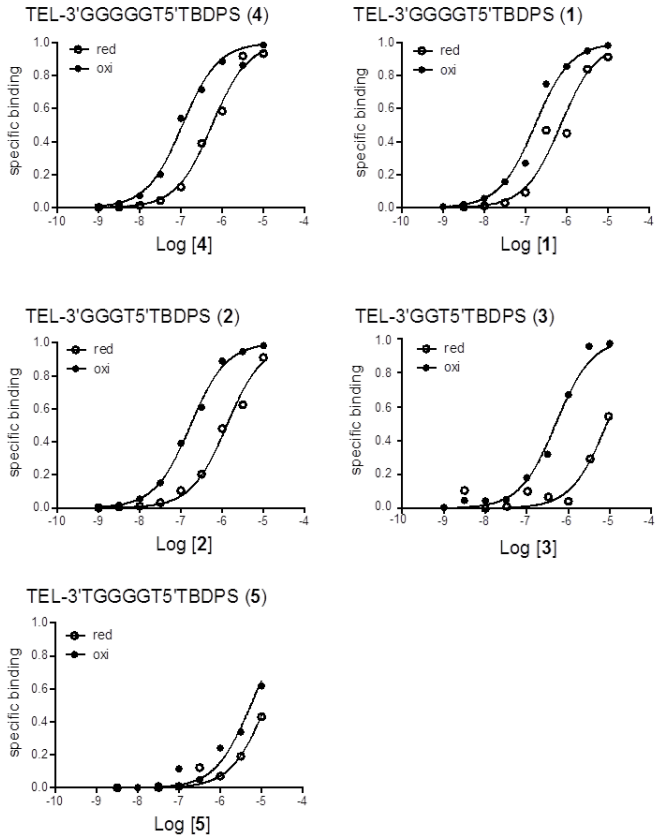

Figure 6. Affinity of TEL-ODNs 1-5 for reduced V35-Fluo (red, empty circles) and oxidized V35-Fluo-oxi (oxi, full circles).

As regards the anti-HIV activity, the biological assays have been undertaken in collaboration with Dr. Jan Balzarini at Rega Institute for Medical Research of Leuven, Belgium. The antiviral activity against HIV-1 and HIV-2 was measured as the concentration of aptamer able to reduce the virus-induced cytopathicity by 50% (EC50) in human CD4+ T-lymphocyte CEM cell cultures. As we can see from table 3, the new analogues **1** and **2** retain high antiviral activity, in the submicromolar range. Interestingly, consistently with docking findings, also **3** shows significant antiviral activity, even if it does not fold into a stable G-Q structure.

Table 1. Anti-HIV studies on TEL-ODNs **1-5**

	EC_{50}[a] (μM)		IC_{50}[b] (μM)	CC_{50}[c] (μM)
	HIV-1	HIV-2	HUT-78/HIV-1+SupT1	
1	0.18 ± 0.0071	6.3 ± 0.71	3.9 ± 0.21	>100
2	0.16 ± 0.028	1.3 ± 0.21	1.8 ± 1.3	>100
3	0.74 ± 0.11	5.1 ± 0.92	10 ± 0.7	>100
4	0.041± 0.007*	≥ 2*		>2*
5	≥ 2*	2*		>2*

In the second part of the project, we focused our attention on the synthesis and structural characterization of new high ordered G-Q aptamers. In 2013 D'Atri *et al*. demonstrated that the ON sequence CGGXGGT, where X is A,T,C or G, is able to form dimers of tetramolecular G-Qs through the 5'-5' stacking of two G-Q subunits in presence of suitable concentrations of potassium cations. The resulting octamers show high thermal stability and reproducible folding assembly, that are interesting features in view of developing novel putative aptamers. Taking into account these considerations, we designed TEL-ONs embodying the sequence $^{5'}$CGGAGG$^{3'}$, where the dG residues at the 3'-end are conjugated to the tetra-end-linker moiety, while the dC residues at the 5' termini are required for the dimerization process, as highlighted by Borbone *et al.* [14, 15] Moreover, we decided to synthesize two analogues of the TEL-$[G_2AG_2C]_4$resulting sequence, characterized by the 5' termini capped with two different groups, the lipophilic dimetoxytritil- group and the hydrophilic glucose derivative respectively, in order to assess the influence of these different conjugations on the dimerization process and, eventually, on the biological activity.

The resulting sequences, TEL-$[CG_2AG_2]_4$,**I**, TEL-$[^{DMT}CG_2AG_2]_4$,**II**, TEL-$[^{Glu}CG_2AG_2]_4$, **III**, have been synthesized through the standard phosphoramidite chemistry. Moreover, to obtain **II** we did not perform the final deblocking step, while for the obtaining of **III** we performed the final coupling step with a non-standard, manually synthesized glucose derivative phosphoramidite. The higher apolarity of **II** was exploited to facilitate the successive purification by means of RP-HPLC, whereas **I** and **III** were purified by means of anion exchange. After synthesis and purification, the biophysical characterization has been carried out. In order to verify if the TEL-ONs are able to fold into stable G-Q structures and eventually form high ordered assemblies, preliminary dichroic experiments have been performed (Fig. 16). Notably, the annealing procedure, *i.e.* the folding process, and the CD experiments have been undertaken adopting the same protocols as those used for CGGXGGT sequences to promote the multimerization process. The dichroic experiments highlighted the presence in solution of G-Q structures, showing the typical shape diagnostic for parallel G-Q assemblies. Interestingly, an additional negative peak is detectable at 290 nm and, as already reported, is ascribable to additional stacking interactions involved in high ordered quadruplex species.

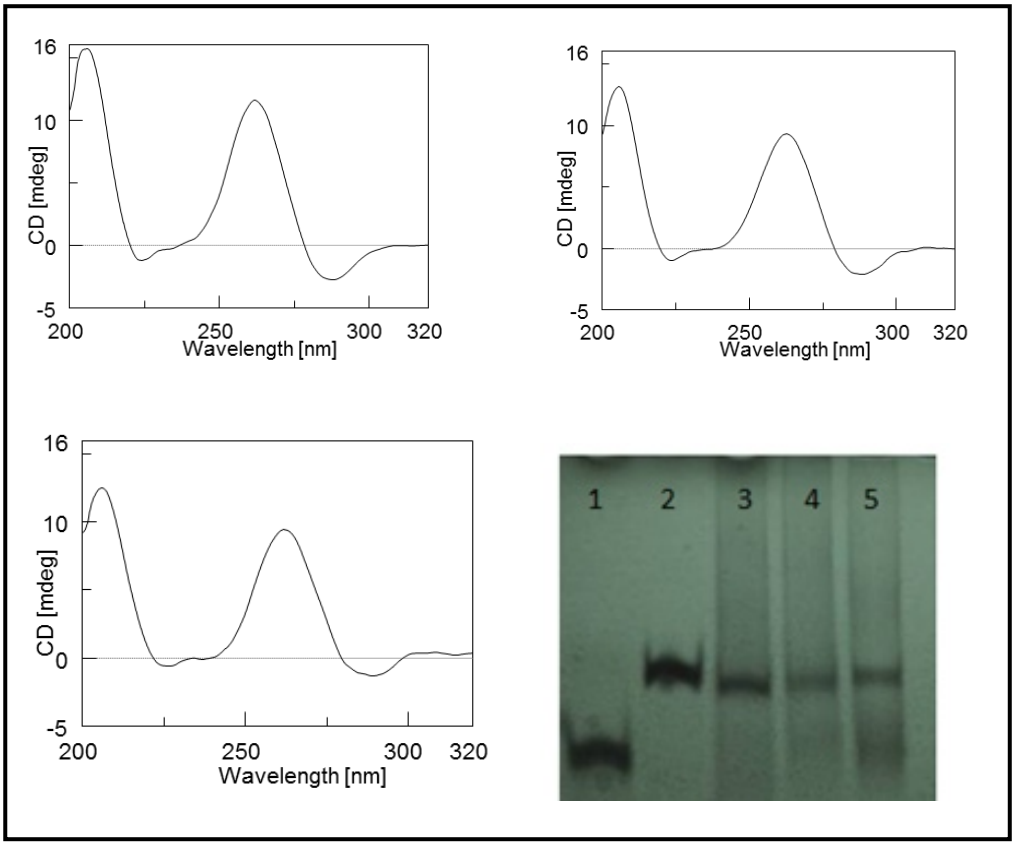

Figure 16. Dichroic profiles of **I-III** in 1 M K^+ buffer and, in the bottom right, non denaturing gel analysis for the sequences TGGGGT (line 1), CGGAGGT (line 2), **I**, (line 3), **II**, (line 4), **III**, (line 5).

To further provide an insight on the molecular size of our species, native polyacrylamide gel electrophoresis has been performed. Figure 16 shows the PAGE of: TGGGGT (line 1) used as tetramolecular quadruplex size marker, CGGAGGT (line 2) used as dimeric quadruplex size marker, TEL-[CG_2AGG_2]4 (**I**, lane 3), TEL-[$^{DMT}CG_2AG_2$]4 (**II**, lane 4), TEL-[$^{Glu}CG_2AG_2$]4 (**III**, lane 5). As expected, CGGAGGT forms stable octamers in solution in our conditions, thus showing a typical slow-migrating band. The comparison between CGGAGGT, used as control, and **I** and **II** demonstrate the formation of high ordered assemblies also for these last sequences; whereas the migration profile of **III**, that shows a major band migrating like an octamer and a faster less defined band, may be diagnostic for the presence in solution of both high order structures and tetrameric quadruplexes.
Finally, to assess whether the formation of stable octamers is somehow connected to antiviral activity, biological assays have been carried out. On the basis of the structural features of these novel sequences, we decided to test them for their activity against HIV. As in the previous case, the antiviral activity is calculated as the concentration of aptamer able to reduce the virus-induced cytopathicity by 50% (EC50) in human CD4+ T-lymphocyte CEM cell cultures. The results show that, even though the overall sequences are able to form octamers and possess very similar sequences, only **II** has significant biological activity.

2.3 Conclusions

The first part of the search allowed us to obtain a new solid and cost-effective method for the rapid measure of the affinities between aptamers, as drug candidates, and their target. By combining *in silico* simulations and a novel and rapid binding assay, we succeeded in developing new aptamers that, despite the smaller dimensions, are still endowed with significant antiviral properties. Importantly, this platform is suited to the feasible optimization of aptamers and other drug candidates.
In the second part of this research work, we developed new TEL-ONs, conveniently modified at their 5'-termini, and studied their capability to undergo multimerization process together with their biological properties. Thanks to the techniques for the biophysical characterization, we observed that suitable modifications at the 5'-sticky ends did not prevent the formation of stable high ordered structures based on G-Q building blocks. Moreover, the findings on the biological activity of these putative TEL-aptamers led us to conclude that the apolarity of the groups attached at the 5'-ends is a fundamental discriminating factor on the mechanism of action. However further studies are required to elucidate the role of the conjugations on this kind of sequences.

2.4 Experimental Section

2.4.1General Instrumentation

Automated solid-phase oligonucleotide synthesis was performed on a 8909 DNA Synthesizer(Applied Biosystems). UV measures for the determination of the ON concentrations were performed on a . CD measurements were performed on a JASCO J-715spectropolarimeter equipped with a Peltier Thermostat JASCO ETC-505T using 0.1cm path length cuvettes. NMR spectra were acquired on Varian UNITYINOVA 500MHz, 700 MHz and Mercury Plus 400 MHz spectrometers and processed using the Varian VNMR software package.

2.4.2 Synthesis of TEL-ONs

The syntheses of TEL-ONs **1**-**3** and **I**-**III** were performed on an automated synthesizer through the standard solid-phase phoshoramidite chemistry. In the case of TEL-ON **II**, we did not perform the final deblocking step, while **III** was obtained using 50 mg/mL of the glucose derivative phosphoramidite, whose synthesis has been reported by Adinolfi *et al*. [20] After the synthesis, deprotection and detachment of the ONs from the solid support were achieved via treatment of the resin in aqueous ammonia at 55°C for 17 h. The combined filtrates and washings were dried, redissolved in water, analysed and purified by HPLC on an anion exchange column (Macherey-Nagel, 1000-8/46, 4.4x50mm, 5 µm) as regards **1**-**3** and **I** and **III**, whereas for **II** we used a reverse-phase column (). In the former case, purification was achieved using a linear gradient from 0 to 100% B in 30 min, flow rate = 1 mL/min and detection at 260 nm (buffer A: 20 mM NaH_2PO_4 aq. solution pH 7.0, containing20% (v/v) CH_3CN; buffer B: 20 mM NaH_2PO_4 aq. solution pH 7.0, containing 1MNaCl and 20% (v/v) CH_3CN); in latter we used a linear gradient from 0% to 100% B in 30 min, flow rate = 1,2 mL/min and detection at 260 nm (buffer A: 0,1 M triethylammonium bicarbonate buffer, eluent B: CH_3CN). After HPLC purification, the oligonucleotide samples were desalted on a biogel column (BIORAD) eluted with H_2O/CH_3CH_2OH (9:1 v/v).

2.4.3 Synthesis and oxidation of V35 and V35-Fluo peptides

The manual syntheses of **V35** and **V35-Fluo** peptides were carried out using the standard Fmoc protocol for the Solid Phase Peptide Synthesis (SPPS) on a 2-Chlorotrytil resin. To obtain **V35-Fluo**, 5-Carboxyfluorescein coupling on the free N-terminal group was performed using 1.5 equivalent of 5-FAM and 3.0 equivalents of DIPEA in DCM:DMF 1:1 by volume. The peptides were released from the resin with TFA/Et_3SiH/H_2O 90:5:5 for 3 h. The reaction crudes were purified by RP-HPLC on a semi-preparative C18-bonded silica column (Phenomenex, Jupiter 4µ Proteo 90Å, 1.0 x 25 cm) using a gradient of CH_3CN in 0.1% aqueous TFA (from 10 to 90% in 40 min) at a flow rate of 5.0 mL/min. The product was obtained by lyophilization of the appropriate fractions after removal of the CH_3CN by rotary evaporation. The correct three-dimensional structure was adopted by the peptides by means of an oxidation treatment. A final concentration of 2 mM of DL-Dithiothreitol (DTT) was added to a solution containing 60 µM of **V35-Fluo**. The solution was gently stirred for 2 h to obtain the preliminary intermolecular and intramolecular disulphide bridges reduction. The sample was then treated with 4 mM of the oxidizing agent *N,N,N′,N′*-tetramethylazodicarboxamide (DIA) and analyzed by RP-HPLC, in the same conditions as reported above, to compare the retention times before and after the treatment with the reducing and oxidizing reagents (Fig. 17)

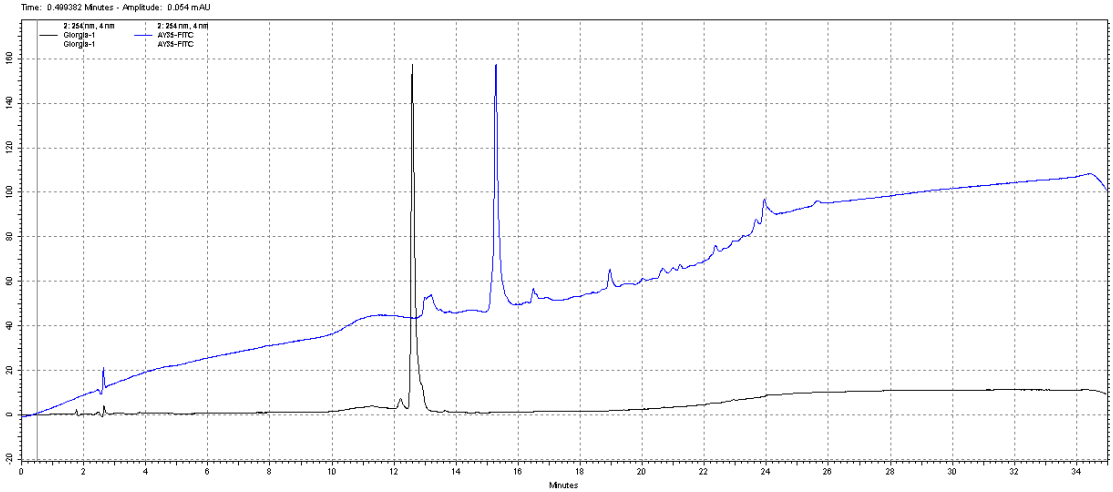

Figure 17. HPLC purification profiles of **V35-Fluo** peptide before (black line) and after (**V35-Fluo-oxi**; blue line) the oxidation process with DTT/DIA.

2.4.4 CD spectroscopy measurements

TEL-ODN samples (1×10^{-5} M) were annealed adopting the standard reported protocol for **1**-**3**, whereas a different procedure was used for **I**-**III.** In this case, the dimerization process was promoted by dissolving the ONs in 1 M Potassium buffer (100 mM KH_2PO_4 and 900 mM KCl) and heating at 90 °C for 5 min followed by 10 min at high temperature and quick cooling at 4 °C. The overall samples were stored at 4°Covernight before measurements. CD spectra were recorded in the 320-200 nmwavelength range, in 0.1 cm path length cuvette, as an average of 3 scans (100 nm/min, 1 s response time, 1 nm band width) and normalized by subtraction of the background scan containing only the buffer. Thermal denaturation experiments were carried out in the temperature range of 5-90 °C by monitoring CD values at 264 nm at a heating rate of0.5 °C/min.

2.4.5 NMR spectroscopy measurements

The NMR samples were prepared in 0.2 ml of buffer (90% H2O/10% D2O), containing 0.1 M K^+ at pH 7.0, and NMR spectra were recorded in the temperature range 25-90 °C on Varian UNITYINOVA 700 MHz spectrometer.

2.4.6 Biological evaluation assays

The methodology of the anti-HIV assays was as follows: ~ 3 x 10_5 human CD_4Tlymphocyte(CEM) cells were infected with 100 $CCID_{50}$ of HIV(III_B) or HIV-2(ROD)/mland seeded in 200 µL wells of a 96-well microtiter plate containing appropriate dilutions of the test compounds. After 4 days of incubation at 37°C, HIV-induced syncytia formation in the CEM cell cultures was examined microscopically. Data represent the mean (± SD) of 3 independent experiments.

2.5 References

1. Negri P, Chen G, Kage A, Nitsche A, Naumann D, Xu B, Dluhy RA, **2012**. *Direct optical detection of viral nucleoprotein binding to an anti-Influenza aptamer.* Anal. Chem. 84: 5501–08.
2. Ruslinda RA, Tanabe K, Ibori S, Wang X, Kawarada H, **2013**. *Effects of diamond-FET-based RNA aptamer sensing for detection of real sample of HIV-1 Tat protein*. Biosens. Bioelectron. 40: 277–282.
3. Tombelli S, Minunni M, Luzi E, Mascicni M, **2005**. *Aptamer-based biosensors for the detection of HIV-1 Tat protein.* Bioelectrochemistry 67: 135–141.
4. Liu J, Yang Y, Hu B, Ma Z, Huang H, Yu Y, Liu S, Lu M, Yang D, **2010**. *Development of HBsAg-binding aptamers that bind HepG2.2.15 cells via HBV surface antigen*. Virol. Sin. 25: 27–35.
5. Chen F, Hu Y, Li D, Chen H, Zhang X, **2009**. *CS-SELEX generates high-affinity ssDNA aptamers as molecular probes for Hepatitis C Virus envelope glycoprotein E2.* PLOS ONE 4: e8142.
6. Toscano-Garibay JD, Benitez-Hess ML, Alvarez-Salas LM, **2011**.*Isolation and characterization of an RNA aptamer for the HPV-16 E7 oncoprotein. Arch. Med. Res*. 42: 88–96.
7. Cho SJ, Woo HM, Kim KS, Oh JW, Jeong YJ, **2011**. *Novel system for detecting SARS coronavirus nucleocapsid protein using an ssDNA aptamer. J. Biosci. Bioeng.*112: 535–540.
8. Cohen S, Tuen M, Hioe CE, **2003**. *Propagation of CD4+ T cells specific for HIV type 1 envelope gp120 from chronically HIV type 1-infected subjects*.AIDS Res Hum. Retroviruses. 19(9):793-806.
9. Phan AT, Kuryavyi V, Ma JB, Faure A, Andréola ML, Patel DJ, **2005**. *An interlocked dimeric parallel-stranded DNA quadruplex: a potent inhibitor of HIV-1 integrase*. Proc Natl Acad Sci U S A. 102(3):634-9.
10. Hotoda H, Koizumi M, Koga R, Kaneko M, Momota K, Ohmine T, Furukawa H, Agatsuma T, Nishigaki T, Sone J, Tsutsumi S, Kosaka T, Abe K, Kimura S, Shimada K, **1998**. *Biologically active oligodeoxyribonucleotides. 5. 5'-End-substituted d(TGGGAG) possesses anti-human immunodeficiency virus type 1 activity by forming a G-quadruplex structure*.J. Med. Chem. 41(19):3655-63.
11. Koizumi M, Koga R, Hotoda H, Ohmine T, Furukawa H, Agatsuma T, Nishigaki T, Abe K, Kosaka T, Tsutsumi S, Sone J, Kaneko M, Kimura S, Shimada K, **1998**. *Biologically active oligodeoxyribonucleotides. Part 11: The least phosphate-modification of quadruplex-forming hexadeoxyribonucleotide TGGGAG, bearing 3-and 5-end-modification, with anti-HIV-1 activity.* Bioorg Med Chem. 6(12):2469-75.
12. Oliviero G, Amato J, Borbone N, D'Errico S, Galeone A, Mayol L, Haider S, Olubiyi O, Hoorelbeke B, Balzarini J, Piccialli G, **2010**. *Tetra-end-linked oligonucleotides forming DNA G-quadruplexes: a new class of aptamers showing anti-HIV activity.* Chem. Commun. 46: 8971-73.
13. D'Atri V, Oliviero G, Amato J, Borbone N, D'Errico S, Mayol L, Piccialli V, Haider S, Hoorelbeke B, Balzarini J, Piccialli G, **2012**. *New anti-HIV aptamers based on tetra-end-linked DNA G-quadruplexes: effect of the base sequence on anti-HIV activity*. Chem Commun. 48(76):9516-8.
14. Borbone N, Amato J, Oliviero G, D'Atri V, Gabelica V, De Pauw E, Piccialli G, Mayol L, **2011**. *d(CGGTGGT) forms an octameric parallel G-quadruplex via*

stacking of unusual G(:C):G(:C):G(:C):G(:C) octads. Nucleic Acids Res. 39(17):7848-57.

15. D'Atri V, Borbone N, Amato J, Gabelica V, D'Errico S, Piccialli G, Mayol L, Oliviero G, **2014**. *DNA-based nanostructures: The effect of the base sequence on octamer formation from d(XGGYGGT) tetramolecular G-quadruplexes*. Biochimie. 99:119-28.

16. Kwong PD, Wyatt R, Robinson J, Sweet RW, Sodroski J, Hendrickson WA, **1998**. *Structure of an HIV gp120 envelope glycoprotein in complex with the CD4 receptor and a neutralizing human antibody.*Nature. 393(6686):648-59.

17. Mergny JL, De Cian A, Ghelab A, Saccà B, Lacroix L, **2005**.*Kinetics of tetramolecular quadruplexes.* Nucleic Acids Res. 33: 81-94.

18. Hardin CC, Perry AG, White K, **2001**. *Thermodynamic and Kinetic Characterization of the Dissociation and Assembly of Quadruplex Nucleic Acids.*Biopolymers (Nucleic Acid Sciences). 56: 147-194.

19. Junker LM, Clardy J,**2007**. *High-Throughput Screens for Small-Molecule Inhibitors of Pseudomonas aeruginosa Biofilm Development.* Antimicrob. Agents Chemother. 51 (10): 3582-90.

20. Adinolfi M, De Napoli L, Di Fabio G, Iadonisi A, Montesarchio D, Piccialli G, **2002**. *Solid phase synthesis of oligonucleotides tethered to oligo-glucose phosphate tail*. Tetrahedron. 58 (33): 6697-04

CHAPTER 3

Conjugation of oligonucleotides onto solid supports: studies on DNA-based biosensors

3.1 Introduction

Biosensors are microelectronic devices normally consisting of two components: a highly specific recognition element and a transducer that converts the molecular recognition event into a quantifiable signal. Depending on the biological elements employed, biosensors have found applications in a variety of fields, such as clinical diagnosis, food analysis, environmental monitoring. However, the choice of the most suitable materials, in the context of the fabrication process, in not trivial, in particular as regards the individuation of sensitive, cheap and simple transducer material. [1] In the last decades, the development of science in this field allowed the recognition of Porous Silicon (PSi) as smart material for the design of different sensors with improved features. [2] For example, the limited surface area of many traditional sensors is one of the main factors inhibiting efficient detection of small molecules. In this sense, PSi offers several advantages for biosensing applications due to their large available surface area for molecular detection and size-selective filtering of contaminant species. However, many other properties make it an attractive transducer material; first of all, its refreactive index is widely tuneable and is changed by each substance that penetrates into its pore, moreover, once oxidized, the porous silicon surface can be further functionalized using common silane chemistry. These attractive properties explain the great number of reports concerning the use of PSi in chemical and biological sensing.[3-6]
In general, a great number of biosensors applications require the functionalization onto their the surface of oligonucleotides. [7] ON biochips rely on the selective recognition phenomenon resulting from the hybridization between the ON probe and the sought-for target and, thanks to the robust interaction between the complementary strands, they have been so far proposed for the detection of the viral genetic material or inherited diseases, and many other applications.
In effect, one of the main hurdle in the fabrication of a biosensor is represented by the bio-conjugation, *i.e.* the immobilization of the biological probe onto the solid surface. [8-10] Historically, the preparation of PSi surface for the bio-conjugation has been achieved through two main processes: (i) direct absorption via hydrophobic interactions, (ii) formation of intermediate layers that allow the attachment of the biomolecules through covalent bonds. [11, 12] In this frame, lots of chemical protocols have been reported in literature to achieve surface functionalization of PSi nano-materials and they include the “activation” of the PSi surfaces by specific chemical groups, such as -SH, -NH_2, -COOH, which can form stable bonds with the biological probe.[13] In this context, it is important to note that, even if far from simple, *in situ* synthesis of biomolecules, ONs in our case, exhibit lots of advantages comparing to *ex situ* absorption. In particular they include: the increasing of DNA probe density, the process automation and the possibility of surface local functionalization. [14]
Recently, De Stefano *et al.* proposed the *in situ* synthesis of a polythimine oligonucleotide strand on PSi matrices, previously passivated with the alkylisilane 3-aminopropyltriethoxysilane (APTES) and 3-aminopropyldimethylethoxysilane

(APDMES), to explore the feasibility of the common ON synthetic protocols for the growth of ON sequences on silicon matrices. [15, 16] The choice of a polythimine strand can be found in the consideration that, giving the dT residue chemical structure, synthesis and deprotection processes do not need the use of chemicals corrosive against PSi (Fig. 1).

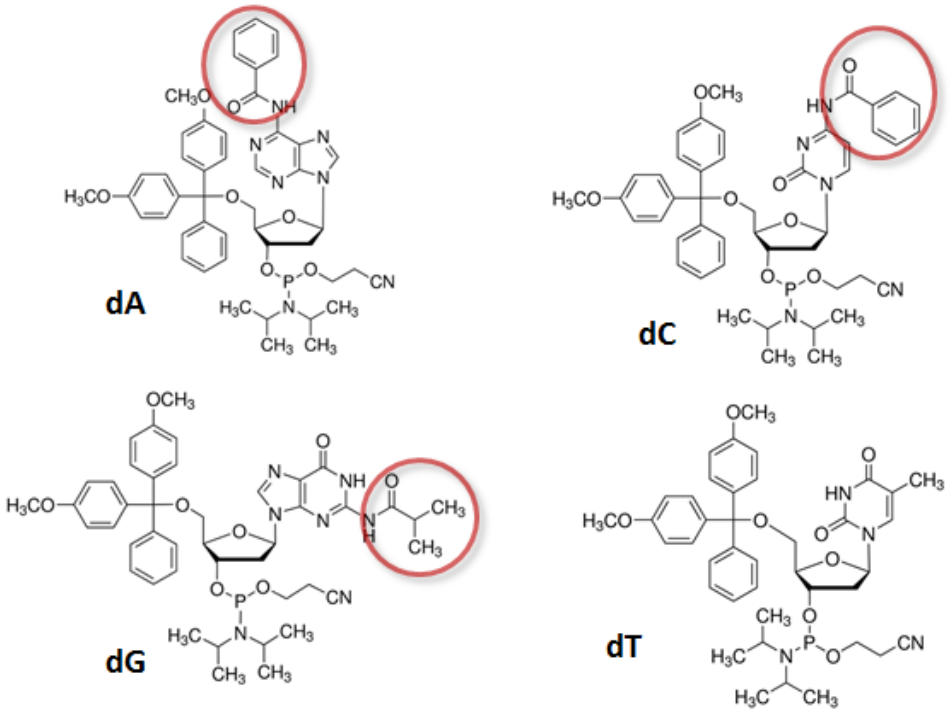

Figure 1. Chemical structures of the common phosphoramidites used for the ON synthesis. Round circles underline the base labile protecting groups on the nucleobases.

In effect, the *in situ* synthesis of mixed ON sequences, *i.e.* composed by the other nucleobases as well, is not trivial due to the chemistry used for the ONs growth, quite aggressive against PSi solid support: PSi suffers from the exposure to alkaline solutions, normally required for the deprotection of the nucleobases. In the first instance, we eluded this problem by the direct synthesis of the above-mentioned polythimine strand on PSi matrix. Furthermore, this preliminary study gave us the possibility to optimize the protocols for the passivation of the support with alkylsilanes and for the ON growth.
However, the common DNA biochip applications need mixed ON sequences for the selective detection of the target. For this reason we focused our efforts on the exploitation of various chemical protocols for the ON deprotection, to allow the direct synthesis on PSi matrices of mixed ON sequences by standard reagents and protocols, with noteworthy economic advantages, and to preserve the stability of PSi during all the phases of growth and sensing.

3.2 Results and Discussion

The principal issue to be solved in facing direct ON synthesis on PSi matrices consists in the structure sensitivity of PSi towards basic solutions. [17] Taking into

account that aqueous ammonia disrupts the silicon skeleton but it is required for the deprotection of the common nucleobases, we firstly addressed our searches to the individuation of reported protocols for the *in situ* DNA synthesis which could be PSi-friendly. It is well known that exposure to K_2CO_3/MeOH dry is a suitable deprotection strategy for ON sequences covalently bonded to PSi support. However this kind of approach requires expensive ultra-mild phosphoramidites. For this reason, in the attempt to find a cheaper protocol, compatible with the common phosphoramidites and reagents, we tested a saturated methanolic dry ammonia solution (NH_3/MeOH) for its ability to preserve PSi skeleton and at the same time deprotect DNA nucleobases.

First of all, we performed preliminary studies on controlled pore glasses resins (CPG resins), namely the traditional supports used for the standard ONs solid phases synthesis. The resins, dG/dC/dA-CPG were treated with dry ammonia and Thin Layer Chromatography (TLC) was performed to check the progress of the detachment 5 and 24 hours later. The TLCs demonstrate that dry ammonia allows the complete deprotection of the monomers, succeeding even in the faster removal of the protecting groups with respect to the standard aqueous ammonia.

Once obtained this positive outcome, we explored the exposure of PSi devices to dry ammonia to verify if this alternative strategy could preserve the chemical stability of the silicon layer. To this aim, two kinds of devices were exploited: APTMES-functionalized PSi device and APDMES-functionalized PSi device (PSi-M_a-NH_2 and PSi-M_b-NH_2 respectively). The comparison between the devices after exposure to the standard aqueous ammonia solution and after treatment with our deprotecting solution highlighted the feasibility of the proposed conditions. In fact, as showed in figure 2, no blue shift is detectable after exposure to dry ammonia for both the explored devices, thus indicating that corrosion did not occur.

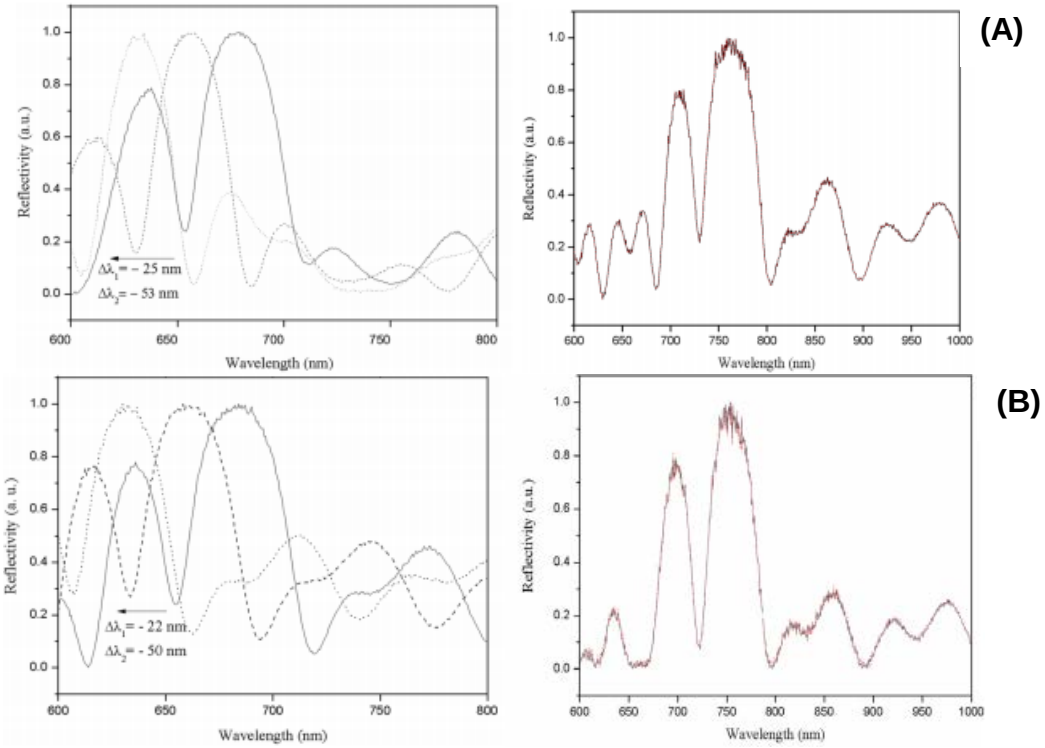

Figure 2. (**A**) Left: Reflectivity spectra of APTES-modified PSi microcavity before (solid line) and after 30 (dashed line) and 60 (dotted line) min of incubation in 33% NH3 at 55°C. Right: Reflectivity spectra of APTES-modified PSi microcavity before (solid line) and after (red dashed line) exposure to NH_3/MeOH dry solution at RT. (**B**) Left: Reflectivity spectra of APDMES-modified PSi microcavity before (solid line) and after 30 (dashed line) and 60 (dotted line) min of incubation in 33% NH3 at 55°C. Right: Reflectivity spectra of APDMES-modified PSi microcavity before (solid line) and after (red dashed line) exposure to NH_3/MeOH dry solution at RT.

These results gave us confidence to perform direct synthesis on PSi supports of a mixed ON sequence.
Therefor, we choose the 19-mer sequence $^{5'}$GATTGATGTGGTTGATTTT$^{3'}$and performed its synthesis on both the functionalised devices, APTES- and APDMES-modified PSi supports, with standard protocols, by intoducing them in a suitable column reactor to be used in the automated synthesizer. [18]In particuar, considering the chemical-physical nature of the supports, the common protocol adopted for ON growth on the commercially available resins was modified in order to enhance the coupling yield, by increasing the coupling times. The protocol requires iterative cycles of:

- *Deblocking*: removal of the 5′-dimethoxytrityl (DMT) protecting group from the support-bound 5′-terminal nucleotide with the deblocking solution of trichloroacetic acid in dichloromethane
- *Coupling*: reaction of the protected phosphoramidite dissolved in dry acetonitrile and activated via protonation by weakly acidic tetrazole (0.45 M in acetonitrile with the 5'-OH ON terminal group
- *Oxidazion*: oxidation of the unstable phosphite triester linkage to the more stable phosphotriester by a standard oxidizing solution of iodine in pyridine/acetonitrile
- *Capping*: acylation of the unreacted 5′-OH ON terminal groups by acetic anhydride in pyridine and tetrahydrofuran to minimize deletion products and simplify the purification process

The amount of dimetoxytrytil- group (DMT) released during the growth steps was used to obtain a measure of the functionalization yield. In particular, the DMT concentration, calculated through UV spectroscopy, led us to conclude that for both the devices after the fifth coupling cycle, at about tha halfway of the growth, the functionalization yield dropped (Fig. 3). Contextually, we performed optical reflectivity experiemts to check the stability of the supports,toward the standard reagents, after the syntheses. Figure 3 also shows the reflectivity spectra for APTES- and APDMES-modified devices, which, by showingred shifts of 60 and 70 nm respectively, indicate that ON had growth on both the supports.

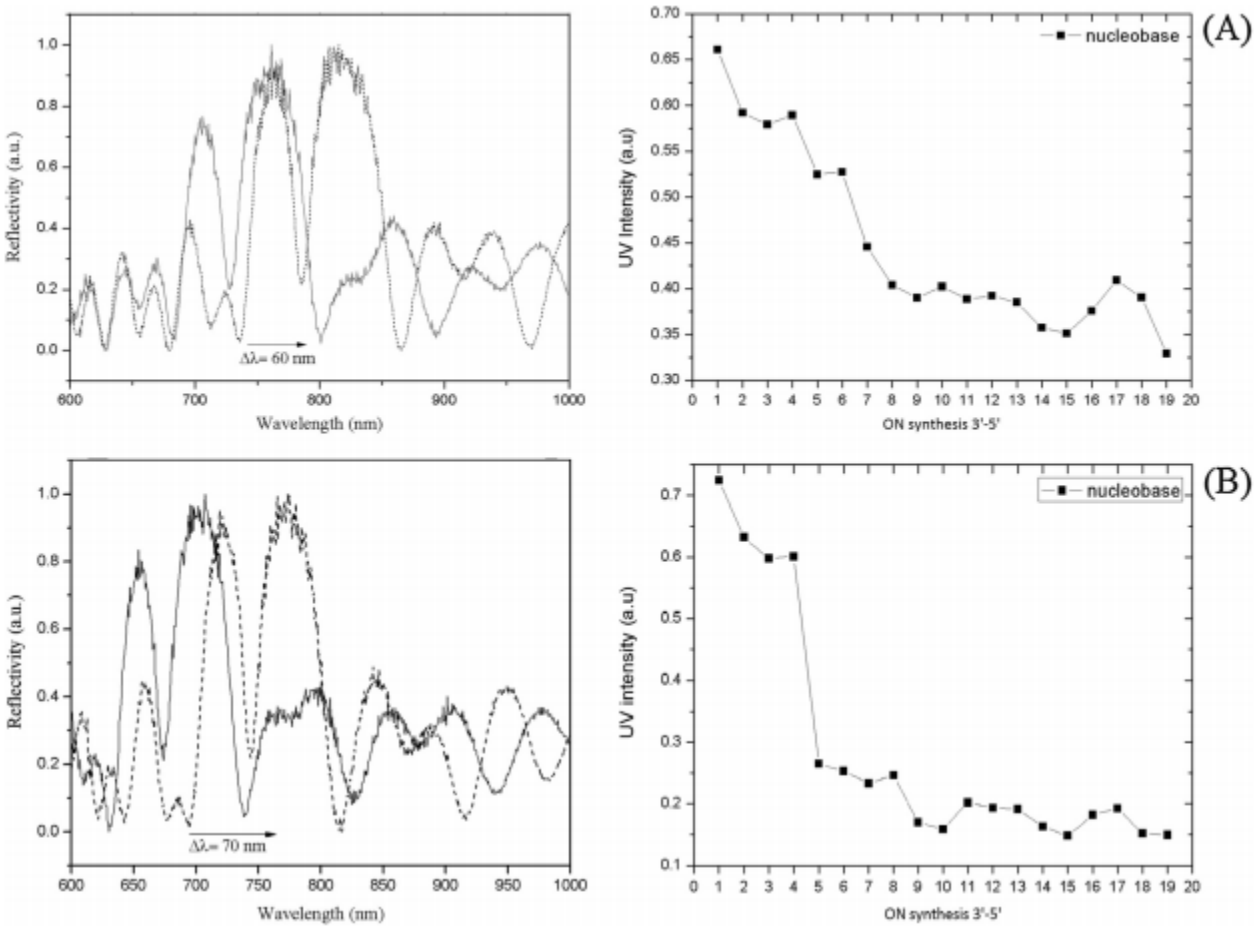

Figure 3. Reflectivity spectra of APTES- and APDMES-modified PSi microcavities before and after ON synthesis. (A) Left: reflectivity spectra of APTES-modified PSi microcavity before (solid line) and after (dashed line) ON synthesis. Right: corresponding UV intensity vs ON synthesis. (B) Left: reflectivity spectra of APDMES-modified PSi microcavity before (solid line) and after (dashed line) ON synthesis. Right: corresponding UV intensity vs ON synthesis.

Once verified the feasibility of the synthetic protocols and the integrity of the supports, the deprotection of the ONs from the base labile phosphates and nucleobases protecting groups, was performed by the previously validated exposure of the devices to the dry ammonia solution over night at room temperature. Once again, the characterization of the supports was performed via optical reflectivity.

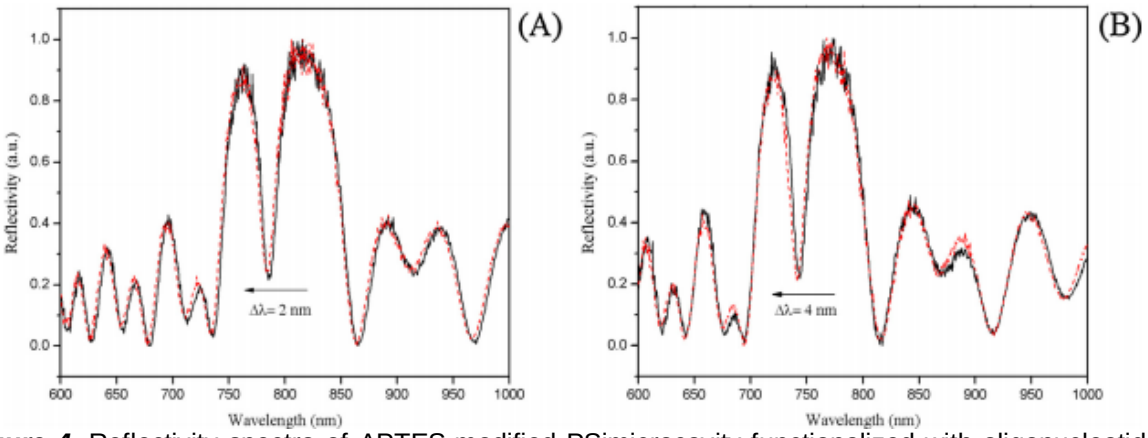

Figure 4. Reflectivity spectra of APTES-modified PSimicrocavity functionalized with oligonucleotides before (solid line) and after (red dashed line) the deprotection process with gaseous ammonia solution. (B) Reflectivity spectra of APDMES-modified PSimicrocavity functionalized with oligonucleotides before (solid line) and after (red dashed line) the deprotection process with gaseous ammonia solution.

The blue shifts of only 2 and 4 nm, ascribable to the removal of the protecting groups from the nucleobases, clearly indicate the chemical stability of the ON-functionalized PSi devices to our proposed deprotection strategy.
Finally, a further confirm of the medium yield of the entire process came from the HPLC purification of the ON strands ultimately detached from the supports. The purification profile shows multiple less defined peaks, confirming the presence on the PSi supports of different length ON sequences (Fig. 5).

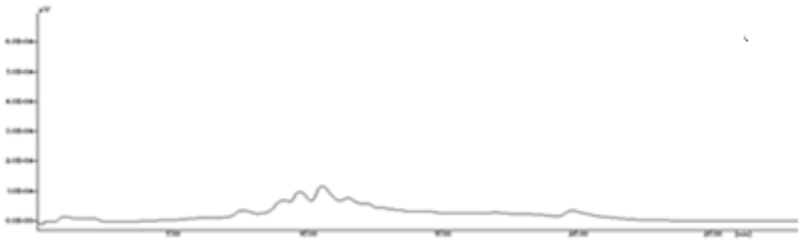

Figure 5. HPLC assay performed on PSi-APDMES-ON device after the removal of the ON sequences

3.3 Conclusions

In this study, we firstly demonstrated the ability of dry NH_3 as alternative and effective deprotecting strategy to preserve the integrity of silicon supports. To perform direct ON synthesis on PSi supports, we used standard protocols and reagents, with noteworthy time and cost saving. The strategy here presented can, in the next future, allow the easy and rapid synthesis of mixed sequences of ONs, in view of the design of optical DNA biosensors. The medium-yield synthetic process observed could be principally due to the average pore size and, for this reason, projecting photonic devices with pore dimensions greater than that value could significantly increase the yield synthesis.

3.4 Experimental Section

3.4.1 ON in situ synthesis

Solid-phase ON syntheses were performed on a PerSeptive Biosystem Expedite 8909 DNA automated synthesizer. The 19-mer mixed-sequence oligonucleotide 5′-GATTGATGTGGTTGATTTT-3′ was assembled on two different aminosilane-modified microcavities, following phosphoramidite chemistry by 19 growing cycles. PSi structures PSi-Mg,h-NH2 (Mg = APTES, Mh = APDMES) were introduced in a suitable column reactor to be used in the automated synthesizer; the syntheses were performed according to the scheme reported in Figure 6, through the standard protocols that involves iterative cycles of: *deblocking, coupling, oxidation, capping*.

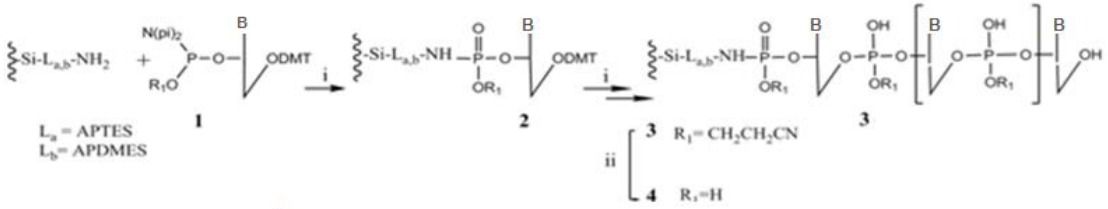

Figure 6. Synthetic procedure for solid-phase synthesis of aminosilane-modified mesoporous silicon

3.4.2 Deprotection strategies

The devices PSi-Ma,b-NH2 (Ma = APTES, Mb = APDMES) were left in contact with 33% aqueous ammonia at 55°C for different times to investigate the effect of standard ON deprotection condition (55°C for 17 h) on the PSi matrix. Contextually, the exposure to dry ammonia solution (NH3/MeOH dry) was also explored as an alternative deprotection strategy. To this aim, the aminosilane-modified samples PSi-Me,fNH2 (Me = APTES, Mf = APDMES) were exposed to dry ammonia overnight at RT. The dry ammonia was generated by dissolving NaOH pellets in a sidearm flask containing aqueous ammonia; the generated gas was passed through a KOH drying tube and bubbled into a flask equipped with a rubber septum and containing anhydrous MeOH at 0°C.

3.4.3 Spectroscopic reflectometry measurements

Reflectivity spectra of PSi optical structures were obtained by a simple experimental setup: a white light was sent on PSi samples through a Y optical fibre (Avantes, Apeldoorn, The Netherlands). The same fibre was used to guide the output signal to an optical spectrum analyser (Ando AQ6315A, Tokyo, Japan). The spectra were acquired at normal incidence over the range 600 to 1,200 nm with a resolution of 5 nm. The reflectivity spectra shown in the graphs are the average of three measurements for each sample.

3.4.4 High-performance liquid chromatography studies

The purification and control of the synthesized ONs was carried out using a Jasco PU2089 PLUS HPLC system (Easton, MD, USA) equipped with an anion exchange column (1000-8/46, 4.4 × 50 mm, 5 µm, Macherey-Nagel, Düren, Germany) using a linear gradient from 0% to 100% B in 30 min, flow rate = 1 mL/min and detection at 260 nm (buffer A: 20 mM NaH2PO4 aq. solution, pH 7.0, containing 20% (v/v) CH3CN; buffer B: 20 mM NaH_2PO_4 aq. solution, pH 7.0, containing 1 M NaCl and 20% (v/v) CH_3CN).

3.4 References

1. Grieshaber D, MacKenzie R, Voros J, Reimhult E, **2008**. *Electrochemical Biosensors - Sensor Principles and Architecture.* Sensors. 1400-58.
2. Jane A,Dronov R, Hodges A, Voelcker NH, **2009**. *Porous silicon biosensors on the advance.* Trends Biotechnol. 27(4):230-9.
3. Ouyang H, Fauchet PM, **2005**. *Biosensing using porous silicon photonic bandgap structures*. Proc. of SPIE. 6005, 60058-1 .
4. Pacholski C, Sartor M, Sailor MJ, Cunin F, Miskelly GM, **2005**. *Biosensing using porous silicon doublelayer interferomenters: reflectice interferometric Fourier transform spectroscopy*. J, Am. Chem. Soc. 127(33): 11636-45.
5. Cunin F, Schmedake TA, Link JR, Li YY, Koh J, Bhatia SN, Sailor MJ, **2002**. *Biomolecular screening with encoded porous silicon photonic crystals.* Nat. Mater. 1: 39-41.
6. Ouyang H, Christophersen M, Viard R, Miller BL, Fauchet PM, **2005**. *Macroporous Silicon Microcavities for Macromolecule Detection*. Advanced Functional Materials 15(11): 1851-59.
7. Marques M, Mansur AAP, Mansur H, **2013**. *Chemical functionalization of surfaces for building three-dimensional engineered biosensors.* Applied Surface Science. 275: 347-60.
8. Kasemo B, **2002**.*Biological surface science.* Surf. Sci. 500: 656–677.
9. Rusciano G, De Luca AC, Pesce G, Sasso A, Oliviero G, Amato J, Borbone N, D'Errico S, Piccialli V, Piccialli G, Mayol L, **2011**. *Label-free probing of G-quadruplex formation by surface-enhanced Raman scattering.*Anal Chem.83(17):6849-55.
10. Musumeci D, Oliviero G, Roviello GN, Bucci EM, Piccialli G, **2012**. *G-quadruplex-forming oligonucleotide conjugated to magnetic nanoparticles: synthesis, characterization, and enzymatic stability assays*. Bioconjug. Chem. 23: 382–391.
11. Zhang F, Sautter K, Larsen AM, Findley DA, Davis RC, Samha H, Lindford MR, **2010**.*Chemical vapor deposition of three aminosilanes on silicon dioxide: surface characterization, stability, effects of silane concentration, and cyanine dye adsorption*. Langmuir 26: 14 648–54.
12. Aissaoui N, Bergaoui L, Landoulsi J, Lambert JF, Boujday S,**2012***Silane layers on silicon surface: mechanism of interaction, stability, and influence on protein adsorption*. Langmuir 28: 656–66.
13. Gooding JJ, Ciampi S,**2011**. *The molecular level modification of surfaces: from self-assembled monolayers to complex molecular assemblies*. Chem. Soc. Rev. 40, 2704–2718.
14. Rea I, Orabona E, Lamberti A, Rendina I, De Stefano L, **2011***A microfluidics assisted porous silicon array for optical label-free biochemical sensing*. Biomicrofluidics 5: 034120.
15. Rea I, Oliviero G, Amato J, Borbone N, Piccialli G, Rendina I, De Stefano L,**2010**. *Direct Synthesis of Oligonucleotides on Nanostructured Silic Multilayers*. The Journal of Physical Chemistry C. 114 (6):2617-2621.
16. De Stefano L, Oliviero G, Amato J, Borbone N, Piccialli G, Mayol L, Rendina I, Terracciano M, Rea I, **2013**. *Aminosilane functionalizations of mesoporous oxidized silicon for oligonucleotide synthesis and detection.* J. R. Soc. Interface 2013 10 20130160.

17. Kuijpers WHA, Huskens J, van Boeckel CAA, **1990**. *The 2-(acetoxymethyl)benzoyl (AMB) group as a new base-protecting group, designed for the protection of (phosphate) modified oligonucleotides*. Tetrahedron Lett.31 (46): 6729-32.

18. Ellington A, Pollard D, **2001**. *Current Protocols in Molecular Biology. New York: Wiley. Synthesis and purification of oligonucleotides*. 2.11.1–2.11.25.

CHAPTER 4

Oligonucleotide analogues: PNA and its use as miRNA inhibitor

4.1 Introduction

Peptide Nucleic Acid (PNA) is an oligonucleotide mimic characterized by a pseudopeptide backbone with the standard nucleobases attached as side chains. As it was first reported in 1991 [1, 2], the number of papers and applications of this ON mimic has exponentially growth, principally due to its broad range of exciting properties. [3] The PNA hallmarks, in fact, are its stability and hybridation properties, that, together with the neutral charge of its backbone, make it a versatile tool in the diagnostic and gene modulation fields.PNA is commonly exploited as gene targeting agent for both elucidation of gene function and drugs development, as versatile tool for the design of diagnostics, as molecular beacon. [4-9] However, recent progresses highlight the great promise of another fascinating application, i.e. the use of PNA as microRNA modulator [10, 11].
MicroRNAs (miRNAs) are small, noncoding RNAs that regulate gene expression post-transcriptionally, by targeting specific mRNA molecules and inhibiting their translation. [12] A markedly high number of evidences showed that they play a pivotal role in diverse physiological and disease processes and, as a consequence, have been so far proposed as potential therapeutic targets. [13-17] The discovery of miRNAs has drastically revolutionized the approaches for gene modulation; since they were discovered, an incredibly high number of agents have been proposed as anti-miRNA tools, thus allowing the elucidation of their biological role and, eventually, their inhibition in pathological processes. Synthetic anti-miRNA oligonucleotides (AMOs) have been extensively explored in this context and proved to work primarily by steric blocking the miRNA recognition and binding to the target. [18-20] Giving the drawbacks of the therapeutic use of oligonucleotides, various chemical modification have been exploited to improve ON performances and potency as anti-miRNA agents. In this context, PNAs has showed chemical and structural features successful for blocking miRNA expression. Among the genetic disorders for which AMOs approach has been proposed, Cystic Fibrosis takes on a great relevance. Cystic fibrosis (CF),the most common, genetically acquired, life-shortening chronic illness affecting young Caucasians today, is an inherited disorder characterized by chronic airway inflammation. CF is a disease that affect the secretory glands and is caused by mutations in the *CFTR* gene encoding the *CFTR* chloride channel expressed by most epithelial cells. [21] This gene is expressed, at different level, in specialized epithelial cells of the airway, in pancreatic duct, intestinal and male genital duct epithelium. A complex pattern of regulatory elements has been characterized within the gene, such as elements flanking the locus and elements within the introns, but, although these *cis*-elements are probably the most relevant for CFTR regulation, it is well established that post-transcriptional regulation plays a key role as well. For example, various miRNAs have emerged as elements involved in the post-transcriptional CFTR regulation. In this sense, it is important to note that little is understood regarding miRNA functions in the airway epithelium under normal or diseased conditions, but there is a growing understanding that altered expression of miRNA is involved in the CF phenotype. [22] As demonstrated by the increasing number of papers in this scientific topic, modulation of miRNAs involved in the CF

phenotype represents a new therapeutic paradigm for CF.
In 2013 Amato *et al.* showed that mutations in the 3'-UTR of the *CFTR* gene may play a pathogenic effect increasing the affinity for a miRNA, known as miR-509-3p, thus confirming the potential of miRNAs as therapeutic targets. [23] In a recent work, Yin and co-workers explored the capability of a PNA sequence to selectively inhibitmiRNA-4661-3p. [24]
The promising results reported in this kind of approaches led our group to propose the use of peptide nucleic acids (PNAs) as inhibitors of miR-509-3p. In a previous work, a negatively charged PNA, 14 bases long, conveniently modified at its termini, in order to allow its delivery and individuation within the cells, and complementary to the 5'-terminus of miR-509-3p,was proposed for the selective inhibition of the miRNA. The *in vitro* studies demonstrated that the PNA was able to recognize the target within the cells, thus preventing the recognition and down regulation of the gene. [25] However, taking into account that the synthesis of long (14-20 bases) and conjugated PNAs is difficult, expensive and, most important, longer PNAs suffer from poor solubility, which is a fundamental property for their manipulation and delivery, we decided to focus our attention on a shorter sequence. In particular we projected and carried out the synthesis and structural characterization of a short PNA sequence aimed at binding and inhibiting miR-509-3pand proved its ability as efficient miRNA modulator.

4.2 Results and Discussion

As demonstrated by various reports [23, 26], miR-509-3p is able to repress CFTR expression by binding the 3'-UTR of the gene. Considering that its expression is enhanced in CF epithelia and, in particular, increases during infection and inflammation, it has been generally recognized as an important therapeutic target to rescue CFTR expression and prevent the pathogenic effects of the disease in those phenotypes where a correct copy of the gene is available.
In this frame, we designed a 7 base long PNA fully complementary to the 5'-end of miR-509-3p and tested it as miRNA inhibitor. In fact, taking into account the previous positive findings reported by us on a 14 base long PNA as miR-509-3p inhibitor, but, at the same time the drawbacks associated to its synthesis, quite long, difficult and expensive, we decided to prove the effectiveness of a smaller PNA sequence as miRNA function modulator, complementary for only 7 nt to the *seed region* of the target, i.e. the region of a miRNA, of about 6-8 bases, essential for the recognition and binding to its target sequence and, consequently, the most important to achieve miRNA inhibition. In this way, we could adopt a synthetic protocol more simple and rapid, compatible with the PNA functionalization and, at the same time, with the production of soluble molecules. To this purpose, preliminary Molecular Dynamics (MD) simulations have been exploited to predict the behaviour of the new PNA/RNA heteroduplexes and evaluate the feasibility of our hypothesis about the effectiveness of the shorter anti-miRNA PNA sequence. The comparison between the long PNA (PNA1) and the novel shorter PNA (PNA2) showed that both PNAs form similar heteroduplexes, assuming a conformation resembling the canonical A-type RNA helix (Figure 1).

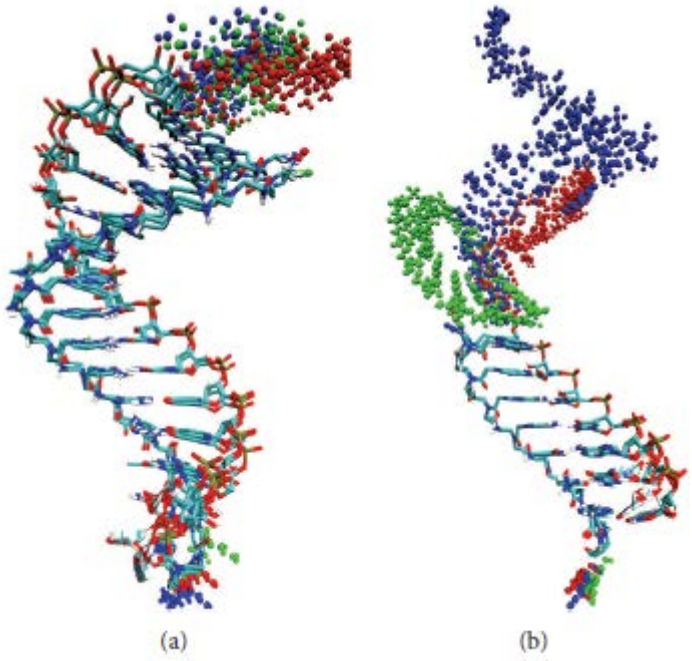

Figure 1. Superimposition of the MD average structures of miR-509-3p/PNA1 complex (a)and of miR-509-3p/PNA2 complex (b). Duplexes regions are represented in licorice colored by atomtype (carbon in cyan, oxygen in red, nitrogen in blue, phosphate in brown, and hydrogen in white). The miR-509-3p single strand regions are represented in spheres colored by MD run (blue, run 1; green, run 2; red, run 3).

On the basis of the positive outcomes, we proceeded with the synthesis of the 7-bases long PNA. The oligomer was provided with a negatively charged tetra peptide tail at the C-end in order to facilitate the cellular uptake and enhance its water solubility and conjugated at the N-terminus to the fluorescent group, to allow its simple visualization during *in vitro* experiments. Contextually a PNA oligomer with the same size and different composition in bases was synthesized as scramble sequence, i.e. negative control. Figure 2 shows the base composition of our anti-miRNA PNA2, the scramble sequence, PNA3, and the previously tested PNA1, i.e. the 14-base long anti-miRNA PNA.

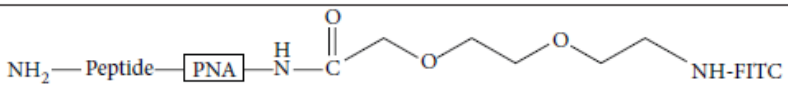

miRNA		U	G	A	U	U	G	G	U	A	C	G	U	C	U	G	U	G	G	G	U	A	G
PNA1	G-S(P)-S(p)-G-a	c	t	a	a	c	c	a	t	g	c	a	g	a	Linker-FITC								
PNA2	G-S(P)-S(p)-G-a	c	t	a	a	c	c	Linker-FITC															
PNA3	G-S(P)-S(p)-G-t	t	t	t	t	t	t																

Figure 2. Structures and sequences of miR-509-3p and PNA1–3. PNA sequences are written from C- to N-terminus.

The overall sequences were synthesized through the Fmoc-solid phase protocol on a Rink amide resin and were equipped with the same conjugations at both their termini:

a peptide tail composed by two glycines and two negatively charged serines at the C-end and, as regards PNA1 and PNA2, a Fluorescein Isothiocynate (FITC) residue attached at the N-terminal using an ethoxyehtyl (AEEA) linker. To this scope, we used an "on line" synthetic approach in which, at first, the peptide tract was assembled, then the PNA portion was constructed and, in the case of PNA1 and 2, conjugated to the fluorophore group. After the synthesis, the oligomers were detached from the support, lyophilized and characterized by means of spectroscopic techniques.
Circular Dichroism and UV-vis spectroscopic techniques, in fact, were exploited to obtain an insight into the occurrence of the recognition between the RNA sequence and our PNA. To this aim, we preliminarily prepared the miR-509-3p/PNA heteroduplexes, in the ratio 1:1.5 and 1:5.
The UV spectrum of miR-509-3p/PNA2 complex displays a lower value of absorbance than the arithmetic sum of each component alone. These findings, in line with those reported for PNA1, highlight the occurrence of stacking interactions between the miRNA and the PNA sequence (Fig. 3).

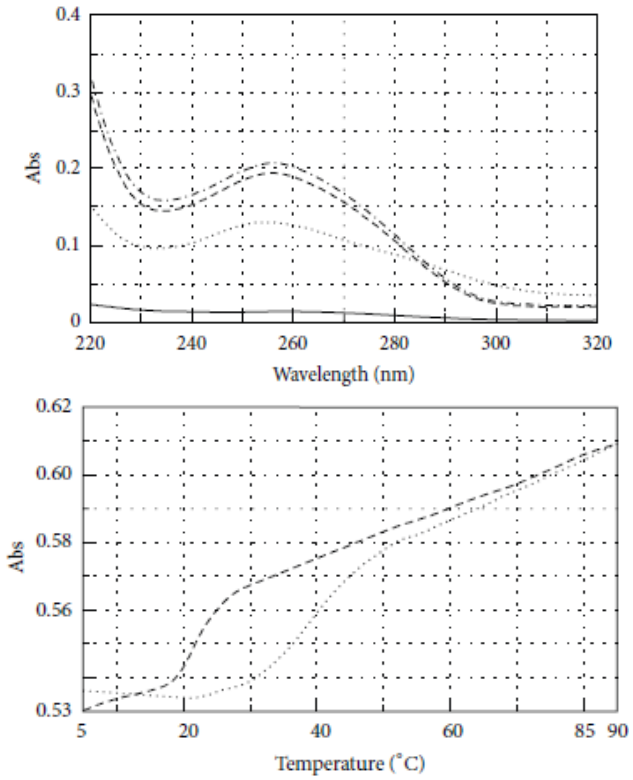

Figure 3. (A) UV spectra of miR-509-3p (dashed line), PNA2 (solid line), miR-509-3p/PNA2 mixture (1 : 1.5) (dotted line), and the arithmetical sum (dashed-dotted line). (B) UV melting profile of miR-509-3p alone (dashed line) andmiR-509-3p/PNA2 mixture (1 : 1.5 dotted line).

The figure above shows also the UV-melting profile of the miR-509-3p/PNA2 mixture in the ratio 1:1.5. This experiment further confirm the formation of the heteroduplex, since a sigmoid curve at 260 nm, typical of duplex/single strand transition is observed. Moreover, the calculated apparent melting Temperature of the mixture is 40°C, while the same value for the RNA alone is 20°C, which can be ascribed to the less stable secondary structures of the RNA alone.

Circular Dichroism was also exploited to characterize our structures. CD spectra of each component alone and of the mixture are reported in figure 4 and, once again, confirm the capability of the PNA to bind the target. Indeed, the dichroic profile of the mixture is that of a typical antiparallel RNA/PNA heteroduplex, showing maxima near 220 and 260 nm and minima at 196 and 235 nm.

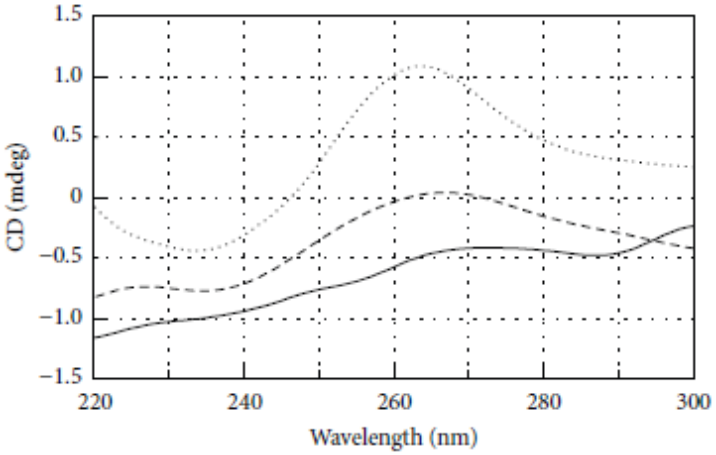

Figure 4. CD spectra of miR-509-3p alone (dashed line), PNA2 alone (solid line), and miR-509-3p/PNA2 mixture (1: 1.5) (dotted line).

To further investigate on the recognition phenomena, we also carried out Electophoresis Mobility Shift Assay (EMSA) experiments (Fig. 5).

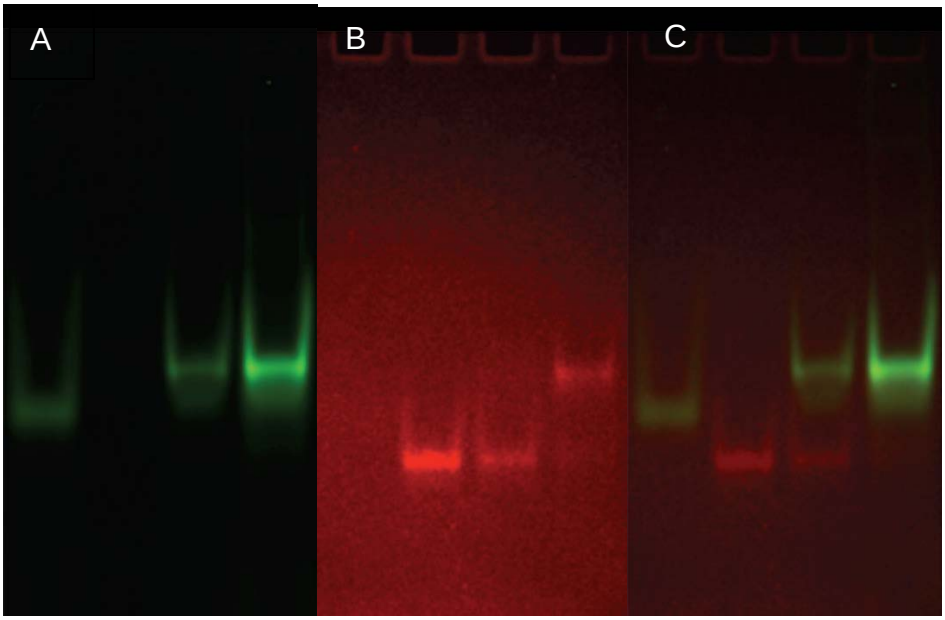

Figure 5. EMSA of PNA2 alone (lanes 1), miR-509-3p alone (lanes 2), miR-509-3p/PNA2 1 : 1.5 (lanes 3), and miR-509-3p/PNA2 1 : 5 (lanes 4) visualized by FITC (a) or EtBr (b) staining. The superimposition of FITC and EtBr stained gels is shown in (c).

The figure above shows the same gel visualized by FITC and ethidium bromide stains and their superimposition. PNA 2 alone, in lane 1, is able to migrate by virtue of its negatively charged peptide tail; the formation of the RNA/PNA complex is

evidenced by the visualization of a upwards-shifted band, slower than the two components alone, for both the 1:1.5 and 1:5 ratios, in lanes 3 and 4 respectively.
Once obtained robust proves concerning the binding events, we wanted to explore the recognition phenomena in a biological context, by setting *in vitro* experiments. To this aim, we examined the ability of PNA2 to revert the decrease of luciferase activity due to the transfection of miR-509-3p in A549 cells. A reporter luciferase construct sensitive to miR-509-3p for the presence of the 3'-UTR of the gene, the pLuc-CFTR-3'UTR plasmid, was used to transfect A549 cells. Then, the cells were transfected with miR-509-3p; as expected, the introduction of the miRNA induces the luciferase activity reduction up to 40%. Successively, PNA2 was transfected by means of commercially available Attractene cationic lipid transfection reagent. As we can see from figure 6, that shows microscopy image of A549 cells 24 hours after the transfection, PNA2 was uptaken by the cells.

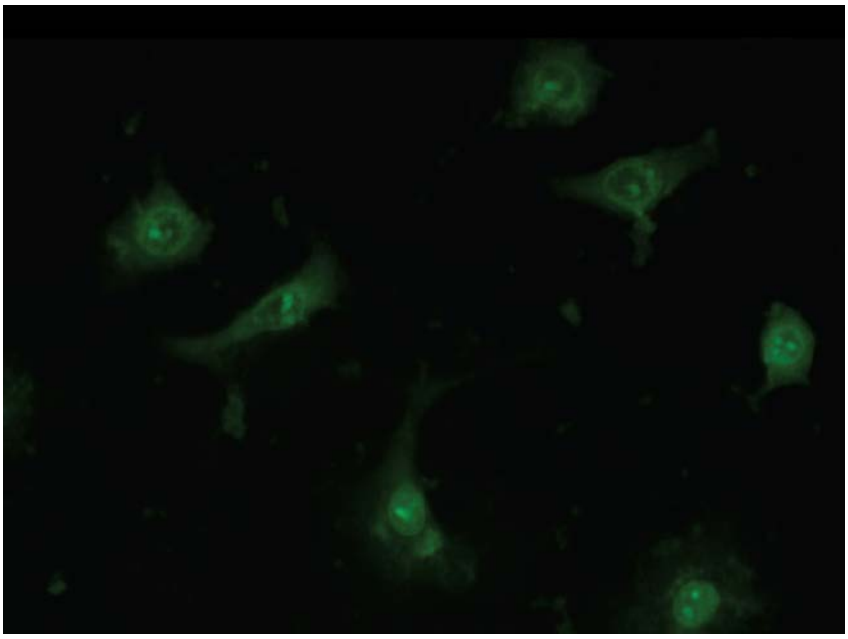

Figure 6. Representative uptake of FITC-labelled PNA2 by A54 cells

More interestingly, PNA2, but no PNA3, was able to rescue luciferase activity in a dose-dependent manner. This last result led us to conclude that, even within the cells, our anti-miRNA PNA is able to selectively recognize and bind its target, thus preventing its recognition to the 3'-UTR of the gene (Fig. 7).

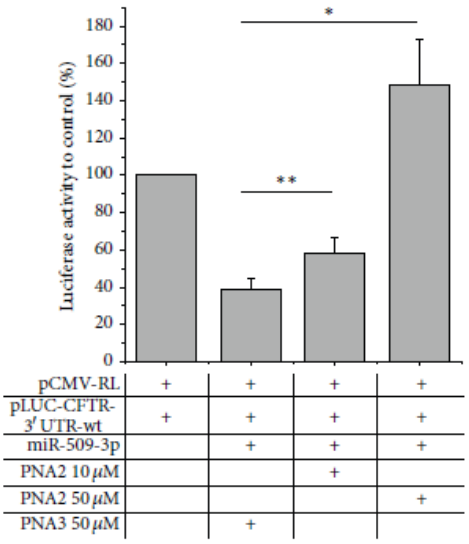

Figure 7. Inhibition of miR-509-3p effect by PNA2. Different dosesof PNA2 were transfected in A549 cells. A significant inhibition ofmiR-509-3pwas observed using PNA2 in a dose-dependent manner. *P values < 0.02, **P values < 0.002.The 7-mer poly-thymine PNA3had no effect on miR-509-3p.

4.3 Conclusions

In this work, we presented the use of a small PNA sequence as miRNA function modulator. The chemical features of PNA make it a versatile tool in the field of gene modulation and, to date, several works have witnessed its potency in this context. However, beyond the classical and consolidated application as antigene and antisense agent, another interesting and less explored field can benefit from its properties, the miRNA modulation field. The RNA/PNA heteroduplexes are exceptionally stable and this aspect, in association to the PNA stability in biological media, are extremely intriguing for the exploration of miRNA role and the modulation of their function in pathological processes.
In a previous work, our group reported the positive findings relative to the use of a 14 base long PNA complementary to the 5'-terminal region of miR-509-3p, a miRNA involved in the pathological progress of Cystisc Fibrosis. [25]In 2011 Obad *et al.* reported the efficient silencing of a miRNA by a very small LNA, only 8 base long.[27] In this frame, our interest towards short PNA sequences was triggered by the experimental observation that the synthesis of long PNA sequences in not trivial, in particular for conjugated PNAs, and, above all, long PNAs suffer from poor solubility in water. These considerations, in addition to the numerous computational evidences that showed that a complementarity of only 7 bases at the 5'-terminus of miRNAs is sufficient for their activity modulation *in vivo*, led us to design and test a novel very small PNA sequence as miR-509-3p modulator. A combination of spectroscopic techniques was firstly used to explore the capability of our PNA to bind the RNA target and the successful findings obtained were then confirmed by the biological assays. These studies demonstrate that the activity of miR-509-3p can be inhibited by a short PNA targeting only the seed region of the miRNA. Therefore the here presented results further strengthen the potential of PNA as anti-miRNAs agent, in particular considering the significant advantages in terms of cost and times required by the PNA synthesis.

4.4 Experimental Section

4.4.1 Molecular Modelling

The initial structures of the heteroduplexes formed by miR-509-3p with PNA1 and PNA2 were built by using the NMR structure of the 6-mer RNA(GAGUUC)/PNA(GAACTC) heteroduplex (PDB ID = 176D) [28]. Starting from the lowest energy NMR structure, one nucleotide was added aligning a duplicate of the reference structure on the PNA backbone. Once the 7-mer heteroduplex was obtained, the bases were mutated to match the PNA2 sequence. Watson-Crick canonical pairs were then refined using distance restraints on the first seven bases of miR- 509-3p/PNA2 heteroduplex. The same procedure was used to build the miR-509-3p/PNA1 heteroduplex, starting from the refined structure of miR509-3P/PNA2 heteroduplex. The equilibration of the systems and production of MD simulations were performed using the Amber 12 suite of programs [29, 30]. The Leap module of Ambertools13 was used to create parameter and topology files for the MD simulations using the ff99SB force field for RNA and standard amino acids. For PNAs parameterization we used the Sanders et al. force field for PNA [31] downloaded from the RESP and ESP charge database (R.E.DD.B. http://q4md-forcefieldtools.org/REDDB Project ID = F93) [32], whereas the parameters for serine phosphate were taken from reference [33]. TIP3P water molecules were added with a minimum spacing of 10.0A from the box edges to the ˚ RNA:PNA molecules and Na+ counterions were added to each system to reach the neutralization of the system. The geometry of the system was minimized in four steps as follows: (1) optimization of hydrogen atoms (500 steps of steepest descent and 4,500 steps of conjugate gradient); (2) optimization of water molecules and counterions (2,000 steps of steepest descent and 8,000 steps of conjugate gradient); (3) further optimization of hydrogen atoms, water molecules, and counterions (3,500 steps of steepest descent and 11,500 steps of conjugate gradient); (4) final optimization of the whole system (2,500 steps of steepest descent and 8,500 steps of conjugate gradient). Thermalization of the system was performed in four steps of 60 ps, increasing the temperature from 10 to 298 K. Concomitantly, interstrand distance restraints were applied to the RNA:PNA heteroduplex to preserve all base pairs canonical Watson-Crick bond, allowing 0.1A movement from the equilibrium bond distance ˚ (either closer or farther). Thus, the force constant applied during thermalization was set to 32 kcal mol−1 A˚ −2 and was gradually reduced in the next step to 10 kcal mol−1 A˚ −2 and subsequently decreased by increments of 5 kcal mol−1 A˚ −2in the next stages. Then, an additional step of 250 ps was performed in order to equilibrate the system density at constant pressure (1 bar) and temperature (298 K). Finally, an extended trajectory covering was run using a time step of 2 fs. SHAKE was used for those bonds containing hydrogen atoms in conjunction with periodic boundary conditions at constant pressure and temperature, particle mesh Ewald was used for the treatment of long range electrostatic interactions, and a cutoff of 9A was used for nonbonded interactions. ˚All production simulations were repeated in triplicate with random seeding for initial velocities and extended to 20 ns. In order to further assay the stability of the RNA:PNA heteroduplexes, we extended one run of PNA2 up to 50 ns, for a total simulation time of 90 ns for PNA2 and 60 ns for PNA1. The structural features were determined using the Curves+ software package [40], and visualization of trajectories was performed in VMD, while the trajectory analyses were performed using Ambertools13.

4.4.2 Synthesis of miR-509-3p and PNAs

Synthesis of miR-509-3p and PNAs. The miR-509-3p mimic (2-OMe modified) was synthesized and purified by the oligonucleotide synthesis facility at CEINGE-Biotecnologie Avanzate (Naples, Italy).

PNA 2 and PNA3 were synthesized by standard Fmoc-solid phase strategy, using Fmoc-Bhoc protected monomers purchased from Link Technologies. MBHA resin, after swelling in DCM for 30 minutes and washings in DMF, was treated with deblocking solution (20% piperidine in DMF) to allow the deprotection of the $–NH_2$ functions on the resin. During the peptide and PNA synthesis the Fmoc group was removed by a treatment with a 5% DBU in DMF solution (5 min).Couplings of the standard aminoacids and the PNA monomers were performed using 5 equivalents of monomer, HATU and DIPEA and 6.5 equivalents of Lutidine, for 1 hour at room temperature. For Fmoc-L-Ser(PO(OBzl)OH)-OH coupling time was prolonged to 15 hours. For the coupling with the fluorescent group the FITC monomer (5 eq., 0.2 M) was dissolved in DMF/DIPEA (2.5:97.5 v/v) and the solution was added to the resin, which was gently shaken in the dark for 15 h. The detachment of the oligomers from the support was achieved by treating the resin with TFA/anisole/ethanedithiol (9:0.5:0.5; v/v/v) for 3.5 h and the products were precipitated with cold diethyl ether. After centrifugation and washings with diethyl ether, the oligomers were dissolved in water and lyophilized.

4.4.3 PNA purification

The purifications were performed by HPLC using a RP-18 column (Merck, RT 250–10 5 μm) eluted with a linear gradient from 10% to 90% of eluent B in eluent A in 30 min, where eluent A is 0.1% TFA in water eluent B: 0.1% TFA in acetonitrile. For these purifications the UV/VIS detector was set at 495 nm corresponding to the maximum of absorption of FITC. The collected yellow fractions were lyophilized and stored at −20◦ C in the dark. The structures of PNA2 and PNA3 were confirmed by MALDI-TOF mass spectrometry on a Bruker Autoflex I instrument using α-cyano-4-hydroxycinnamic acid, 10 mg/mL in acetonitrile-3% aqueous TFA (1 : 1, v/v) as the matrix.

PNA2 m/z calculated 2812, found 2813 $[M + H]^+$

PNA3 m/z calculated 2864, found 2865 $[M + H]^+$

4.4.4 Preparation of miRNA/PNA heteroduplexes

The miR-509-3p/PNA heteroduplexes (1:1.5 or 1:5) were prepared in100mM KCl and 10mMK_2HPO_4 containing buffer, by heating the mixture of the samples at 90°C for 5min and slowly cooling at room temperature for 12 h. The concentration of each PNA sample was estimated by quantitative UV at 90°Cusing the following molar extinction coefficients: PNA1 ε=149.6mL μmol−1 cm−1, PNA2 ε = 69.7mL μmol^{-1} cm^{-1},PNA3 ε=61.6mL$\mu mol^{-1}cm^{-1}$, and miR-509-3p ε=205.0mL μmol^{-1} cm^{-1}.

4.4.5 UV and UV-melting studies

The UV spectra were recorded on a Jasco V-530 UV spectrophotometer equipped with a Peltier-type temperature control system (model PTC-348WI). Thermal denaturation experiments were performed in the temperature range 5–90°C by monitoring the absorbance at 260 nm at the heating rate of 0.5◦C/min. The apparent T_m was estimated from the maximum in the first derivative of the melting profile.

4.4.6 CD and CD-melting studies

CD spectra were recorded with a JascoJ-715 spectropolarimeter equipped with a Peltier Thermostat Jasco ETC-505T using 0.1 cm path length cuvettes. CD measurements were registered in the range 220–320 nm with a scan rate of 100 nm/min and 2nm bandwidth. The concentration of miR-509-3p/PNA2 and miR-509-3p was 1.0×10^{-5} M. The spectra were signal-averaged over at least three scans and baseline was corrected by subtracting the buffer spectrum.

4.4.7 Cell line, construct and transfection

A549 human lung carcinoma cells were purchased from ATCC (Manassas, USA). Cells were maintained in Dulbecco's modified Eagle'smedium (Gibco Invitrogen, USA) with 10% heat inactivated fetal bovine serum (HyClone, USA) without the addition of antibiotics. Luciferase construct bearing the 3'-UTR of CFTR gene [23] was used as miR-509-3p sensitive. Transfection of A549 cells with miRNA-mimics (Qiagen, Germany, EU) or PNA was performed with Attractene Transfection Reagent (Qiagen) as previously reported [25]. Briefly, cells seeded in 96-well plates were co-transfected with the luciferase reporter constructs and the miR-509-3p mimic. 24 h after, the cells were transfected with anti-miR-509-3p PNA. The transfection efficiency (≈ 80%) was assessed by measuring the percentage of fluorescent cells relative to the total number of cells. The luciferase activity level was measured 24 h after transfection using the Dual-Glo Luciferase Assay System (Promega Corporation).The relative reporter activity was obtained by normalization to the Renilla luciferase activity.

4.4.8 Electrophoresis Mobility Shift Assay

The miR-509-3p mimic (2'-OMe-modified) was synthesized by the oligonucleotide synthesis facility at CEINGE-Biotecnologie Avanzate(Naples, Italy). As previously reported [25], the miRNA and PNA were annealed in 1X NE Buffer 2 (50mMNaCl, 10mMTris-HCl, 10mMMgCl2, 1mMDTT, and pH 7.9 at 25◦C) for2 h at room temperature. All the reactions were loaded into 20% polyacrylamide gels in 0.5X Tris-Borate-EDTA (TBE) buffer and run at 140V for 3 h. The fluorescence signal was acquired placing the wet gel directly on the plate of the Typhoon 8600 scanner.

4.5 References

1. Nielsen PE, Egholm M, Berg RH, Buchardt O, **1991**. *Sequence-selective recognition of DNA by strand displacement with a thymine-substituted polyamide.*Science. 254(5037):1497-500.
2. Hyrup B, Nielsen PE, **1996**. Peptide nucleic acids (PNA): synthesis, properties and potential applications. Bioorg. Med. Chem. 4:5–23
3. Eriksson M, Nielsen PE, **1996**. *Solution structure of a peptide nucleic acid-DNA duplex.* Nat. Struct. Biol. 3:410–413.
4. Fraser GL, Holmgren J, Clarke PBS, Wahlestedt C, **2000**. *Antisense inhibition of delta-opioid receptor gene function in vivo by peptide nucleic acids*. Mol. Pharmacol. 57: 725–731.
5. Gotfredsen CH, Schultze P, Feigon J, **1998**. *Solution structure of an intramolecular pyrimidine–purine–pyrimidine triplex containing an RNA third strand*. J. Am. Chem. Soc. 120:4281–4289.
6. Hamilton SE, Simmons CG, Kathiriya IS, Corey DR, **1999**.*Cellular delivery of peptide nucleic acids and inhibition of human telomerase*. Chem. Biol 6:343–351.
7. Kuhn H, Demidov VV, Coull JM, Fiandaca MJ, Gildea BD, FrankKamenetskii MD, **2002**. *Hybridization of DNA and PNA molecular beacons to single-stranded and double-stranded DNA targets*. J. Am. Chem. Soc. 124:1097–1103.
8. Mologni L, Nielsen PE, Gambacorti-Passerini C, **1999**. *In vitro transcriptional and translational block of the bcl-2 gene operated by peptide nucleic acid*. Biochem. Biophys. Res. Commun. 264:537–543.
9. Norton JC, Piatyszek MA, Wright WE, Shay JW, Corey DR, **1996**. *Inhibition of human telomerase activity by peptide nucleic acids.* Nat. Biotechnol. 14:615–619.
10. Oh SY, Ju YS, Park H, **2009**.*A highly effective and long-lasting inhibition of miRNAs with PNA-based antisense oligonucleotides*. Molecules and Cells. 28: 341-345
11. Fabani MM, Gait MJ, **2008**.*miR-122 targeting with LNA/2'-O-methyl oligonucleotide mixmers, peptide nucleic acids (PNA), and PNA-peptide conjugates.* Rna 14: 336–346.
12. Rana TM, **2007**. *Illuminating the silence: understanding the structure and function of small RNAs.* Nature Reviews Molecular Cell Biology. 8: 23-36.
13. Mann M, Barad O, Agami R, Geiger B, Hornstein E, **2010.***miRNA-based mechanism for the commitment of multipotent progenitors to a single cellular fate*. Proc Natl Acad Sci USA. 107: 15804–09.
14. Hornstein E, **2010**.*miRNA activity directs stem cell commitment to a particular fate.* Cell Cycle. 9: 4041–4042.
15. Haramati S, Chapnik E, Sztainberg Y, Eilam R, Zwang R, Gershoni N, McGlinn E, Heiser PW, Wills AM, Wirguin I, Rubin LL, Misawa H, Tabin CJ, Brown R Jr, Chen A, Hornstein E, **2010**. *miRNA malfunction causes spinal motor neuron disease*. Proc Natl Acad Sci, 107: 13111–13116.
16. Thum T, Gross C, Fiedler J, Fischer T, Kissler S, Bussen M, Galuppo P, Just S, Rottbauer W, Frantz S, Castoldi M, Soutschek J, Koteliansky V, Rosenwald A, Basson MA, Licht JD, Pena JT, Rouhanifard SH, Muckenthaler MU, Tuschl T, Martin GR, Bauersachs J, Engelhardt S, **2008**. *MicroRNA-21 contributes to*

myocardial disease by stimulating MAP kinase signalling in fibroblasts. Nature. 456(7224):980-4.

17. Garzon R, Marcucci G, Croce CM, **2010**. *Targeting microRNAs in cancer: rationale, strategies and challenges. Nat. Rev. Drug. Discov*. 9: 775–789.

18. Freier SM, Altmann KH, **1997**.*The ups and downs of nucleic acid duplex stability: structure-stability studies on chemically-modified DNA:RNA duplexes*. Nucleic Acids Res. 25: 4429–43.

19. Lennox KA, Behlke MA, **2010**. *A direct comparison of anti-microRNA oligonucleotide potency*. Pharm. Res.27: 1788–99.

20. Eder PS, DeVine RJ, Dagle JM, Walder JA, **1991**. *Substrate specificity and kinetics of degradation of antisense oligonucleotides by a 3' exonuclease in plasma.* Antisense Res. Dev. 1(2):141-51.

21. Cheng SH, Gregory RJ, Marshall J, Paul S, Souza DW, White GA, O'Riordan CR, Smith AE, **1990**. *Defective intracellular transport and processing of CFTR is the molecular basis of most cystic fibrosis*. Cell. 63(4):827-34.

22. Gillen AE, Gosalia N, Leir SH, Harris A, **2011***. MicroRNA regulation of expression of the cystic fibrosis transmembrane conductance regulator gene*.Biochem. J. 438(1):25-32.

23. Amato F, Seia M, Giordano S, Elce A, Zarrilli F, Castaldo G, Tomaiuolo R, **2013**. *Gene mutation in microRNA target sites of CFTR gene: a novel pathogenetic mechanism in cystic fibrosis*. *PLoS One*. 8(3): e60448

24. Brown PN, Yin H, **2013**. *PNA-based microRNA inhibitors elicit anti-inflammatory effects in microglia cells*. Chem Commun (Camb). 49(39):4415-7.

25. Amato F, Tomaiuolo R, Borbone N, Elce A, Amato J, D'Errico S, De Rosa G, Mayol L, Piccialli G, Oliviero G, Castaldo G, **2014**. *Design, synthesis and biochemical investigation, by in vitro luciferase reporter system, of peptide nucleic acids as new inhibitors of miR-509-3p involved in the regulation of cystic fibrosis disease-gene expression.* Med. Chem. Commun. 5: 68-71.

26. Ramachandran S, Karp PH, Osterhaus SR, Jiang P, Wohlford-Lenane C, Lennox KA, Jacobi AM, Praekh K, Rose SD, Behlke MA, Xing Y, Welsh MJ, McCray PB Jr, **2013**. *Post-transcriptional regulation of cystic fibrosis transmembrane conductance regulator expression and function by microRNAs*. Am. J. Respir. Cell. Mol. Biol. 49(4):544-51.

27. Obad S, dos Santos CO, Petri A, Heidenblad M, Broom O, Ruse C, Fu C, Lindow M, Stenvang J, Straarup EM, Hansen HF, Koch T, Pappin D, Hannon GJ, Kauppinen S, 2011. *Silencing of microRNA families by seed-targeting tiny LNAs.* Nat. Genet. 43(4):371-8.

28. Brown SC, Thomson SA, Veal JM, Davis DG, **1998**. *NMR solution structure of a peptide nucleic acid complexed with RNA.* Science. 265(5173):777-80.

29. Hornak V, Abel R, Okur A, Strockbine B, Roitberg A, Simmerling C, **2006**. *Comparison of multiple Amber force fields and development of improved protein backbone parameters.* Proteins. 65(3):712-25.

30. Case DA, Darden TA, Cheatham TE III, et al., **2012**. "AMBER 12" University of California**.**

31. Sanders JM, Wampole ME, Chen CP, Sethi D, Singh A, Dupradeau FY, Wang F, Gray BD, Thakur ML, Wickstrom E, **2013**. *Effects of Hypoxanthine Substitution in Peptide Nucleic Acids Targeting KRAS2 Oncogenic mRNA Molecules: Theory and Experiment.* J. Phys. Chem. B. 117 (39): 11584-95.

32. Dupradeau FY, Cézard C, Lelong R, Stanislawiak E, Pêcher J, Delepine JC, Cieplak P, **2008**. *R.E.DD.B.: a database for RESP and ESP atomic charges, and force field libraries.* Nucleic Acids Res. 36 (1) (Database issue):D360-7.
33. Craft JW Jr, Legge GB, **2005**. *An AMBER/DYANA/MOLMOL phosphorylated amino acid library set and incorporation into NMR structure calculations.* J Biomol NMR. 33(1):15-24.

APPENDIX

A1

List of publications:

1. “A rapid screening platform towards new anti-HIV aptamers set on molecular docking and fluorescence quenching techniques”. Giorgia Oliviero, Mariano Stornaiuolo, Valentina D’Atri, **Fabrizia Nici**, Ali Munaim Yousif, Stefano D’Errico, Gennaro Piccialli, Luciano Mayol, Ettore Novellino, Luciana Marinelli, Paolo Grieco, Alfonso Carotenuto, Sam Noppen, Sandra Liekens, Jan Balzarini and Nicola Borbone. A*nalytical Chemistry,* 2015, 88, 2327-2334; doi: 10.1021/acs.analchem.5b04268

2. “Synthesis and Evaluation of the Antiproliferative Properties of a Tethered Tubercidin–Platinum(II) Complex”. Stefano D'Errico, Giorgia Oliviero, Nicola Borbone, Elena Di Gennaro, Andrea Ilaria Zotti, Alfredo Budillon, Vincenzo Cerullo, **Fabrizia Nici**, Luciano Mayol, Vincenzo Piccialli and Gennaro Piccialli. *Eur. J. Org. Chem,* 2015, 7550-7556; 2015 doi: 10.1002/ejoc.201500998.

3. “Synthesis of C6 -Pyridylpurine Nucleosides by Reaction of Nebularine N1 -Oxide with Pyridinyl Grignard Reagents”. Stefano D’Errico,Giorgia Oliviero, Nicola Borbone, **Fabrizia Nici**, Vincenzo Piccialli, Brunella Pinto, Daniele D’Alonzo, Luciano Mayol, and Gennaro Piccialli. *Eur. J. Org. Chem*, 2015, 2244–2249; 2015 doi: 10.1002/ejoc.201403648.

4. “Synthesis and Pharmacological Evaluation of Modified Adenosines Joined to Mono-Functional Platinum Moieties”. Stefano D’Errico, Giorgia Oliviero, Nicola Borbone, Vincenzo Piccialli, Brunella Pinto, Francesca De Falco, Maria Chiara Maiuri, Rosa Carnuccio, Valeria Costantino, **Fabrizia Nici** and Gennaro Piccialli. *Molecules,* 2014, 19, 9339-9353; doi:10.3390/molecules19079339.

5. “Synthesis of mixed-sequence oligonucleotides on mesoporous silicon: chemical strategies and material stability”. Monica Terracciano, Ilaria Rea, Luca Stefano, Ivo Rendina, Giorgia Oliviero, **Fabrizia Nici**, Stefano D'Errico, Gennaro Piccialli, Nicola Borbone. *Nanoscale Res Lett*, 2014, 9, 317; doi:10. 1186/1556-276X-9-317.

6. ”Exploitation of a Very Small Peptide Nucleic Acid as a New Inhibitor of miR-509-3p Involved in the Regulation of Cystic Fibrosis Disease-Gene Expression”. Felice Amato, Rossella Tomaiuolo, **Fabrizia Nici**, Nicola Borbone, Ausilia Elce, Bruno Catalanotti, Stefano D'Errico, Carmine Marco Morgillo, Giuseppe De Rosa, Laura Mayol, Gennaro Piccialli, Giorgia Oliviero,

Giuseppe Castaldo. *BioMed research international*, 2014 doi: 10.1155/2014/610718.

List of Communications:

1. "*In silico* driven techniques for the design and synthesis of new Tetra-End-Linked analogues of the anti-HIV aptamer SA-1042 and a novel binding assay". International School of Organic Synthesis. Gargnano (MI), 14-19 June 2015

2. "Chemical stability studies of mesoporous oxidized silicon for the synthesis of mixed-sequence oligonucleotides" **F. Nici**, M. Terracciano, N. Borbone, L. De Stefano, S. D'Errico, G. Piccialli, I. Rea, G. Oliviero – Workshop: Functional DNA Technology. Rome, 19-20 June 2014

A2

Copy of the publications

analytical chemistry

Article

pubs.acs.org/ac

Screening Platform toward New Anti-HIV Aptamers Set on Molecular Docking and Fluorescence Quenching Techniques

Giorgia Oliviero,[†,∥] Mariano Stornaiuolo,[†,∥] Valentina D'Atri,[‡,§] Fabrizia Nici,[†] Ali Munaim Yousif,[†] Stefano D'Errico,[†] Gennaro Piccialli,[†,¶] Luciano Mayol,[†] Ettore Novellino,[†] Luciana Marinelli,[†] Paolo Grieco,[†] Alfonso Carotenuto,[†] Sam Noppen,[⊥] Sandra Liekens,[⊥] Jan Balzarini,[⊥] and Nicola Borbone*[,†]

[†]University of Naples Federico II, Department of Pharmacy, Napoli, 80131, Italy

[‡]University of Bordeaux, IECB, ARNA laboratory, Pessac, 33600, France

[§]INSERM, U869, ARNA laboratory, Bordeaux, 33000, France

[¶]CNR, Institute of Protein Biochemistry, Napoli, 80131, Italy

[⊥]KU Leuven, Rega Institute for Medical Research, Leuven, 3000, Belgium

Supporting Information

ABSTRACT: By using a new rapid screening platform set on molecular docking simulations and fluorescence quenching techniques, three new anti-HIV aptamers targeting the viral surface glycoprotein 120 (gp120) were selected, synthesized, and assayed. The use of the short synthetic fluorescent peptide **V35-Fluo** mimicking the V3 loop of gp120, as the molecular target for fluorescence-quenching binding affinity studies, allowed one to measure the binding affinities of the new aptamers for the HIV-1 gp120 without the need to obtain and purify the full recombinant gp120 protein. The almost perfect correspondence between the calculated K_d and the experimental EC_{50} on HIV-infected cells confirmed the reliability of the platform as an alternative to the existing methods for aptamer selection and measuring of aptamer−protein equilibria.

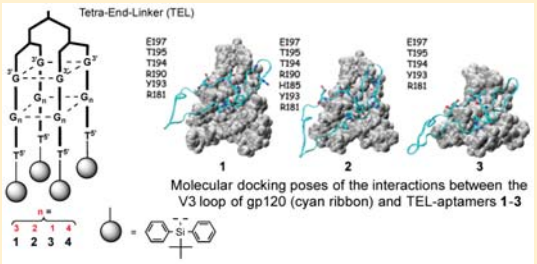

Human immunodeficiency virus (HIV) resistance to therapy relies, at least in part, on antigenic drifts and shifts, changes in the amino acids sequences of viral proteins causing drug resistance and evasion from host immune response and drug pressure. Compared to neutralizing antibodies and small drugs, oligonucleotide aptamers targeting viral proteins represent a promising source of new anti-HIV drugs capable of overcoming the consequences of the drift. In fact, due to the bigger area buried at the aptamer−protein interface, the binding affinity of aptamers for the target protein is less affected by amino acid substitutions.

In the last decades, several RNA and DNA aptamers targeting HIV have been reported.[1−10] However, new, faster, and more reliable screening platforms toward aptamers targeting HIV proteins remain to be developed. We here propose an innovative platform, to the best of our knowledge never explored so far, which uses a virtual binding assay approach for aptamer selection and a quick in vitro fluorescence quenching assay for the measurement of aptamer−protein equilibria. Aptamers targeting the HIV envelope glycoprotein 120 (gp120) are more effective in the protection of human cells from infection than those targeting viral protease or reverse transcriptase (2−3 logs higher protection).[4] The first active anti-HIV aptamers, namely, SA-1042[11] and ISIS 5320,[12] were shown to be capable of binding to the third hyper variable region of gp120 (known as the V3 loop) thus protecting the target cells from HIV infection. Upon binding, these aptamers block the first event leading to cell infection, the interaction of gp120 with the coreceptor glycoprotein CD4 expressed on the surface of target cells. The crystal structure of the complex formed by gp120 with CD4 and the neutralizing antibody X5 (PDB ID: 2B4C)[13] enlightened the structural features of the V3 loop and its role in the binding of gp120 to CD4. The V3 loop is typically 35-amino acids in length, protrudes from the protein core, and is closed by two cysteines forming a disulfide bridge.

SA-1042 and ISIS 5320 are DNA quadruplex-forming aptamers. DNA quadruplexes (G4s) are peculiar nucleic acid tertiary structures that form rapidly when suitable guanine-rich oligonucleotides are annealed in near physiological conditions. G4s are characterized by the presence of stacked planar arrangements of four guanines (G tetrads) held together by eight Hoogsteen hydrogen bonds and stabilized by the

Received: November 10, 2015
Accepted: January 25, 2016

 © XXXX American Chemical Society

DOI: 10.1021/acs.analchem.5b04268
Anal. Chem. XXXX, XXX, XXX−XXX

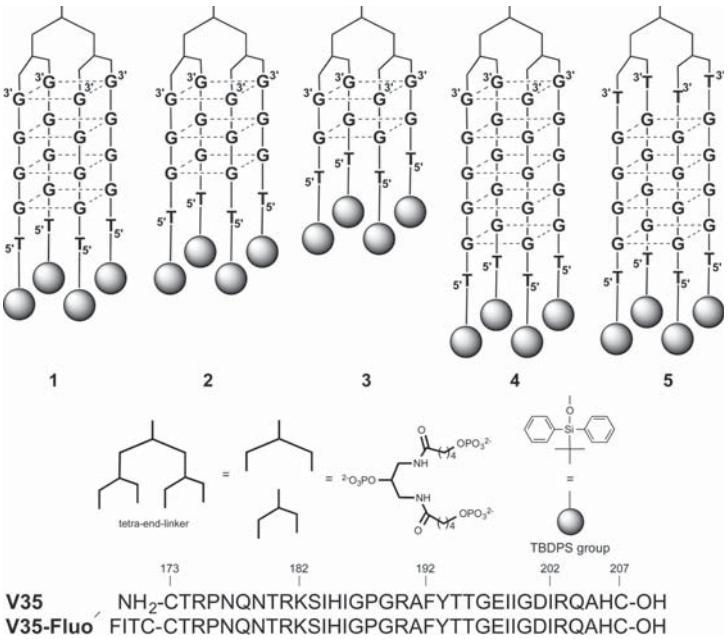

Figure 1. Schematic representation of TEL–ODNs **1**–**5** and primary structure of **V35** and **V35-Fluo**.

coordination with central monovalent cations.[14,15] The melting temperatures of G4s are typically higher than the physiological temperature, and the existence in vivo of G4s in human cells was recently demonstrated.[16,17] To improve both the resistance to nucleases and the kinetics of quadruplex formation, we initiated a study aimed at the synthesis of a series of new monomolecular analogues of SA-1042 by exploiting the Tetra-End-Linker (TEL)-oligonucleotides strategy.[18,19] By varying the TEL size and position and by changing the fifth and sixth nucleobases in SA-1042, we selected the TEL-(3′GGGGGT5′TBDPS)$_4$ species (**4**, Figure 1) as the best candidate for further SAR studies.[20,21]

EXPERIMENTAL PROCEDURES

General Instrumentation. Automated solid phase oligonucleotide synthesis was performed on a 8909 DNA-Synthesizer (Applied Biosystems). Mass spectra of peptides were recorded by using a MALDI-TOF-MS, Voyager DE STR MALDI TOF mass spectrometer. CD measurements were performed on a JASCO J-715 spectropolarimeter equipped with a Peltier Thermostat JASCO ETC-505T using 0.1 cm path length cuvettes. NMR spectra were acquired on Varian ^{UNITY}INOVA 500 MHz, 700 MHz and Mercury Plus 400 MHz spectrometers and processed using the iNMR software package (http://www.inmr.net). For the experiments in H_2O, water suppression was achieved by including a double pulsed-field gradient spin-echo (DPFGSE) module[26,27] in the pulse sequence prior to acquisition. Chemical shifts are reported in parts per million (δ) relative to the residual solvent signals.

Synthesis of TEL–ODNs 1–3. TEL–aptamers TEL–(3′GGGGT5′-TBDPSi)$_4$ (**1**), TEL–(3′GGGT5′-TBDPSi)$_4$ (**2**), and TEL–(3′GGT5′-TBDPSi)$_4$ (**3**) were chemically synthesized according to the previously described procedure.[20] After automated solid phase synthesis, the oligonucleotides were detached from the support and deprotected using a 33% aqueous ammonia solution at 55 °C for 17 h. The combined filtrates and washings were dried, redissolved in water, analyzed, and purified by HPLC on C-18 reverse phase column (Purosphere STAR, 5 μm, 250 × 10 mm, Merck) using a linear gradient from 0 to 100% B in 30 min, flow rate = 1.2 mL/min, and detection at 260 nm (eluent A: TEAB 0.1 M; eluent B: CH_3CN). The retention time of **1** (24 min), **2** (24.5 min), and **3** (26 min) corresponded to that of the most retained pick in each HPLC profile due to the presence of the terminal TBDPS lipophilic groups.

TEL–ODN Samples Annealing. 1–5 were dissolved in 100 mM potassium buffer (10 mM KH_2PO_4 aq. solution containing 90 mM KCl, pH 7.0), and the corresponding quadruplexes were formed by heating at 90 °C for 5 min and slowly cooling at room temperature for 12 h. Samples were stored at 4 °C for 24 h before measurements. TEL–ODNs concentrations were determined in water by measuring the absorbance at 260 nm at 90 °C using the nearest-neighbor calculated molar extinction coefficient (ε) of d(5′TG$_n$3′) (for **1**–**4**) or d(5′TGGGGT3′) (for **5**) multiplied by 4 (the number of strands in each TEL–ODN complex). A contribution of 8658 cm^{-1} M^{-1} was added for each TBDPS group;[28] **1**: calculated ε = 231 832 cm^{-1} M^{-1}; **2**: calculated ε = 191 432 cm^{-1} M^{-1}; **3**: calculated ε = 151 032 cm^{-1} M^{-1}; **4**: calculated ε = 272 232 cm^{-1} M^{-1} (from ref 21); **5**: calculated ε = 265 832 cm^{-1} M^{-1} (from ref 21).

CD Spectroscopy Measurements. TEL–ODN samples (2×10^{-5} M) were annealed as described above and stored at 4 °C overnight before measurements. CD spectra of **1**–**3** (Figure S-2, left panels) alone or mixed with **V35-Fluo** or **V35-Fluo-oxi** at 1.5:1 aptamer/peptide ratio (data not shown) were recorded at 25 °C in the 360–200 nm wavelength range as an average of 5 scans (100 nm/min, 1 s response time, 1 nm bandwidth) and normalized by subtraction of the background scan containing only the buffer. Thermal denaturation experiments on **1**–**3** alone (Figure S-2, right panels) or mixed with **V35-Fluo** or **V35-Fluo-oxi** (data not shown) were also carried out in the

DOI: 10.1021/acs.analchem.5b04268
Anal. Chem. XXXX, XXX, XXX–XXX

temperature range of 20−90 °C by monitoring CD values at 264 nm at a heating rate of 0.5 °C/min. The CD data of aptamer/peptide mixtures were all superimposable with those of the corresponding aptamer alone.

Manual Synthesis and Characterization of V35 and V35-Fluo. The peptide synthesis (Scheme S-1) was done manually using the Fmoc chemistry solid phase approach on a 2-chlorotrityl Resin (0.312 g, 0.8 mmol/g), swelled for 30 min in DCM.[29,30] The first coupling was carried out using 1.0 equiv of N^{α}-Fmoc-Cys(Trt)-OH, dissolved in 5 mL of DCM. The amino acid solution was added to 2-chlorotrityl Resin. To this mixture was added 1.0 equiv of DIEA, agitated in the shaker for 10 min, and then was added 1.5 equiv of DIEA. The mixture was agitated vigorously for 60 min. To end-cap any remaining reactive 2-chlorotrityl groups, a mixture of DCM/MeOH/DIEA (80%:15%:5%) was added and mixed for 30 min. For removing the Fmoc protecting group from the first amino acid, the resin was suspended in a 25% solution of piperidine in DMF (1 × 5 min and 1 × 20 min). The following protected amino acids were then added stepwise, N^{α}-Fmoc-His(Trt)-OH, N^{α}-Fmoc-Ala-OH, N^{α}-Fmoc-Gln(Trt)-OH, N^{α}-Fmoc-Arg-(Pbf)-OH, N^{α}-Fmoc-Ile-OH, N^{α}-Fmoc-Asp(OtBu)-OH, N^{α}-Fmoc-Gly-OH, N^{α}-Fmoc-Glu-OH, N^{α}-Fmoc-Thr(tBu)-OH, N^{α}-Fmoc-Tyr(tBu)-OH, N^{α}-Fmoc-Phe-OH, N^{α}-Fmoc-Lys-(Boc)-OH, N^{α}-Fmoc-His(Trt)-OH, N^{α}-Fmoc-Asn(Trt)-OH, N^{α}-Fmoc-Asp(OtBu)-OH, and N^{α}-Fmoc-Cys(Trt)-OH. Each coupling reaction was accomplished using a 3-fold excess of amino acid with HBTU and HOBt in the presence of DIEA. The N^{α}-Fmoc protecting groups were removed by treating the protected peptide resin with a 20% solution of piperidine in DMF (1 × 5 min and 1 × 20 min). The peptide resin was washed three times with DCM, and the next coupling step was initiated in a stepwise manner. The peptide resin was washed with DCM (3×) and DMF (3×), and the deprotection protocol was repeated after each coupling step. The N-terminal Fmoc group was removed as described above. Fluorescein 5-carboxyfluorescein, coupling on the free N-terminal in **V35-Fluo**, was carried out using 1.5 equiv of 5-FAM and 3.0 equiv of DIPEA in DCM:DMF 1:1 by volume. The peptide was released from the resin with TFA/Et_3SiH/H_2O 90:5:5 for 3 h. The resin was removed by filtration, and the crude peptide was recovered by precipitation with cold anhydrous ethyl ether to give a white powder which was purified by RP-HPLC on a semipreparative C18-bonded silica column (Phenomenex, Jupiter 4 μ Proteo 90 Å, 1.0 × 25 cm) using a gradient of CH_3CN in 0.1% aqueous TFA (from 10% to 90% in 40 min) at a flow rate of 5.0 mL/min. The product was obtained by lyophilization of the appropriate fractions after removal of the CH_3CN by rotary evaporation. Analytical RP-HPLC (Figure S-5) indicated for all synthesized compounds a purity of >95%, and the correct molecular weights were confirmed by MALDI-TOF-MS; **V35**: purified purity: 95.83%; t_R: 8.992 (analytical μHPLC, 10% to 90% acetonitrile in water (0.1% TFA) over 25 min, flow rate of 1.0 mL/min); MALDI-TOF-MS for chemical formula $C_{166}H_{269}N_{57}O_{49}S_2$, calculated mass m/z $[M + H]^+$ 3912.21, found 3912.45. **V35-Fluo**: purified purity: 95.45%; t_R: 9.512 (analytical μHPLC, 10% to 90% acetonitrile in water (0.1% TFA) over 25 min, flow rate of 1.0 mL/min); MALDI-TOF-MS for chemical formula $C_{187}H_{279}N_{57}O_{55}S_2$, calculated mass m/z $[M + H]^+$ 4270.32, found 4270.73.

Fluorescence Measurements. 50 μL of a final solution containing 50 nM **V35-Fluo** or **V35-Fluo-oxi** in K^+ buffer (10 mM KH_2PO_4 aq. solution containing 90 mM KCl, pH 7.0) was incubated in 96 well black Optiplates (PerkinElmer) with or without the indicated amount of aptamers. Five minutes after the incubation, the plates were inserted in a 2104 Envision Multilabel plate reader (PerkinElmer). Each sample was excited with Envision filter 102 (485 ± 14 nM; 60% T) (PerkinElmer) and fluorescence filtered with an emission filter Envision filter 206 (535 ± 25 nM; 50% T) (PerkinElmer) using a normal top mirror. For the time course experiments, the measurements were done in a continuous mode with time intervals of 0.5 min. After 5 and 50 min, the indicated amount of **1**−**5** and **V35** or **V35-oxi** (25 μM) dissolved in K^+ buffer was added to each well, respectively. The addition was performed using the automatic liquid dispenser of the Envision. Plots were fitted in Prism5 (GraphPad Software Inc., La Jolla, CA) using an inhibition sigmoidal curve to calculate IC_{50}.

Oxidation of V35-Fluo with DTT/DIA. A final concentration of 2 mM of DL-dithiothreitol (DTT) was added to a solution containing 60 μM of **V35-Fluo**. The solution was gently stirred for 2 h to obtain the preliminary intermolecular and intramolecular disulfide bridges reduction. The sample was then treated with 4 mM of the oxidizing agent *N,N,N′,N′*-tetramethylazodicarboxamide (DIA) and analyzed by RP-HPLC on a semipreparative C18-bonded silica column (Phenomenex, Jupiter 4μ Proteo 90 Å, 1.0 × 25 cm) using a gradient of CH_3CN in 0.1% aqueous TFA (from 10% to 90% in 40 min) at a flow rate of 5.0 mL/min to compare the retention times before and after the treatment with the reducing and oxidizing reagents (Figure S5).

Docking Protocol. The HIV gp120 protein structure was downloaded by the Protein Data Bank (PDB ID 2B4C). The molecular models of TEL−ODNs were manually generated using the InsightII suite of programs (Accelrys, Inc.). The Biopolymer module was employed to make the quadruplexes; the Builder module was used to add the modified linkers at 3′- and 5′-ends, and the Discovery3 module was applied to bring the molecular models to their energetically minimized structures after parametrization with the AMBER force field. The minimization steps were performed with a distance-dependent macroscopic dielectric constant of 4.0 and an infinite cutoff for nonbonded interactions, using 1000 cycles of the steepest descent method followed by conjugate gradient calculation until convergence at 0.1 rms was reached. Notably, the Hoogsteen H-bonds maintaining the geometry of the G-tetrads of **1** and **2** were kept during the minimization procedure. Conversely, those of the G-tetrads of **3** were lost, because they were affected by the presence of the TEL at the 3′-end and TBDPS groups at the 5′-end. The ZDOCK server (http://zdock.umassmed.edu)[22] was used to perform all the dockings between the TEL−ODNs and the V3 loop in gp120. The program uses a fast Fourier transform to perform a 3D search of all possible binding modes in the translational and rotational space between the two molecules and evaluates each pose by utilizing a pairwise statistical potential in the scoring function. The resulting output is a list of transformation values, from which models can be generated.[31] A list of 2000 transformations was calculated for each docking, ranked on the basis of the internal scoring functions, and presented through a global energy term. The best solution from each dock was taken into account, and to relieve any steric clashes that might have arisen in docking, the chosen models underwent a further minimization process with no restraints. Finally, the PyMOL Molecular Graphics System (Version 1.5.0.4 Schrö-

DOI: 10.1021/acs.analchem.5b04268
Anal. Chem. XXXX, XXX, XXX−XXX

dinger, LLC) was used to visualize the binding between protein and aptamer and to define their electrostatic interactions.

Anti-HIV Activity Assays. Inhibition of HIV-1(III_B)- and HIV-2(ROD)-induced cytopathicity in CEM cell cultures was measured in microtiter 96-well plates containing ~3 × 10^5 CEM cells/mL infected with 100 $CCID_{50}$ of HIV per milliliter and containing appropriate dilutions of the test compounds. After 4−5 days of incubation at 37 °C in a CO_2-controlled humidified atmosphere, CEM giant (syncytium) cell formation was examined microscopically (Figure S-6). The EC_{50} (50% effective concentration) was defined as the compound concentration required to inhibit HIV-induced giant cell formation by 50%.

Cocultivation Assays. After washing persistently HIV-1-infected Hut-78/HIV-1 cells to remove free virions, 10^5 Hut-78/HIV-1 cells were added to 10^5 SupT1 cells in 200 μL wells of a 96-well plate. The appropriate concentrations of the test compounds were added at 5-fold serial dilutions ranging between 100 and 0.006 μg/mL. After 20 h of incubation at 37 °C, the cells were microscopically examined for syncytia formation. The EC_{50} was calculated as the concentration of an agent required to suppress syncytia formation by 50%.

RESULTS AND DISCUSSION

Using our new screening platform, we here measured the activity of three shorter analogues of **4** in which the four TGGGGG strands were shortened by one, two, or three guanosines (**1**−**3** in Figure 1, respectively) to ease their synthetic production on larger scale. At first, we started anticipating the binding of the putative TEL−aptamers **1**−**3** to the V3 loop by performing an in silico molecular study by docking **1**−**3** to the V3 loop of gp120 (PDB ID 2B4C)[13] using the ZDOCK server.[22] The results showed that **1**−**3** can indeed bind the V3 loop by direct interaction of the phosphate backbone atoms and the heteroatoms of the guanines. In particular, in all the complexes, the phosphates of three different strands interact with the side chains of Thr195, Thr194, and Tyr193 defining a common binding site (Figure 2). Furthermore, the side chain of Arg181 plays a key role for the specificity of the binding, being the only one to interact directly with the guanines involved in the formation of G-tetrads. Additional H-bond and electrostatic interactions, responsible for the different interaction energies of the three complexes, are listed in Table S-1. The results of the computational docking study confirmed in full the aptness of **1**−**3** to bind the V3 loop and gave us confidence about their potentiality as new anti-HIV aptamers.

Accordingly, TEL−aptamers **1**−**3** were synthesized and purified following a previously described procedure,[21] and CD and NMR measurements were performed to assess whether the reduction in the ODN length affected the ability of **1**−**3** to fold into the expected parallel TEL-G4s. Before measurements, the samples were annealed in 100 mM K^+ buffer and stored at 4 °C overnight. The NMR (Figure S-1) and CD spectra (Figure S-2) of **1** and **2** supported the presence in solution of parallel G4s, whereas the data did not confirm the ability of **3** to fold into the desired G4 structure, at least in the used annealing buffer. In fact, the characteristic imino proton signals (10−12 ppm) of the exchange-protected imino protons of guanosines involved in the formation of G-tetrads,[23] and CD profiles having a minimum at about 240 nm and a maximum at about 260 nm, indicative for the presence in solution of parallel

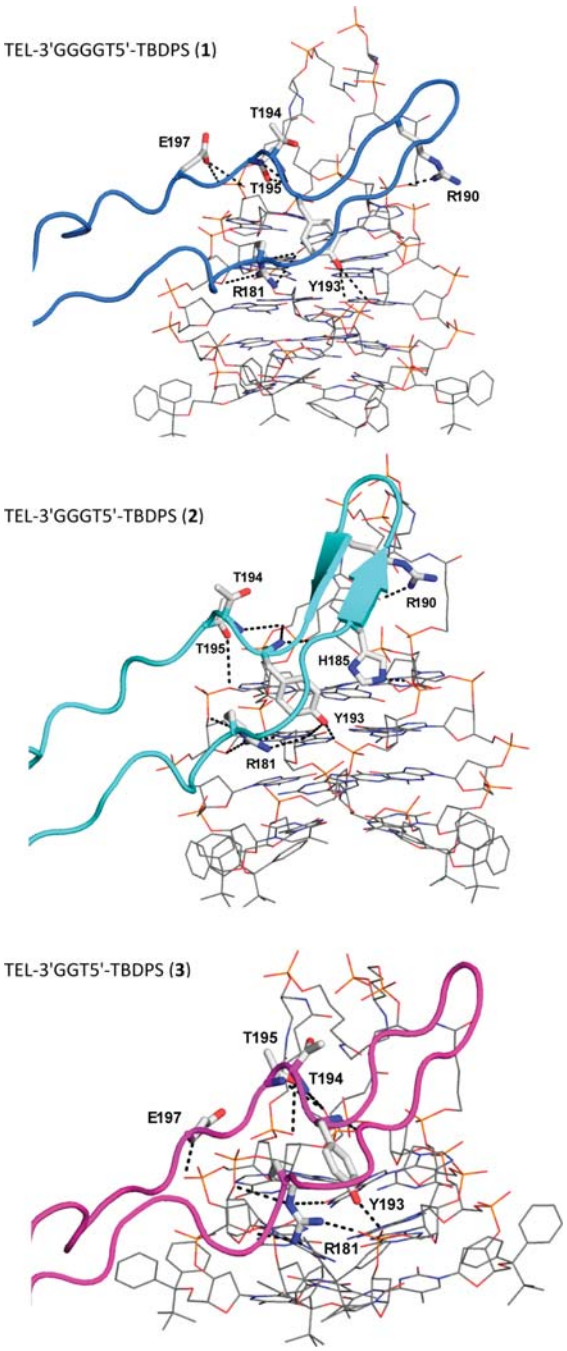

Figure 2. Molecular models of the interactions between aptamers **1**−**3** and the V3 loop of gp120. The aptamers are drawn as lines; the V3 loop is shown as a cartoon, and hydrogen bonding interactions between the V3 loop and the aptamers are drawn as dashed lines.

G4 species,[24] were observed only in the NMR and CD spectra, respectively, of TEL−ODNs **1** and **2**.

Differently from the existing screening platforms that use the full-length gp120 to measure the binding affinity of new aptamers, we attempted to assess the affinity of **1**−**3** for gp120 by using a 35 amino acids long peptide (**V35** in Figure 1), as a

DOI: 10.1021/acs.analchem.5b04268
Anal. Chem. XXXX, XXX, XXX−XXX

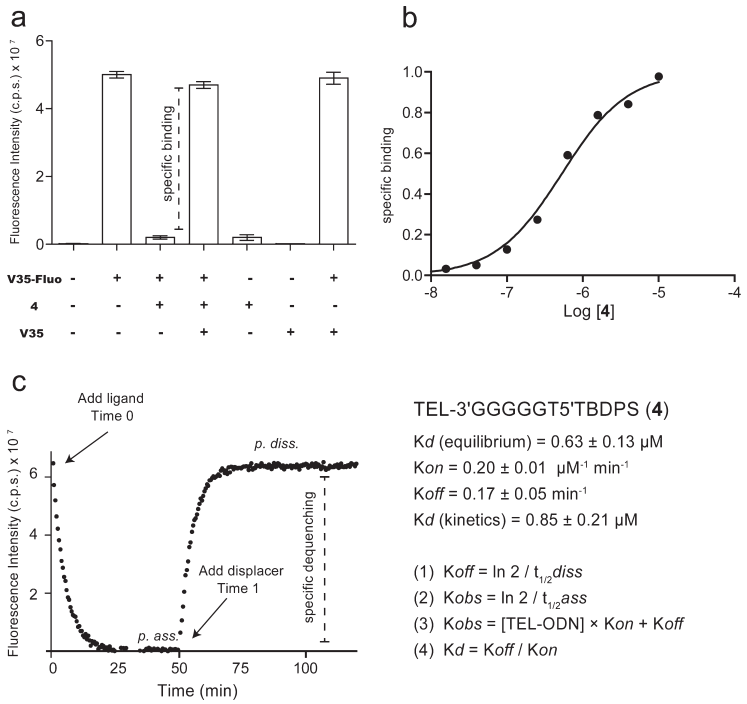

Figure 3. Affinity of **4** for **V35-Fluo**. Equilibrium binding: (a) 50 nM **V35-Fluo**, 10 μM **4**, and 25 μM **V35** were mixed according the scheme. Specific binding correlates with the amount of **V35-Fluo** fluorescence dequenched in the presence of an excess of **V35**. (b) **V35-Fluo** was incubated with the indicated concentration of **4**. Specific binding values (normalized to the maximum response) are plotted vs concentration of the aptamer. Kinetic binding: (c) Binding of **4** to **V35-Fluo** was measured in a time course experiment. At time 0, **4** (10 μM) was added to **V35-Fluo** (50 nM) and fluorescence was recorded at 0.5 min time intervals. Then, **V35** (25 μM) was added (Time 1) to displace **4** specifically bound to **V35-Fluo** (association plateau, p_{ass}, and dissociation plateau, p_{diss}, are indicated).

Table 1. Equilibrium Binding Parameters (Kd, μM) of TEL−ODNs 1−5 for V35-Fluo and V35-Fluo-oxi

peptide	1	2	3	4	5
V35-Fluo	0.79 ± 0.16	1.26 ± 0.47	10.0 ± 2.1	0.63 ± 0.13	≫10
V35-Fluo-oxi	0.20 ± 0.07	0.20 ± 0.04	0.50 ± 0.25	0.10 ± 0.02	6.3 ± 2.3

synthetic mimic of the V3 loop, using a fluorescence quenching assay.[25] Hence, fluorescein isothiocyanate (FITC) was installed at the N-terminal cysteine of **V35** to give the fluorescently labeled peptide **V35-Fluo** as described in Scheme S-1. The amino acids sequence we chose for **V35-Fluo** matched that of the V3 loop used for the docking simulations. **V35** and **V35-Fluo** were manually synthesized using the Fmoc-based solid phase approach, purified by RP-μHPLC, and characterized by electrospray mass spectrometry.

Equilibrium and kinetic binding experiments were initially performed by incubating **V35-Fluo** with **4**, whose binding with the gp120 V3 loop was already studied by SPR.[21] In the presence of **4**, the fluorescence signal of **V35-Fluo** decreased compared to that of the same amount of peptide dissolved in pure buffer (Figure 3a). Fluorescence quenching could be ascribed specifically to **V35-Fluo** binding to the aptamer since, in the presence of an excess of unconjugated **V35**, the fluorescence signal of **V35-Fluo** was not affected by the addition of **4** (Figure 3a). Quenching (or increase) in fluorescence of a FITC tagged molecule can be expected upon an event of binding mainly because of the change in the environment surrounding the fluorescence moiety and thus affecting its emission. Specific binding (amount of **V35-Fluo** fluorescence recovered upon addition of an excess of **V35**) was measured for several dilutions of **4** and resulted in an equilibrium K_d value of 0.63 ± 0.13 μM for **V35-Fluo** (Figure 3b). The binding of **4** to **V35-Fluo** was also measured in a time course experiment at 0.5 min time intervals. Upon addition of **4** (Time 0; Figure 3c), a decrease in fluorescence was observed. Then, **V35** was added (Time 1) to displace **4** specifically bound to **V35-Fluo**. As already seen with the measurements at equilibrium, the addition of **V35** allowed **V35-Fluo** to regain its original fluorescence. The half time needed to displace **4** by **V35-Fluo** directly correlates to its apparent k_{off} rate (eq 1 in Figure 3). k_{off} rate of displacement resulting from our measurement was 0.17 ± 0.05 min^{-1}. k_{obs} directly correlates with the half time of association of **4** and together with the measured k_{off} can be used to calculate the apparent k_{on} and K_d (eq 2−4 in Figure 3). K_{on} and K_d measured by kinetic measurements were 0.20 ± 0.01 μM^{-1} min^{-1} and 0.85 ± 0.21 μM, respectively.

Given the positive outcome from pilot experiments on **4**, **V35-Fluo** was used to estimate the affinity of the new aptamers **1**−**3** for the V3 loop of gp120. The fluorescent assay was also performed on **5**, a quadruplex forming analogue of **1**−**3** lacking marked anti-HIV activity,[21] and the specific binding and

DOI: 10.1021/acs.analchem.5b04268
Anal. Chem. XXXX, XXX, XXX−XXX

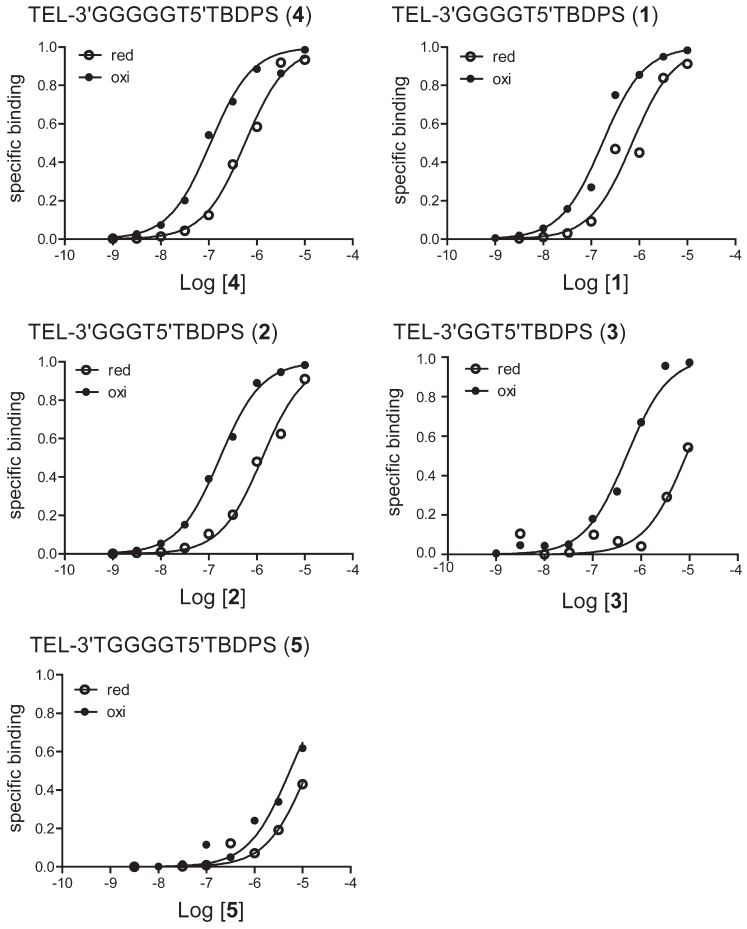

Figure 4. Affinity of TEL−ODNs **1**−**5** for reduced **V35-Fluo** (red, empty circles) and oxidized **V35-Fluo-oxi** (oxi, full circles).

equilibrium K_d of **1**−**3** and **5** were obtained as done for **4**. The results shown in Table 1 and in Figure S-3 indicated that **1** and **2** retain almost the same binding affinity as **4** for **V35-Fluo**, whereas weaker specific binding and higher K_d values were found for **3** and **5**.

Despite the fluorescence assay set on synthetic **V35-Fluo** discriminated well among aptamers binding to gp120 with high or low affinity, the K_d measured for **4** was somehow higher than that measured by SPR for the full length gp120 (0.8 vs 0.2 μM).[21] We thought that one of the possible reasons for this decreased affinity could have been the 3D conformation adopted by **V35-Fluo** in solution. In fact, in the crystal structure 2B4C, the V3 loop acquires a hairpin conformation stabilized by a disulfide bond (Cys173 and Cys207). This arrangement could influence the binding site for the aptamer that in turn could bind better to a structured than to an unstructured V3 loop. To stabilize **V35-Fluo** in a conformation similar to the one adopted in the full-length gp120, we oxidized **V35-Fluo** in a redox dithiothreitol/diamide (DTT/DIA) buffer in an attempt to create a disulfide bond between Cys1 and Cys35 (**V35-Fluo-oxi**).

As shown by the chromatographic profile in Figure S-4, **V35-Fluo-oxi** runs as a discrete monomeric peak proving the oxidation reaction successful and excluding the presence of covalently linked dimers, oligomers, and aggregates. Then, we measured the affinity of **V35-Fluo-oxi** for **1**−**5**. While the affinity for **5** was still very low, the affinities (K_d values) of the oxidized peptide for **1**−**4** were much higher than those of the untreated peptide (Figure 4 and Table 1), thus confirming the preference of the aptamers to interact with the **V35-Fluo** peptide endowed with a specific conformation. In particular, after the oxidation of **V35-Fluo**, the binding affinity of **1** and **2** for **V35-Fluo-oxi** reached that of the parent aptamer **4** previously measured by SPR.

The anti-HIV activity of **1**−**3** against HIV-1 and HIV-2 was determined in vitro by measuring the concentration of aptamer required to reduce the virus-induced cytopathicity by 50% (EC_{50}) in human $CD4^+$ T-lymphocyte CEM cell cultures. All shorter analogues of **4** retained a potent anti-HIV activity, with EC_{50} values in the submicromolar range (see Table 2). It is noteworthy that, in agreement with the molecular docking and fluorescence quenching studies, also the shortest aptamer **3** still displayed a submicromolar anti-HIV activity (EC_{50} = 0.74 μM), notwithstanding its CD and NMR spectra did not confirm the structuration into a stable G4 structure. Considering that in a previous paper[21] we demonstrated that neither the TEL nor the TBDPS groups themselves, but the formation of a stable G4, is responsible for the anti HIV activity of TEL analogues of the Hotoda's aptamer, the latter observation suggests that **3** could finally fold into the bioactive G4 in the presence of the full

DOI: 10.1021/acs.analchem.5b04268
Anal. Chem. XXXX, XXX, XXX−XXX

Table 2. Anti-HIV Studies on TEL−ODNs 1−5

	EC_{50}[a] (μM)		IC_{50}[b] (μM)	
	HIV-1	HIV-2	HUT-78/HIV-1+SupT1	CC_{50}[c] (μM)
1	0.18 ± 0.0071	6.3 ± 0.71	3.9 ± 0.21	>100
2	0.16 ± 0.028	1.3 ± 0.21	1.8 ± 1.3	>100
3	0.74 ± 0.11	5.1 ± 0.92	10 ± 0.7	>100
4	0.041 ± 0.007[d]	≥2[d]		>2[d]
5	≥2[d]	2[d]		>2[d]

[a]EC_{50} = 50%-effective concentration or concentration required to protect CEM cells against the cytopathicity of HIV by 50%. [b]IC_{50} = 50%-inhibitory concentration or compound concentration required to inhibit syncytium formation in cocultures of HUT-78/HIV-1 and SupT1 cells by 50%. [c]CC_{50} = 50%-cytostatic concentration or compound concentration required to inhibit CEM cell proliferation by 50%. [d]Data taken from ref 21.

gp120 protein. **1**−**3** were also evaluated for their inhibitory activity against the syncytia formation in cocultures of persistently HIV-1-infected HUT-78/HIV-1 cells and $CD4^+$ T-lymphocyte SupT1 cells. **1** and **2** markedly inhibited the syncytia formation in the low micromolar range.

In conclusion, we here propose a new screening platform toward aptamers targeting the HIV gp120. Candidates are selected and ranked by molecular docking simulations and assayed for their binding affinity to the V3 loop of gp120 using a fluorescence quenching assay. Three new shorter analogues (**1**−**3**) of the anti-HIV aptamer **4** were synthesized and tested. Although the anti HIV activities of **1**−**3** were not higher than that of their precursor **4**, the almost perfect correspondence between the calculated binding affinities and the experimental EC_{50} values in HIV-infected cells confirmed in full the reliability of this rapid and cost-effective alternative to the existing methods for selecting new aptamers and measuring aptamer−protein equilibria.

■ ASSOCIATED CONTENT

Supporting Information

The Supporting Information is available free of charge on the ACS Publications website at DOI: 10.1021/acs.analchem.5b04268.

Molecular models of top dock structures; table of interactions, interaction energies, number of H-bonds between **1**−**3** and the V3 loop; NMR spectra of **1**−**3**; CD spectra and CD melting of **1**−**3**; synthetic scheme for the obtainment of **V35** and **V35-Fluo**; specific binding of **1**−**3** and **5** for **V35-Fluo**; HPLC purification of **V35** and **V35-Fluo**; HPLC profiles of **V35-Fluo** before and after oxidation with DTT/DIA. (PDF)

■ AUTHOR INFORMATION

Corresponding Author

*E-mail: nicola.borbone@unina.it. Fax: +39 081 678552.

Author Contributions

[‖]G.O. and M.S. contributed equally to this work.

Author Contributions

G.O. designed the study and contributed to synthesis of TEL−aptamers. M.S. performed the fluorescence-quenching experiments and wrote the paper. V.D. performed the molecular docking simulations. A.M.Y., P.G., L.M., and A. C. proposed the use and synthesized the labeled and unlabeled peptides used in the study. F.N. performed CD characterization. S.D. and G.P. contributed to the synthesis and purification of TEL−aptamers. G.P., L.M., and E.N. contributed to the design of the study. S.N., S.L., and J.B. performed biological assays on HIV-infected human cell cultures. N.B. designed the study, performed the NMR characterization, coordinated the activity of the different research groups, and wrote the paper. All authors approved the manuscript and this submission.

Notes

The authors declare no competing financial interest.

■ ACKNOWLEDGMENTS

This research was funded by Regione Campania under POR Campania FESR 2007-2013-O.O. 2.1 (FarmaBioNet).

■ REFERENCES

(1) Phan, A. T.; et al. *Proc. Natl. Acad. Sci. U.S.A.* **2005**, *102* (3), 634−639.

(2) Di Fabio, G.; D'Onofrio, J.; Chiapparelli, M.; Hoorelbeke, B.; Montesarchio, D.; Balzarini, J.; De Napoli, L. *Chem. Commun.* **2011**, *47* (8), 2363−2365.

(3) Sánchez-Luque, F. J.; Stich, M.; Manrubia, S.; Briones, C.; Berzal-Herranz, A. *Sci. Rep.* **2014**, *4*, 6242.

(4) Held, D. M.; Kissel, J. D.; Patterson, J. T.; Nickens, D. G.; Burke, D. H. *Front. Biosci., Landmark Ed.* **2006**, *11*, 89−112.

(5) Khati, M.; Schüman, M.; Ibrahim, J.; Sattentau, Q.; Gordon, S.; James, W. *J. Virol.* **2003**, *77* (23), 12692−12698.

(6) Zhou, J.; Li, H.; Li, S.; Zaia, J.; Rossi, J. J. *Mol. Ther.* **2008**, *16* (8), 1481−1489.

(7) Neff, C. P.; Zhou, J.; Remling, L.; Kuruvilla, J.; Zhang, J.; Li, H.; Smith, D. D.; Swiderski, P.; Rossi, J. J.; Akkina, R. *Sci. Transl. Med.* **2011**, *3* (66), 66ra6−66ra6.

(8) Shum, K.-T.; Zhou, J.; Rossi, J. J. *Pharmaceuticals* **2013**, *6* (12), 1507−1542.

(9) Musumeci, D.; Riccardi, C.; Montesarchio, D. *Molecules* **2015**, *20* (9), 17511−17532.

(10) Virgilio, A.; Esposito, V.; Citarella, G.; Mayol, L.; Galeone, A. *ChemBioChem* **2012**, *13*, 2219.

(11) Hotoda, H.; Momota, K.; Furukawa, H.; Nakamura, T.; Kaneko, M.; Kimura, S.; Shimada, K. *Nucleosides Nucleotides* **1994**, *13* (6−7), 1375−1395.

(12) Wyatt, J. R.; Vickers, T. A.; Roberson, J. L.; Buckheit, R. W.; Klimkait, T.; Debaets, E.; Davis, P. W.; Rayner, B.; Imbach, J. L.; Ecker, D. J. *Proc. Natl. Acad. Sci. U. S. A.* **1994**, *91* (4), 1356−1360.

(13) Huang, C.-C.; Tang, M.; Zhang, M.-Y.; Majeed, S.; Montabana, E.; Stanfield, R. L.; Dimitrov, D. S.; Korber, B.; Sodroski, J.; Wilson, I. A.; Wyatt, R.; Kwong, P. D. *Science* **2005**, *310* (5750), 1025−1028.

(14) Parkinson, G. N. In *Quadruplex Nucleic Acids*; Neidle, S., Balasubramanian, S., Eds.; Royal Society of Chemistry: London, 2006; pp 1−30.

(15) Davis, J. T. *Angew. Chem., Int. Ed.* **2004**, *43* (6), 668−698.

(16) Biffi, G.; Tannahill, D.; McCafferty, J.; Balasubramanian, S. *Nat. Chem.* **2013**, *5* (3), 182−186.

(17) Biffi, G.; Di Antonio, M.; Tannahill, D.; Balasubramanian, S. *Nat. Chem.* **2014**, *6* (1), 75−80.

(18) Oliviero, G.; Borbone, N.; Galeone, A.; Varra, M.; Piccialli, G.; Mayol, L. *Tetrahedron Lett.* **2004**, *45* (25), 4869−4872.

(19) Oliviero, G.; Amato, J.; Borbone, N.; Galeone, A.; Petraccone, L.; Varra, M.; Piccialli, G.; Mayol, L. *Bioconjugate Chem.* **2006**, *17* (4), 889−898.

(20) Oliviero, G.; Amato, J.; Borbone, N.; D'Errico, S.; Galeone, A.; Mayol, L.; Haider, S.; Olubiyi, O.; Hoorelbeke, B.; Balzarini, J.; Piccialli, G. *Chem. Commun.* **2010**, *46* (47), 8971−8973.

(21) D'Atri, V.; Oliviero, G.; Amato, J.; Borbone, N.; D'Errico, S.; Mayol, L.; Piccialli, V.; Haider, S.; Hoorelbeke, B.; Balzarini, J.; Piccialli, G. *Chem. Commun.* **2012**, *48* (76), 9516−9518.

DOI: 10.1021/acs.analchem.5b04268
Anal. Chem. XXXX, XXX, XXX−XXX

(22) Pierce, B. G.; Wiehe, K.; Hwang, H.; Kim, B.-H.; Vreven, T.; Weng, Z. *Bioinformatics* **2014**, *30* (12), 1771−1773.
(23) Adrian, M.; Heddi, B.; Phan, A. T. *Methods* **2012**, *57* (1), 11−24.
(24) Vorlícková, M.; Kejnovská, I.; Sagi, J.; Renčiuk, D.; Bednárová, K.; Motlová, J.; Kypr, J. *Methods* **2012**, *57* (1), 64−75.
(25) Bruno, A.; Lembo, F.; Novellino, E.; Stornaiuolo, M.; Marinelli, L. *Sci. Rep.* **2014**, *4*, 3757.
(26) Hwang, T. L.; Shaka, A. J. *J. Magn. Reson., Ser. A* **1995**, *112* (2), 275−279.
(27) Dalvit, C. *J. Biomol. NMR* **1998**, *11* (4), 437−444.
(28) D'Onofrio, J.; Petraccone, L.; Erra, E.; Martino, L.; Di Fabio, G.; De Napoli, L.; Giancola, C.; Montesarchio, D. *Bioconjugate Chem.* **2007**, *18* (4), 1194−1204.
(29) Young, J. D.; Stewart, J. M. *Solid phase peptide synthesis*; Pierce Chemical Co.: Rockford, IL, 1984.
(30) Barlos, K.; Gatos, D.; Schäfer, W. *Angew. Chem., Int. Ed. Engl.* **1991**, *30* (5), 590−593.
(31) Pierce, B. G.; Hourai, Y.; Weng, Z. *PLoS One* **2011**, *6* (9), e24657.

DOI: 10.1021/acs.analchem.5b04268
Anal. Chem. XXXX, XXX, XXX−XXX

DOI: 10.1002/ejoc.201403648

Synthesis of C^6-Pyridylpurine Nucleosides by Reaction of Nebularine N^1-Oxide with Pyridinyl Grignard Reagents

Stefano D'Errico,[a] Giorgia Oliviero,*[a] Nicola Borbone,[a] Fabrizia Nici,[a] Vincenzo Piccialli,[b] Brunella Pinto,[a] Daniele D'Alonzo,[b] Luciano Mayol,[a] and Gennaro Piccialli[a]

Keywords: Synthetic methods / Grignard reaction / Transmetallation / Nucleosides / Nucleobases

A general synthesis of C^6-pyridylpurine nucleosides is described. The reported synthetic procedure exploits the regioselective addition of pyridinyl Grignard reagents, obtained by bromine/magnesium exchange between mono- or dihalopyridines and *i*PrMgCl, to the C6–N1–O$^-$ moiety of nebularine N^1-oxide. The regioselective transmetallation of unsymmetrical dihalopyridines with *i*PrMgCl allowed C^6-halopyridylpurine nucleosides to be obtained through the addition of halopyridinyl Grignard reagents. The presence of a halogenated pyridine ring in these nucleosides allows for further useful synthetic transformations.

Introduction

Natural nucleosides and nucleotides play a central role in cell metabolism and in signal transduction, acting as synthetic precursors and regulatory agents. In addition, they are substrates of polymerases and, in some cases, can control the activity of these enzymes so as to regulate nucleic acid construction. Several nucleoside and nucleotide analogues have been approved for the treatment of viral diseases and some of them are in clinical trials for cancer treatment.[1] Therefore the preparation of modified nucleosides and nucleotides continues to attract the interest of chemical and biomedical research. Modifications of nucleobases can affect the hydrogen-bonding patterns and base-pairing in nucleic acids or confer on them peculiar properties such as fluorescence, which allows monitoring of their fate in cells and analysis of DNA and RNA structures.[2] Purine nucleosides bearing a C substituent at C-6 represent an important subclass of nucleoside analogues possessing a broad spectrum of biological activities[3] and this has prompted synthetic efforts towards these substances. The introduction of C substituents at C-6 in the purine nucleus has been mostly accomplished by metal-mediated cross-coupling processes starting from 6-halopurines,[3b,4] whereas N, O, and S substituents have been introduced by direct nucleophilic aromatic substitution.[5] We have recently discovered a new approach to accessing C^6-alkyl/aryl nucleosides. In particular, we observed that the sugar-protected nebularine N^1-oxide[6a] (**1**, Scheme 1) can regioselectively react with Grignard reagents at the more electrophilic C-6 position leading to adduct **2**, which is re-aromatized by treatment with Ac_2O/pyridine to furnish the C^6-substituted purine nucleoside **3** in high yields. We have also shown that a second alkyl/aryl substituent can be introduced at C-2 by a similar strategy, that is, by the addition of a Grignard reagent to the C^6-substituted nebularine N^1-oxides **4** through the opening/reclosing of the pyrimidine ring induced by the Grignard reagent itself. Through this approach we have synthesized new collections of 6-alkyl(aryl)purine nucleosides **3** and 2,6-dialkyl(aryl)purine nucleosides **5**.[6]

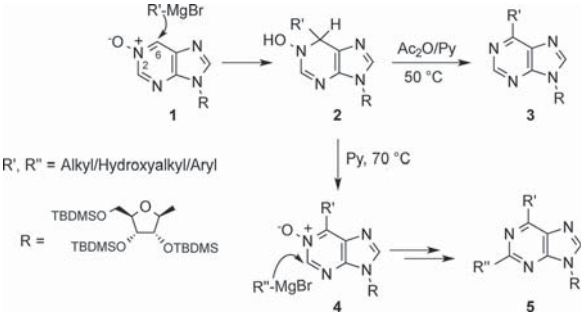

Scheme 1. Reaction of nebularine N^1-oxide **1** with Grignard reagents. Functionalization of the C-6 and C-2 positions of the purine.

C^6-Pyridinyl nucleosides are appealing nucleoside analogues because the presence of a nitrogen atom in the C-6 residue can potentially alter the hydrogen-bonding capabilities of the nucleoside as well as promote its coordination to

[a] Dipartimento di Farmacia, Università degli Studi di Napoli Federico II,
Via D. Montesano 49, 80131 Napoli, Italy
E-mail: golivier@unina.it
http://www.unina.it
[b] Dipartimento di Scienze Chimiche, Università degli Studi di Napoli Federico II,
Via Cinthia 4, 80126 Napoli, Italy
Supporting information for this article is available on the WWW under http://dx.doi.org/10.1002/ejoc.201403648.

 © 2015 Wiley-VCH Verlag GmbH & Co. KGaA, Weinheim

biologically important metals, such as platinum and ruthenium.[7] In addition, a number of pharmaceuticals, natural products, and active products for agriculture are pyridine derivatives.[8] However, the introduction of a pyridinyl residue at the C-6 position of purine nucleosides has scarcely been studied. As far as we know, the only known substances of this type are 6-(2-pyridyl)nebularine and the nucleotide corresponding to 6-(5-bromo-3-pyridyl)nebularine (see **9a** and **9e** in Table 1), both displaying interesting biological activities. These compounds were synthesized by the Pd-catalyzed cross-coupling of 6-chloropurine riboside with Rieke organozinc reagents[9] and 5-bromopyridine-3-boronic acid,[10] respectively. However, Hocek et al. reported the failure to introduce 3- and 4-pyridyl residues at C-6 by Suzuki–Miyaura coupling with the more reactive catalytic system $Pd(OAc)_2$/2-(dicyclohexylphosphanyl)biphenyl.[11] These precedents and the lack of a general synthetic procedure for obtaining C^6-pyridylpurine nucleosides prompted us to explore the addition of pyridinyl Grignard reagents **7a**–**h** (Scheme 2) to nebularine N^1-oxide (**1**) by using our procedure. We report here that it can be successfully applied to the synthesis of various C^6-pyridinyl nucleosides **9a**–**c** and C^6-halopyridinyl nucleosides **9d**–**h** (Table 1) in moderate-to-good yields.

Table 1. Product yields of compounds **9a**–**j**.

PyBr	PyMgCl	Py	Product yields (%) from **1**
6a	**7a**		**9a** (55%)
6b	**7b**		**9b** (60%)
6c	**7c**		**9c** (55%)
6d	**7d**	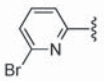	**9d** (50%)
6e	**7e**	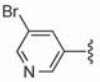	**9e** (60%)
6f	**7f**	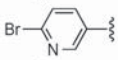	**9f** (55%)
6g	**7g**		**9g** (48%)
6h	**7h**		**9h** (65%)
6i	**7i**	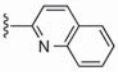	**9i** (20%)
6j	**7j**	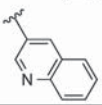	**9j** no reaction

Results and Discussion

The required pyridinyl Grignard reagents **7a**–**h** (Table 1) were prepared by bromine/magnesium exchange between bromopyridines **6a**–**h** and *i*PrMgCl (Scheme 2). This procedure has previously been efficiently employed by Trécourt et al. for the transmetallation of 2-, 3-, and 4-bromopyridines, as well as for the regioselective transmetallation of 2,3-, 2,5-, 2,6-, and 3,5-dibromopyridines to obtain various pyridinyl Grignard reagents.[12] Our general strategy for the bromine/magnesium exchange makes use of a 1:1 ratio of *i*PrMgCl and bromopyridines **6a**–**h** (2 h at room temp.). The complexes **7a**–**h** (5 equiv.) obtained in this way were added in one portion to **1** and the reaction mixtures were left at room temp. for 2 h. After work-up (see the Exp. Sect.), the crude products **8a**–**h** were treated with Ac_2O/pyridine to form the purine rings **9a**–**h** by re-aromatization.

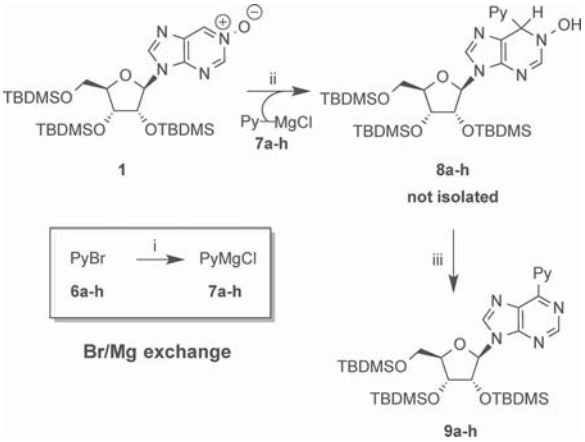

Scheme 2. Reagents and conditions: i) *i*PrMgCl, THF, 2 h, room temp., N_2; ii) **7a**–**h**, THF, 2 h, room temp., N_2; iii) Ac_2O/pyridine (4:6, v/v), 1 h, 50 °C.

Reactions of Bromopyridines 6a–c

Following our procedure, the 2-pyridyl residue could be easily introduced at the C-6 purine position by the reaction of **1** with 2-pyridylmagnesium chloride (**7a**, Table 1), and compound **9a** was obtained in a yield higher than previously reported (55%, reported 27%).[9] Compound **9b**, embodying a 3-pyridyl residue, was obtained by treating **1** with 3-pyridylmagnesium chloride (**7b**). The process proceeded smoothly and the product was obtained in 60% yield. In contrast, 4-brompyridine (**6c**) is an unstable compound and has to be prepared immediately prior to use by neutralization of the corresponding hydrochloride salt (commercially available). Initially we used the recommended procedure in which the hydrochloride salt is treated with a 5% aqueous Na_2CO_3 solution, followed by extraction with Et_2O, and drying with $MgSO_4$.[12] Disappointingly, 4-bromopyridine prepared in this way, when treated

 © 2015 Wiley-VCH Verlag GmbH & Co. KGaA, Weinheim

with *i*PrMgCl, gave a very low yield of the corresponding Grignard reagent **7c**, as suggested by its unproductive reaction with **1**.

We ascribed this failure to the difficulty in obtaining very dry 4-bromopyridine after aqueous treatment and drying with $MgSO_4$. On the other hand, bromopyridine is a volatile liquid and it could not be dried effectively under reduced pressure. We succeeded in obtaining 4-bromopyridine suitable for the preparation of the Grignard reagent by treatment of its hydrochloride salt with 1 equiv. of NaH in dry THF. The pyridine **6c** obtained was transmetallated in situ by the addition of *i*PrMgCl to give the 4-bromopyridinyl Grignard reagent **7c**, which was immediately treated with **1**. By this procedure, compound **9c** was obtained in 55% yield, which compares well with the yields of **9a** and **9b**. Therefore the 3- and 4-pyridyl nucleosides **9b** and **9c** could be synthesized by our procedure, whereas the Suzuki–Miyaura coupling reaction was unsuccessful.[11]

Reactions of Dihalopyridines 6d–h

Halopyridines are known to undergo a number of useful synthetic transformations.[13] Therefore the introduction of a halopyridine ring at the C-6 position of a purine nucleoside would allow its further synthetic elaboration. Thus, dibromopyridines **6d**–**g** and the 2-chloro-3-bromopyridine (**6h**) were transmetallated with *i*PrMgCl, as described for bromopyridines **6a**–**6c**, to furnish the corresponding Grignard reagents **7d**–**h**. Bromopyridinyl nucleosides **9d** and **9e** were obtained from symmetrical dibromopyridines **6d** and **6e** in yields of 50 and 60%, respectively, on coupling with **1**. The fully ribose-deprotected compound **9e** was recently prepared by the reaction of 6-chloropurine riboside under Suzuki–Miyaura cross-coupling conditions in 40% yield. Interestingly, its nucleotide derivative was active towards human and rat DNHP1 enzymes, showing itself to be a competitive inhibitor of dGMP binding with a micromolar affinity.[10]

Grignard reagents prepared in the usual manner from unsymmetrical 2,5- and 2,3-dibromopyridines **6f** and **6g** and used in the coupling/aromatization sequence afforded compounds **9f** and **9g**, respectively, which were analyzed by 2D NMR experiments. In particular, the correlations observed in the HMBC spectrum of **9f** between the 2′′-H and 4′′-H protons of the pyridine ring, which resonate at δ = 10.2 and 8.86 ppm, respectively, and C-6 at δ = 152.2 ppm of the purine nucleus (Figure 1) clearly indicate the formation of the C3′′–C6 bond during the coupling step. This confirms the expected preferential transmetallation at C-5 of the 2,5-dibromopyridine ring. On the other hand, in the case of compound **9g**, a significant correlation in the HMBC spectrum was seen between the 4′′-H proton at δ = 8.00 ppm and the C-6 purine carbon at δ = 156.5 ppm (Figure 1), which indicates the connection C3′′–C6 in this compound and, accordingly, confirms the preferential transmetallation at C-3 of the 2,3-dibromopyridine ring.

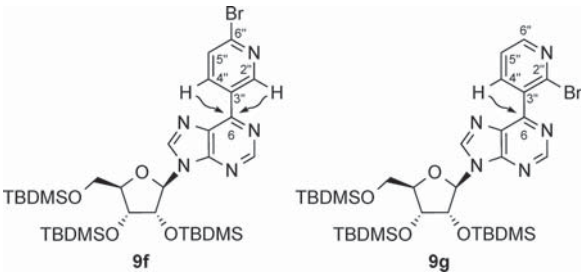

Figure 1. HMBC correlations between 4′′-H, 2′′-H and C-6 for **9f** and 4′′-H and C-6 for **9g**.

In addition, we tested the preparation and reactivity of the Grignard reagent **7h** obtained from 3-bromo-2-chloropyridine (**6h**). The transmetallation of the latter proved to be chemoselective giving the 2-chloro-3-pyridinyl Grignard reagent and then compound **9h**, which was obtained in 65% yield on reaction with **1**. In an attempt to further expand the scope of the process and access new C^6-heteroaryl nucleosides, we tested the introduction at this position of a quinolyl residue. Purine ribonucleosides bearing a quinoline ring at C-6 are unprecedented. Application of the strategy used for bromopyridines was initially attempted and the required Grignard reagents were prepared in the usual manner by treating 2-bromoquinoline (**6i**) and 3-bromoquinoline (**6j**) with *i*PrMgCl (1 equiv.). However, the subsequent reaction with **1** gave complex reaction mixtures from which the expected C^6-quinolyl derivative **9i** was obtained in 20% yield after purification, whereas no compound corresponding to **9j** could be recovered. We attributed these unsatisfactory results to the low-yielding formation or the absence of any formation of Grignard reagents **7i** and **7j**, respectively. In fact, it is reported that bromoquinolines preferably undergo nucleophilic attack at C–Br rather than transmetallation due to the low energy of their LUMO levels.[14] An alternative approach to the use of quinolyl Grignard reagents exploits the reactivity of lithium tri(quinolyl)magnesate complexes, obtained by the transmetallation reaction of lithium tributylmagnesate and 2- or 3-bromoquinolines, a procedure reported to yield *C*-functionalized quinolones.[14] Disappointingly, by using this procedure (data not shown), we could not improve on the yield of compound **9i**, and again the formation of compound **9j** was not observed in this case. The structures of all the synthesized compounds were ascertained by spectroscopic investigations (^{1}H and ^{13}C NMR, UV, IR, and MS data).

Conclusions

In this paper we describe the synthesis of a collection of C^6-pyridylpurine ribonucleosides exploiting the electrophilicity of the C-6 purine position of the sugar-protected nebularine N^1-oxide towards a series of pyridinyl Grignard reagents, prepared by transmetallation reactions between *i*PrMgCl and mono- and dihalopyridines. The bromine/magnesium exchange reactions proved to be regioselective

 © 2015 Wiley-VCH Verlag GmbH & Co. KGaA, Weinheim

when using unsymmetrical dihalopyridines, allowing bromo- and chloropyridylpurine nucleosides to be obtained. The presence of a halogen atom on the pyridinyl residue in the latter allows for further synthetic elaborations towards more diverse substituted nucleosides. An attempt to extend the synthetic strategy to the preparation of unprecedented C^6-quinolylpurine nucleosides was also made by using 2- and 3-bromoquinolines; a C^6-(2-quinolyl)purine nucleoside was obtained, but in a low yield. This result, although unsatisfactory, is promising and prompts further efforts towards the synthesis of this type of substance. Studies are ongoing in our laboratories both towards this goal and to explore the reactivity of the halogenated pyridine ring in the newly prepared nucleosides.

Experimental Section

General Methods: All the reagents were obtained from commercial sources (Sigma–Aldrich) and were used without further purification. ^{1}H and ^{13}C NMR spectra were acquired with a Varian Mercury Plus 400 MHz spectrometer in CD_3OD or C_6D_6. Chemical shifts (δ) are reported in parts per million (ppm) relative to the residual solvent signals: CD_2HOD 3.31 ppm, C_6D_5H 7.15 ppm for ^{1}H NMR; CD_3OD 49.0 ppm, C_6D_5H 128.6 ppm for ^{13}C NMR. The ^{1}H NMR chemical shifts were assigned on the basis of 2D NMR experiments. The abbreviations s, d, dd, and m represent singlet, doublet, doublet of doublets, and multiplet, respectively. UV spectra were recorded with a Jasco V-530 UV spectrophotometer. High-resolution MS spectra were recorded with a Bruker APEX II FT-ICR mass spectrometer using the electrospray ionization (ESI) technique in positive mode. IR spectra were recorded with a Jasco FT-IR 430 spectrophotometer. Optical rotations were determined with a Jasco polarimeter using a 1-dm cell at 25 °C; concentrations are given in g/100 mL. Column chromatography was performed on silica gel 60 (70–230 mesh ASTM, Merck) and analytical TLC analyses were performed on F_{254} silica gel plates (0.2 mm thick, Merck) with TLC spots being detected under UV light (254 nm).

General Procedure for the Reaction of 1 with Grignard Reagents 7a–i. Synthesis of 9a–i: In a representative experiment, *i*PrMgCl (0.12 mL, 0.24 mmol) was added to 2-bromopyridine (**6a**; 0.023 mL, 0.24 mmol) in dry THF (0.5 mL) at room temperature under nitrogen. After 2 h, **1** (30 mg, 0.049 mmol) dissolved in dry THF (0.5 mL) was added to the reaction mixture, which was then stirred for a further 2 h (TLC monitoring: hexane/AcOEt, 3:7) at room temperature. The reaction was then quenched by the addition of a 1 M solution of NH_4Cl (1 mL), diluted with AcOEt (10 mL), and washed with brine (10 mL). The organic layer was separated, dried (Na_2SO_4), filtered, and concentrated under rotary evaporation. The crude **8a** was dissolved in a mixture of Ac_2O/pyridine (4:6, 0.5 mL) and the solution kept at 50 °C for 1 h (TLC monitoring: AcOEt/MeOH, 9.5:0.5). The mixture was evaporated in vacuo and purified on a column of silica gel eluted with increasing amounts of MeOH in AcOEt (up to 5%). The fractions containing the product were collected and evaporated to afford pure **9a**.

2′,3′,5′-Tri-*O*-(*tert*-butyldimethylsilyl)-6-(3-pyridyl)nebularine (9b): TLC monitoring (hexane/AcOEt, 1:1), purification through a column of silica gel eluted with increasing amounts of AcOEt in hexane (up to 30%). Amorphous solid (19 mg, 60%). $[\alpha]_D$ = –42.0 (c = 1.1, CH_3OH). ^{1}H NMR (400 MHz, CD_3OD): δ = 9.92–9.88 (m, 1 H, arom.), 9.18–9.13 (m, 1 H, arom.), 9.0 (s, 1 H, 2-H), 8.75 (s, 1 H, 8-H), 8.72–8.69 (m, 1 H, arom.), 7.69–7.63 (m, 1 H, arom.), 6.21 (d, J = 5.6 Hz, 1 H, 1′-H), 4.95–4.90 (m, 1 H, 2′-H), 4.49–4.44 (m, 1 H, 3′-H), 4.20–4.15 (m, 1 H, 4′-H), 4.09 (dd, J = 11.3, 4.6 Hz, 1 H, 5′-H_a), 3.87 (dd, J = 11.3, 3.1 Hz, 1 H, 5′-H_b), 0.98 [s, 9 H, $C(CH_3)_3$], 0.96 [s, 9 H, $C(CH_3)_3$], 0.78 [s, 9 H, $C(CH_3)_3$], 0.18 (s, 3 H, CH_3), 0.17 (s, 3 H, CH_3), 0.16 (s, 6 H, 2 CH_3), –0.016 (s, 3 H, CH_3), –0.28 (s, 3 H, CH_3) ppm. ^{13}C NMR (100 MHz, CD_3OD): δ = 153.8, 153.5, 152.9, 151.9, 151.3, 146.4, 138.9, 133.2, 132.9, 125.3, 89.6, 87.4, 77.1, 73.7, 63.8, 26.6, 26.4, 26.2, 19.4, 18.9, 18.7, –4.1, –4.2, –4.3, –4.9, –5.2, –5.3 ppm. IR (neat): ν_{max} = 2950, 2923, 2857, 1577, 1465, 1320, 1256, 1127, 834, 779 cm^{-1}. UV (CH_3OH): λ_{max} = 288 nm. HRMS (ESI): calcd. for $C_{33}H_{58}N_5O_4Si_3$ $[M + H]^+$ 672.3797; found 672.3794.

2′,3′,5′-Tri-*O*-(*tert*-butyldimethylsilyl)-6-(4-pyridyl)nebularine (9c): 4-Bromopyridine hydrochloride (47 mg, 0.24 mmol) was suspended in dry THF (1 mL) under nitrogen and the mixture cooled to 0 °C. NaH (5.8 mg, 0.24 mmol) was added in one portion and the mixture stirred for 15 min. After warming to room temp., *i*PrMgCl (0.12 mL, 0.24 mmol) was added as for **6a**. TLC monitoring (hexane/AcOEt, 6:4), purification through a column of silica gel eluted with increasing amounts of AcOEt in hexane (up to 30%). Amorphous solid (18 mg, 55%). $[\alpha]_D$ = –34.3 (c = 0.5, CH_3OH). ^{1}H NMR (400 MHz, CD_3OD): δ = 9.06 (s, 1 H, 2-H), 8.81–8.74 (complex signal, 5 H, 4 arom., 8-H), 6.22 (d, J = 5.6 Hz, 1 H, 1′-H), 4.95–4.91 (m, 1 H, 2′-H), 4.49–4.45 (m, 1 H, 3′-H), 4.20–4.17 (m, 1 H, 4′-H), 4.09 (dd, J = 11.4, 4.5 Hz, 1 H, 5′-H_a), 3.88 (dd, J = 11.3, 2.9 Hz, 1 H, 5′-H_b), 0.99 [s, 9 H, $C(CH_3)_3$], 0.97 [s, 9 H, $C(CH_3)_3$], 0.79 [s, 9 H, $C(CH_3)_3$], 0.19 (s, 3 H, CH_3), 0.17 (s, 3 H, CH_3), 0.16 (s, 6 H, 2 CH_3), –0.009 (s, 3 H, CH_3), –0.28 (s, 3 H, CH_3) ppm. ^{13}C NMR (100 MHz, CD_3OD): δ = 154.2, 153.4, 152.6, 150.8, 146.9, 144.9, 133.5, 125.0, 89.7, 87.4, 77.1, 73.7, 63.8, 26.6, 26.4, 26.2, 19.4, 18.9, 18.7, –4.1, –4.3, –4.9, –5.2, –5.3 ppm. IR (neat): ν_{max} = 2956, 2923, 2851, 1569, 1412, 1254, 1091, 793 cm^{-1}. UV (CH_3OH): λ_{max} = 290 nm. HRMS (ESI): calcd. for $C_{33}H_{58}N_5O_4Si_3$ $[M + H]^+$ 672.3797; found 672.3792.

2′,3′,5′-Tri-*O*-(*tert*-butyldimethylsilyl)-6-(6-bromo-2-pyridyl)nebularine (9d): TLC monitoring (CH_2Cl_2/AcOEt, 95:5), purification through a column of silica gel eluted with increasing amounts of AcOEt in CH_2Cl_2 (up to 5%). Oil (18 mg, 50%). $[\alpha]_D$ = –36.7 (c = 1.1, CH_3OH). ^{1}H NMR (400 MHz, CD_3OD): δ = 9.0 (s, 1 H, 2-H), 8.88–8.84 (m, 1 H, arom.), 8.79 (s, 1 H, 8-H), 7.97–7.90 (m, 1 H, arom.), 7.80–7.75 (m, 1 H, arom.), 6.22 (d, J = 5.7 Hz, 1 H, 1′-H), 4.95–4.90 (m, 1 H, 2′-H), 4.48–4.44 (m, 1 H, 3′-H), 4.20–4.15 (m, 1 H, 4′-H), 4.08 (dd, J = 11.3, 4.5 Hz, 1 H, 5′-H_a), 3.87 (dd, J = 11.3, 2.9 Hz, 1 H, 5′-H_b), 0.98 [s, 9 H, $C(CH_3)_3$], 0.95 [s, 9 H, $C(CH_3)_3$], 0.78 [s, 9 H, $C(CH_3)_3$], 0.17 (s, 3 H, CH_3), 0.16 (s, 3 H, CH_3), 0.15 (s, 6 H, 2 CH_3), –0.021 (s, 3 H, CH_3), –0.29 (s, 3 H, CH_3) ppm. ^{13}C NMR (100 MHz, CD_3OD): δ = 154.8, 154.4, 153.4, 147.1, 143.6, 141.0, 133.1, 131.3, 126.8, 89.7, 87.5, 77.1, 73.7, 63.8, 26.6, 26.4, 26.2, 19.4, 19.0, 18.7, –4.1, –4.3, –4.9, –5.2 ppm. HRMS (ESI): calcd. for $C_{33}H_{57}BrN_5O_4Si_3$ $[M + H]^+$ 750.2902; found 750.2907. IR (neat): ν_{max} = 2956, 2928, 2857, 1566, 1429, 1256, 1072, 834, 790 cm^{-1}. UV (CH_3OH): λ_{max} = 304 nm.

2′,3′,5′-Tri-*O*-(*tert*-butyldimethylsilyl)-6-(5-bromo-3-pyridyl)nebularine (9e): TLC monitoring (hexane/AcOEt, 8:2), purification through a column of silica gel eluted with increasing amounts of AcOEt in hexane (up to 10%). Oil (22 mg, 60%). $[\alpha]_D$ = –41.6 (c = 0.7, CH_2Cl_2). ^{1}H NMR (400 MHz, C_6D_6): δ = 10.48–10.46 (m, 1 H, arom.), 9.49–9.46 (m, 1 H, arom.), 8.96 (s, 1 H, 2-H), 8.71–8.68 (m, 1 H, arom.), 8.37 (s, 1 H, 8-H), 6.22 (d, J = 4.4 Hz, 1 H, 1′-H), 4.95–4.90 (m, 1 H, 2′-H), 4.55–4.50 (m, 1 H, 3′-H), 4.29–4.24 (m, 1 H, 4′-H), 4.01 (dd, J = 11.4, 4.2 Hz, 1 H, 5′-H_a), 3.72

 © 2015 Wiley-VCH Verlag GmbH & Co. KGaA, Weinheim

(dd, J = 11.4, 2.6 Hz, 1 H, 5′-H_b), 1.00 [s, 9 H, $C(CH_3)_3$], 0.96 [s, 9 H, $C(CH_3)_3$], 0.91 [s, 9 H, $C(CH_3)_3$], 0.13 (s, 3 H, CH_3), 0.12 (s, 3 H, CH_3), 0.094 (s, 3 H, CH_3), 0.078 (s, 3 H, CH_3), 0.048 (s, 3 H, CH_3), –0.082 (s, 3 H, CH_3) ppm. ^{13}C NMR (100 MHz, C_6D_6): δ = 153.4, 153.2, 152.9, 151.7, 150.4, 144.9, 139.7, 134.1, 133.1, 121.7, 89.9, 85.9, 76.6, 72.5, 62.9, 26.8, 26.6, 26.5, 19.2, 18.9, 18.7, –3.6, –3.9, –4.0, –4.1, –4.7, –4.8 ppm. IR (neat): ν_{max} = 2956, 2923, 2857, 1580, 1459, 1325, 1256, 1105, 834, 779 cm^{-1}. UV (CH_3OH): λ_{max} = 302 nm. HRMS (ESI): calcd. for $C_{33}H_{57}BrN_5O_4Si_3$ $[M + H]^+$ 750.2902; found 750.2898.

2′,3′,5′-Tri-*O*-(*tert*-butyldimethylsilyl)-6-(6-bromo-3-pyridyl)nebularine (9f): TLC monitoring (hexane/AcOEt, 85:15), purification through a column of silica gel eluted with increasing amounts of AcOEt in hexane (up to 10%). Amorphous solid (20 mg, 55%). $[\alpha]_D$ = –41.3 (c = 0.6, CH_2Cl_2). ^1H NMR (400 MHz, C_6D_6): δ = 10.2 (d, J = 2.2 Hz, 1 H, arom.), 8.92 (s, 1 H, 2-H), 8.86 (dd, J = 8.4, 2.4 Hz, 1 H, arom.), 8.35 (s, 1 H, 8-H), 7.03 (d, J = 8.4 Hz, 1 H, arom.), 6.20 (d, J = 4.2 Hz, 1 H, 1′-H), 4.88–4.83 (m, 1 H, 2′-H), 4.51–4.46 (m, 1 H, 3′-H), 4.25–4.20 (m, 1 H, 4′-H), 3.96 (dd, J = 11.5, 4.1 Hz, 1 H, 5′-H_a), 3.68 (dd, J = 11.4, 2.5 Hz, 1 H, 5′-H_b), 0.96 [s, 9 H, $C(CH_3)_3$], 0.93 [s, 9 H, $C(CH_3)_3$], 0.88 [s, 9 H, $C(CH_3)_3$], 0.075 (s, 3 H, CH_3), 0.067 (s, 3 H, CH_3), 0.059 (s, 3 H, CH_3), 0.043 (s, 3 H, CH_3), 0.013 (s, 3 H, CH_3), –0.10 (s, 3 H, CH_3) ppm. ^{13}C NMR (100 MHz, C_6D_6): δ = 153.1, 153.0, 152.8, 152.2, 145.8, 144.7, 139.6, 132.9, 131.7, 128.5, 89.9, 85.8, 76.6, 72.4, 62.8, 26.8, 26.6, 26.5, 19.3, 18.9, 18.7, –3.6, –3.9, –4.0, –4.7, –4.8 ppm. IR (neat): ν_{max} = 2950, 2923, 2851, 1580, 1459, 1322, 1256, 1072, 834, 773 cm^{-1}. UV (CH_3OH): λ_{max} = 299 nm. HRMS (ESI): calcd. for $C_{33}H_{57}BrN_5O_4Si_3$ $[M + H]^+$ 750.2902; found 750.2910.

2′,3′,5′-Tri-*O*-(*tert*-butyldimethylsilyl)-6-(2-bromo-3-pyridyl)nebularine (9g): TLC monitoring (hexane/AcOEt, 7:3), purification through a column of silica gel eluted with increasing amounts of AcOEt in hexane (up to 25%). Oil (18 mg, 48%). $[\alpha]_D$ = –32.1 (c = 0.7, CH_3OH). ^1H NMR (400 MHz, CD_3OD): δ = 9.05 (s, 1 H, 2-H), 8.76 (s, 1 H, 8-H), 8.54 (dd, J = 4.8, 1.8 Hz, 1 H, arom.), 8.00 (dd, J = 7.6, 1.8 Hz, 1 H, arom.), 7.63 (dd, J = 7.6, 4.9 Hz, 1 H, arom.), 6.23 (d, J = 5.9 Hz, 1 H, 1′-H), 4.95–4.90 (m, 1 H, 2′-H), 4.48–4.43 (m, 1 H, 3′-H), 4.22–4.16 (m, 1 H, 4′-H), 4.08 (dd, J = 11.3, 4.7 Hz, 1 H, 5′-H_a), 3.88 (dd, J = 11.3, 3.0 Hz, 1 H, 5′-H_b), 0.98 [s, 9 H, $C(CH_3)_3$], 0.95 [s, 9 H, $C(CH_3)_3$], 0.78 [s, 9 H, $C(CH_3)_3$], 0.18 (s, 3 H, CH_3), 0.16 (s, 3 H, CH_3), 0.15 (s, 6 H, 2 CH_3), –0.012 (s, 3 H, CH_3), –0.29 (s, 3 H, CH_3) ppm. ^{13}C NMR (100 MHz, CD_3OD): δ = 156.5, 153.4, 153.2, 152.1, 147.1, 141.9, 141.3, 135.2, 133.6, 124.3, 89.7, 87.8, 77.2, 73.9, 63.9, 26.6, 26.4, 26.2, 19.4, 19.0, 18.8, –4.1, –4.2, –4.3, –4.8, –5.2, –5.3 ppm. IR (neat): ν_{max} = 2956, 2923, 2857, 1594, 1462, 1391, 1253, 1163, 1108, 834, 774 cm^{-1}. UV (CH_3OH): λ_{max} = 272 nm. HRMS (ESI): calcd. for $C_{33}H_{57}BrN_5O_4Si_3$ $[M + H]^+$ 750.2902; found 750.2911.

2′,3′,5′-Tri-*O*-(*tert*-butyldimethylsilyl)-6-(2-chloro-3-pyridyl)nebularine (9h): TLC monitoring (hexane/AcOEt, 7:3), purification through a column of silica gel eluted with increasing amounts of AcOEt in hexane (up to 25%). Oil (22 mg, 65%). $[\alpha]_D$ = –28.0 (c = 0.8, CH_2Cl_2). ^1H NMR (400 MHz, C_6D_6): δ = 9.12 (s, 1 H, 2-H), 8.34 (s, 1 H, 8 H), 8.04 (dd, J = 4.8, 1.9 Hz, 1 H, arom.), 7.76 (dd, J = 7.6, 1.9 Hz, 1 H, arom.), 6.51 (dd, J = 7.5, 4.8 Hz, 1 H, arom.), 6.24 (d, J = 4.5 Hz, 1 H, 1′-H), 4.99–4.94 (m, 1 H, 2′-H), 4.57–4.52 (m, 1 H, 3′-H), 4.30–4.25 (m, 1 H, 4′-H), 4.03 (dd, J = 11.4, 4.4 Hz, 1 H, 5′-H_a), 3.74 (dd, J = 11.4, 2.7 Hz, 1 H, 5′-H_b), 1.01 [s, 9 H, $C(CH_3)_3$], 0.94 [s, 9 H, $C(CH_3)_3$], 0.91 [s, 9 H, $C(CH_3)_3$], 0.13 (s, 3 H, CH_3), 0.12 (s, 3 H, CH_3), 0.076 (s, 6 H, 2 CH_3), 0.064 (s, 3 H, CH_3), 0.039 (s, 3 H, CH_3), –0.087 (s, 3 H, CH_3) ppm. ^{13}C NMR (100 MHz, CD_3OD): δ = 155.8, 153.1, 152.8, 151.2, 150.9, 145.1, 141.1, 134.3, 132.3, 122.4, 89.9, 86.0, 76.6, 72.6, 63.0, 26.8, 26.6, 26.5, 19.2, 18.9, 18.7, –3.6, –3.9, –4.0, –4.2, –4.7, –4.8 ppm. IR (neat): ν_{max} = 2956, 2923, 2857, 1591, 1462, 1399, 1328, 1254, 1064, 834, 774 cm^{-1}. UV (CH_3OH): λ_{max} = 273 nm. HRMS (ESI): calcd. for $C_{33}H_{57}ClN_5O_4Si_3$ $[M + H]^+$ 706.3407; found 706.3412.

2′,3′,5′-Tri-*O*-(*tert*-butyldimethylsilyl)-6-(2-quinolyl)nebularine (9i): TLC monitoring (hexane/AcOEt, 7:3), purification through a column of silica gel eluted with increasing amounts of AcOEt in hexane (up to 30%). Oil (7.1 mg, 20%). $[\alpha]_D$ = –39.5 (c = 0.5, CH_3OH). ^1H NMR (400 MHz, CD_3OD): δ = 9.14 (s, 1 H, 2-H), 8.88–8.81 (complex signal, 2 H, arom., 8-H), 8.59–8.54 (m, 1 H, arom.), 8.39–8.37 (m, 1 H, arom.), 8.05–8.03 (m, 1 H, arom.), 7.87–7.83 (m, 1 H, arom.), 7.72–7.68 (m, 1 H, arom.), 6.27 (d, J = 5.8 Hz, 1 H, 1′-H), 5.00–4.95 (m, 1 H, 2′-H), 4.51–4.46 (m, 1 H, 3′-H), 4.22–4.18 (m, 1 H, 4′-H), 4.11 (dd, J = 11.3, 4.7 Hz, 1 H, 5′-H_a), 3.90 (dd, J = 11.3, 3.1 Hz, 1 H, 5′-H_b), 0.99 [s, 9 H, $C(CH_3)_3$], 0.97 [s, 9 H, $C(CH_3)_3$], 0.79 [s, 9 H, $C(CH_3)_3$], 0.19 (s, 3 H, CH_3), 0.18 (s, 3 H, CH_3), 0.17 (s, 6 H, 2 CH_3), –0.003 (s, 3 H, CH_3), –0.27 (s, 3 H, CH_3) ppm. ^{13}C NMR (100 MHz, CD_3OD): δ = 154.6, 154.5, 154.4, 153.5, 149.4, 147.1, 138.5, 133.4, 131.4, 130.8, 130.1, 129.2, 128.9, 123.5, 89.7, 87.6, 77.1, 73.9, 63.9, 26.6, 26.4, 26.2, 19.4, 19.0, 18.8, –4.1, –4.3, –4.8, –5.1, –5.2 ppm. IR (neat): ν_{max} = 2956, 2923, 2857, 1572, 1459, 1377, 1256, 1072, 834, 779 cm^{-1}. UV (CH_3OH): λ_{sh} = 243, 257 nm. HRMS (ESI): calcd. for $C_{37}H_{60}N_5O_4Si_3$ $[M + H]^+$ 722.3953; found 722.3960.

Supporting Information (see footnote on the first page of this article): ^1H and ^{13}C NMR spectra of all new compounds.

Acknowledgments

This work was supported by the Compagnia di San Paolo Foundation (Progetto FARO 2011, Finanziamento per l'Avvio di Ricerche Originali). The authors are grateful to Dr. Luisa Cuorvo and Dr. Andrea De Fortis Nadi for their technical assistance and to the Centro di Servizio Interdipartimentale di Analisi Strutturale (CSIAS) for the NMR facilities.

[1] a) L. P. Jordheim, D. Durantel, F. Zoulim, C. Dumontet, *Nat. Rev. Drug Discovery* **2013**, *12*, 447–464; b) E. De Clercq, *Nat. Rev. Drug Discovery* **2002**, *1*, 13–25; c) D. Komiotis, S. Manta, E. Tsoukala, N. Tzioumaki, *Curr. Med. Chem. Anti-Infect. Agents* **2008**, *7*, 219–244; d) C. M. Galmarini, J. R. Mackey, C. Dumontet, *Lancet Oncol.* **2002**, *3*, 415–424.

[2] a) D. A. Malyshev, K. Dhami, T. Lavergne, T. Chen, N. Dai, J. M. Foster, I. R. Corrêa, F. E. Romesberg, *Nature* **2014**, *509*, 385–388; b) D. Dziuba, V. Y. Postupalenko, M. Spadafora, A. S. Klymchenko, V. Guérineau, Y. Mély, R. Benhida, A. Burger, *J. Am. Chem. Soc.* **2012**, *134*, 10209–10213; c) G. Oliviero, S. D′Errico, N. Borbone, J. Amato, V. Piccialli, G. Piccialli, L. Mayol, *Eur. J. Org. Chem.* **2010**, *8*, 1517–1524; d) S. D'Errico, G. Oliviero, N. Borbone, J. Amato, V. Piccialli, M. Varra, L. Mayol, G. Piccialli, *Molecules* **2011**, *16*, 8110–8118; e) S. D'Errico, G. Oliviero, N. Borbone, J. Amato, D. D'Alonzo, V. Piccialli, L. Mayol, G. Piccialli, *Molecules* **2012**, *17*, 13036–13044; f) S. D'Errico, G. Oliviero, N. Borbone, J. Amato, V. Piccialli, M. Varra, L. Mayol, G. Piccialli, *Molecules* **2013**, *18*, 9420–9431; g) L. Zilbershtein, A. Silberman, B. Fischer, *Org. Biomol. Chem.* **2011**, *9*, 7763–7773; h) A. A. Tanpure, M. G. Pawar, S. G. Srivatsan, *Isr. J. Chem.* **2013**, *53*, 366–378; i) A. Dumas, N. W. Luedtke, *Chem. Eur. J.* **2012**, *18*, 245–254; j) G. Mata, N. W. Luedtke, *J. Org. Chem.* **2012**, *77*, 9006–9017.

[3] a) M. Hocek, P. Nauš, R. Pohl, I. Votruba, P. Furman, P. Tharnish, M. Otto, *J. Med. Chem.* **2005**, *48*, 5869–5873; b)

 © 2015 Wiley-VCH Verlag GmbH & Co. KGaA, Weinheim

A. E. A. Hassan, R. A. I. Abou-Elkhair, J. M. Riordan, P. W. Allan, W. B. Parker, R. Khare, W. R. Waud, J. A. Montgomery, J. A. Secrist III, *Eur. J. Med. Chem.* **2012**, *47*, 167–174; c) Y. Ding, J.-L. Girardet, Z. Hong, V. C. H. Lai, H. An, Y.-H. Koh, S. Z. Shaw, W. Zhong, *Bioorg. Med. Chem. Lett.* **2005**, *15*, 709–713; d) L. L. Gundersen, J. Nissen-Meyer, B. Spilsberg, *J. Med. Chem.* **2002**, *45*, 1383–1386.

[4] a) L. A. Agrofoglio, I. Gillaizeau, Y. Saito, *Chem. Rev.* **2003**, *103*, 1875–1916; b) M. Lakshman, J. Hilmer, J. Martin, J. Keeler, Y. Dinh, F. Ngassa, L. Russon, *J. Am. Chem. Soc.* **2001**, *123*, 7779–7787; c) L. Gundersen, A. K. Bakkestuen, A. J. Aasen, *Tetrahedron* **1994**, *50*, 9743–9756; d) M. Hocek, *Eur. J. Org. Chem.* **2003**, 245–254.

[5] a) E. Véliz, P. Beal, *J. Org. Chem.* **2001**, *66*, 8592–8598; b) H. P. Kokatla, M. K. Lakshman, *Org. Lett.* **2010**, *12*, 4478–4481.

[6] a) S. D'Errico, V. Piccialli, G. Oliviero, N. Borbone, J. Amato, V. D'Atri, G. Piccialli, *Tetrahedron* **2011**, *67*, 6138–6144; b) S. D'Errico, G. Oliviero, J. Amato, N. Borbone, V. Cerullo, A. Hemminki, V. Piccialli, S. Zaccaria, L. Mayol, G. Piccialli, *Chem. Commun.* **2012**, *48*, 9310–9312; c) S. D'Errico, G. Oliviero, N. Borbone, V. Piccialli, V. D'Atri, L. Mayol, G. Piccialli, *Eur. J. Org. Chem.* **2013**, 6948–6954.

[7] a) M. Coluccia, A. Boccarelli, C. Cermelli, M. Portolani, G. Natile, *Met.-Based Drugs* **1995**, *2*, 249–256; b) S. D'Errico, G. Oliviero, N. Borbone, V. Piccialli, B. Pinto, F. De Falco, M. C. Maiuri, R. Carnuccio, V. Costantino, F. Nici, G. Piccialli, *Molecules* **2014**, *19*, 9339–9353; c) S. D'Errico, G. Oliviero, V. Piccialli, J. Amato, N. Borbone, V. D'Atri, F. D'Alessio, R. Di Noto, F. Ruffo, F. Salvatore, G. Piccialli, *Bioorg. Med. Chem. Lett.* **2011**, *21*, 5835–5838; d) D. Montesarchio, G. Mangiapia, G. Vitiello, D. Musumeci, C. Irace, R. Santamaria, G. D'Errico, L. Paduano, *Dalton Trans.* **2013**, *42*, 16697–16708.

[8] a) A. E. Goetz, N. K. Garg, *Nat. Chem.* **2013**, *5*, 54–60; b) M. Baumann, I. R. Baxendale, *Beilstein J. Org. Chem.* **2013**, *9*, 2265–2319.

[9] M. Hocek, A. Holý, I. Votruba, H. Dvořáková, *Collect. Czech Chem. C* **2001**, *66*, 483–499.

[10] C. Amiable, J. Paoletti, A. Haouz, A. Padilla, G. Labesse, P. A. Kaminski, S. Pochet, *Eur. J. Med. Chem.* **2014**, *85*, 418–437.

[11] M. Hocek, P. Nauš, R. Pohl, I. Votruba, P. Furman, P. Tharnish, M. Otto, *J. Med. Chem.* **2005**, *48*, 5869–5873.

[12] F. Trécourt, G. Breton, V. Bonnet, F. Mongin, F. Marsais, G. Quéguiner, *Tetrahedron* **2000**, *56*, 1349–1360.

[13] a) F. Marsais, F. Trécourt, P. Bréant, G. Quéguiner, *J. Heterocycl. Chem.* **1988**, *25*, 81–87; b) S. V. Amosova, G. M. Gavrilova, *Russ. J. Org. Chem.* **2004**, *40*, 1657–1661; c) C. Gosmini, C. Bassene-Ernst, M. Durandetti, *Tetrahedron* **2009**, *65*, 6141–6146; d) S. Gamsey, A. Miller, M. M. Olmstead, C. M. Beavers, L. C. Hirayama, S. Pradhan, R. A. Wessling, B. Singaram, *J. Am. Chem. Soc.* **2007**, *129*, 1278–1286; e) S. Zhang, L.-Y. Liao, F. Zhang, X. F. Duan, *J. Org. Chem.* **2013**, *78*, 2720–2725; f) P. S. Fier, J. F. Hartwig, *Science* **2013**, *342*, 956–960; g) G. D. Henry, *Tetrahedron* **2004**, *60*, 6043–6061; h) M. Schlosser, F. Mongin, *Chem. Soc. Rev.* **2007**, *36*, 1161–1172.

[14] S. Dumouchel, F. Mongin, F. Trécourt, G. Queguiner, *Tetrahedron Lett.* **2003**, *44*, 2033–2035.

Received: December 18, 2014
Published Online: February 19, 2015

 © 2015 Wiley-VCH Verlag GmbH & Co. KGaA, Weinheim

DOI: 10.1002/ejoc.201500998

Synthesis and Evaluation of the Antiproliferative Properties of a Tethered Tubercidin–Platinum(II) Complex

Stefano D'Errico,[a] Giorgia Oliviero,*[a] Nicola Borbone,[a] Elena Di Gennaro,[b] Andrea Ilaria Zotti,[b] Alfredo Budillon,[b] Vincenzo Cerullo,[c] Fabrizia Nici,[a] Luciano Mayol,[a] Vincenzo Piccialli,[d] and Gennaro Piccialli[a,e]

Keywords: Platinum / Nucleosides / Antitumor agents / Medicinal chemistry

Herein, the synthesis of a nucleoside platinum(II) complex in which a cisplatin-like unit is joined to 7-deazaadenosine through an amino alkyl chain installed at the C6 position of purine was explored. The capability of the new complex to react with DNA purine bases was confirmed by a model reaction with deoxyguanosine monophosphate, whereas its antiproliferative activity against A549 and Cal27 human cancer cell lines was studied by sulforhodamine B assay in comparison with its unplatinated precursor and cisplatin.

Introduction

More than 50 years after its discovery,[1] cisplatin (**1**, Figure 1) is still one of the most effective drugs for the treatment of several types of tumors, including testicular, ovarian, bladder, cervical, and lung cancer and head and neck carcinomas.[2] The mechanism of action of cisplatin involves DNA as the final target. In fact, cisplatin essentially binds the guanine bases at the N7 position and forms stable intrastrand adducts or interstrand crosslinks that cause severe local changes in the secondary structure of DNA.[3] This DNA distortion hampers its binding with crucial cellular proteins and is recognized as DNA damage that eventually leads to cell death by apoptosis.[4] The clinical use of cisplatin is partially limited by intrinsic resistance of many tumors and by the insurgence of acquired resistance during treatments.[2,5] Carboplatin (**2**) and oxaliplatin (**3**), second- and third-generation platinum-based antineoplastic agents, respectively, have dosages and clinical administration protocols that ameliorate the quality of life of patients, even if they do not resolve the problems of drug resistance.[6]

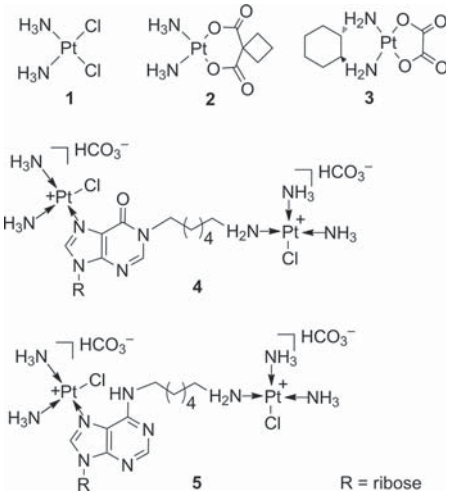

Figure 1. Structures of platinum drugs **1**–**3** and bis-platinated nucleoside complexes **4** and **5** carrying purine nucleoside scaffolds.

For these reasons, research in this field is still very active, proposing multinuclear platinum complexes[7–10] and composite molecules in which the platinum complex is conjugated to biologically important substances, drugs, and carriers.[11–18] Furthermore, thanks to the synergistic effect that may result, tethering between biologically active molecules and platinum units could afford novel complexes with improved drug-targeting and drug-delivery properties.[12]

Nucleosides and nucleotides (NNs) and their analogues play a key role in the regulation of cellular processes and in signal transduction.[19–22] Furthermore, NN analogues are

[a] Dipartimento di Farmacia, Università degli Studi di Napoli Federico II,
Via Domenico Montesano 49, 80131 Napoli, Italy
E-mail: giorgia.oliviero@unina.it
http://www.unina.it
[b] Experimental Pharmacology, Istituto Nazionale Tumori Fondazione G. Pascale – IRCCS,
Via Mariano Semmola 52, 80131 Napoli, Italy
[c] Division of Biopharmaceutics and Pharmacokinetics, Faculty of Pharmacy, University of Helsinki,
Viikinkaari 5 E, 00790 Helsinki, Finland
[d] Dipartimento di Scienze Chimiche, Università degli Studi di Napoli Federico II,
Via Cinthia 4, 80126 Napoli, Italy
[e] Institute of Protein Biochemistry, National Research Council of Italy,
Via Pietro Castellino 111, 80131 Napoli, Italy
Supporting information for this article is available on the WWW under http://dx.doi.org/10.1002/ejoc.201500998.

 © 2015 Wiley-VCH Verlag GmbH & Co. KGaA, Weinheim

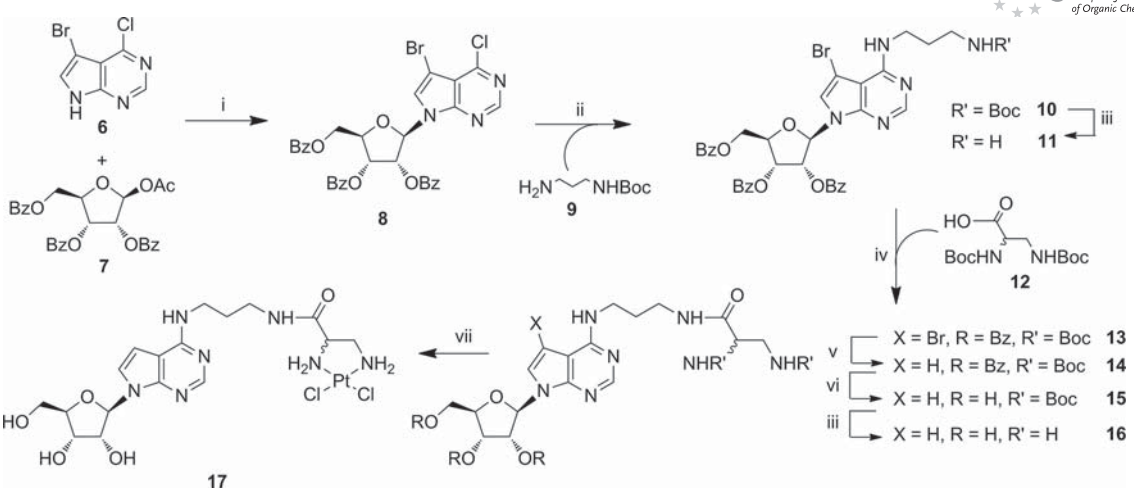

Scheme 1. Reagents and conditions: (i) *N,O*-Bis(trimethylsilyl)acetamide (BSA), trimethylsilyl trifluoromethanesulfonate (TMSOTf), CH_3CN, 2 h, 80 °C, 60%; (ii) **9**, EtOH, 5 h, reflux, 80%; (iii) trifluoroacetic acid (TFA)/CH_2Cl_2 (1:1), 1 h, r.t., 99%; (iv) **12**, 1-ethyl-3-(3-dimethylaminopropyl)carbodiimide (EDC), hydroxybenzotriazole (HOBt), *N,N*-diisopropylethylamine (DIPEA), 16 h, r.t., 83%; (v) MeOH, AcONa, H_2/Pd/C, 2 h, r.t., 99%; (vi) MeONa, MeOH, 1 h, r.t., 95%; (vii) K_2PtCl_4, H_2O/MeOH (1:1), 16 h, r.t., in the dark, 70%. Bz = benzoyl, Boc = *tert*-butoxycarbonyl.

known to inhibit the growth of several cancer lines[23–26] and many of them are clinically used as antiviral drugs.[27–29] Despite this, only a few platinum complexes carrying nucleoside scaffolds have been proposed.[30–33] In principle, a platinum complex conjugated to a biologically active nucleoside could combine the reactivity of the platinum center with the pharmacological properties of the nucleoside analogue (e.g., antimetabolite activity or active transmembrane transport). However, the properties of such a composite molecule are not predictable because each moiety of the complex can strongly influence the chemical and pharmacological behavior of the other. In this context, we recently focused our attention on the development of new nucleoside dinuclear platinum(II) complexes.

In particular, we synthesized bis-platinated nucleoside complexes **4** and **5** (Figure 1)[34,35] carrying two monofunctional platinum(II) centers, the first coordinating the N7 position of the purine system and the second coordinating the terminal amino group of an alkyl chain installed on the purine base. These substances showed moderate (or low) antiproliferative activities upon testing against A278, HeLa, A549, and MCF7 cell lines.

In this paper, we describe the synthesis and the preliminary biological evaluation of a novel nucleoside platinum complex (i.e., **17**, Scheme 1) carrying a neutral cisplatin unit conjugated to the 1,2-diamine moiety of 7-deazaadenosine (7-deaza-A) analogue **16**. 7-Deaza-A (also known as tubercidin) is an interesting antimetabolite endowed with antibiotic and antitumor properties.[36,37] In particular, tubercidin shows significant in vitro cytotoxicity against the murine P388 and the human lung adenocarcinoma A549 cell lines.[38,39] In our context, the absence of the N7 purine atom in 7-deaza-A avoids the issue of the fast reactivity of N7 with platinum during the coordination reaction, which thus allows the construction of a monoplatinated complex involving exclusively the exocyclic 1,2-diamine function of the linker. The capability of **17** to mimic the reactivity of cisplatin with the DNA bases was assessed by monitoring a model reaction of **17** with deoxyguanosine 5′-monophosphate (dGMP) by ^1H NMR spectroscopy.[40,41] The preliminary information on the antiproliferative activity of **17** and its unplatinated precursor **16** against Cal27 and A549 tumor cell lines are also reported.

Results and Discussion

Synthesis and Characterization

Our synthetic route started with the construction of bis-halogenated 7-deazapurine-β-D-riboside **8** (Scheme 1). The nucleoside scaffold was prepared according to a procedure by Seela and Ming,[42] which performs the glycosylation step by using 7-bromo-6-chloro-7-deazapurine **6** as the aglycon moiety. As outlined in that paper, the presence of the electron-withdrawing bromine atom at the C7 position of the purine atom makes the formation of the glycosidic bond with suitably protected ribose moiety **7** possible in good yields and with complete β stereoselectivity. Nucleoside **8** was then treated with mono-Boc-protected 1,3-diaminopropane unit **9** to afford derivative **10**. After quantitative removal of the Boc group (TFA in CH_2Cl_2), resulting nucleoside **11** was treated with bis-Boc-protected 2,3-diaminopropanoic acid (racemic mixture, **12**)[43] by using EDC/HOBt as the activating agents of the carboxylic function to give **13** (83% yield) as a mixture of diastereoisomers. Compound **13** was then subjected to hydrogenolysis in a Parr apparatus by using Pd/C as the catalyst to remove the C7 bromine. It was reported that the presence of a base (AcONa) in the reaction mixture is indispensable to neutralize HBr that is formed during the reaction.[44] The

 © 2015 Wiley-VCH Verlag GmbH & Co. KGaA, Weinheim

hydrogenolysis proceeded very cleanly to give **14** quantitatively after a standard workup procedure. The benzoate protecting groups were then removed from **14** with a solution of MeONa in MeOH to give **15** after chromatographic purification (95% yield). Finally, the Boc protecting groups in **15** were removed by TFA treatment, and the crude was treated with a concentrated aqueous solution of NH_4OH to affording 7-deaza-A derivative **16**, as the free diamine almost quantitatively (98%). The reaction of **16** with K_2PtCl_4 in a H_2O/MeOH (1:1) solution gave platinum complex **17** as a pale-yellow solid that precipitated from the reaction mixture in 70% yield.

The structures of all intermediates and of complex **17** were supported by spectroscopic analyses. High-resolution mass spectrometry and CHN analysis further confirmed the structure and purity of final complex **17**.

NMR Spectroscopy Study of the Reactivity of 17 towards dGMP

To assess the capability of **17** to react with the guanine bases of DNA as a bifunctional coordinating agent, such as cisplatin, we incubated **17** with a fourfold excess amount of dGMP in a water buffer containing 50 mM KH_2PO_4 and 50 mM KCl in a NMR tube in the dark at 37 °C. It is well known that the chemical shifts of H8 and H1′ of dGMP complexed with platinum(II) species are very sensitive to the geometry and the composition of the complex.[40] Thus, we monitored the reaction by recording the ^{1}H NMR spectrum every 30 min for the first 6 h and then every 6 h until no further changes were noticed. 10% [D_7]DMF was added to the buffer to assure the complete water solubility of **17**.

The reactivity of the *cis*-dichloroplatinum moiety of **17** towards dGMP was confirmed by the appearance of downfield-shifted aromatic signals (δ = 8.4–9.0 ppm), attributable to H8 of dGMP complexed with **17**, already in the first hour of incubation (Figure 2). Because of the asymmetry of the diaminoalkyl moiety coordinated with the platinum(II) center, up to six aromatic signals belonging to H8 of dGMP complexed with **17** were expected [two signals for each of the two complexes 7-deaza-A-Pt(dGMP)(Cl) and 7-deaza-A-Pt(dGMP)(H_2O); two signals for 7-deaza-A-Pt-(dGMP)$_2$]. This spectral complexity was observed in the NMR spectra recorded at an incubation time ≥3 h. Although the detailed assignment of all the dGMP H8 signals was not accomplished, because it is beyond the scope of this paper, the analysis of the literature data and the relative intensity of the NMR signals recorded at increasing incubation times (Figure 2) allowed us to tentatively assign (1) the signals at δ = 8.55 and 8.62 ppm of the dGMP H8 proton of the complexes 7-deaza-A-Pt(dGMP)(Cl) and 7-deaza-A-Pt(Cl)(dGMP) (**+** in Figure 2); (2) the signal at δ = 8.99 ppm (visible at incubation times ≥ 6 h) of the dGMP H8 proton of one of the two aqua complexes 7-deaza-A-Pt(dGMP)(H_2O) or 7-deaza-A-Pt(H_2O)(dGMP) (●); (3) the signals at δ = 8.52 and 8.65 ppm of the H8 protons of the two dGMP in the 7-deaza-A–Pt(dGMP)$_2$ complex (♦). The formation of platinum–d(GMP) complexes during the incubation time was also confirmed by the appearance of new upfield-shifted signals for the H2, H7, H8, and H1′ protons of **17** in the NMR spectra. In particular, the relative intensity of the NMR signals of H7 and H8 before and after coordination with d(GMP) disclosed that more than 50% of **17** reacted with one or two molecules of d(GMP) at incubation times within 12 and 36 h (Figure 2).

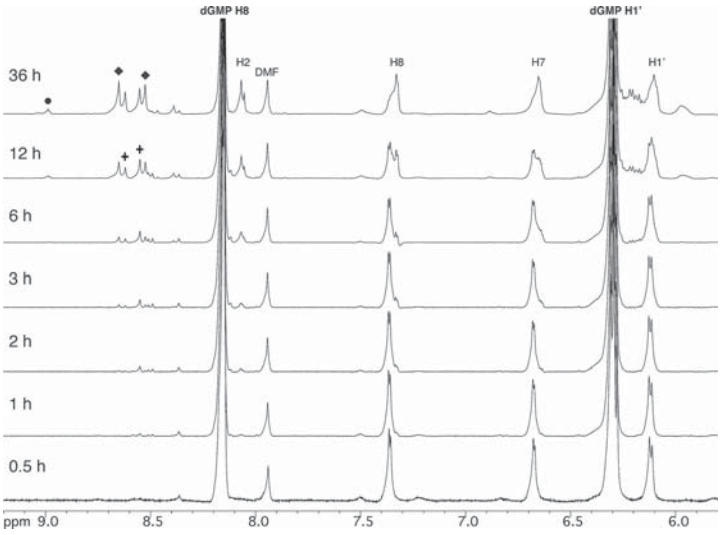

Figure 2. Aromatic region of the ^{1}H NMR spectra recorded at different time points monitoring the reaction between **17** and a fourfold excess amount of dGMP (50 mM KH_2PO_4, 50 mM KCl, pH 7.0, 37 °C in H_2O/D_2O = 9:1 containing 10% [D_7]DMF). The signals of **17** and dGMP are labeled by using regular and bold-type fonts, respectively. The H8 NMR signals of dGMP complexed with **17** are labeled with ●, ♦, and **+** (see also the Results and Discussion section).

 © 2015 Wiley-VCH Verlag GmbH & Co. KGaA, Weinheim

Antiproliferative Studies on the A549 and Cal27 Cell Lines

Compound **17**, its unplatinated precursor **16**, and cisplatin were examined by sulforhodamine B (SRB) assay[45] for their capability to inhibit growth of the A549 and Cal27 cell lines. To this end, cisplatin was dissolved in phosphate-buffered saline (PBS), whereas compound **16** and complex **17** were dissolved in 10% DMSO/PBS. All compounds were diluted immediately to the final concentrations by using the cell growth medium. The results showed that, although less active than cisplatin, both compounds induced dose-dependent growth inhibition in both cell lines after 96 h of treatment (Figure 3). Unexpectedly, for the tested cell lines, we observed that the antiproliferative activity of unplatinated precursor **16** was 1.5-fold higher than that of platinated complex **17** (Table 1). Further studies are needed to ascertain whether the lower activity of **17** is due to the residual "tubercidin-like" activity found for **16** or to the target "cisplatin-like alkylation" of purine bases by the dichloroplatinum moiety.

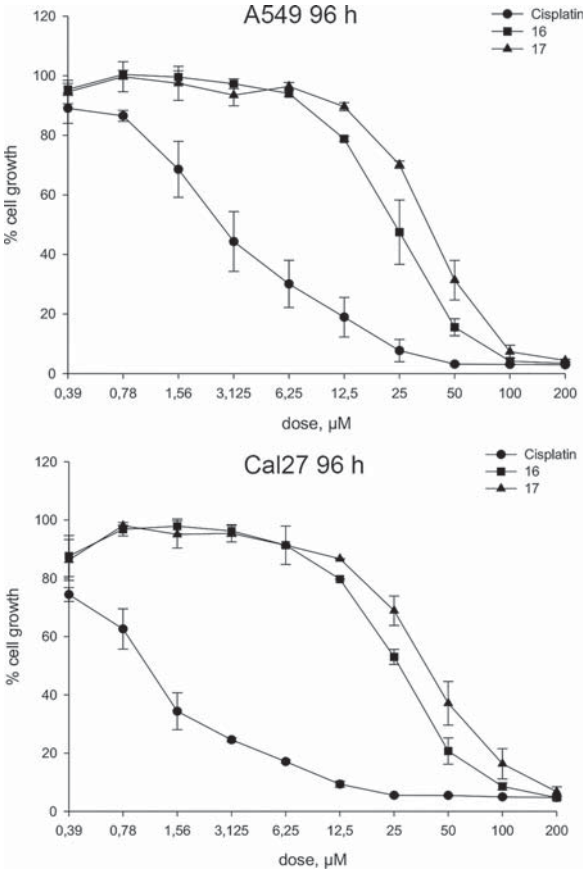

Figure 3. Antiproliferative effect of cisplatin, **16**, and **17** in the A549 (top) and Cal27 (bottom) cell lines. Cell growth assessment was performed by sulforhodamine B colorimetric assay (see the Experimental Section) and is expressed as the percentage of control for each time point. Values are the mean ± SD from at least three independent experiments performed in quadruplicate.

Table 1. Sensitivity of the A549 and Cal27 cell lines to cisplatin, **16**, and **17**.

Compound	IC_{50}[a] at 96 h [μM] ± SD	
	A549	Cal27
Cisplatin	2.69 ± 0.80	1.04 ± 0.20
16	23.62 ± 4.83	26.44 ± 1.64
17	36.20 ± 2.72	37.75 ± 5.58

[a] The half-maximal inhibitory concentration (IC_{50}) values were computed after 96 h of treatment (mean ± SD from at least three separate experiments performed in quadruplicate). SD: standard deviation.

Conclusions

In this paper, we described the synthesis of a new nucleoside platinum(II) complex (i.e., **17**) in which a cisplatin-like unit is joined to 7-deazaadenosine through an amino alkyl chain installed at the C6 position of purine. The cisplatin-like capability of **17** to react with the purine bases of DNA was confirmed by monitoring a model reaction with dGMP, whereas preliminary antiproliferative data on **17** and on unplatinated precursor **16** demonstrated that both compounds, although less potent than cisplatin, were able to inhibit the proliferation of the A549 and Cal27 human cell lines in a dose-dependent manner. Interestingly, the antiproliferative activity of free diamine **16** was 1.5-fold higher than that of platinated complex **17** on both cell lines. Studies are ongoing in our laboratories to assess the suitability of compound **16** to chelate other metals involved in cancer research and to construct novel unprecedented tubercidin derivatives with polyaminoalkyl chains at the C6 position of purine.

Experimental Section

General Methods: All reagents and solvents for the chemical syntheses were obtained from commercial sources and were used without further purification. All cell culture media, serum, antibiotics, and glutamine were purchased from LONZA (Basel, Switzerland). Sulforhodamine B (SRB) was from ICN Biomedicals (Irvine, CA, USA). ^1H NMR and ^{13}C NMR spectra were acquired with Varian Mercury Plus 400 MHz and Varian UNITY Inova 500 MHz instruments by using CD_3OD, $(CD_3)_2SO$, or C_6D_6 as solvents. A total of 450 μL of a 50 mM KH_2PO_4, 50 mM KCl, pH 7 buffer in H_2O/D_2O (9:1) was used to record the ^1H NMR spectra required to monitor the reaction of **17** (dissolved in 50 μL of [D_7]DMF) with dGMP. A double pulsed gradient spin echo (DPFGSE) module was included in the NMR pulse sequences to suppress the water signal.[46,47] Chemical shifts are reported in parts per million (δ) relative to the residual solvent signal [^1H: CD_2HOD δ = 3.31 ppm, $(CD_3)(CD_2H)SO$ δ = 2.54 ppm, C_6D_5H δ = 7.15 ppm; ^{13}C: CD_3OD δ = 49.0 ppm, $(CD_3)_2SO$ δ = 40.4 ppm, C_6D_6 δ = 128.6 ppm] and were assigned by 2D NMR experiments. UV spectra were recorded with a Jasco V-530 UV spectrophotometer. IR spectra were recorded with a Jasco FTIR 430 spectrophotometer. Optical rotations were determined with a Jasco polarimeter by using a 1 dm cell at 25 °C; concentrations are expressed in g 100 mL^{-1}. High-resolution MS spectra were recorded with a Thermo Orbitrap XL mass spectrometer by using the electrospray ionization (ESI) tech-

 © 2015 Wiley-VCH Verlag GmbH & Co. KGaA, Weinheim

nique in positive mode. Elemental analyses were performed with a Thermo Finnigan Flash EA 1112 CHN analyzer.

Cell Culture and Proliferation Assay: Human lung-cancer-derived A549 cells and human tongue squamous-carcinoma-derived Cal27 cells were grown in adhesion in Dulbecco's modified Eagle's medium. The medium was supplemented with 10% heat-inactivated fetal bovine serum, penicillin (50 U mL^{-1}), streptomycin (500 μg mL^{-1}), and glutamine (4 mmol L^{-1}) in a humidified atmosphere of 95% air and 5% CO_2 at 37 °C. Cell proliferation of A549 and Cal27 was evaluated in the presence and absence of increasing concentrations of the compounds by colorimetric assay with sulforhodamine B (SRB, ICN Biomedicals, Irvine, CA, USA). In detail, 1000 cells well^{-1} were seeded in 96-multiwell plates (Falcon, Becton Dickinson Labware, Franklin Lakes, NJ, USA) in quadruplicate. After 24 h, the cells were treated with the indicated compounds for 96 h and then the SRB assay was performed as described before.[45] The growth was evaluated as percentage compared to untreated cells.

Compound 10: A mixture of compound **8** (300 mg, 0.44 mmol), *tert*-butyl (3-aminopropyl)carbamate (**9**; 383 mg, 2.2 mmol), and Et_3N (61 μL, 0.44 mmol) was heated at reflux in EtOH (12 mL). During the reaction, a colorless solid, identified as compound **10**, precipitated. After 5 h (TLC monitoring: CH_2Cl_2/MeOH, 98:2), the system was cooled to room temperature, and the solid was then filtered, washed with cold EtOH, and dried. Colorless amorphous solid (287 mg, 80%). $[\alpha]_D$ = –122.1 (c = 0.1, CH_2Cl_2). ^{1}H NMR (400 MHz, C_6D_6): δ = 8.46 (s, 1 H, 2-H), 8.31–8.24 (m, 2 H, arom.), 8.02–7.92 (complex signal, 4 H, arom.), 7.20–6.81 (complex signal partially covered by residual solvent signal, 10 H, 8-H and arom.), 6.75 (d, J = 5.6 Hz, 1 H, 1′-H), 6.37–6.31 (m, 1 H, 2′-H), 6.25–6.16 (complex signal, 2 H, 3′-H and NH), 4.74–4.65 (m, 1 H, 4′-H), 4.64–4.56 (br. t, J = 6.1 Hz, 1 H, NH), 4.40–4.32 (m, 2 H, 5′-$H_{a,b}$), 3.41–3.31 (m, 2 H, CH_2NH), 2.96–2.87 (m, 2 H, CH_2NHBoc), 1.44 (s, 9 H, Boc), 1.37–1.26 (m, 2 H, CH_2) ppm. ^{13}C NMR (100 MHz, C_6D_6, 40 °C): δ = 166.0, 165.3, 165.2, 156.9, 156.4, 153.7, 150.4, 133.3, 133.2, 130.4, 130.1, 129.8, 129.5, 128.8, 128.6, 128.5, 120.6, 103.0, 89.1, 86.9, 80.6, 78.6, 75.0, 72.3, 64.1, 37.5, 30.7, 28.6 ppm. IR (KBr pellet): $\tilde{\nu}$ = 3411, 3382, 2980, 2936, 1728, 1687, 1602, 1562, 1513, 1451, 1270, 1175, 1127, 1027, 711 cm^{-1}. UV (CH_2Cl_2): λ_{max} = 235, 280 nm. HRMS (ESI): m/z = 836.1911 [M + Na]$^+$ ($C_{40}H_{40}BrN_5O_9Na$ requires 836.1907).

Compound 11: A solution of compound **10** (250 mg, 0.29 mmol) in CH_2Cl_2 (1.0 mL) was cooled to 0 °C. TFA (1.0 mL) was added in one portion. The mixture was then warmed to room temperature and stirred for 1 h (TLC monitoring: CH_2Cl_2/MeOH, 8:2). Solvents were evaporated under reduced pressure, and the crude material containing compound **11** as its TFA salt was used for the next step without purification. Oil (238 mg, 99%). $[\alpha]_D$ = –76.8 (c = 0.5, CH_2Cl_2). ^{1}H NMR (400 MHz, CD_3OD): δ = 8.18 (s, 1 H, 2-H), 8.10–8.05 (m, 2 H, arom.), 8.01–7.96 (m, 2 H, arom.), 7.85–7.89 (m, 2 H, arom.), 7.65–7.30 (complex signal, 10 H, 8-H and arom.), 6.61 (d, J = 5.3 Hz, 1 H, 1′-H), 6.26–6.19 (m, 1 H, 2′-H), 6.16–6.11 (m, 1 H, 3′-H), 4.95–4.80 (complex signal partially covered by residual solvent signal, 2 H, 4′-H and 5′-H_a), 4.67 (dd, J = 11.7, 3.5 Hz, 1 H, 5′-H_b), 3.71 (t, J = 6.7 Hz, 2 H, CH_2NH), 3.01 (t, J = 7.2 Hz, 2 H, C$H_2NH_3^+$), 2.08–1.97 (m, 2 H, CH_2) ppm. ^{13}C NMR (100 MHz, CD_3OD): δ = 167.5, 166.7, 166.4, 161.2 (q, J = 37.7 Hz), 156.6, 151.5, 149.8, 134.9, 134.6, 130.9, 130.8, 130.7, 130.2, 129.8, 129.6, 123.9, 115.8, 103.4, 89.8, 88.1, 81.5, 75.4, 72.8, 64.8, 38.5, 37.9, 28.7 ppm. IR (neat): $\tilde{\nu}$ = 3060, 2884, 1722, 1682, 1599, 1448, 1269, 1204, 1127, 711 cm^{-1}. UV (MeOH): λ_{max} = 277 nm. HRMS (ESI): m/z = 736.1390 [M + Na]$^+$ ($C_{35}H_{32}BrN_5NaO_7$ requires 736.1383).

Compound 13: Racemic acid **12** (177 mg, 0.58 mmol) was dissolved in dry DMF (4 mL) and then DIPEA (0.4 mL, 2.3 mmol), EDC (222 mg, 1.2 mmol), and HOBt (157 mg, 1.2 mmol) were added. The mixture was stirred for 30 min at room temperature. Compound **11** (200 mg, 0.24 mmol), dissolved in dry DMF (2 mL), was added to the previous solution, and the mixture was stirred for 16 h at room temperature (TLC monitoring: *n*-hexane/AcOEt, 4:6). The solvents were removed under reduced pressure, and the crude material was diluted with AcOEt (20 mL) and extracted with brine (3× 20 mL). The organic layer was separated, dried (Na_2SO_4), filtered, and concentrated under reduced pressure. The crude material containing compound **13** was purified by chromatography (silica gel, EtOAc in *n*-hexane, gradient up to 70%). The fractions containing the product were collected and concentrated to afford pure **13** as a mixture of diastereomers. Amorphous white solid (200 mg, 83%). ^{1}H NMR (400 MHz, CD_3OD): δ = 8.19 (s, 2 H, 2×2-H), 8.12–8.07 (m, 4 H, arom.), 8.02–7.97 (m, 4 H, arom.), 7.91–7.86 (m, 4 H, arom.), 7.66–7.33 (complex signal, 20 H, 2×8-H and arom.), 6.61 (d, J = 5.5 Hz, 2 H, 2×1′-H), 6.25–6.19 (m, 2 H, 2×2′-H), 6.18–6.12 (m, 2 H, 2×3′-H), 4.93–4.78 (complex signal partially covered by residual solvent signal, 4 H, 2×4′-H and 2×5′-H_a), 4.67 (dd, J = 3.6, 12.2 Hz, 2 H, 2×5′-H_b), 4.15–4.08 (m, 2 H, 2×CH), 3.71–3.54 (m, 4 H, 2×CH_2NH), 3.41 (dd, J = 4.7, 14.1 Hz, 2 H, 2×CH_aNHBoc), 3.36–3.26 (2 H, 2×CH_bNHBoc, covered by residual solvent signal), 3.24–3-14 (m, 4 H, 2×CH_2NHCO), 1.83–1.72 (m, 4 H, 2×CH_2), 1.41 (s, 9 H, Boc), 1.39 (s, 9 H, Boc), 1.37 (s, 9 H, Boc), 1.36 (s, 9 H, Boc) ppm. ^{13}C NMR (100 MHz, CD_3OD): δ = 173.2, 167.5, 166.7, 166.4, 158.9, 157.9, 157.7, 153.9, 150.4, 134.8, 134.7, 134.5, 130.9, 130.8, 130.7, 130.3, 129.9, 129.7, 129.6, 129.5, 122.5, 103.4, 89.7, 87.7, 81.4, 80.9, 80.5, 75.4, 72.9, 64.9, 57.4, 43.1, 38.4, 37.0, 30.7, 28.7 ppm. IR (KBr pellet): $\tilde{\nu}$ = 3330, 2923, 1723, 1597, 1262, 1160, 1117, 708 cm^{-1}. UV (MeOH): λ_{max} = 275 nm. HRMS (ESI): m/z = 1000.3085 [M + H]$^+$ ($C_{48}H_{55}BrN_7O_{12}$ requires 1000.3092).

Compound 14: Compound **13** (150 mg, 0.15 mmol) was dissolved in MeOH (10 mL) in a Parr reactor; NaOAc (13 mg, 0.16 mmol) and Pd/C (10% w/w, 42 mg, 0.04 mmol) were added and air was removed by insufflating H_2. The apparatus was then charged with H_2 (1.0 MPa), and the system was stirred for 2 h (TLC monitoring: *n*-hexane/AcOEt, 3:7) at room temperature. H_2 was removed, and the mixture was filtered through a Celite 545 pad that was then washed with MeOH (3× 10 mL). The solvent was evaporated under reduced pressure, and the crude was diluted with AcOEt (20 mL) and extracted with brine (3× 20 mL). The organic layer was separated, dried (Na_2SO_4), filtered, and concentrated under reduced pressure. The crude material containing compound **14** was used for the next reaction step without purification. Oil (137 mg, 99%). ^{1}H NMR (400 MHz, CD_3OD): δ = 8.21 (s, 2 H, 2×2-H), 8.16–8.08 (m, 4 H, arom.), 8.04–7.97 (m, 4 H, arom.), 7.92–7.83 (m, 4 H, arom.), 7.66–7.34 (complex signal, 18 H, arom.), 7.23 (d, J = 3.7 Hz, 2 H, 2×8-H), 6.67 (d, J = 5.9 Hz, 2 H, 2×1′-H), 6.58 (d, J = 3.7 Hz, 2 H, 2×7-H), 6.28–6.20 (m, 2 H, 2×2′-H), 6.19–6.12 (m, 2 H, 2×3′-H), 4.93–4.77 (complex signal partially covered by residual solvent signal, 4 H, 2×4′-H and 2×5′-H_a), 4.71–4.64 (m, 2 H, 2×5′-H_b), 4.15–4.08 (m, 2 H, 2×CH), 3.70–3.45 (m, 4 H, 2×CH_2NH), 3.44–3.36 (m, 2 H, 2×CH_aNHBoc), 3.36–3.26 (2 H, 2×CH_bNHBoc, covered by residual solvent signal), 3.22–3.11 (m, 4 H, 2×CH_2NHCO), 1.83–1.73 (m, 4 H, 2×CH_2), 1.40 (s, 9 H, Boc), 1.38 (s, 9 H, Boc), 1.36 (s, 9 H, Boc), 1.35 (s, 9 H, Boc) ppm. ^{13}C NMR (100 MHz, CD_3OD): δ = 173.0, 167.5, 166.7, 166.5, 158.9, 158.3, 157.7, 153.1, 150.8, 134.8, 134.7, 134.5, 130.9, 130.8, 130.7, 130.3, 129.9, 129.7, 129.6, 129.5, 122.5, 105.2, 101.6, 87.2, 81.2, 80.9, 80.5, 75.3, 73.0, 65.2, 57.5, 43.0, 38.5, 37.2, 30.6,

 © 2015 Wiley-VCH Verlag GmbH & Co. KGaA, Weinheim

28.7 ppm. IR (neat): $\tilde{\nu}$ = 3341, 2972, 1723, 1602, 1503, 1262, 1160, 1119, 708 cm^{-1}. UV (MeOH): λ_{max} = 276 nm. HRMS (ESI) *m/z* = 922.3989 $[M + H]^+$ ($C_{48}H_{55}N_7O_{12}$ requires 922.3987).

Compound 15: Compound **14** (115 mg, 0.12 mmol) was dissolved in MeOH (1.5 mL) and then MeONa (32 mg, 0.60 mmol) was added. The solution was stirred for 2 h at room temperature (TLC monitoring: AcOEt/MeOH, 9:1). The solution was neutralized with a few drops of glacial acetic acid; the solvents were removed under reduced pressure, and the crude was diluted with AcOEt (20 mL) and extracted with brine (3× 20 mL). The organic layer was separated, dried (Na_2SO_4), filtered, and concentrated under reduced pressure. The crude material was purified by column chromatography (silica gel, MeOH in AcOEt, gradient up to 10%). The fractions containing the product were collected and concentrated to afford pure **15**. Amorphous solid (67 mg, 95%). ^{1}H NMR (400 MHz, CD_3OD): δ = 8.12 (s, 2 H, 2×2-H), 7.25 (d, *J* = 3.6 Hz, 2 H, 2×8-H), 6.57 (d, *J* = 3.6 Hz, 2 H, 2×7-H), 5.96 (d, *J* = 6.6 Hz, 2 H, 2×1′-H), 4.71–4.65 (m, 2 H, 2×2′-H), 4.30–4.26 (m, 2 H, 2×3′-H), 4.18–4.08 (complex signal, 4 H, 2×4′-H and 2×CH), 3.84 (dd, *J* = 2.1, 12.4 Hz, 2 H, 2×5′-H_a), 3.71 (dd, *J* = 2.3, 12.4 Hz, 2 H, 2×5′-H_b), 3.68–3.48 (m, 4 H, 2×CH_2NH), 3.46–3.39 (m, 2 H, 2×CH_aNHBoc), 3.36–3.26 (2 H, 2×CH_bNHBoc, covered by residual solvent signal), 3.24–3.11 (m, 4 H, 2×CH_2NHCO), 1.86–1.75 (m, 4 H, 2×CH_2), 1.42 (s, 18 H, 2×Boc), 1.38 (s, 18 H, 2×Boc) ppm. ^{13}C NMR (100 MHz, CD_3OD): δ = 173.0, 158.8, 158.3, 157.7, 152.2, 149.5, 124.7, 105.9, 100.0, 91.6, 87.3, 80.9, 80.5, 75.3, 72.7, 63.7, 57.4, 43.0, 38.4, 37.2, 30.6, 28.7 ppm. IR (KBr pellet): $\tilde{\nu}$ = 3307, 2917, 1695, 1607, 1503, 1366, 1256, 1160, 1048 cm^{-1}. UV (MeOH): λ_{max} = 277 nm. HRMS (ESI): *m/z* =610.3184 $[M + H]^+$ ($C_{27}H_{44}N_7O_9$ requires 610.3201).

Compound 16: A solution of compound **15** (50 mg, 0.082 mmol) in CH_2Cl_2 (0.5 mL) was cooled to 0 °C. TFA (0.5 mL) was added in one portion. The mixture was then warmed to room temperature and stirred for 1 h (TLC monitoring: CH_2Cl_2/MeOH, 8:2). The solvents were evaporated under reduced pressure. The crude was treated with conc. NH_4OH solution (1 mL), evaporated under reduced pressure, dissolved in water (1 mL), and eventually lyophilized. The crude material containing compound **16** was used for the next reaction step without purification. Oil (33 mg, 99%). ^{1}H NMR (400 MHz, CD_3OD): δ = 8.12 (s, 2 H, 2×2-H), 7.27 (d, *J* = 3.7 Hz, 2 H, 2×8-H), 6.58 (d, *J* = 3.7 Hz, 2 H, 2×7-H), 5.95 (d, *J* = 6.6 Hz, 2 H, 2×1′-H), 4.69–4.63 (m, 2 H, 2×2′-H), 4.29–4.24 (m, 2 H, 2×3′-H), 4.13–4.08 (m, 2 H, 2×4′-H), 3.84 (dd, *J* = 2.6, 12.4 Hz, 2 H, 2×5′-H_a), 3.72 (dd, *J* = 2.8, 12.4 Hz, 2 H, 2×5′-H_b), 3.58 (t, *J* = 6.7 Hz, 4 H, 2×CH_2NH), 3.33–3.26 (6 H, covered by residual solvent signal, 2×CH and 2×CH_2NHCO), 2.85 (dd, *J* = 5.0, 13.1 Hz, 2 H, 2×C$H_a$$NH_2$), 2.85 (dd, *J* = 6.7, 13.1 Hz, 2 H, 2×C$H_b$$NH_2$), 1.91–1.80 (m, 4 H, 2×$CH_2$) ppm. ^{13}C NMR (100 MHz, CD_3OD): δ = 176.1, 158.1, 152.0, 149.7, 124.6, 105.9, 100.1, 91.5, 87.3, 75.3, 72.7, 63.7, 57.7, 46.7, 38.9, 37.7, 30.4 ppm. IR (neat): $\tilde{\nu}$ = 3269, 1610, 1551, 1365, 1314, 1248, 1079, 725 cm^{-1}. UV (MeOH): λ_{max} = 274 nm. HRMS (ESI): *m/z* = 410.2147 $[M + H]^+$ ($C_{17}H_{28}N_7O_5$ requires 410.2152).

Compound 17: Compound **16** (20 mg, 0.031 mmol) was dissolved in H_2O/MeOH (1:1, 1 mL). K_2PtCl_4 (13 mg, 0.031 mmol) was added, and the solution was stirred in the dark at room temperature for 16 h. The pale-yellow precipitate (15 mg, 70%) was collected by filtration, washed sequentially with H_2O and MeOH, and then dried. ^{1}H NMR (400 MHz, [D_6]DMSO): δ = 8.21 (br. t, 2 H, 2×N*H*CO), 8.12 (s, 2 H, 2×2-H), 7.55–7.50 (m, 2 H, 2×N*H*CH_2), 7.33 (br. d, *J* = 3.6 Hz, 2 H, 2×8-H), 6.60 (br. d, *J* = 3.6 Hz, 2 H, 2×7-H), 5.98 (br. d, *J* = 6.3 Hz, 2 H, 2×1′-H), 5.50–5.41 (br. s, 8 H, 2×PtN$H_2$$CH_2$ and 2×PtNH_2CH), 5.29 (br. t, 2 H, 2×5′-OH), 5.23 (br. d, 2 H, 2×2′-OH), 5.09 (br. d, 2 H, 2×3′-OH), 4.38–4.45 (m, 2 H, 2×2′-H), 4.11–4.04 (m, 2 H, 2×3′-H), 3.93–3.85 (m, 2 H, 2×4′-H), 3.66–3.40 (complex signal partially covered by residual solvent signal, 14 H, 2×5′-$H_{a,b}$, 2×CH_2NH, 2×PtNH_2CH_2, 2×PtNHC*H*), 3.19–3.11 (m, 4 H, CH_2NHCO), 1.80–1.66 (m, 4 H, 2×CH_2) ppm. ^{13}C NMR (100 MHz, [D_6]DMSO): δ = 167.0, 157.0, 152.3, 150.1, 123.1, 104.3, 100.1, 88.4, 86.0, 74.6, 71.6, 62.7, 61.9, 38.4, 37.7, 29.7 ppm. IR (KBr pellet): $\tilde{\nu}$ = 3247, 1665, 1610, 1561, 1363, 1311, 1245, 1089, 721 cm^{-1}. UV (H_2O): λ_{max} = 274 nm. HRMS (ESI): *m/z* = 717.1531 $[M – Cl + DMSO]^+$ ($C_{19}H_{33}ClN_7O_6PtS$ requires 717.1549). $C_{17}H_{27}Cl_2N_7O_5Pt$ (675.44): calcd. C 30.23, H 4.03, N 14.52; found C 30.27, H 4.08, N 14.58.

Reaction of 17 with dGMP: Complex **17** (2 mg, 3.0×10^{-3} mmol) was dissolved in [D_7]DMF (50 μL) and then added to 450 μL of a solution of dGMP (4 equiv.) in H_2O/D_2O (9:1) containing 50 mM KH_2PO_4 and 50 mM KCl, pH 7. The mixture was transferred to a NMR tube and was incubated at 37 °C. Water-suppressed ^{1}H NMR spectra (500 MHz, 37 °C) were then recorded as described in the general methods section and in the text.

Acknowledgments

This work was supported by POR Campania FESR 2007-2013 – Rete delle Biotecnolgie in Campania (project "FARMABIONET").

[1] B. Rosenberg, L. VanCamp, J. E. Trosko, V. H. Mansour, *Nature* **1969**, *222*, 385–386.
[2] A.-M. Florea, D. Büsselberg, *Cancers* **2011**, *3*, 1351–1371.
[3] A. Sigel, H. Sigel, *Metal Ions in Biological Systems: Metal Complexes in Tumor Diagnosis and as Anticancer Agents*, CRC Press, London, UK, **2004**.
[4] E. Wexselblatt, E. Yavin, D. Gibson, *Inorg. Chim. Acta* **2012**, *393*, 75–83.
[5] L. Kelland, *Nat. Rev. Cancer* **2007**, *7*, 573–584.
[6] B. W. Harper, A. M. Krause-Heuer, M. P. Grant, M. Manohar, K. B. Garbutcheon-Singh, J. R. Aldrich-Wright, *Chem. Eur. J.* **2010**, *16*, 7064–7077.
[7] L. R. Kelland, N. P. Farrell (Eds.), *Platinum-Based Drugs in Cancer Therapy*, Humana Press, Totowa, NJ, USA, **2000**.
[8] F. Arnesano, G. Natile, *Coord. Chem. Rev.* **2009**, *253*, 2070–2081.
[9] J. Zhang, L. Wang, Z. Xing, D. Liu, J. Sun, *Curr. Med. Chem. Anti-Cancer Agents* **2010**, *10*, 272–282.
[10] K. Wang, E. Gao, *Curr. Med. Chem. Anti-Cancer Agents* **2014**, *14*, 147–169.
[11] P. Sengupta, S. Basu, S. Soni, A. Pandey, B. Roy, M. S. Oh, K. T. Chin, A. S. Paraskar, S. Sarangi, Y. Connor, V. S. Sabbisetti, J. Kopparam, A. Kulkarni, K. Muto, C. Amarasiriwardena, I. Jayawardene, N. Lupoli, D. M. Dinulescu, J. V. Bonventre, R. A. Mashelkar, S. Sengupta, *Proc. Natl. Acad. Sci. USA* **2012**, *109*, 11294–11299.
[12] R. Cincinelli, L. Musso, S. Dallavalle, R. Artali, S. Tinelli, D. Colangelo, F. Zunino, M. De Cesare, G. L. Beretta, N. Zaffaroni, *Eur. J. Med. Chem.* **2013**, *63*, 387–400.
[13] J. S. Butler, P. J. Sadler, *Curr. Opin. Chem. Biol.* **2013**, *17*, 175–188.
[14] A. Arouri, A. H. Hansen, T. E. Rasmussen, O. G. Mouritsen, *Curr. Opin. Colloid Interface Sci.* **2013**, *18*, 419–431.
[15] C. Tomuleasa, O. Soritau, A. Orza, M. Dudea, B. Petrushev, O. Mosteanu, S. Susman, A. Florea, E. Pall, M. Aldea, G. Kacso, V. Cristea, I. Berindan-Neagoe, A. Irimie, *J. Gastrointestin. Liver. Dis.* **2012**, *21*, 187–196.

 © 2015 Wiley-VCH Verlag GmbH & Co. KGaA, Weinheim

[16] Y. H. Quan, B. Kim, J.-H. Park, Y. Choi, Y. H. Choi, H. K. Kim, *Exp. Lung. Res.* **2014**, *40*, 475–484.
[17] Y. Min, C.-Q. Mao, S. Chen, G. Ma, J. Wang, Y. Liu, *Angew. Chem. Int. Ed.* **2012**, *51*, 6742–6747; *Angew. Chem.* **2012**, *124*, 6846–6851.
[18] S. Wang, W. Chu, Y. Wang, S. Liu, J. Zhang, S. Li, H. Wei, G. Zhou, X. Qin, *Appl. Organomet. Chem.* **2013**, *27*, 373–379.
[19] Dubyak, G. R, *Am. J. Physiol. Cell Physiol.* **2013**, *304*, C403–C405.
[20] A. H. Guse, *Curr. Mol. Med.* **2002**, *2*, 273–282.
[21] H. C. Lee, *J. Biol. Chem.* **2012**, *287*, 31633–31640.
[22] G. Oliviero, S. D'Errico, N. Borbone, J. Amato, V. Piccialli, M. Varra, G. Piccialli, L. Mayol, *Tetrahedron* **2010**, *66*, 1931–1936.
[23] R. S. Hosmane, *Curr. Top. Med. Chem.* **2002**, *2*, 1093–1109.
[24] S. D'Errico, G. Oliviero, J. Amato, N. Borbone, V. Cerullo, A. Hemminki, V. Piccialli, S. Zaccaria, L. Mayol, G. Piccialli, *Chem. Commun.* **2012**, *48*, 9310–9312.
[25] R. M. Huang, Y. N. Chen, Z. Zeng, C. H. Gao, X. Su, Y. Peng, *Mar. Drugs* **2014**; *12*, 5817–5838.
[26] S. Meike, T. Yamamori, H. Yasui, M. Eitaki, A. Matsuda, M. Morimatsu, M. Fukushima, Y. Yamasaki, O. Inanami, *Mol. Cancer* **2011**, *10*, 92.
[27] C. K. Chu, *Antiviral Nucleosides: Chiral Synthesis and Chemotherapy*, Elsevier, Amsterdam, The Netherlands, **2003**.
[28] L. P. Jordheim, D. Durantel, F. Zoulim, C. Dumontet, *Nat. Rev. Drug Discovery* **2013**, *12*, 447–464.
[29] M. F. Caso, D. D'Alonzo, S. D'Errico, G. Palumbo, A. Guaragna, *Org. Lett.* **2015**, *17*, 2626–2629.
[30] D. Montagner, V. Gandin, C. Marzano, B. Longato, *J. Inorg. Biochem.* **2011**, *105*, 919–926.
[31] P. Starha, I. Popa, Z. Trávníček, J. Vančo, *Molecules* **2013**, *18*, 6990–7003.
[32] M. Coluccia, A. Boccarelli, C. Cermelli, M. Portolani, G. Natile, *Met. Based Drugs* **1995**, *2*, 249–256.
[33] C. Nervi, M. A. Vigna, G. Cavigiolio, M. Ravera, D. Osella, *Inorg. Chim. Acta* **2005**, *358*, 2799–2803.
[34] S. D'Errico, G. Oliviero, V. Piccialli, J. Amato, N. Borbone, V. D'Atri, F. D'Alessio, R. Di Noto, F. Ruffo, F. Salvatore, G. Piccialli, *Bioorg. Med. Chem. Lett.* **2011**, *21*, 5835–5838.
[35] S. D'Errico, G. Oliviero, N. Borbone, V. Piccialli, B. Pinto, F. De Falco, M. C. Maiuri, R. Carnuccio, V. Costantino, F. Nici, G. Piccialli, *Molecules* **2014**, *19*, 9339–9353.
[36] L. V. Frolova, I. V. Magedov, A. E. Romero, M. Karki, I. Otero, K. Hayden, N. M. Evdokimov, L. M. Y. Banuls, S. K. Rastogi, W. R. Smith, S.-L. Lu, R. Kiss, C. B. Shuster, E. Hamel, T. Betancourt, S. Rogelj, A. Kornienko, *J. Med. Chem.* **2013**, *56*, 6886–6900.
[37] G. Acs, E. Reich, M. Mori, *Proc. Natl. Acad. Sci. USA* **1964**, *52*, 493–501.
[38] M. F. Biabani, S. P. Gunasekera, *Pharm. Biol.* **2002**, *40*, 302–303.
[39] B. K. Hwang, B. S. Kim, *Pestic. Sci.* **1995**, *44*, 255–260.
[40] A. Marcelis, C. G. Van Kralingen, J. Reedijk, *J. Inorg. Biochem.* **1980**, *13*, 213–222.
[41] E. Pantoja, A. Gallipoli, S. van Zutphen, S. Komeda, D. Reddy, D. Jaganyi, M. Lutz, D. M. Tooke, A. L. Spek, C. Navarro-Ranninger, J. Reedijk, *J. Inorg. Biochem.* **2006**, *100*, 1955–1964.
[42] F. Seela, X. Ming, *Tetrahedron* **2007**, *63*, 9850–9861.
[43] S. Moradell, J. Lorenzo, A. Rovira, S. van Zutphen, F. X. Avilés, V. Moreno, R. de Llorens, M. A. Martinez, J. Reedijk, A. Llobet, *J. Inorg. Biochem.* **2004**, *98*, 1933–1946.
[44] E. A. Véliz, P. A. Beal, *J. Org. Chem.* **2001**, *66*, 8592–8598.
[45] E. Di Gennaro, F. Bruzzese, S. Pepe, A. Leone, P. Delrio, P. R. Subbarayan, A. Avallone, A. Budillon, *Cancer Biol. Ther.* **2009**, *8*, 782–791.
[46] T. L. Hwang, A. J. Shaka, *J. Magn. Reson., Ser. A* **1995**, *112*, 275–279.
[47] C. Dalvit, *J. Biomol. NMR* **1998**, *11*, 437–444.

Received: July 29, 2015
Published Online: November 3, 2015

 © 2015 Wiley-VCH Verlag GmbH & Co. KGaA, Weinheim

Molecules **2014**, *19*, 9339-9353; doi:10.3390/molecules19079339

OPEN ACCESS

molecules

ISSN 1420-3049

www.mdpi.com/journal/molecules

Article

Synthesis and Pharmacological Evaluation of Modified Adenosines Joined to Mono-Functional Platinum Moieties

Stefano D'Errico [1], Giorgia Oliviero [1,*], Nicola Borbone [1], Vincenzo Piccialli [2], Brunella Pinto [1], Francesca De Falco [1], Maria Chiara Maiuri [1,3], Rosa Carnuccio [1], Valeria Costantino [1], Fabrizia Nici [1] and Gennaro Piccialli [1]

[1] Dipartimento di Farmacia, Università degli Studi di Napoli "Federico II", via D. Montesano, 49, 80131 Napoli, Italy; E-Mails: stefano.derrico@unina.it (S.D.); borbone@unina.it (N.B.); brunella.pinto87@gmail.com (B.P.); francesca.defalco@unina.it (F.D.F.); mariachiara.maiuri@unina.it (M.C.M.); rosa.carnuccio@unina.it (R.C.); valeria.costantino@unina.it (V.C.); fabrizia.nici@unina.it (F.N.); picciall@unina.it (G.P.)

[2] Dipartimento di Scienze Chimiche, Università degli Studi di Napoli "Federico II", via Cintia, 21, 80126 Napoli, Italy; E-Mail: vinpicci@unina.it

[3] INSERM U848, IGR, 39 rue C. Desmoulins, 94805 Villejuif, France

* Author to whom correspondence should be addressed; E-Mail: golivier@unina.it; Tel.: +39-081-679-896.

Received: 26 March 2014; in revised form: 23 June 2014 / Accepted: 25 June 2014 / Published: 3 July 2014

Abstract: The synthesis of four novel platinum complexes, bearing N^6-(6-amino-hexyl)adenosine or a 1,6-di(adenosin-N^6-yl)-hexane respectively, as ligands of mono-functional cisplatin or monochloro(ethylendiamine)platinum(II), is reported. The chemistry exploits the high affinity of the charged platinum centres towards the N7 position of the adenosine base system and a primary amine of an alkyl chain installed on the C6 position of the purine. The cytotoxic behaviour of the synthesized complexes has been studied in A549 adenocarcinomic human alveolar basal epithelial and MCF7 human breast adenocarcinomic cancer cell lines, in order to investigate their effects on cell viability and proliferation.

Keywords: platinum complexes; nucleosides; cisplatin; chemotherapy

1. Introduction

The discovery of the anti-proliferative properties of cisplatin [1] marked the beginning of modern chemotherapy based on the use of metal complexes capable of blocking the replication of cancer cells targeting the nuclear DNA [2,3]. In fact, it is widely accepted that cisplatin, once inside the cell, may form a highly reactive species [4,5] that can react with DNA through the formation of intra-strand linkages [6,7]. Such linkages alter the secondary structure of DNA, resulting in an inhibition of transcription and replication, ultimately leading to cell death [4]. However, the poor solubility in biological fluids [8], the serious side effects [9,10], and, more importantly, the intrinsic and acquired resistance of many types of tumors [5], have limited its use in the clinic. Carboplatin and oxaliplatin, second and third generation anti-neoplastic agents, respectively, are able to enhance the quality of life of patients in terms of dosage and drug administration. However, they can still trigger mechanisms of resistance (intrinsic and/or acquired) during repeated cycles of oncological treatment [5]. It was then discovered that the presence of more charged metal centres separated by unbranched alkylamine chains leads to complexes capable of being uptaken by cells via active import [11] and of overcoming the intrinsic and/or acquired resistance in some tumors [6,12–15]. Based on the understanding that they may exert anti-tumoral activities through inter-strand linkages with DNA that cannot be repaired by enzymes [16], many multinuclear platinum complexes have recently been synthesized, by varying the diamine backbone chain length, or by introducing modified linkers [8,10–12,17,18]. In addition, new Pt-based compounds have been obtained by conjugating biologically important substances or drugs to Pt-containing subunits [19–24] and novel drug-delivery based methodologies have been explored to vehiculate platinum-based anti-cancer complexes directly against tumors [25,26].

Nucleoside and nucleotide anti-metabolites and their base analogues are able to inhibit specific pathways of the cancer cell metabolism by blocking the biosynthesis or the function of nucleic acids. For example, the combination of cisplatin and 5-fluorouracil, a chemotherapeutic agent that inhibits thymidylate synthase, has been extensively used in clinical practice to treat various types of cancer. Acyclovir, a guanosine nucleoside analogue containing an open-chain sugar surrogate, has been used as a ligand for platinum and the corresponding complex exhibits high *in vitro* activity against various *herpes* viruses [27]. Furthermore, the synthesis and the preliminary pharmacological activity of novel modified adenosines and thymidines, employed as N-donor ligands of platinum(II) dichloride complexes, have been recently reported [28,29].

Recently, we have reported the solid-phase synthesis and the pharmacological activity of the first examples of bis-platinated nucleoside complexes in which the mono-functional metal is linked both to N-7 of the purine nucleus of inosine and to the terminal amino-group of a hexylamine side chain installed on N-1 (compounds **1**–**3**, Figure 1) [30]. The amino-alkyl chain was introduced on the purine base system through a chemical strategy recently developed by us [30–36]. These complexes showed very good water solubility thanks to the charged platinum centres and to the ribose hydroxyl groups. They were tested against four different human tumor cell lines and, in particular, the complex bearing two monofunctional cisplatin units was revealed to be more cytotoxic than cisplatin against the MCF7 cancer cell line in a short-term exposure assay [30].

Figure 1. Bis-platinated nucleoside complexes synthesized starting from inosine [30].

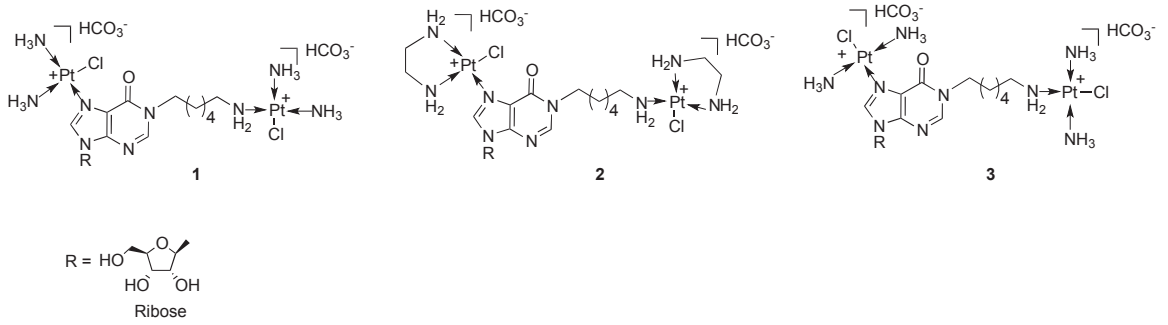

In the light of the above results, to investigate the importance of nucleoside scaffolds in the construction of novel platinum complexes we have speculated about the antitumoral activity of cisplatin-adenosine complexes. As a result, in this paper we report on the synthesis of four dinuclear platinum complexes **8a**,**b** and **10a**,**b** (Scheme 1) carrying N^6-(6-aminohexyl)adenosine (compound **5**, Scheme 1) or a 1,6-di-(adenosin-N^6-yl)-hexane (compound **9**, Scheme 1) respectively, as ligands of mono-functional cisplatin or monochloro(ethylene diamine)platinum(II) (compounds **7a** and **7b**, respectively, Scheme 1).

Scheme 1. Synthesis of complexes **8** and **10**.

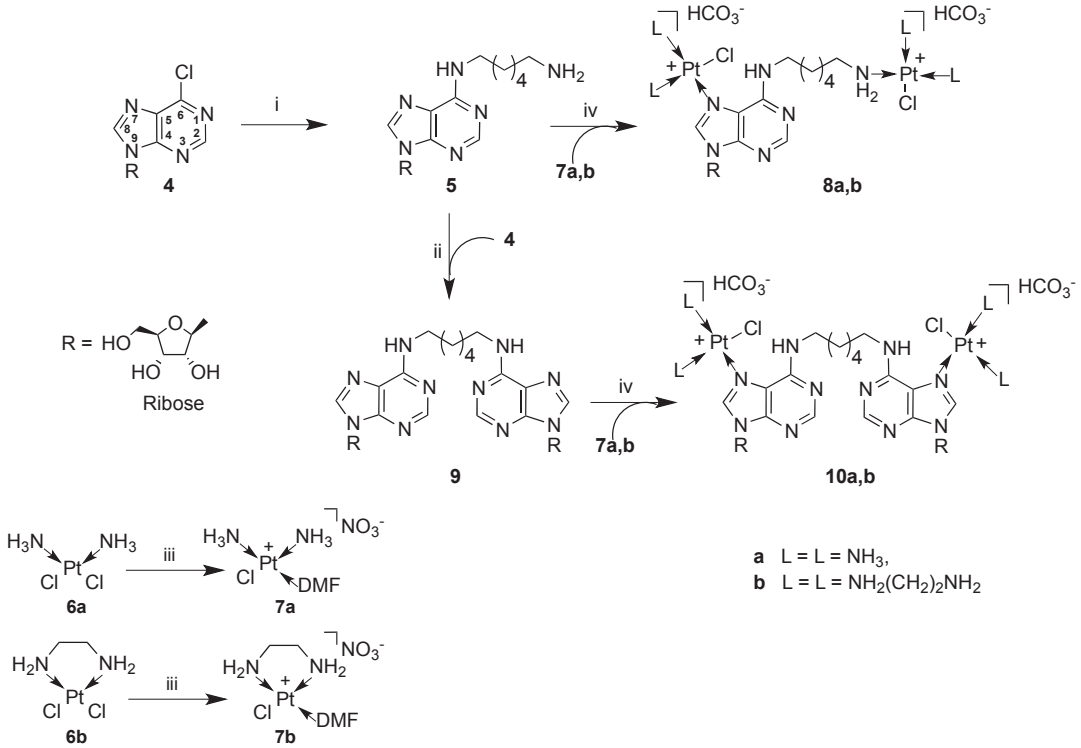

Reagents and conditions: (i) $NH_2(CH_2)_6NH_2$ (7 equiv.), TEA, EtOH, 3 h, reflux; (ii) **4** (1.5 equiv.), TEA, EtOH, 5 h, reflux; (iii) $AgNO_3$ (0.9 equiv.), DMF, 16 h, r.t.; (iv) **7a**,**b**, 16 h, r.t..

In the case of complexes **8a**,**b** the monofunctional platinum centres are linked to the N-7 of the purine base and to the terminal amino group of a hexylamine side chain bonded to N-6, whereas for the complexes **10a**,**b** they are both linked to N-7.

Platinum complexes, endowed with particular structural strains, have been designed to evaluate alternative interactions with DNA strands [8,12,17,37,38]. The novel prepared complexes **8a**,**b** and **10a**,**b** are characterized by a rigid planar purine substructure joined to a flexible hexylamine chain. On this basis, it could be expected that they may alter the binding mode with DNA through, for example, base-stacking or by the formation of multiple hydrogen bonds. Therefore, we have investigated the preliminary effects of these compounds on viability and proliferation in two different human cancer cell lines.

2. Results and Discussion

2.1. Synthesis and Characterization

The synthesis of the novel modified adenosine-based platinum complexes **8a**,**b** and **10a**,**b** is depicted in Scheme 1. 6-Cloropurine riboside **4** proved to be a good candidate to obtain the key intermediate **5** from which the construction of complexes **8a**,**b** and **10a**,**b** has been accomplished. As reported by Schammells *et al.* [39] seven equivalents of 1,6-diaminohexane have proved sufficient to convert **4** into **5** in a very good yield (86%), avoiding the formation of dimeric species, which would complicate the purification procedure. In fact, the recovery of **5** from the reaction mixture was easily performed thanks to its insolubility in EtOH upon cooling. Compound **9** was prepared by reacting **4** with a slight excess of **5**. During the reaction, this substance precipitated from the reaction mixture as a white solid which was then collected in 93% yield by filtration. This represents a very good improvement on the reported yield for **9** (12%) [40].

Next, the platinum-containing moieties were installed. In particular, treatment of **5** and **9** with a seven-fold excess of the suitable platinating complex **7a**,**b**, activated by overnight reaction with $AgNO_3$ (0.9 equiv.) in DMF, furnished the bisplatinated compounds **8a**,**b** and **10a**,**b**. Purification of these substances could be accomplished by reverse-phase HPLC only using a gradient of CH_3CN in 0.1 M triethylammonium bicarbonate buffer (TEAB) as the solvent mixture, whereas complex chromatographic patterns were observed in the absence of the TEAB.

The structures of complexes **8a**,**b** and **10a**,**b** (yields 58%–62%) were supported by 2D-NMR and positive mode high resolution mass spectrometry (HRMS) data; whereas their purity was ascertained by CHN analyses.

In Figure 2 (panel A) the representative HRMS spectrum of complex **8a** is reported; in particular, the isotopic pattern of the base peak (expansion, panel B) perfectly fits with that of the calculated one (expansion, panel C), confirming the presence of two Pt and two Cl atoms and a net 2+ charge.

In the ^{1}H-NMR spectra of **8a**,**b** and **10a**,**b** the downfield shift of H-8, compared with the resonance of the same proton in **5** and **7** ($\Delta\delta$ = 0.6 and 0.5, respectively), confirmed the presence of the N(7) → Pt bond in all these substances [41,42]. In Table 1 the differences between the ^{13}C-NMR shifts of the Pt-coordinated and not-coordinated purine carbon atoms ($\Delta\delta = \delta_{complex} - \delta_{ligand}$, ppm) are listed: in the case of complexes **8a**,**b** significant coordination shifts were found for the C-5 and C-8 atoms,

whereas for the complexes **10a**,**b** the C-5 atoms underwent the major shifts. Further evidence of metallation at N-7 come from the increased acidity of the H-8 as indicated by the reduced intensity of the pertinent signal in the ^{1}H-NMR spectra of **8a**,**b** and **10a**,**b**, when these complexes were dissolved in D_2O and the spectra acquired after several hours [43]. ^{1}H-NMR analyses excluded also the presence of equilibria involving migrations of the platinum moieties from N-7 to N-1 of the nucleobases; such migrations would shift the H-2 resonances of complexes **8a**,**b** and **10a**,**b** to higher frequences in comparison to the same signals of compounds **5** and **9**, respectively [44]. The resonances of the methylene protons belonging to the CH_2-NH_2-Pt moieties were seen as broad partly overlapped triplets in the range 2.3–2.7 ppm, in the proton spectra of **8b** and **10b**, likewise the protons of the methylene group geminal to platinum in **8a** resonated as a triplet at δ 2.6. In ^{13}C-NMR spectra of **8a** and **8b** the 5 ppm downfield shift of the ω-methylene carbon could be a consequence of the NH_2 platination.

Figure 2. HRMS spectrum of complex **8a** (panel **A**). Expansion of the isotopic pattern of the base peak (panel **B**) and of the corresponding calculated one (panel **C**).

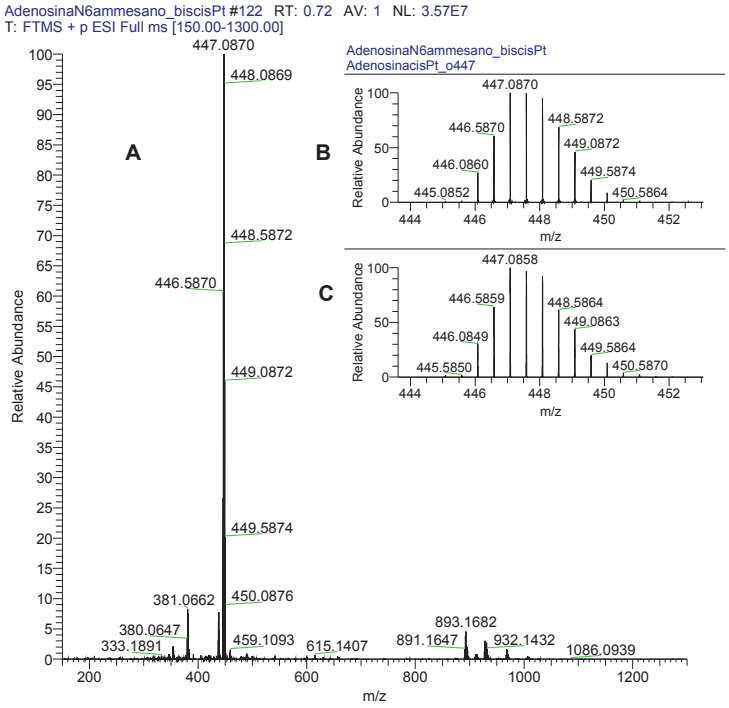

In the UV spectra of the complexes **8a**,**b** and **10a**,**b** the maxima of absorption appeared red-shifted (Δλ = 10–13 nm) in respect to those of the free ligands, in accordance with literature data [45]. Comparison of the IR spectra of the ligands and complexes did not provide evidence about the bonding mode of the ligands in the complexes; in fact in the 4000–2700 cm^{-1} region very little information could be obtained about the nature of metal-ligand interaction, because of the presence of broad and intense bands belonging to hydrogen-bonded hydroxyls of the ribose moieties. The 1800–400 cm^{-1} region, where vibration frequencies of purine and ribose skeletons fall, did not furnish significant differences between platinated and not-platinated nucleosides. Furthermore, in the region 550–400 cm^{-1}, where the resonances of Pt-N could be expected [45,46], no distinctive bands were observed.

Table 1. Differences between the ^{13}C-NMR shifts of the Pt-coordinated and not-coordinated purine carbons ($\Delta\delta = \delta_{complex} - \delta_{ligand}$, ppm).

Entry	^{13}C-NMR (Δδ, ppm)				
	C-2	C-4	C-5	C-6	C-8
8a [39]	−1.0	−1.4	−2.9	0.9	2.1
8b [39]	−1.0	−1.3	−2.8	0.9	2.1
10a	−1.9	−2.3	−4.2	−0.1	0.9
10b	−2.0	−2.5	−4.2	0.1	1.1

2.2. Cytotoxicity Studies

The synthesized complexes were subjected to preliminary cell viability and proliferation assays. In particular, the cytotoxic behaviour was studied in A549 adenocarcinomic human alveolar basal epithelial and MCF7 human breast adenocarcinomic cancer cell lines by MTT and BrdU assays, to investigate the potential effects of platinum complexes on cell viability and proliferation, respectively. The incubation of A549 cells with **8a**,**b** and **10a,b** (50, 100 and 200 μM) for 72 h caused a concentration-dependent reduction of cell survival (Figure 3, panel A) as well as an inhibition of cell proliferation at the higher concentrations (Figure 3, panel B) compared to untreated cells. Indeed, comparable results were obtained when the cell number was directly determined by cell counting (data not shown).

Figure 3. Effect of **8a**, **8b**, **10a** and **10b** on cell viability and proliferation. A549 cells were incubated with cisplatin, **8a**, **8b**, **10a** and **10b** (50, 100 and 200 μM) for 72 h. Thereafter, cell viability (panel **A**) and proliferation (panel **B**) were determined, respectively, by MTT and BrdU assay as described in the Experimental Section (*** $p < 0.001$, ** $p < 0.01$, * $p < 0.05$ *vs.* untreated cells).

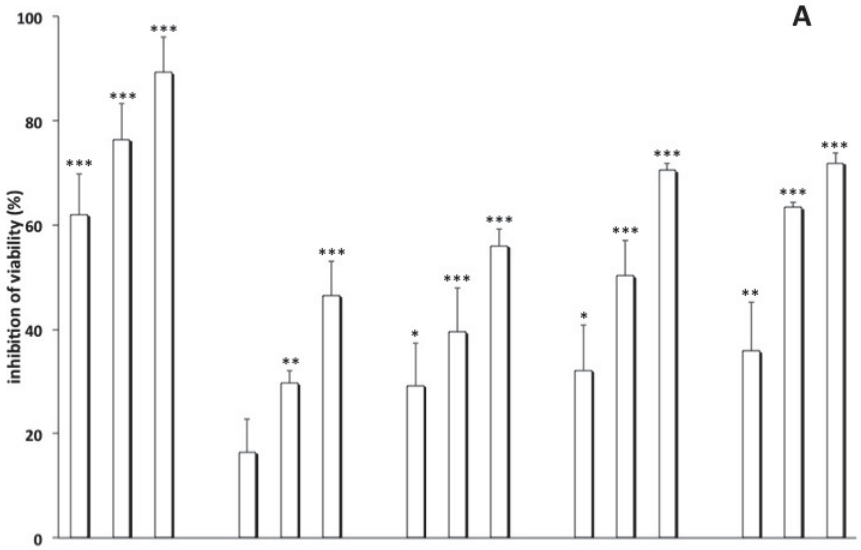

Figure 3. *Cont.*

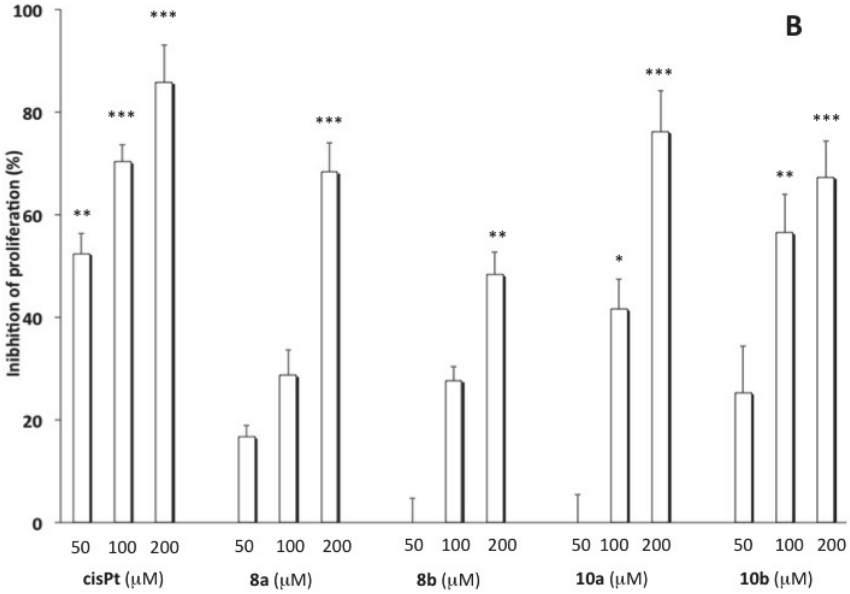

The compounds **8b**, **10a** and **10b** (50, 100 and 200 μM) modified the viability and proliferation of MCF7 cells at higher concentrations, according to the published evidence that these cells have been associated with cisplatin resistance [47]. The compound **8a** proved to reduce the proliferation of the MCF7 cell line with a greater ability than the other compounds. Strikingly, compound **8a** was able to inhibit the cell proliferation slightly better than cisplatin, but only at 50 μM concentration (Figure 4).

Figure 4. Effect of **8a**, **8b**, **10a** and **10b** on cell viability and proliferation. MCF7 cells were incubated with cisplatin, **8a**, **8b**, **10a** and **10b** (50, 100 and 200 μM) for 72 h. Thereafter, cell viability (panel **A**) and proliferation (panel **B**) were determined, respectively, by MTT and BrdU assay as described in the Experimental Section (*** $p < 0.001$, ** $p < 0.01$, * $p < 0.05$ *vs.* untreated cells).

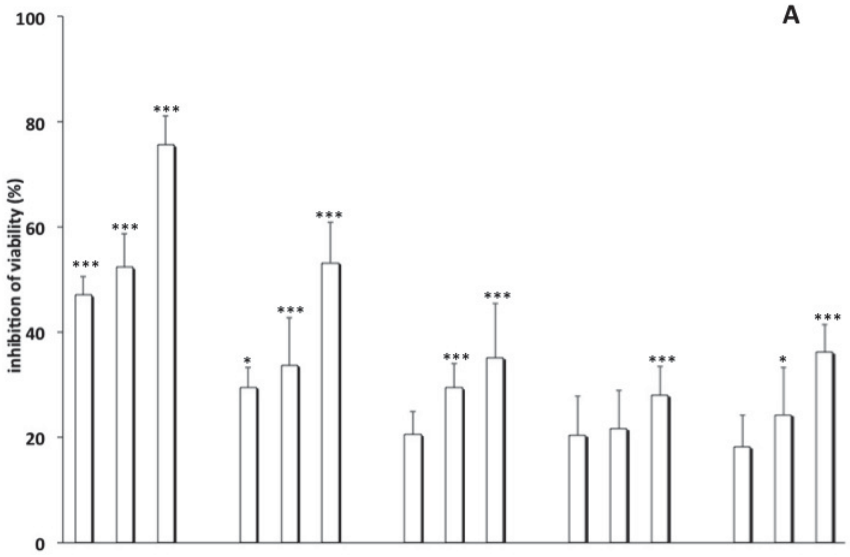

Figure 4. *Cont.*

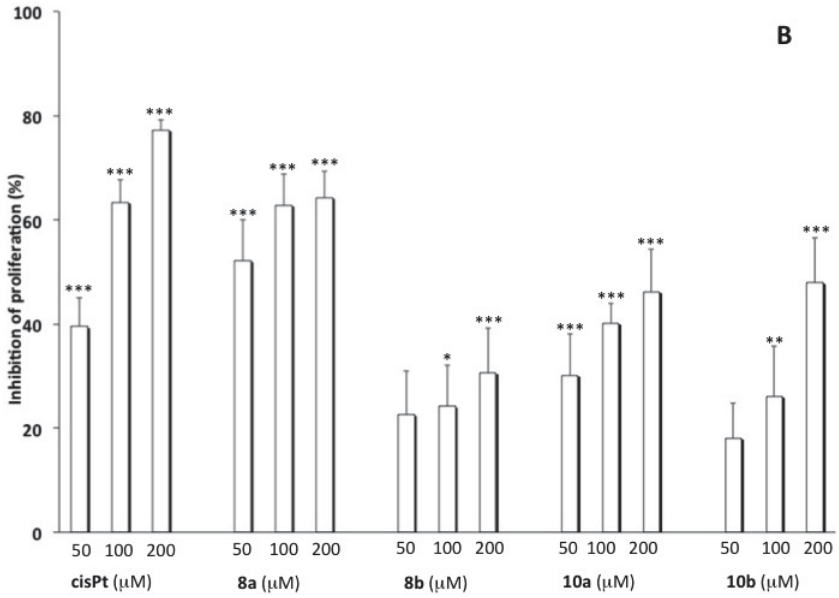

3. Experimental Section

3.1. General Methods

All the reagents and solvents were obtained from commercial sources and used without further purification. ^{1}H- and ^{13}C-NMR spectra were acquired on Varian Mercury Plus 400 MHz instrument using D_2O or $(CD_3)_2SO$ as solvents. Chemical shifts were reported in parts per million (δ) relative to the residual solvent signal (^{1}H: HDO 4.80; ^{13}C: $(CD_3)(CD_2H)SO$ 40.4) and assigned by 2D-NMR experiments. UV spectra were recorded on a Jasco V-530 UV spectrophotometer. IR spectra were recorded on a Jasco FT-IR 430 spectrophotometer. High-resolution MS spectra were recorded on a Thermo Orbitrap XL mass spectrometer using the electrospray ionization (ESI) technique in positive mode. Elemental analyses were performed on a Thermo Finnigan Flash EA 1112 CHN analyzer. RP-HPLC analyses and purifications were carried out on a Jasco UP-2075 Plus pump, equipped with a Jasco UV-2075 Plus UV detector, using a C-18 reverse-phase column (5 μm, 4.8 × 150 mm), eluted with a linear gradient of CH_3CN in 0.1 M triethylammonium bicarbonate (TEAB) buffer (System A: from 0% to 50% in 90 min, flow 1.3 mL/min, or System B: from 0% to 100% in 90 min, flow 1.3 mL/min). Human alveolar basal carcinoma epithelial cells (A549) and human breast cancer cells (MCF7) were grown in Dulbecco's modified Eagle's medium (DMEM) supplemented with 10% Foetal bovine serum (FBS), 100 U/mL penicillin and 100 U/mL streptomycin at 37 °C under 5% CO_2. The cell lines were all from the ATCC catalogue. All media and supplements for cell culture were purchased from Gibco-Invitrogen (GE Healthcare).

N^6-(6-Aminohexyl)adenosine (**5**). Compound **5** (326 mg) was obtained by reaction of **4** (297 mg, 01.04 mmol) in accordance to the procedure by Schammells *et al.* [37]. Spectroscopic data and yields were in agreement with those reported by the authors.

1,6-Di-(adenosin-N^6-yl)-hexane (**9**). Compound **5** (100 mg, 0.27 mmol), 6-chloropurine riboside (**4**, 116 mg, 0.40 mmol), Et_3N (41 μL, 0.30 mmol) were refluxed in EtOH (1 mL). During the reaction, a colourless solid precipitated from the reaction. After 5 h it was filtered, washed with boiling EtOH and dried, giving **9** as a colourless powder (164 mg, 93%). El. An. Calcd. for $C_{26}H_{36}N_{10}O_8$: C, 50.64; H, 5.88; N, 22.72. Found: C, 50.68; H, 5.90; N, 22.69. ^{1}H-NMR and UV data were in agreement with those reported in literature [38]. ^{13}C-NMR (100 MHz, $(CD_3)_2SO$) δ 155.6 (C-2), 153.3 (C-6), 149.1 (C-4), 140.5 (C-8), 120.7 (C-5), 88.9 (C-1'), 86.9 (C-4'), 74.4 (C-2'), 71.6 (C-3'), 62.6 (C-5'), 40.8 (CH_2NH, covered by residual solvent signal), 30.0 (CH_2), 27.1 (CH_2); IR (KBr pellet) 3336, 2935, 2861 1630, 1587, 1537, 1474, 1418, 1369, 1334, 1307, 1221, 1185, 1130, 1097, 1058, 985, 866, 822, 793, 641, 554 cm^{-1}; *m/z* 639.2620 (HRESIMS) ($[M + Na]^+$, $C_{26}H_{36}N_{10}NaO_8$, requires 639.2615).

3.2. General Procedure for the Preparation of Dinuclear Platinum Complexes **8a**,**b** *and* **10a**,**b**

In a representative experiment, cisplatin (57 mg, 0.19 mmol) was activated by treatment with $AgNO_3$ (29.0 mg, 0.17 mmol) in DMF (2 mL) in the dark (16 h, r.t.). AgCl was removed by filtration and the resulting solution of $[Pt(NH_3)_2(Cl)DMF]^+(NO_3)^-$ in DMF was added to compound **5** (10 mg, 0.027 mmol). The solution was shaken in the dark (16 h, r.t.) and then filtered over a GHP Acrodisc 13 mm syringe filter (0.45 μm GHP membrane). The filter was washed with the minimal amount of DMF and the clarified solution was then subjected to HPLC purification [system A for **8a**,**b** (t_R: 38.7 min and 38.4 min respectively) and system B for **10a**,**b** (t_R: 31.0 min and 31.5 min respectively), see General Methods]; the fractions containing the title compound were evaporated under reduced pressure and then lyophilized affording pure **8a**.

Compound **8a**. Bis-bicarbonate salt (17 mg, 60%). El. An. Calcd. for $C_{18}H_{40}Cl_2N_{10}O_{10}Pt_2$: C, 21.24; H, 3.96; N, 13.76. Found: C, 21.21; H, 3.98; N, 13.79. ^{1}H-NMR (400 MHz, D_2O) δ 8.84 (s, 1H, H-8), 8.33 (s, 1H, H-2), 6.12 (bs, 1H, H-1'), 4.78–4.76 (m, 1H, H-2', partially covered by solvent signal), 4.43–4.36 (m, 1H, H-3'), 4.31–4.25 (m, 1H, H-4'), 3.97–3.76 (m, 2H, $H_{a,b}$-5'), 3.67–3.55 (m, 2H, CH_2N), 2.62 (t, *J* = 6.4 Hz, 1H, C*H*$_2$NH$_2$Pt), 1.86–1.72 (m, 2H, CH_2), 1.71–1.59 (m, 2H, CH_2), 1.57–1.34 (complex signal, 4H, 2 × CH_2); ^{13}C-NMR (100 MHz, D_2O) δ 160.2 (2 × HCO_3^-), 153.7 (C-2), 153.2 (C-6), 146.8 (C-4), 141.6 (C-8), 116.8 (C-5), 89.1 (C-1'), 85.9 (C-4'), 73.9 (C-2'), 70.1 (C-3'), 61.0 (C-5'), 45.7 (CH_2NH_2), 40.7 (CH_2NH), 29.8 (CH_2), 28.0 (CH_2), 25.4 (CH_2), 25.2 (CH_2). IR (KBr pellet) 3246, 2930, 1626, 1589, 1492, 1339, 1084, 1058, 835, 790, 553 cm^{-1}; UV (H_2O) λ_{max} = 277 nm; HRESI-MS: (*m*/*z*) 447.0870, calcd. $[M]^{2+}$ 447.0859.

Compound **8b**. Bis-bicarbonate salt (17 mg, 58%). El. An. Calcd. for $C_{22}H_{44}Cl_2N_{10}O_{10}Pt_2$: C, 24.70; H, 4.15; N, 13.09. Found: C, 24.73; H, 4.13; N, 13.06. ^{1}H-NMR (400 MHz, D_2O) δ 8.85 (s, 1H, H-8), 8.39 (s, 1H, H-2), 6.16 (d, *J* = 5.0 Hz, 1H, H-1'), 4.80 (m, 1H, H-2', covered by solvent signal), 4.48–4.41 (m, 1H, H-3'), 4.37–4.30 (m, 1H, H-4'), 4.00–3.84 (m, 2H, $H_{a,b}$-5'), 3.78–3.67 (m, 2H, CH_2N), 2.85–2.50 (complex signal, 10H, C*H*$_2$NH$_2$Pt and 4 × CH_2 ethylene diamine moieties) 1.91–1.78 (m, 2H, CH_2), 1.77–1.62 (m, 2H, CH_2), 1.61–1.36 (complex signal, 4H, 2 × CH_2); ^{13}C-NMR (100 MHz, D_2O) δ 160.2 (2 × HCO_3^-), 153.7 (C-2), 153.2 (C-6), 146.9 (C-4), 141.6 (C-8), 116.9 (C-5), 89.1 (C-1'), 85.9 (C-4'), 73.9 (C-2'), 70.1 (C-3'), 61.0 (C-5'), 48.3, 48.0, 47.1 (4 × CH_2 ethylene diamine moieties), 45.9 (CH_2NH_2), 40.7 (CH_2NH), 29.9 (CH_2), 28.1 (CH_2), 25.5 (CH_2), 25.2 (CH_2); IR

(KBr pellet) 3406, 3208, 2931, 1627, 1589, 1470, 1336, 1303, 1232, 1079, 1054, 834, 790, 555, 472 cm^{-1}; UV (H_2O) λ_{max} = 278 nm; HRESI-MS: (*m*/*z*) 473.1037, calcd. $[M]^{2+}$ 473.1031.

Compound **10a**. Bis-bicarbonate salt (12 mg, 60%). El. An. Calcd. for $C_{28}H_{50}Cl_2N_{14}O_{14}Pt_2$: C, 26.53; H, 3.97; N, 15.47. Found: C, 26.50; H, 3.95; N, 15.45. ^{1}H-NMR (400 MHz, D_2O) δ 8.85 (s, 2H, 2 × H-8), 8.26 (s, 2H, 2 × H-2), 6.14 (bs, 2H, 2 × H-1'), 4.80 (m, 2H, 2 × H-2', covered by solvent signal), 4.50–4.40 (m, 2H, 2 × H-3'), 4.38–4.29 (m, 2H, 2 × H-4'), 4.03–3.76 (complex signal, 6H, 2 × $H_{a,b}$-5' and 2 × CH_aN), 3.67–3.53 (m, 2H, 2 × CH_bN), 1.94–1.75 (m, 4H, 2 × CH_2), 1.73–1.51 (m, 4H, 2 × CH_2); ^{13}C-NMR (100 MHz, D_2O) δ 160.2 (HCO_3^-), 153.7 (C-2), 153.2 (C-6), 146.8 (C-4), 141.4 (C-8), 116.5 (C-5), 89.1 (C-1'), 85.8 (C-4'), 74.0 (C-2'), 70.0 (C-3'), 61.0 (C-5'), 40.5 (CH_2NH), 27.8 (CH_2), 25.2 (CH_2); IR (KBr pellet) 3280, 2933, 1626, 1589, 1492, 1415, 1339, 1306, 1230, 1085, 1059, 985, 864, 790, 552 cm^{-1}; UV (H_2O) λ_{max} = 277 nm; HRESI-MS: (*m*/*z*) 572.1213, calcd. $[M]^{2+}$ 572.1226.

Compound **10b**. Bis-bicarbonate salt (13 mg, 62%). El. An. Calcd. for $C_{32}H_{54}Cl_2N_{14}O_{14}Pt_2$: C, 29.12; H, 4.12; N, 14.86. Found: C, 29.15; H, 4.10; N, 14.83. ^{1}H-NMR (400 MHz, D_2O) δ 8.81 (s, 2H, 2 × H-8), 8.24 (s, 2H, 2 × H-2), 6.14 (bs, 2H, 2 × H-1'), 4.80 (m, 2H, 2 × H-2', covered by solvent signal), 4.49–4.41 (m, 2H, 2 × H-3'), 4.37–4.31 (m, 2H, 2 × H-4'), 4.04–3.83 (m, 4H, 2 × $H_{a,b}$-5'), 3.81–3.60 (m, 4H, 2 × CH_2N), 2.84–2.50 (complex signal, 8H, 4 × CH_2, ethylene diamine moieties), 1.95–1.74 (m, 4H, 2 × CH_2), 1.72–1.52 (m, 4H, 2 × CH_2); ^{13}C-NMR (100 MHz, D_2O) δ 160.1 (HCO_3^-), 153.6 (C-2), 153.2 (C-6), 146.6 (C-4), 141.6 (C-8), 116.5 (C-5), 89.1 (C-1'), 85.7 (C-4'), 74.1 (C-2'), 70.1 (C-3'), 61.2 (C-5'), 48.1, 47.3 (2 × CH_2 ethylene diamine moieties) 40.5 (CH_2NH), 27.7 (CH_2), 25.1 (CH_2); IR (KBr pellet) 3284, 2930, 1625, 1592, 1490, 1417, 1338, 1310, 1233, 1083, 1061, 980, 860, 791, 554 cm^{-1}; UV (H_2O) λ_{max} 276 nm; HRESI-MS: (*m*/*z*) 598.1391, calcd. $[M]^{2+}$ 598.1382.

3.3. MTT Viability Assay

The cells were plated in 96 culture wells (20 × 10^4 cells/well) and allowed to adhere overnight. Thereafter, the medium was replaced with fresh medium and the cells were incubated in the absence or presence of cisplatin, **8a**, **8b**, **10a** and **10b** (50, 100 and 200 μM). After 72 h, the cell viability was determined by using 3-(4,5-dimethylthiazol-2yl)-2,5-diphenyl-2H-tetrazoliumbromide (MTT) conversion assay [48]. Briefly, 10 μL of MTT (5 mg/mL) were added to the cells and incubated for an additional 3 h. After this time point, the cells were lysed and the dark blue crystals solubilized with 150 μL of a solution containing 50% (*v:v*) DMF, 20% (*w:v*) SDS with an adjusted pH of 4.5. The optical density (OD) of each well was measured with a microplate spectrophotometer (Multiskan MCCC/340, Titertek, Huntsville, AL, USA) equipped with a 620 nm filter. The experiment was performed twice in triplicate. The vitality inhibition, induced by each compound at the indicated concentrations, was expressed as a percentage *versus* the untreated cells (the control). The viable cells were also counted by the trypan blue exclusion assay and light microscopy.

3.4. BrdU Cell Proliferation Assay

The cells were plated onto 96-well plates (2 × 10^4 cells/well) overnight. Then, the medium was replaced with fresh medium and the cells were incubated in the absence or presence of cisplatin (50,

100 and 200 μM), **8a**, **8b**, **10a** and **10b** (50, 100 and 200 μM). After 72 h, 5-bromo-2'-deoxyuridine (BrdU; 10 μM) was added and the cells were cultured for a further 12 h. The mitogenic activity was determined according to the manufacturer's instructions (BrdU cell proliferation assay kit, Cell Signaling). The experiment was performed three times in triplicate. The proliferation inhibition, induced by each compound at the indicated concentrations, was expressed as a percentage *versus* the untreated cells (the control).

3.5. Statistical Analysis

The results are expressed as the means ± SEM of n experiments. The statistical significance was calculated by one-way analysis of variance (ANOVA) and Bonferroni-corrected *p*-value for multiple comparison testing. The level of statistically significant difference was defined as $p < 0.05$.

4. Conclusions

In summary, in this paper we have reported the synthesis of four novel platinum complexes embodying a N^6-(6-aminohexyl)adenosine or a 1,6-di-(adenosin-N^6-yl)-hexane as ligands of monofunctional cisplatin or monochloro(ethylene diamine)platinum(II) moieties, starting from commercially available 6-chloropurine riboside. The designed synthetic route allowed us to obtain the desired platinum complexes without blocking the ribose hydroxyl groups and through easy purification steps.

The effects of these platinum complexes on cell viability and proliferation have been studied in A549 and MCF7 cell lines. Our data demonstrate that these compounds are able to inhibit the survival and proliferation of sensitive cancer cells. Nevertheless, cisplatin remains the most active molecule under our experimental conditions. Further experiments are necessary to understand the mechanism by which **8a** penetrates into the cells and inhibits cell proliferation in the MCF7 cell line.

Acknowledgments

This work was financially supported by "Progetto FARO 2011" (Finanziamento per l'Avvio di Ricerche Originali). We are grateful to Luisa Cuorvo for her technical assistance and to CSIAS (Centro di Servizio Interdipartimentale di Analisi Strutturale) for the NMR facilities.

Author Contributions

Stefano D'Errico, Brunella Pinto and Fabrizia Nici designed and synthesized the compounds shown in Scheme 1, furthermore Stefano D'Errico wrote the initial draft of the paper and edited the final draft. Vincenzo Piccialli wrote an intermediate draft of the paper and helped write and edit the final draft of the manuscript. Nicola Borbone and Valeria Costantino characterized all the novel platinum complexes, analyzed spectroscopic data from the experiments and wrote the pertinent section in Results and Discussion and in the Experimental Section. Francesca De Falco, Maria Chiara Maiuri and Rosa Carnuccio performed the *in vitro* biological assays, analyzed and processed the data obtained from the experiments and wrote the pertinent section in the Results and Discussion and in the Experimental Section. Giorgia Oliviero and Gennaro Piccialli supervised all experiments, reanalyzed

all data for accuracy, and wrote the final draft of the manuscript. All authors reviewed and approved the final version of the manuscript.

Conflicts of Interest

The authors declare no conflict of interest.

References

1. Rosenberg, B.; Vancamp, L.; Krigas, T. Platinum compounds: A new class of potent antitumour agents. *Nature* **1969**, *222*, 385–386.
2. Kelland, L.R.; Farrell, N. *Platinum Based Drugs in Cancer Therapy*; Humana Press: Totowa, NJ, USA, 2000.
3. Allardyce, C.S.; Dorcier, A.; Scolaro, C.; Dyson, P.J. Development of organometallic (organo-transition metal) pharmaceuticals. *Appl. Organometal. Chem.* **2005**, *19*, 1–10.
4. Wexselblatt, E.; Yavin, E.; Gibson, D. Cellular interactions of platinum drugs. *Inorg. Chim. Acta* **2012**, *393*, 75–83.
5. Harper, B.W.; Krause-Heuer, A.M.; Grant, M.P.; Manohar, M.; Garbutcheon-Singh, K.B.; Aldrich-Wright, J.R. Advances in Platinum Chemotherapeutics. *Chem. Eur. J.* **2010**, *16*, 7064–7077.
6. Sigel, A.; Sigel, H. *Metal Ions in Biological Systems: Metal Complexes in Tumor Diagnosis and as Anticancer Agents*; CRC Press: London, UK, 2004.
7. Florea, A.M.; Büsselberg, D. Cisplatin as an Anti-Tumor Drug: Cellular Mechanisms of Activity, Drug Resistance and Induced Side Effects. *Cancers* **2011**, *3*, 1351–1371.
8. Fan, D.; Yang, X.; Wang, X.; Zhang, S.; Mao, J.; Ding, J.; Lin, L.; Guo, Z. A dinuclear monofunctional platinum(II) complex with an aromatic linker shows low reactivity towards glutathione but high DNA binding ability and antitumor activity. *J. Biol. Inorg. Chem.* **2007**, *12*, 655–665.
9. Boulikas, T. Clinical overview on Lipoplatin™: A successful liposomal formulation of cisplatin. *Expert Opin. Investig. Drugs* **2009**, *18*, 1197–1218.
10. Abu-Surrah, A.S.; Kettunen, M. Platinum group antitumor chemistry: Design and development of new anticancer drugs complementary to cisplatin. *Curr. Med. Chem.* **2006**, *13*, 1337–1357.
11. Arnesano, F.; Natile, G. Mechanistic insight into the cellular uptake and processing of cisplatin 30 years after its approval by FDA. *Coord. Chem. Rev.* **2009**, *253*, 2070–2081.
12. Zhang, J.; Wang, L.; Xing, Z.; Liu, D.; Sun, J.; Li, X.; Zhang, Y. Status of Bi- and Multi-Nuclear Platinum Anticancer Drug Development. *Anti Cancer Agents Med. Chem.* **2010**, *10*, 272–282.
13. Wheate, N.; Collins, J.G. Multi-nuclear platinum complexes as anti-cancer drugs. *Coord. Chem. Rev.* **2003**, *241*, 133–145.
14. Roberts, J.D.; Peroutka, J.; Farrell, N. Cellular pharmacology of polynuclear platinum anti-cancer agents. *J. Inorg. Biochem.* **1999**, *77*, 51–57.
15. Pratesi, G.; Perego, P.; Polizzi, D.; Righetti, S.C.; Supino, R.; Caserini, C.; Manzotti, C.; Giuliani, F.C.; Pezzoni, G.; Tognella, S.; *et al*. A novel charged trinuclear platinum complex effective against cisplatin-resistant tumours: Hypersensitivity of p53-mutant human tumour xenografts. *Br. J. Cancer* **1999**, *80*, 1912–1919.

16. Kasparkova, J.; Zehnulova, J.; Farrell, N.; Brabec, V. DNA interstrand cross-links of the novel antitumor trinuclear platinum complex BBR3464. Conformation, recognition by high mobility group domain proteins, and nucleotide excision repair. *J. Biol. Chem.* **2002**, *277*, 48076–48086.
17. Jansen, B.A.J.; Wielaard, P.; Kalayda, G.V.; Ferrari, M.; Molenaar, C.; Tanke, H.J.; Brouwer, J.; Reedijk, J. Dinuclear platinum complexes with N,N'-bis(aminoalkyl)-1,4-diaminoanthraquinones as linking ligands. Part I. Synthesis, cytotoxicity, and cellular studies in A2780 human ovarian carcinoma cells. *J. Biol. Inorg. Chem.* **2004**, *9*, 403–413.
18. Mitova, V.; Bogomilova, A.; Shestakova, P.; Momekov, G.; Momekova, D.; Abbas, R.K.; Koseva, N. Synthesis of a new polynuclear platinum (ii) complex and its prodrug forms. Evaluation of their cytotoxic properties. *J. Chem. Technol. Metall.* **2013**, *48*, 17–27.
19. Cincinelli, R.; Musso, L.; Dallavalle, S.; Artali, R.; Tinelli, S.; Colangelo, D.; Zunino, F.; de Cesare, M.; Beretta, G.L.; Zaffaroni, N. Design, modeling, synthesis and biological activity evaluation of camptothecin-linked platinum anticancer agents. *Eur. J. Med. Chem.* **2013**, *63*, 387–400.
20. Robillard, M.S.; Valentijn, A.; Meeuwenoord, N.J.; van der Marel, G.A.; van Boom, J.H.; Reedijk, J. The First Solid-Phase Synthesis of a Peptide-Tethered Platinum (II) Complex. *Angew. Chem. Int. Ed.* **2000**, *112*, 3226–3229.
21. Robillard, M.S.; van Alphen, S.; Meeuwenoord, N.J.; Jansen, B.A.J.; van der Marel, G.A.; van Boom, J.H.; Reedijk, J. Solid-phase synthesis of peptide-platinum complexes using platinum-chelating building blocks derived from amino acids. *New J. Chem.* **2005**, *29*, 220–225.
22. Holmes, R.J.; McKeage, M.J.; Murray, V.; Denny, W.A.; McFadyen, W.D. cis-Dichloroplatinum (II) complexes tethered to 9-aminoacridine-4-carboxamides: Synthesis and action in resistant cell lines *in vitro*. *J. Inorg. Biochem.* **2001**, *85*, 209–217.
23. Cai, L.; Lim, K.; Ren, S.; Cadena, R.S.; Beck, W.T. Synthesis and *in Vitro* Antitumor Activity of Oligonucleotide-Tethered and Related Platinum Complexes. *J. Med. Chem.* **2001**, *44*, 2959–2965.
24. Schmidt, K.S.; Boudvillain, M.; Schwartz, A.; van der Marel, G.A.; van Boom, J.H.; Reedijk, J.; Lippert, B. Monofunctionally trans-Diammine Platinum (II)-Modified Peptide Nucleic Acid Oligomers: A New Generation of Potential Antisense Drugs. *Chem. Eur. J.* **2002**, *8*, 5566–5570.
25. Butler, J.S.; Sadler, P.J. Targeted delivery of platinum-based anticancer complexes. *Curr. Opin. Chem. Biol.* **2013**, *17*, 175–188.
26. Sengupta, P.; Basu, S.; Soni, S.; Pandey, A.; Roy, B.; Oh, M.S.; Chin, K.T.; Paraskar, A.S.; Sarangi, S.; Connor, Y. Cholesterol-tethered platinum II-based supramolecular nanoparticle increases antitumor efficacy and reduces nephrotoxicity. *Proc. Natl. Acad. Sci. USA* **2012**, *109*, 11294–11299.
27. Coluccia, M.; Boccarelli, A.; Cermelli, C.; Portolani, M.; Natile, G. Platinum(II)-Acyclovir Complexes: Synthesis, Antiviral and Antitumour Activity. *Metal-Based Drugs.* **1995**, *2*, 249–256.
28. Nervi, C.; Vigna, M.A.; Cavigiolio, G.; Ravera, M.; Osella, D. Synthesis and characterization of functionalized thymidine as a potential carrier for cisplatin-like drugs. *Inorg. Chim. Acta* **2005**, *358*, 2799–2803.
29. Štarha, P.; Popa, I.; Trávníček, Z.; Vančo, J. N6-Benzyladenosine Derivatives as Novel *N*-Donor Ligands of Platinum(II) Dichlorido Complexes. *Molecules* **2013**, *18*, 6990–7003.

30. D'Errico, S.; Oliviero, G.; Piccialli, V.; Amato, J.; Borbone, N.; D'Atri, V.; D'Alessio, F.; Di Noto, R.; Ruffo, F.; Salvatore, F.; *et al*. Solid-phase synthesis and pharmacological evaluation of novel nucleoside-tethered dinuclear platinum (II) complexes. *Bioorg. Med. Chem. Lett.* **2011**, *21*, 5835–5838.
31. Oliviero, G.; D'Errico, S.; Borbone, N.; Amato, J.; Piccialli, V.; Piccialli, G.; Mayol, L. Facile Solid-Phase Synthesis of AICAR 5'-Monophosphate (ZMP) and Its 4-N-Alkyl Derivatives. *Eur. J. Org. Chem.* **2010**, *2010*, 1517–1524.
32. Oliviero, G.; Amato, J.; Borbone, N.; D'Errico, S.; Piccialli, G.; Bucci, E.; Piccialli, V.; Mayol, L. Synthesis of 4-N-alkyl and ribose-modified AICAR analogues on solid support. *Tetrahedron* **2008**, *64*, 6475–6481.
33. Oliviero, G.; D Errico, S.; Borbone, N.; Amato, J.; Piccialli, V.; Varra, M.; Piccialli, G.; Mayol, L. A solid-phase approach to the synthesis of N-1-alkyl analogues of cyclic inosine-diphosphate-ribose (cIDPR). *Tetrahedron* **2010**, *66*, 1931–1936.
34. D'Errico, S.; Oliviero, G.; Borbone, N.; Amato, J.; Piccialli, V.; Varra, M.; Mayol, L.; Piccialli, G. Solid-Phase Synthesis of a New Diphosphate 5-Aminoimidazole-4-carboxamide Riboside (AICAR) Derivative and Studies toward Cyclic AICAR Diphosphate Ribose. *Molecules* **2011**, *16*, 8110–8118.
35. D'Errico, S.; Oliviero, G.; Borbone, N.; Amato, J.; D'Alonzo, D.; Piccialli, V.; Mayol, L.; Piccialli, G. A Facile Synthesis of 5'-Fluoro-5'-deoxyacadesine (5'-F-AICAR): A Novel Non-phosphorylable AICAR Analogue. *Molecules* **2012**, *17*, 13036–13044.
36. D'Errico, S.; Oliviero, G.; Borbone, N.; Amato, J.; Piccialli, V.; Varra, M.; Mayol, L.; Piccialli, G. Synthesis of New Acadesine (AICA-riboside) Analogues Having Acyclic D-Ribityl or 4-Hydroxybutyl Chains in Place of the Ribose. *Molecules* **2013**, *18*, 9420–9431.
37. Park, G.Y.; Wilson, J.J.; Song, Y.; Lippard, S.J. Phenanthriplatin, a monofunctional DNA-binding platinum anticancer drug candidate with unusual potency and cellular activity profile. *Proc. Natl. Acad. Sci. USA* **2012**, *109*, 11987–11992.
38. Johnstone, T.C.; Alexander, S.M.; Lin, W.; Lippard, S.J. Effects of Monofunctional Platinum Agents on Bacterial Growth: A Retrospective Study. *J. Am. Chem. Soc.* **2014**, *136*, 116–118.
39. Gregg, A.; Bottle, S.E.; Devine, S.M.; Figler, H.; Linden, J.; White, P.; Pouton, C.W.; Urmaliya, V.; Scammells, P.J. Dual acting antioxidant A1 adenosine receptor agonists. *Bioorg. Med. Chem. Lett.* **2007**, *17*, 5437–5441.
40. Agathocleous, D.C.; Page, P.B.C.; Cosstick, R.; Galpin, J.J.; McLennan, A.G.; Prescott, M. Synthesis of bridged nucleosides. *Tetrahedron* **1990**, *46*, 2047–2058.
41. Amo-Ochoa, P.; González, V.M.; Pérez, J.M.; Masaguer, J.R.; Alonso, C.; Navarro-Ranninger, C. Cytotoxicity, DNA binding, and reactivity against nucleosides of platinum (II) and (IV) spermine compounds. *J. Inorg. Biochem.* **1996**, *64*, 287–299.
42. Van Rijt, S.; van Zutphen, S.; den Dulk, H.; Brouwer, J.; Reedijk, J. Structure–activity relationship studies for three new asymmetric cis-platinum(II) aminoethanol-based complexes. *Inorg. Chim. Acta* **2006**, *359*, 4125–4129.
43. Girault, J.O.; Chottard, G.; Lallemand, J.Y.; Chottard, J.C. Interaction of cis-$[Pt(NH_3)_2(H_2O)_2](NO_3)_2$ with ribose and deoxyribose diguanosine phosphates. *Biochemistry* **1982**, *21*, 1352–1356.

44. Arpalahti, J.; Klika, K.D.; Sillanpää, R.; Kivekäs, R. Dynamic processes in platinum(II)-adenosine complexes. Preparation, NMR spectroscopic characterisation and crystal structure of isomeric Pt II (dien)-adenosine complexes. *J. Chem. Soc. Dalton Trans.* **1998**, 1397–1402.
45. Wang, S.; Chu, W.; Wang, Y.; Liu, S.; Zhang, J.; Li, S.; Wei, H.; Zhou, G.; Qin, X. Synthesis, characterization and cytotoxicity of Pt(II), Pd(II), Cu(II) and Zn(II) complexes with 4'-substituted terpyridine. *Appl. Organometal. Chem.* **2013**, *27*, 373–379.
46. Li, L.J.; Wang, C.; Qiao, Y.; Yang, X.Y.; Hua, X.X.; Du, J.L. Platinum(II) complexes of reduced amino acid ester Schiff bases: Synthesis, characterization, and antitumor activity. *Res. Chem. Intermed.* **2014**, *40*, 413–424.
47. Fan, S.; Smith, M.L.; Rivet, D.J.; Duba, D.; Zhan, Q.; Kohn, K.W.; Fornace, A.J.; O'Connor, P.M. Disruption of p53 function sensitizes breast cancer MCF-7 cells to cisplatin and pentoxifylline. *Cancer Res.* **1995**, *55*, 1649–1654.
48. De Stefano, D.; Tommonaro, G.; Malik, S.A.; Iodice, C.; de Rosa, S.; Maiuri, M.C.; Carnuccio, R. Cacospongionolide and Scalaradial, Two Marine Sesterterpenoids as Potent Apoptosis-Inducing Factors in Human Carcinoma Cell Lines. *PLoS One* **2012**, *7*, e33031.

Sample Availability: Samples of the compounds **8a**,**b** and **10a**,**b** are available from the authors.

© 2014 by the authors; licensee MDPI, Basel, Switzerland. This article is an open access article distributed under the terms and conditions of the Creative Commons Attribution license (http://creativecommons.org/licenses/by/3.0/).

Terracciano et al. Nanoscale Research Letters 2014, 9:317
http://www.nanoscalereslett.com/content/9/1/317

Nanoscale Research Letters
a SpringerOpen Journal

NANO EXPRESS Open Access

Synthesis of mixed-sequence oligonucleotides on mesoporous silicon: chemical strategies and material stability

Monica Terracciano[1,2], Ilaria Rea[1], Luca De Stefano[1*], Ivo Rendina[1], Giorgia Oliviero[2], Fabrizia Nici[2], Stefano D'Errico[2], Gennaro Piccialli[2] and Nicola Borbone[2]

Abstract

Rapid screening tests in medical diagnostic and environmental analysis are often based on oligonucleotide biochips. In this paper, we studied the stability of functionalized mesoporous silicon supports in the solid-phase synthesis of oligonucleotides, exploiting several chemical procedures. A 19-mer mixed sequence has been successfully synthesized on aminosilane-modified porous silicon photonic structures. The process and the materials have been characterized by optical reflectivity, atomic force microscopy and high-performance liquid chromatography.

Keywords: Mesoporous silicon functionalization; DNA synthesis; Deprotection conditions; Surface stability

Background

DNA chip technology has greatly evolved over the last decade, moving from pure genomics towards a number of biotechnology applications such as human disease diagnostics [1], environmental monitoring and food control [2,3]. DNA chips can be classified as a special class of biosensors since they are realized by immobilization of single-stranded oligonucleotides (ONs), the bioprobe, on a transducer surface. Any molecular interaction between the bioprobe and its ligands, such as hybridization to the complementary DNA sequence or protein binding, is then transduced into an analytical signal by an electrochemical-, optical- or surface plasmon resonance-based or electrical device, depending on the specific technology used. Porous silicon (PSi) is by far one of the most popular transducer materials due to its peculiar physical and chemical properties [4]. PSi is fabricated by electrochemical etching of crystalline silicon in aqueous hydrofluoric acid. Depending on etch time, current density and acid concentration, several porous morphologies can be obtained, from micropores (average pore size <5 nm) to macropores (average pore size >50 nm) [5]. The resulting sponge-like matrix possesses a very large specific surface area (up to 300 m^2/cm^3): gases and liquids can easily get into pores, thus changing the optical, chemical and electrical properties of PSi [6]. Even if electrochemical etching induces silicon dissolution, the resulting PSi surface is smooth enough to get very good quality optical devices, also in the case of multilayered structures [7]. Periodic, or quasi-periodic, alternation of high- and low-porosity layers is used for fabrication of Bragg reflectors, microcavities and Thue-Morse sequences: all these photonic devices exhibit resonance wavelengths that can be used as monitoring peak in quantifying biomolecular interaction from the optical point of view [8-10]. The PSi surface can be properly passivated and functionalized in order to covalently bind biological molecules such as single- or double-stranded DNA, proteins, enzymes, antibodies, aptamers and so on, which act as bioprobes. There are many routes to achieve surface functionalization which are based on proper chemical or biological processes: the PSi surface can be activated by specific chemical groups, namely -SH, $-NH_2$ or -COOH, that could form very stable bonds, such as sulphide or peptide bond, with the biological molecule considered [11]. For some biomolecules that are usually synthesized *ex situ* and then coupled on the PSi surface, there is also the possibility of directly growing the molecules using PSi as support in the so-called solid-phase synthesis [12].

* Correspondence: luca.destefano@cnr.it
[1]Institute for Microelectronics and Microsystems, National Council of Research, Naples 80131, Italy
Full list of author information is available at the end of the article

Springer

© 2014 Terracciano et al.; licensee Springer. This is an Open Access article distributed under the terms of the Creative Commons Attribution License (http://creativecommons.org/licenses/by/4.0), which permits unrestricted use, distribution, and reproduction in any medium, provided the original work is properly credited.

In this article, we describe the fabrication and the characterization of a PSi-based DNA chip for biochemical optical sensing through *in situ* mixed-sequence ON growth. Since the chemistry used for the solid-phase synthesis of ON can be quite aggressive against the PSi solid support, the chemical stability of PSi supports is a key issue that must be checked and satisfied for each considered substrate. In particular, it is well known that PSi suffers upon exposure to alkaline solutions (commonly used for the deprotection of nucleobases) that can easily corrode the silicon skeleton, so a trade-off between PSi surface passivation and suitable solid-phase synthesis chemistry must be found. We focused our studies on silanization of PSi by using two different siloxanes and also on the exploitation of different chemical approaches for the ON deprotection in order to preserve the stability of PSi during all phases of synthesis and sensing.

Methods

Mesoporous silicon microcavity fabrication

PSi microcavities constituted by a $\lambda/2$ layer (optical thickness) sandwiched between two 9.5-period Bragg reflectors (BRs) were obtained alternating low (L) and high (H) refractive index layers whose thicknesses satisfy the Bragg relationship $n_H d_H + n_L d_L = m\lambda_B/2$, where m is an integer and λ_B is the Bragg wavelength. The microcavities were prepared by electrochemical etching of highly doped p^+ crystalline silicon (0.001-Ω cm resistivity, <100 > -oriented, 500 μm thick) in HF solution (HF:ethanol 1:1) in the dark at room temperature (RT). Before the anodization process, the silicon substrate was immersed in HF solution for 2 min to remove the native oxide layer. Since the PSi fabrication process is self-stopping, it is possible to obtain adjacent layers with different porosities by changing the current density during the electrochemical etching [4]. A current density of 200 mA/cm^2 for 1.2 s was applied to obtain low refractive index layers ($n_L = 1.542$; $d_L = 125$ nm) while a current density of 100 mA/cm^2 was applied for 1.4 s for high refractive index layers ($n_H = 1.784$; $d_H = 108$ nm). After the electrochemical process, the pore dimension was increased to favour the infiltration of biological matter by rinsing the fresh-made PSi microcavities in a KOH ethanol solution (1.5 mM) for 15 min [5]. The structures were then thermally oxidized against uncontrolled environmental aging and corrosion in alkaline solutions. The thermal oxidation has been performed in pure O_2 by a two-step process: pre-oxidation at 400°C for 30 min followed by oxidation at 900°C for 15 min.

Silane surface modifications

Eight oxidized PSi microcavities (PSi-$M_{a\text{-}h}$) were immersed in piranha solution (H_2O_2:H_2SO_4 1:4) at RT for 30 min to generate Si-OH groups on the PSi surface. After that, the samples were extensively washed in Milli-Q® water flow (Millipore, Billerica, MA, USA) and dried with nitrogen gas. Structures were then silanized by immersion in different 5% aminosilane solutions, (3-aminopropyl)triethoxysilane (APTES) or (3-aminopropyl)-dimethyl-ethoxysilane (APDMES), in dry toluene for 30 min at RT. Samples PSi-$M_{a,c,e,g}$ were silanized by APTES and samples PSi-$M_{b,d,f,h}$ by APDMES. The reaction conditions were optimized on a crystalline silicon-varying solvent for silane dissolution and incubation time [12]. The PSi-silanized samples were rinsed three times in the solvent used for the process so as to remove the ungrafted silanes. The last step of silanization is curing at 100°C for 10 min.

Oligonucleotide synthesis

Chemicals and solvents were purchased from Sigma-Aldrich (St. Louis, MO, USA). Reagents and phosphoramidites for DNA synthesis were purchased from Glen Research (Sterling, VA, USA). Solid-phase ON syntheses were performed on a PerSeptive Biosystem Expedite 8909 DNA automated synthesizer (Framingham, MA, USA). The 19-mer mixed-sequence oligonucleotide 5′-GATTG ATGTGGTTGATTTT-3′ was assembled on two different aminosilane-modified microcavities, following phosphoramidite chemistry by 19 growing cycles [13]. PSi structures, PSi-$M_{g,h}$-NH_2 (M_g = APTES, M_h = APDMES), were introduced in a suitable column reactor to be used in the automated synthesizer; the syntheses were performed according to the scheme reported in Figure 1. In all cases, the first reaction step involved the attachment of the

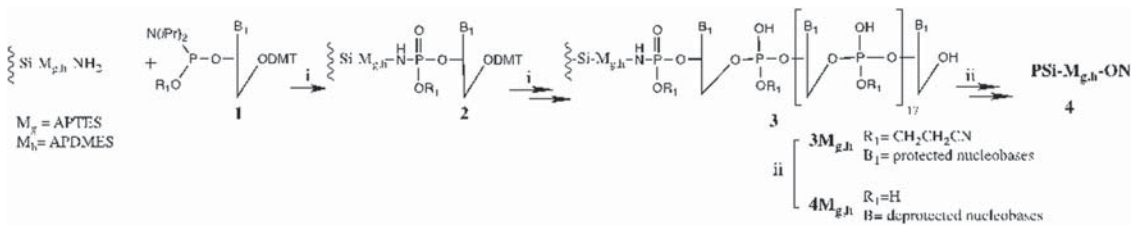

Figure 1 Synthetic procedure for solid-phase synthesis of aminosilane-modified mesoporous silicon. (i) Standard procedure for automated ON synthesis. (ii) NH_3/MeOH dry.

3′-ending nucleobase to the amino group of PSi-bound APTES or APDMES. This step required the activation of the protected phosphoramidite dissolved in dry acetonitrile via protonation by weakly acidic tetrazole (0.45 M in acetonitrile). Once the first nucleobase was installed on the solid support, the ON growth was obtained by repeating the following sequential steps of the automated ON synthesis:

- Coupling: reaction of the protected phosphoramidite dissolved in dry acetonitrile and activated via protonation by weakly acidic tetrazole (0.45 M in acetonitrile) with the 5′-OH ON terminal group.
- Oxidation: oxidation of the unstable phosphite triester linkage to the more stable phosphotriester by a standard oxidizing solution of iodine in pyridine/acetonitrile.
- Capping: acylation of the unreacted 5′-OH ON terminal groups by acetic anhydride in pyridine and tetrahydrofuran to minimize deletion products and simplify the purification process.
- Detritylation: removal of the 5′-dimethoxytrityl (DMT) protecting group from the support-bound 5′-terminal nucleotide with the deblocking solution of trichloroacetic acid in dichloromethane (3% *w*/*w*).

The amount of DMT cation released by acid treatment was used as a direct measure of the efficiency of the ongoing synthesis. The release of the protecting group generates a bright red-orange colour solution in which the quantity of the DMT cation can be measured online by UV-vis spectroscopy at 495 nm ($\varepsilon = 71{,}700\ M^{-1}\ cm^{-1}$). At the end of each growing cycle, the support was thoroughly washed with acetonitrile before the beginning of the successive cycle.

Deprotection strategies

The devices PSi-$M_{a,b}$-NH_2 (M_a = APTES, M_b = APDMES) were left in contact with 33% aqueous ammonia at 55°C for different times to investigate the effect of standard ON deprotection condition (55°C for 17 h) on the PSi matrix [14]. Two additional aminosilane-modified devices, PSi-$M_{c,d}$-NH_2, (M_c = APTES, M_d = APDMES) were incubated in anhydrous K_2CO_3 (0.05 M)/dry methanol solution at 55°C for different times to investigate the 'ultra-mild' ON deprotection condition (55°C for 2 h) [14]. Finally, the exposure to dry ammonia solution (NH_3/MeOH dry) was also explored as an alternative deprotection strategy [15]. To this aim, the aminosilane-modified samples PSi-$M_{e,f}$-NH_2 (M_e = APTES, M_f = APDMES) were exposed to dry ammonia overnight at RT. The dry ammonia was generated by dissolving NaOH pellets in a sidearm flask containing aqueous ammonia; the generated gas was passed through a KOH drying tube and bubbled into a flask equipped with a rubber septum and containing anhydrous MeOH at 0°C.

The explored deprotection strategies carried out on aminosilane-modified PSi microcavities are summarized in Table 1.

Atomic force microscopy

A XE-100 AFM (Park Systems, Suwon, South Korea) was used to study sample morphology. Surface imaging was obtained in non-contact mode using silicon/aluminium-coated cantilevers (PPP-NCHR 10 M, Park Systems, Suwon, South Korea) 125 mm long with a resonance frequency of 200 to 400 kHz and nominal force constant of 42 N/m. The scan frequency was typically 1 Hz per line. The scan area in surface analysis was 1 μm × 1 μm.

Spectroscopic reflectometry

Reflectivity spectra of PSi optical structures were obtained by a simple experimental setup: a white light was sent on PSi samples through a Y optical fibre (Avantes, Apeldoorn, The Netherlands). The same fibre was used to guide the output signal to an optical spectrum analyser (Ando AQ6315A, Tokyo, Japan). The spectra were acquired at normal incidence over the range 600 to 1,200 nm with a resolution of 5 nm. The reflectivity spectra shown in the graphs are the average of three measurements for each sample.

High-performance liquid chromatography

The purification and control of the synthesized ONs was carried out using a Jasco PU2089 PLUS HPLC system (Easton, MD, USA) equipped with an anion exchange column (1000-8/46, 4.4 × 50 mm, 5 μm, Macherey-Nagel, Düren, Germany) using a linear gradient from 0% to 100% B in 30 min, flow rate = 1 mL/min and detection at 260 nm (buffer A: 20 mM NaH_2PO_4 aq. solution, pH 7.0, containing 20% (*v*/*v*) CH_3CN; buffer B: 20 mM NaH_2PO_4 aq. solution, pH 7.0, containing 1 M NaCl and 20% (*v*/*v*) CH_3CN).

Table 1 Deprotection strategies

Deprotection strategy	Exposition time	Sample
NH_3(l) @55°C	30 min; 1 h; 2 h	PSi-$M_{a\text{-}NH2}$
		PSi-$M_{b\text{-}NH2}$
K_2CO_3/MeOH @55°C	30 min; 1 h; 2 h; 5 h; 8 h; overnight	PSi-$M_{c\text{-}NH2}$
		PSi-$M_{d\text{-}NH2}$
NH_3(g) @RT	Overnight	PSi-$M_{e\text{-}NH2}$
		PSi-$M_{f\text{-}NH2}$
		PSi-$M_{g\text{-}NH2\text{-}oligo}$
		PSi-$M_{h\text{-}NH2\text{-}oligo}$

Results and discussion

In our previous work [16], we investigated the passivation ability of oxidized PSi multilayered structures by two aminosilane compounds (APTES and APDMES) used for the *in situ* synthesis of a 13-mer polythymine ON strand. We successfully demonstrated that even using the less aggressive carbonate/methanol solution as the ON deprotection system, hybridization with the complementary ON target took place, thus confirming that ONs can be synthesized and deprotected on the PSi surface. However, the synthesis of mixed-sequence ONs using the carbonate/methanol solution in the final ON deprotection step would require the use of highly expensive ultra-mild nucleobase-protected phosphoramidites characterized by having non-standard very labile protecting groups. In the present paper, we describe the results of alternative PSi-friendly ON deprotection conditions during the *in situ* synthesis of mixed-sequence ONs on PSi supports by using standard phosphoramidite nucleoside monomers, without using ultra-mild reagents.

Measurement of optical spectra by spectroscopic reflectometry is very useful since both the position of resonance wavelength and the shape of lateral fringes give quantitative information about PSi corrosion or stability: the peak wavelengths of each PSi-$M_{a\text{-}h}$ microcavity before and after silanization are reported in Table 2. Both APTES and APDMES covered the pore walls by a thin film: the aminosilane layer substitutes air in the pores and increases the average refractive index of PSi layers, resulting in a shift of reflectivity spectra towards greater wavelengths. The thicknesses of the APTES and APDMES layers coating the pore walls were estimated from red shifts: in the first case, we observed a 22 nm red shift, corresponding to a silane layer of 0.7 nm; in the second, the red shift was about 10 nm, corresponding to a silane layer of 0.2 nm [16]. These numbers are consistent with the different behaviours of the polymers: APTES generally cross-links after curing, producing a compact and thicker sheet of silane, whereas APDMES does not polymerize. A direct evidence of the slightly distinct morphologies of aminosilane-modified surfaces was given by atomic force microscopy (AFM). The AFM images of bare oxidized PSi and APTES- and APDMES-modified porous PSi surfaces are reported in Figure 2. The AFM image of porous SiO_2 reveals a sponge-like structure characterized by hillocks and voids randomly distributed on the whole surface; pore size can be estimated to be on the order of 20 nm. After APTES grafting (porous SiO_2 + APTES), most voids disappear due to partial pore cloaking by the silane layer coating the pore walls. Quite the same result is obtained in the case of APDMES modification (porous SiO_2 + APDMES): even if APDMES forms a thinner layer, voids in the porous matrix are strongly reduced. Further investigations about the effect of this steric hindrance on oligonucleotide synthesis are also required.

Table 2 Peak shift of devices after surface modification by APTES or APDMES

Sample	Pre-silanization	Post-silanization	Peak shift (nm)
	Peak wavelength (nm) Er±	Peak wavelength (nm) Er±	
PSi-M_a	631.3 ± 0.3	653.3 ± 0.1	22.2
PSi-M_b	640.1 ± 0.1	651.0 ± 0.2	11
PSi-M_c	635.7 ± 0.5	656.9 ± 0.4	21.2
PSi-M_d	628.4 ± 0.6	640.7 ± 0.3	12.3
PSi-M_e	708.2 ± 0.2	730.3 ± 0.6	22.3
PSi-M_f	714.7 ± 0.1	722.3 ± 0.4	8
PSi-M_g	706.5 ± 0.3	727.8 ± 0.1	21.3
PSi-M_h	665.6 ± 0.4	673.7 ± 0.2	8.1

The reflectivity spectra and graphs of peak shift vs incubation time for PSi-$M_{a,b}$-NH_2 microcavities (M_a = APTES; M_b = APDMES) before and after treatment with 33% aqueous ammonia (17 h, 55°C) used in the standard deprotection condition are reported in Figure 3. The stability of the surfaces was tested by a full dip in ammonia solution for different times. The results showed that the destructive effect of ammonia solution was about the same for both samples: a blue shift of 25 or 50 nm was detected after 30 min or 1 h, respectively, and the complete dissolution of the silicon matrices occurred after 2 h.

Because aqueous ammonia could not be used in deprotection steps, we checked the stability of PSi-$M_{c,d}$-NH_2 (M_c = APTES; M_d = APDMES) at the so-called ultra-mild deprotection condition (0.05 M K_2CO_3/dry methanol at 55°C for 2 h). Sample PSi-M_c-NH_2 showed better chemical resistance than sample PSi-M_d-NH_2. In particular, a progressive shift of the optical reflectivity spectrum towards shorter wavelength was observed only after more than 2 h of incubation for PSi-M_c-NH_2, whereas PSi-M_d-NH_2 resulted in being partially stable in ultra-mild deprotection condition only up to 30 min (see plots in Figure 4).

As the last route in the deprotection strategy, we tested the saturated dry methanolic ammonia solution. Both the two aminosilane-modified PSi structures (PSi-$M_{e,f}$-NH_2) were highly stable at this condition. In Figure 5, we have reported the reflectivity spectra of PSi microcavities before and after treatment with NH_3/MeOH dry. In both cases, any shift cannot be observed, thus confirming the feasibility of this deprotection condition.

Once deprotection conditions were checked and fixed for PSi samples, two microcavities, namely PSi-$M_{g,h}$-NH_2, were used as supports for automated *in situ* solid-phase ON synthesis using the standard phosphoramidite chemistry. The amount of 5′-dimethoxytrityl released after the

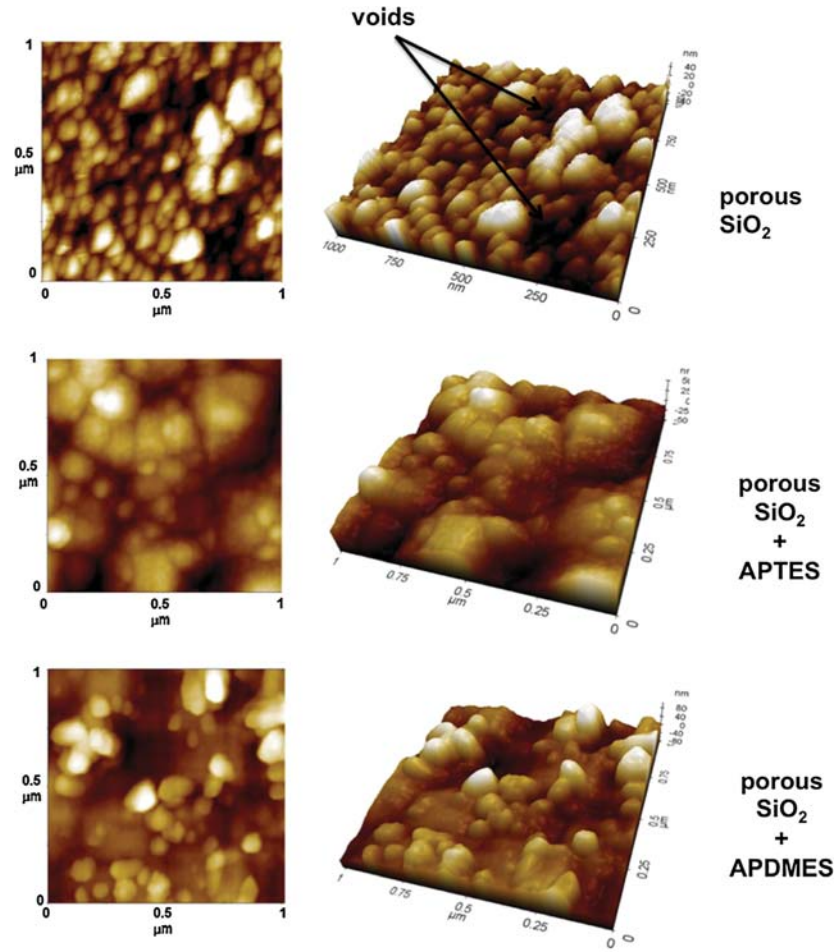

Figure 2 AFM images of bare oxidized PSi and aminosilane-modified oxidized PSi surfaces.

detritylation step was used to quantify the functionalization yield of each synthesis cycle by UV-vis spectroscopy as shown in Figure 6 [16,17]. Up to the fourth coupling cycle, we observed almost the same coupling yield for both aminosilane-functionalized PSi supports. From the fifth cycle on, the coupling yields dropped for both supports, even if higher functionalization yields were generally observed for PSi supports functionalized with APTES.

Figure 6 also shows the reflectivity spectra of devices before and after the *in situ* synthesis process: red shifts of 60 and 70 nm were detected, respectively, for APTES- and APDMES-modified devices, thus indicating that more ON had grown on the latter device with respect to the first one. This experimental result is ascribed to the less steric hindrance of pores due to the thinner APDMES layer, as already demonstrated in our previous work [16].

In both samples, we have measured the red shifts upon exposure to saturated ethanol atmosphere (data not shown here), in order to check if pores could be completely filled up by ON growth: in both cases, we measured red shifts of about 100 nm, just a little bit lower, but of the same order, than those registered in the same experiment after fabrication and silane functionalization. Even if this result is not accurate as standard pore characterization (such as gas adsorption or thermoporometry), it clearly confirms a minor variation in pore dimensions.

We demonstrated the ability of NH_3/dry MeOH solution to completely deprotect the PSi-aminosilane-bound ON by treating the functionalized samples with NH_3/MeOH at room temperature. We observed by chromatographic analysis that the amide-bound N-2 isobutyryl (on G), N-6 benzoyl (on A) and N-4 benzoyl (on C) were

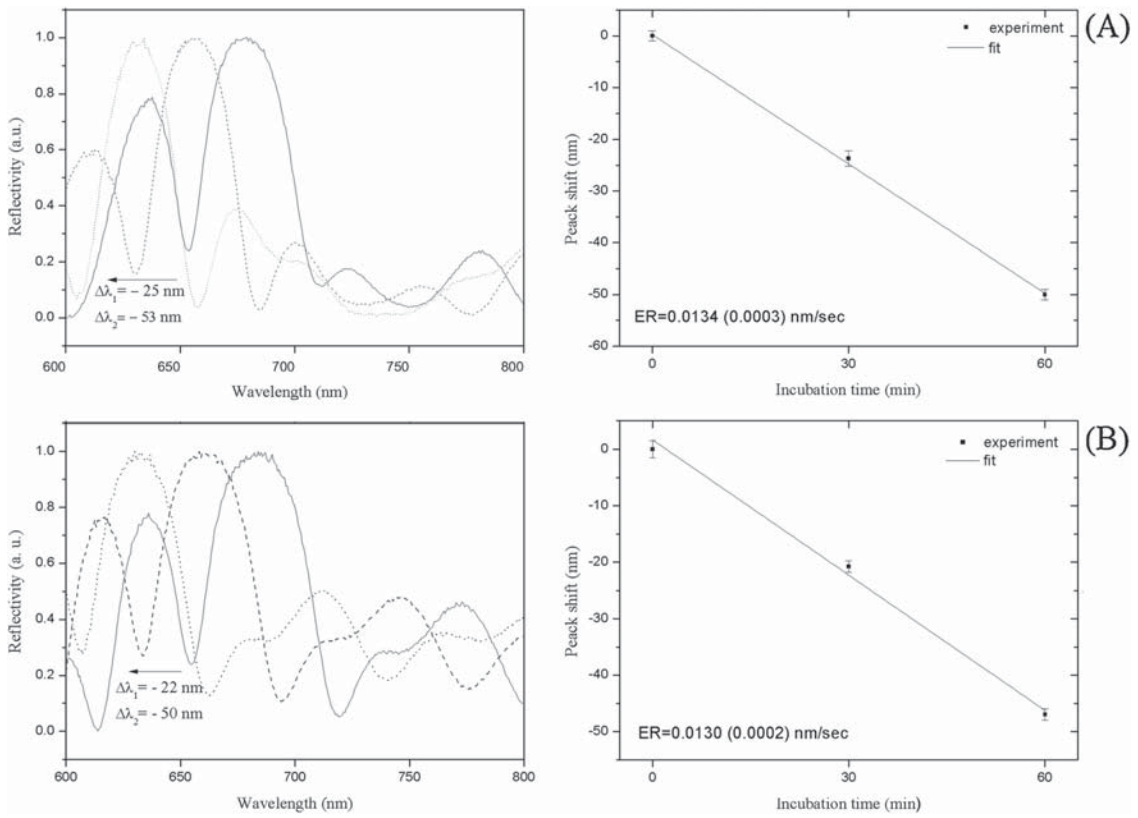

Figure 3 Reflectivity spectra of APTES- and APDMES-modified PSi microcavities before and after incubation in 33% NH_3. (A) Left: reflectivity spectra of APTES-modified PSi microcavity before (solid line) and after 30 (dashed line) and 60 (dotted line) min of incubation in 33% NH_3 at 55°C. Right: corresponding peak shift vs incubation time. **(B)** Left: reflectivity spectra of APDMES-modified PSi microcavity before (solid line) and after 30 (dashed line) and 60 (dotted line) min of incubation in 33% NH_3 at 55°C. Right: corresponding peak shift vs incubation time.

completely cleaved after 3 h at room temperature. Furthermore, it is reported that the ammonia in dry MeOH is able to quickly remove the 2-cyanoethyl phosphate protecting group [15]. This data, together with our findings on the compatibility with the silicon structure, indicates the NH_3/dry MeOH solution as the best choice to deprotect the exocyclic amino groups of nucleobases and the phosphate groups without promoting the basic hydrolysis on the support, which would instead occur in aqueous conditions. The blue shift of only 2 to 4 nm, which we attribute to the removal of N-2, N-4 and N-6 groups, has been detected after this procedure for *in situ* ON synthesis on PSi-APTES or PSi-APDMES supports, respectively (see plots in Figure 7).

Conclusions

In the present study, we propose and validate by optical measurements a new method to achieve the *in situ* synthesis of tailored oligonucleotide sequences on porous silicon supports suitable for label-free optical biosensing. In particular, we demonstrate that, differently from aqueous ammonia, the use of dry ammonia in methanol allows the effective deprotection of nucleobases without harming the structural integrity of the porous silicon matrix, thus opening the way for the direct growing of mixed-sequence ONs on optically active PSi supports using exclusively inexpensive standard phosphoramidites. A 19-mer mixed-sequence 5′-GATTGATGTGGTTGATTTT-3′ has been synthesized in mesoporous PSi microcavities, resulting in a medium-yield process, mainly due to the average pore size (about 20 nm). PSi photonic devices with pore dimensions greater than that value, but always compatible with high optical quality response in the visible-near-infrared, therefore between 50 and 100 nm, will be considered in the next experiments, in order to maximize yield synthesis. Moreover, more stable PSi supports could also be considered, such as those produced by thermal acetylation, which maintains pore size and makes it very stable from the chemical point of view [18].

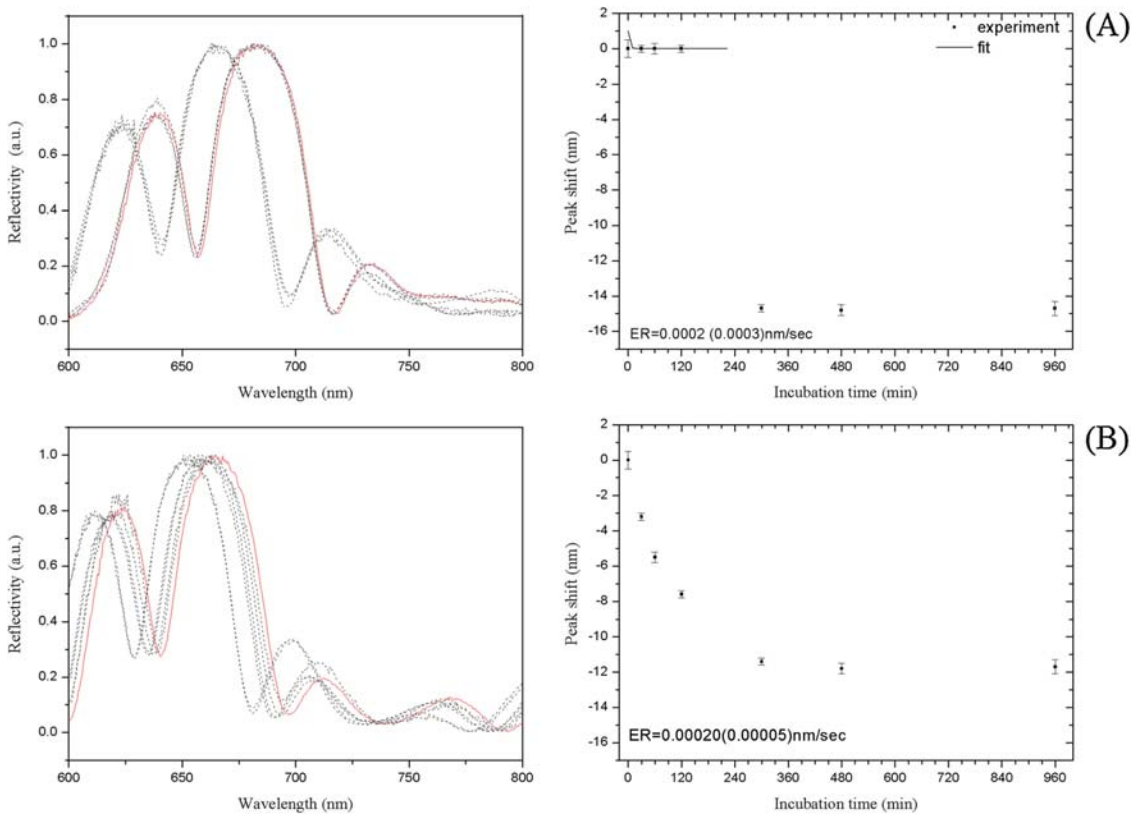

Figure 4 Reflectivity spectra of APTES- and APDMES-modified PSi microcavities before and after incubation in K_2CO_3/MeOH dry. (A) Left: reflectivity spectra of APTES-modified PSi microcavity before (red solid line) and after (dashed line) incubation in K_2CO_3/MeOH dry at 55°C for different times. Right: corresponding peak shift vs incubation time. **(B)** Left: reflectivity spectra of APDMES-modified PSi microcavity before (red solid line) and after (dashed line) incubation in K_2CO_3/MeOH dry at 55°C for different times. Right: corresponding peak shift vs incubation time.

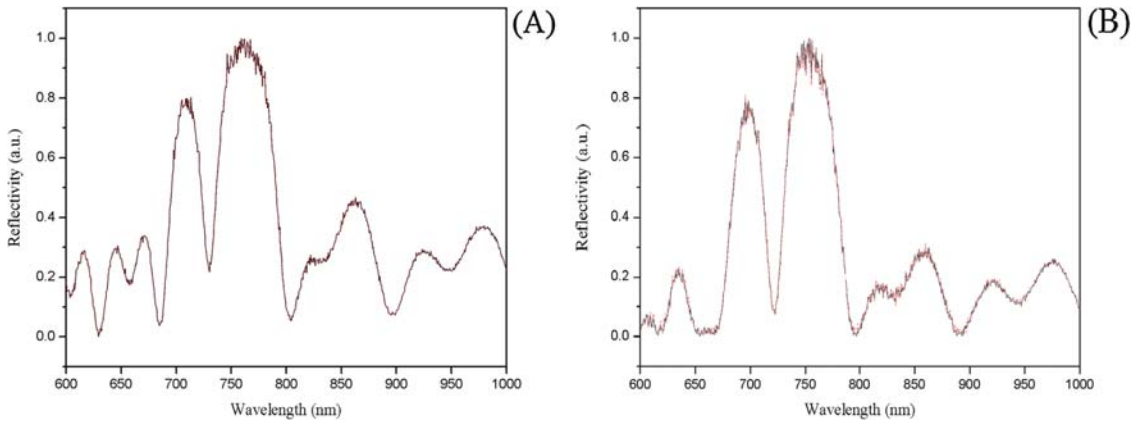

Figure 5 Reflectivity spectra of APTES- and APDMES-modified PSi microcavities before and after exposure to NH_3/MeOH dry and ammonia. (A) Reflectivity spectra of APTES-modified PSi microcavity before (solid line) and after (red dashed line) exposure to NH_3/MeOH dry solution at RT. **(B)** Reflectivity spectra of APDMES-modified PSi microcavity before (solid line) and after (red dashed line) exposure to ammonia solution at RT.

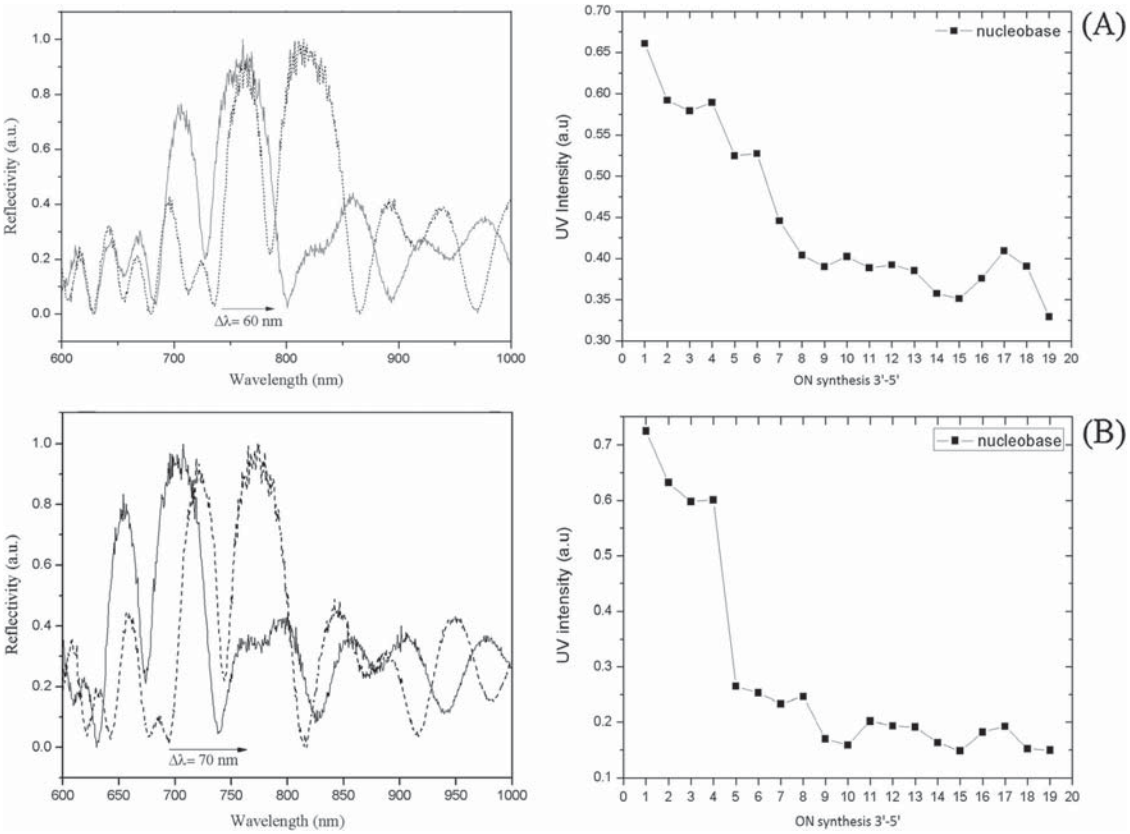

Figure 6 Reflectivity spectra of APTES- and APDMES-modified PSi microcavities before and after ON synthesis. (A) Left: reflectivity spectra of APTES-modified PSi microcavity before (solid line) and after (dashed line) ON synthesis. Right: corresponding UV intensity vs ON synthesis. **(B)** Left: reflectivity spectra of APDMES-modified PSi microcavity before (solid line) and after (dashed line) ON synthesis. Right: corresponding UV intensity vs ON synthesis.

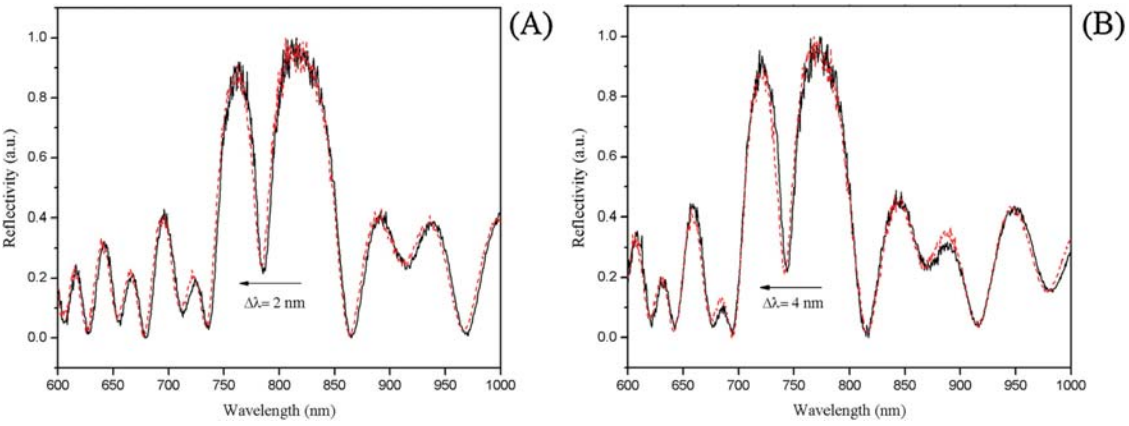

Figure 7 Reflectivity spectra of APTES- and APDMES-modified PSi microcavities before and after the deprotection process. (A) Reflectivity spectra of APTES-modified PSi microcavity functionalized with oligonucleotides before (solid line) and after (red dashed line) the deprotection process with gaseous ammonia solution. **(B)** Reflectivity spectra of APDMES-modified PSi microcavity functionalized with oligonucleotides before (solid line) and after (red dashed line) the deprotection process with gaseous ammonia solution.

Competing interests
The authors declare that they have no competing interests.

Authors' contributions
MT performed the experiments. LDS and IR designed the research. MT and IR analysed the data and wrote the paper. LDS and NB corrected the paper. MT prepared and characterized the samples. GO, SDE and FN performed the oligonucleotide synthesis and characterization. IvR and GP have given final approval of the version to be published. All authors read and approved the final manuscript.

Acknowledgements
This work has been partially supported by the national project PON Oncology.

Author details
[1]Institute for Microelectronics and Microsystems, National Council of Research, Naples 80131, Italy. [2]Department of Pharmacy, University of Naples Federico II, Naples 80138, Italy.

Received: 24 April 2014 Accepted: 12 June 2014
Published: 25 June 2014

References

1. Heller MJ: **DNA microarray technology: devices, systems, and applications.** *Annu Rev Biomed Eng* 2002, **4:**129–153.
2. Wang J, Rivas G, Cai X, Palecek M, Nielsen P, Shiraishi H, Dontha N, Luo D, Parrado C, Chicharro M, Flair MN: **DNA electrochemical biosensors for environmental monitoring. A review.** *Anal Chim Acta* 1997, **347:**1–8.
3. Leonard P, Hearty S, Joanne B, Lynsey D, Chakraborty T, O'Kennedy R: **Advances in biosensors for detection of pathogens in food and water.** *Enzym Microb Technol* 2003, **32:**3–13.
4. Lehman V: *Electrochemistry of Silicon.* New York: Wiley; 2002.
5. Leigh C: *Properties of Porous Silicon.* London: INSPEC/IEE; 1997.
6. Bisi O, Ossicini S, Pavesi L: **Porous silicon: a quantum sponge structure for silicon based optoelectronics.** *Surf Sci Rep* 2000, **38:**1–126.
7. Pavesi L: **Porous silicon dielectric multilayers and microcavities.** *La Rivista del Nuovo Cimento* 1997, **20:**1–76.
8. De Tommasi E, Rendina I, Rea I, Di Sarno V, Rotiroti L, Arcari P, Lamberti A, Sanges C, De Stefano L: **Porous silicon based resonant mirrors for biochemical sensing.** *Sensors* 2008, **8:**6549–6556.
9. De Stefano L, Rea I, Giardina I, Armenante A, Rendina I: **Protein modified porous silicon nanostructures.** *Adv Mat* 2008, **20:**1529–1533.
10. Moretti L, De Stefano L, Rea I, Rendina I: **Periodic versus aperiodic: enhancing the sensitivity of porous silicon based optical sensor.** *Appl Phys Lett* 2007, **90:**191112.
11. Buriak JM: **Illuminating silicon surface hydrosilylation: an unexpected plurality of mechanisms.** *Chem Mater* 2013, **26:**763–772.
12. Terracciano M, Rea I, Politi J, De Stefano L: **Optical characterization of aminosilane-modified silicon dioxide surface for biosensing.** *J Europ Opt Soc Rap Public* 2013, **8:**13075.
13. Ellington A, Pollard D: **Synthesis and purification of oligonucleotides.** In *Current Protocols in Molecular Biology.* New York: Wiley; 2001:2.11.1–2.11.25.
14. Kuijpers WHA, Huskens J, van Boeckel CAA: **The 2-(acetoxymethyl)benzoyl (AMB) group as a new base-protecting group, designed for the protection of (phosphate) modified oligonucleotides.** *Tetrahedron Lett* 1990, **31:**6729.
15. Iyer RP, Dong Y, Jin X, Wen Z, Sudhir A: **The use of gaseous ammonia for the deprotection and cleavage steps during the solid-phase synthesis of oligonucleotides, and analogs.** *Bio Med Chem Lett* 1997, **11:**1443.
16. De Stefano L, Oliviero G, Amato J, Borbone N, Piccialli G, Mayol L, Rendina I, Terracciano M, Rea I: **Aminosilane functionalizations of mesoporous oxidized silicon for oligonucleotides synthesis and detection.** *J R Soc Interface* 2013, **10:**20130160.
17. Rea I, Oliviero G, Amato J, Borbone N, Piccialli G, Rendina I, De Stefano L: **Direct synthesis of oligonucleotides on nanostructured silica multilayers.** *J Phys Chem C* 2010, **114:**2617.
18. Salonen J, Laine E, Niinistö L: **Thermal carbonization of porous silicon surface by acetylene.** *J App Phys* 2002, **91:**456–461.

doi:10.1186/1556-276X-9-317
Cite this article as: Terracciano *et al.*: Synthesis of mixed-sequence oligonucleotides on mesoporous silicon: chemical strategies and material stability. *Nanoscale Research Letters* 2014 **9**:317.

Submit your manuscript to a SpringerOpen journal and benefit from:

► Convenient online submission
► Rigorous peer review
► Immediate publication on acceptance
► Open access: articles freely available online
► High visibility within the field
► Retaining the copyright to your article

Submit your next manuscript at ► springeropen.com

Hindawi Publishing Corporation
BioMed Research International
Volume 2014, Article ID 610718, 10 pages
http://dx.doi.org/10.1155/2014/610718

Research Article

Exploitation of a Very Small Peptide Nucleic Acid as a New Inhibitor of miR-509-3p Involved in the Regulation of Cystic Fibrosis Disease-Gene Expression

Felice Amato,[1,2] Rossella Tomaiuolo,[1,2] Fabrizia Nici,[3] Nicola Borbone,[3] Ausilia Elce,[1,2,4] Bruno Catalanotti,[3] Stefano D'Errico,[3] Carmine Marco Morgillo,[3] Giuseppe De Rosa,[3] Laura Mayol,[3] Gennaro Piccialli,[3] Giorgia Oliviero,[3] and Giuseppe Castaldo[1,2]

[1] *Dipartimento di Medicina Molecolare e Biotecnologie Mediche, Via Pansini 5, 80131 Napoli, Italy*
[2] *CEINGE-Biotecnologie Avanzate, 80131 Napoli, Italy*
[3] *Dipartimento di Farmacia, Università degli Studi di Napoli Federico II, Via D. Montesano 49, 80131 Napoli, Italy*
[4] *Università Telematica Pegaso, 80143 Napoli, Italy*

Correspondence should be addressed to Giorgia Oliviero; golivier@unina.it

Received 6 December 2013; Accepted 18 March 2014; Published 15 April 2014

Academic Editor: Daniela De Stefano

Copyright © 2014 Felice Amato et al. This is an open access article distributed under the Creative Commons Attribution License, which permits unrestricted use, distribution, and reproduction in any medium, provided the original work is properly cited.

Computational techniques, and in particular molecular dynamics (MD) simulations, have been successfully used as a complementary technique to predict and analyse the structural behaviour of nucleic acids, including peptide nucleic acid- (PNA-) RNA hybrids. This study shows that a 7-base long PNA complementary to the seed region of miR-509-3p, one of the miRNAs involved in the posttranscriptional regulation of the CFTR disease-gene of Cystic Fibrosis, and bearing suitable functionalization at its N- and C-ends aimed at improving its resistance to nucleases and cellular uptake, is able to revert the expression of the luciferase gene containing the 3UTR of the gene in A549 human lung cancer cells, in agreement with the MD results that pointed at the formation of a stable RNA/PNA heteroduplex notwithstanding the short sequence of the latter. The here reported results widen the interest towards the use of small PNAs as effective anti-miRNA agents.

1. Introduction

In the last twelve years a new group of endogenous, small, noncoding fragments of RNA, 18–25 nucleotides in length, named microRNAs (miRNAs) emerged for its ability to suppress the gene expression at posttranscriptional level [1, 2]. To date more than 1,400 miRNAs have been identified. MicroRNAs regulate the gene expression by annealing with the complementary mRNAs, thus preventing their translation or inducing their degradation [3, 4]. Although miRNAs usually recognize the 3UTR many of them are capable of binding the 5UTR or even coding regions of target mRNAs. Due to the small number of constituting nucleobases, each miRNA can recognize one or many mRNAs and each mRNA can be the target of many miRNAs. The result of this network of interactions is the coregulatory role of miRNAs on the translation/degradation of one or more mRNAs [5]. Despite the potential occurrence of off-target effects, it is emerging that the modulation of specific miRNAs represents a new approach to achieve the control of gene expression. Potential applications of miRNA inhibitors (antimiR) range from diagnostics to regulation of important proteins involved in numerous cancers [6]. A number of human diseases have been associated with a deregulation of specific miRNAs [7–12]. Among these is the genetic disease Cystic Fibrosis (CF). CF is the most common lethal genetic disorder among Caucasians with one in every 3,000 newborns affected. CF is due to mutations in the CFTR gene encoding the CFTR chloride channel expressed by most epithelial cells [13]. The CF phenotype typically includes the altered sweat test, pancreatic

insufficiency, and pulmonary infections that gradually lead to respiratory insufficiency. To date more than 1,900 mutations of CF gene have been described, and a set of miRNAs inhibiting the CFTR expression at the posttranscriptional level has been described [14]. Furthermore, our group has shown that mutations in the 3UTR of the CFTR gene may have a pathogenic effect by enhancing the affinity for the miR-509-3p miRNA [15].

The approaches to downregulate a specific miRNA essentially use oligonucleotide (ON) analogues which being complementary to miRNAs are able to reduce or inhibit their activity. For this purpose a number of ribose modified ONs, usually bearing a phosphorothioate backbone, have recently been used. Interesting results have been obtained by using 2-O-methyl-ribonucleotides [16, 17] and other 2-modified ONs [18, 19]. In addition, locked nucleic acids (LNAs) have shown interesting activity [20, 21] especially when used in combination with unmodified DNA monomers. Recently, several studies have demonstrated that the DNA mimics named peptide nucleic acids (PNAs) can be effectively used as anti-miRNA [22–24]. In the PNAs a 2-aminoethyl-glycine polymer replaces the ribose-phosphate DNA backbone [25]. PNA molecules are resistant to protease and nuclease degradation and recognize with a high affinity complementary fragments of DNA or RNA [26]. Many studies have been performed on the binding capability of PNAs and on the topological way in which they can recognize nucleic acids in single strand, duplex, or quadruplex arrangements to form heteroduplex, heterotriplex, and heteroquadruplex complexes [27–31] or to act as quadruplex ligands, respectively [32, 33]. The anti-miRNA activity of a PNA can occur in the nucleus by targeting the pre-miRNA or in the cytoplasm by binding the pre-miRNA and/or the mature miRNA [17]. In both cases it is necessary that the PNA can pass through the cell membrane and also through the nuclear membrane for the former case. The main drawback in the use of PNAs as intracellular probes lies in the poor water solubility when their length exceeds the 12–14 bases. Furthermore, the cellular uptake behaviour of a PNA is not easily predictable because it is mostly dependent on the PNA base composition and the overall lipophilicity. Recent studies report on the feasibility of a miRNA regulation approach by using unmodified PNAs and PNAs conjugated with peptides or hydrophilic groups [34, 35].

PNAs having a poly-lysine tail display increased water solubility and cellular uptake [23, 24]. In addition, negatively charged PNAs can be obtained by synthesizing PNA-DNA hybrid strands or by attaching negative groups to the PNA monomers [34, 36]. In the last case, cationic lipids can be used as transfection reagents.

We recently reported that some anionic PNAs, synthesized by our group, are a potential treatment for CF by targeting the miR-509-3p involved in the regulation of CF disease-gene expression [37]. In that study we synthesized a 14-base long PNA fully complementary to the 5-end of miR-509-3p and carrying a tetrapeptide tail containing two serine phosphates at its C-terminus and a fluorescein group at its N-terminus (PNA1, Table 1). We demonstrated, by *in vitro* studies on A549 cell lines, that the serine phosphate tail represents a suitable conjugation to improve both the water solubility and the cellular uptake of a PNA molecule. Hybridization studies on PNA1 in the presence of miR-509-3p, performed by UV and CD spectroscopies and by electrophoretic mobility shift assay (EMSA), prove that the anionic peptide tail does not hamper the formation of the miR-509-3p/PNA1 heteroduplex. Finally, by reverting the expression of the luciferase gene containing the 3UTR of the CFTR gene, we also demonstrated that PNA1 is able to recognize miR-509-3p in A549 cells. In continuing our studies on the Cystic Fibrosis and on the control of the related miR-509-3p miRNA, we decided to test the capability of the short 7-mer PNA2 (Table 1), bearing the same functionalization of PNA1 and complementary to the seed region of miR-509-3p, to bind this miRNA. Our interest towards shorter PNA anti-miRNAs was triggered by the consideration that the synthesis of longer PNAs (14–16 bases long) is an expensive and not an easily achievable task, especially when the PNA is conjugated to peptide tails and/or labelled at both ends. In addition, a recent study has reported that a very short LNA (8 bases long) was able to recognize and silence a family of miRNAs with no off-target effects [38]. Furthermore, experimental and computational evidence for different types of miRNA target sites demonstrated that probes with as few as seven base pairs of complementarity to the 5-end of miRNAs are sufficient to confer regulation *in vivo* and are used in biologically relevant targets [5, 39]. The synthesis of PNA2 was preceded by a molecular modelling study aimed at evaluating the structural behaviour of the goal seven bases long miR-509-3p/PNA2 heteroduplex in comparison with that of the longer miR-509-3p/PNA1 heteroduplex. The stability and the structure of the miR-509-3p/PNA2 duplex were evaluated by molecular modelling and by UV, CD, and EMSA analyses. We here anticipate that PNA2, notwithstanding its reduced length, was still able to recognize miR-509-3p in A549 cells where it reverted the expression of the luciferase gene containing the 3UTR of the CFTR gene.

2. Materials and Methods

Synthesis of miR-509-3p and PNAs (Table 1). The miR-509-3p mimic (2-OMe modified) was synthesized and purified by the oligonucleotide synthesis facility at CEINGE-Biotecnologie Avanzate (Naples, Italy). The 4-methyl-benzhydrylamine-resin (MBHA resin, 0.4 mmol/g), all Fmoc/Boc protected monomers, and the 2-(2-(fluorenylmethoxycarbonylamino)ethoxy) ethoxyacetic (AEEA) spacer-linker were purchased from Link Technologies. Fmoc-L-Ser(PO(OBzl)OH)-OH building block, 2-(1-H-benzotriazol-1-yl)-1,1,3,3-tetramethyluronium hexafluorophosphate (HBTU), 2-(1-H-7-azabenzotriazole-1-yl)-1,1,3,3-tetramethyluronium hexafluorophosphate (HATU), and 1-hydroxybenzotriazole (HOBt) were purchased from Novabiochem. The following abbreviations are used: trifluoroacetic acid (TFA), dimethylformamide (DMF), dichloromethane (DCM), N,N-diisopropylethylamine (DIPEA), N-methylpyrrolidone (NMP), 1,8-diazabicyclo(5,4,0)undec-7-ene (DBU), and 2-(6-hydroxy-3-oxo-3H-xanthen-9-yl)-5-isothiocyanate-benzoic acid (FITC).

Table 1: Structures and sequences of miR-509-3p and PNA1–3. PNA sequences are written from C- to N-terminus.

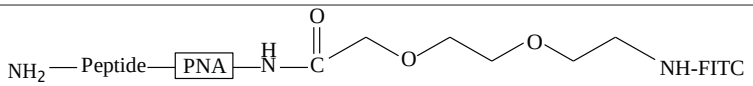

miRNA		U	G	A	U	U	G	G	U	A	C	G	U	C	U	G	U	G	G	G	U	A	G
PNA1	G-S(P)-S(p)-G-a	c	t	a	a	c	c	a	t	g	c	a	g	a	Linker-FITC								
PNA2	G-S(P)-S(p)-G-a	c	t	a	a	c	c	Linker-FITC															
PNA3	G-S(P)-S(p)-G-t	t	t	t	t	t	t																

PNA2 and PNA3 were synthesized using the Fmoc-solid-phase strategy. The MBHA resin (50 mg, 0.02 mmol), after swelling in DCM (30 min) and DMF washings, was treated with a solution of 20% piperidine (2 mL) in DMF for 10 min. After washings in DMF, the resin was reacted with Fmoc-Gly (5 eq., in NMP 0.25 M), HATU (3.6 eq. in DMF 0.2 M), and DIPEA (5 eq.)/lutidine (6 eq.) for 1 h at room temperature. During the peptide and PNA synthesis the Fmoc group was removed by a treatment with a 5% DBU in DMF solution (5 min). In the case of Fmoc-Ser amino acids the basic treatment was prolonged (20 min). Couplings of Fmoc-L-Ser(PO(OBzl)OH)-OH were achieved using the following conditions: Fmoc-Ser monomer (8 eq. in NMP 0.4 M), HATU (8 eq. in DMF 0.4 M), and DIPEA (8 eq.)/lutidine (12 eq.) for 15 h at room temperature. PNA monomers and AEEA-COOH linker were reacted using the following conditions: monomer building block (8 eq. in NMP 0.4 M), HATU (8 eq. in DMF 0.4 M), and DIPEA (8 eq.)/lutidine (12 eq.) for 4 h at room temperature.

For the coupling with the fluorescent group the FITC monomer (5 eq., 0.2 M) was dissolved in DMF/DIPEA (2.5 : 97.5 v/v) and the solution was added to the resin, which was gently shaken in the dark for 15 h. The resin was finally treated with TFA/anisole/ethanedithiol (9 : 0.5 : 0.5; v/v/v) for 3.5 h and the products were precipitated with cold diethyl ether. The precipitates were recovered by centrifugation and following two washings with diethyl ether were dissolved in water and lyophilized. The PNA2 and PNA3 were obtained with a 48–50% overall yield (94-95% medium yield for each coupling).

The purifications were performed by HPLC using a RP-18 column (Merck, RT 250–10 5 □m) eluted with a linear gradient from 10% to 90% of eluent B in eluent A in 30 min. Eluent A: 0.1% TFA in water; eluent B: 0.1% TFA in acetonitrile. For these purifications the UV/VIS detector was set at 495 nm corresponding to the maximum of absorption of FITC. The collected yellow fractions were lyophilized and stored at −20°C in the dark.

The structures of PNA2 and PNA3 were confirmed by MALDI-TOF mass spectrometry on a Bruker Autoflex I instrument using □-cyano-4-hydroxycinnamic acid, 10 mg/mL in acetonitrile-3% aqueous TFA (1 : 1, v/v) as the matrix.

PNA2 m/z calculated 2812, found 2813 $[M+H]^+$.

PNA3 m/z calculated 2864, found 2865 $[M+H]^+$.

Molecular Modelling. The initial structures of the heteroduplexes formed by miR-509-3p with PNA1 and PNA2 were built by using the NMR structure of the 6-mer RNA(GAGUUC)/PNA(GAACTC) heteroduplex (PDB ID = 176D) [43]. Starting from the lowest energy NMR structure, one nucleotide was added aligninga duplicate of the reference structure on the PNA backbone. Once the 7-mer heteroduplex was obtained, the bases were mutated to match the PNA2 sequence. Watson-Crick canonical pairs were then refined using distance restraints on the first seven bases of miR-509-3p/PNA2 heteroduplex. The same procedure was used to build the miR-509-3p/PNA1 heteroduplex, starting from the refined structure of miR509-3P/PNA2 heteroduplex.

The equilibration of the systems and production of MD simulations were performed using the Amber 12 suite of programs [44, 45]. The Leap module of Ambertools13 was used to create parameter and topology files for the MD simulations using the ff99SB force field for RNA and standard amino acids [44, 45]. For PNAs parameterization we used the Sanders et al. force field for PNA [46] downloaded from the RESP and ESP charge database (R.E.DD.B. http://q4md-forcefieldtools.org/REDDB Project ID = F93) [47], whereas the parameters for serine phosphate were taken from reference [48]. TIP3P water molecules were added with a minimum spacing of 10.0 Å from the box edges to the RNA:PNA molecules and Na^+ counterions were added to each system to reach the neutralization of the system.

The geometry of the system was minimized in four steps as follows: (1) optimization of hydrogen atoms (500 steps of steepest descent and 4,500 steps of conjugate gradient); (2) optimization of water molecules and counterions (2,000 steps of steepest descent and 8,000 steps of conjugate gradient); (3) further optimization of hydrogen atoms, water molecules, and counterions (3,500 steps of steepest descent and 11,500 steps of conjugate gradient); (4) final optimization of the whole system (2,500 steps of steepest descent and 8,500 steps of conjugate gradient). Thermalization of the system was performed in four steps of 60 ps, increasing the temperature from 10 to 298 K. Concomitantly, interstrand distance restraints were applied to the RNA:PNA heteroduplex to preserve all base pairs canonical Watson-Crick bond, allowing 0.1 Å movement from the equilibrium bond distance (either closer or farther). Thus, the force constant applied during thermalization was set to 32 kcal mol^{-1} $Å^{-2}$ and was gradually reduced in the next step to 10 kcal mol^{-1} $Å^{-2}$ and subsequently decreased by increments of 5 kcal mol^{-1} $Å^{-2}$

in the next stages. Then, an additional step of 250 ps was performed in order to equilibrate the system density at constant pressure (1 bar) and temperature (298 K). Finally, an extended trajectory covering was run using a time step of 2 fs. SHAKE was used for those bonds containing hydrogen atoms in conjunction with periodic boundary conditions at constant pressure and temperature, particle mesh Ewald was used for the treatment of long range electrostatic interactions, and a cutoff of 9 Å was used for nonbonded interactions.

All production simulations were repeated in triplicate with random seeding for initial velocities and extended to 20 ns. In order to further assay the stability of the RNA:PNA heteroduplexes, we extended one run of PNA2 up to 50 ns, for a total simulation time of 90 ns for PNA2 and 60 ns for PNA1. The structural features were determined using the Curves+ software package [40], and visualization of trajectories was performed in VMD [41], while the trajectory analyses were performed using Ambertools13.

Preparation of miRNA/PNA Heteroduplexes (Annealing). The miR-509-3p/PNA heteroduplexes (1 : 1.5 or 1 : 5) were formed by heating the mixture of the samples dissolved in 100 mM KCl, 10 mM K_2HPO_4, at 90°C for 5 min and slowly cooling at room temperature for 12 h. The amount of each PNA sample was estimated by quantitative UV at 80°C using the following molar extinction coefficients: PNA1 □ = 149.6 mL □mol^{-1} cm^{-1}, PNA2 □ = 69.7 mL □mol^{-1} cm^{-1}, PNA3 □ = 61.6 mL □mol^{-1} cm^{-1}, and miR-509-3p □ = 205.0 mL □mol^{-1} cm^{-1}.

UV and UV Melting Studies. The UV spectra were recorded on a Jasco V-530 UV spectrophotometer equipped with a Peltier-type temperature control system (model PTC-348WI). Thermal denaturation experiments were carried out in the temperature range 5–90°C by monitoring the absorbance at 260 nm at the heating rate of 0.5°C/min. The apparent Tm was estimated from the maximum in the first derivative of the melting profile.

CD Studies. CD spectra were recorded with a Jasco J-715 spectropolarimeter equipped with a Peltier Thermostat Jasco ETC-505T using 0.1 cm path length cuvettes and calibrated with an aqueous solution of 0.06% d-10-(1)-camphorsulfonic acid at 290 nm. The molar ellipticity [Θ] (deg cm^2 $dmol^{-1}$) was calculated from the following equation: [Θ] = [Θ]obs/10 □ □, where [Θ]obs is the ellipticity (mdeg), □ is the oligonucleotide molar concentration, and □ is the optical path length of the cell (cm). CD measurements (220–320 nm) were carried out at a scan rate of 100 nm/min with a 2 nm bandwidth. The concentration of miR-509- 3p/PNA2 and miR-509-3p was 1.0×10^{-5} M. The spectra were signal-averaged over at least three scans and baseline was corrected by subtracting the buffer spectrum.

Cell Line, Construct, and Transfections. A549 human lung carcinoma cells were purchased from ATCC (Manassas, USA). Cells were maintained in Dulbecco's modified Eagle's medium (Gibco Invitrogen, USA) with 10% heat inactivated fetal bovine serum (HyClone, USA) without the addition of antibiotics. Luciferase construct bearing the 3UTR of CFTR gene [15] was used as miR-509-3p sensitive. Transfection of A549 cells with miRNA-mimics (Qiagen, Germany, EU) or PNA was performed with Attractene Transfection Reagent (Qiagen) as previously reported [37]. Briefly, cells seeded in 96-well plates were cotransfected with the luciferase reporter constructs and the miR-509-3p mimic. 24 h after, the cells were transfected with anti-miR-509-3p PNA. The transfection efficiency (≈ 80%) was assessed by measuring the percentage of fluorescent cells relative to the total number of cells. The luciferase activity level was measured 24 h after transfection using the Dual-Glo Luciferase Assay System (Promega Corporation). The relative reporter activity was obtained by normalization to the Renilla luciferase activity.

2.7. Electrophoretic Mobility Shift Assay. The miR-509-3p mimic (2OMe-modified) was synthesized by the oligonucleotide synthesis facility at CEINGE-Biotecnologie Avanzate (Naples, Italy). As previously reported [37], the miRNA and PNA were annealed in 1X NEBuffer 2 (50 mM NaCl, 10 mM Tris-HCl, 10 mM $MgCl_2$, 1 mM DTT, and pH 7.9 at 25°C) for 2 h at room temperature. All the reactions were loaded into 20% polyacrylamide gels in 0.5X Tris-Borate-EDTA (TBE) buffer and run at 140 V for 3 h. The fluorescence signal was acquired placing the wet gel directly on the plate of the Typhoon 8600 scanner.

3. Results and Discussion

With the aim of evaluating the feasibility of our hypothesis of shortening the PNA1 molecule to achieve a more synthetically affordable PNA targeted against miR-509-3p that preserves the hybridization properties of the parent PNA1, PNA2 was designed by deleting all the PNA1 bases that were not complementary to the "seed region" of miR-509-3p (i.e. the first seven bases at its 5end, considered the most important target to achieve the anti-miRNA activity). As previously done for PNA1 [37], to improve the water solubility and the cellular uptake of PNA2 we decided to add the negatively charged tetrapeptide G-S(P)-S(P)-G at the C-end, whereas the fluorescent AEEA linker-FITC was added at the N-end to assess the cellular localization of PNA2. Before proceeding to the in-lab synthesis of PNA2, we estimated the stability and the conformational features of the goal miR-509-3p/PNA2 heteroduplex by means of computational techniques and compared the results with those of the correspondent heteroduplex formed with the PNA1. Computational techniques, and in particular molecular dynamics (MD) simulations, have been successfully used as complementary technique to predict and analyse the structural behaviour of nucleic acids, including PNA-RNA hybrids [46, 49, 50].

Molecular Dynamics Simulations. The miR-509- 3p/PNA2 and miR-509-3p/PNA1 heteroduplexes were built starting from the NMR structure of the RNA (GAGUUC)/PNA(GAACTC) duplex (PDB-ID 176D)

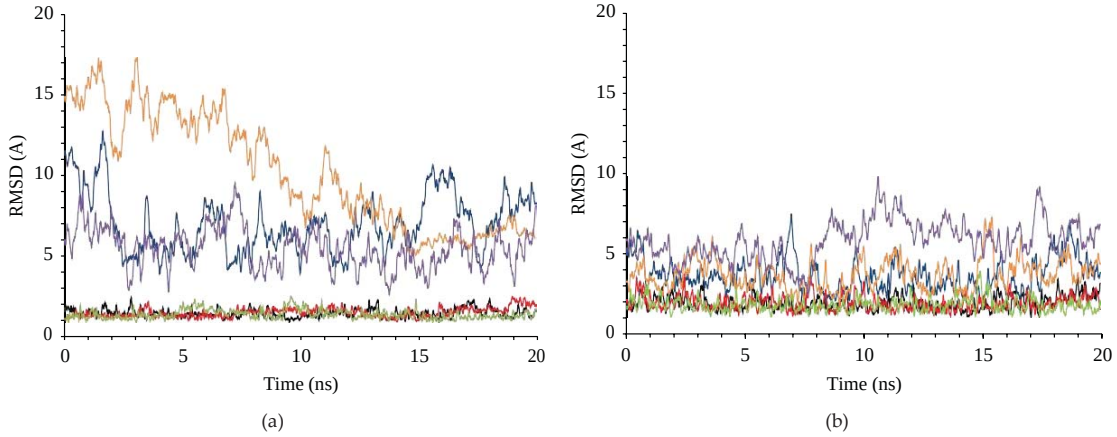

Figure 1: Root-mean-square deviation in the three MD runs on miR-509-3p/PNA2 (a) and miR-509-3p/PNA1 (b) heteroduplexes. Superimpositions were made on the MD-averaged structures for each trajectory taking into account the whole structure (blue, orange, and purple) or only the duplex region (black, red, and green).

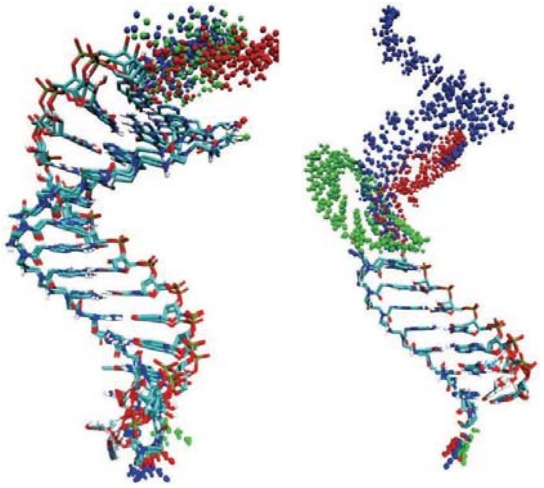

	PNA1		PNA2	
AVG	Run 2	Run 3	Run 2	Run 3
Run 1	0.36	0.36	0.9	0.56
Run 2	//	0.5	//	0.9

(c)

Figure 2: Superimposition of the MD average structures of miR-509-3p/PNA1 complex (a) and of miR-509-3p/PNA2 complex (b). Duplexes regions are represented in licorice coloured by atom type (carbon in cyan, oxygen in red, nitrogen in blue, phosphate in brown, and hydrogen in white). The miR-509-3p single strand regions are represented in spheres coloured by MD run (blue, run 1; green, run 2; red, run 3). (c) RMSD in Å, calculated on phosphates in the duplexes regions, among the average structures of the MD runs.

[43] as described in Materials and Methods. Each system was firstly analysed by means of three runs of 20 ns molecular dynamics in order to better sample the conformational behaviour of the complexes. Secondly, in order to further assay the stability of the miR-509-3p/PNA2 duplex, we extended one run of miR-509-3p/PNA2 up to 50 ns, for a total simulation time of 90 ns for miR-509-3p/PNA2 and 60 ns for miR-509-3p/PNA1.

The macroscopic properties of the systems, such as temperature, pressure, volume, density, and energy, were fairly constant during the whole simulation for both of the systems (data not shown). As expected, the analysis of the RMSD in the trajectories of miR-509-3p/PNA2 and miR-509-3p/PNA1 complexes showed high flexibility of the single stranded miRNA segment (Figure 1). On the contrary, the behaviour of the region of miR-509-3p hybridized with PNAs was characterized by low RMSD values and low fluctuations, thus indicating the presence of a stable secondary structure (Figure 1).

Moreover, the comparison of the average structures obtained from each trajectory (Figure 2) revealed the convergence of the trajectories as shown by the low RMSD values in the duplex region of both complexes with PNA1 and PNA2 (>0.5 Å and >0.9 Å, resp.).

Table 2: Comparison of backbone torsion angles and helicoidal parameters for average structures of each run after 20 ns MD simulation. Highlighted in bold are values for structure obtained by averaging all the three runs. Standard deviation is reported in brackets.

(a)

	Helicoidal parameters						
Duplex name	Twist (°)	Roll (°)	Tilt (°)	Inclination (°)	H.Ris (°)	H.Twi (°)	Groove width (Å)
PNA:RNA-NMR[a]	30.1 (4)	4.9 (4.3)	1.0 (3.3)	9.0 (2.7)	2.98 (0.2)	30.6 (4.2)	6.1 (0.5)
PNA:RNA MD[b]	23.7; 23.2						
A-RNA[c]	32	12	2.8	15.8	3.3		3.8
PNA2 AVG tot	24.5 (1.1)	6.5 (1.6)	1 (0.9)	14.2 (0.6)	2.79 (0.10)	25.3 (1.1)	6.8 (0.6)
PNA1 AVG tot	24.9 (2.8)	5.7 (2.2)	0.9 (1.3)	13 (1.1)	2.77 (0.16)	25.5 (2.9)	6.8 (0.5)

(b)

	Torsional PNA angles (in degrees)						
	N4–C5	C5–C	C–N1	C2–C3	C3–N4	N4–C7	□
PNA:RNA-NMR[a]	−84.9	80	105.7	66	−100.1	9.1	50.6
PNA2	**−79.9**	**125.2**	**78.6**	**70.4**	**−103**	**−2.9**	**78**
PNA1	**−81.3**	**129**	**131.5**	**69.5**	**−103.3**	**−2.1**	**78.5**

(c)

	Torsional RNA angles (in degrees)						
	□	□	□	□	□	□	□
PNA:RNA-NMR[a]	−68.4	111.75	58.4	78.5	−148.7	−72.5	−104.5
A-RNA[c]	−52	175	42	79	−146	−75	−157
miR20a[d]	−99.1	162.6	73.1	88.7	−138	−119.4	−147.6
PNA2 AVG tot	−84.4	172.8	81.3	79.2	−160.4	−70.3	−159.5
PNA1 AVG tot	−88.8	145.8	85.5	81.8	−161.1	−70.9	−158.7

[a] Calculated on the average of the 10 NMR structures of PDB structure 176D; [b]from [40]; [c]from [41]; [d]from [42].

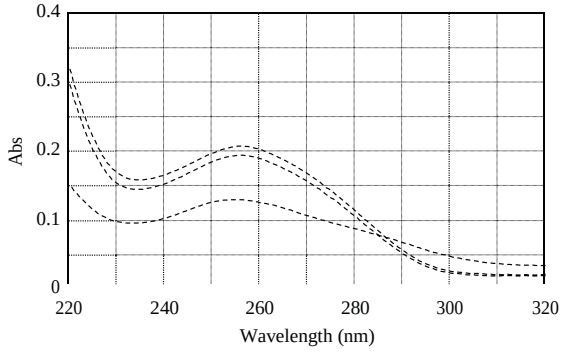

Figure 3: UV spectra of miR-509-3p (dashed line), PNA2 (solid line), miR-509-3p/PNA2 mixture (1:1.5) (dotted line), and the arithmetical sum (dashed-dotted line).

The analysis of the helicoidal parameters and torsion angles (Table 2) demonstrated that both miRNA/PNA duplexes could be described as A-type double helix with few noticeable deviations from the canonical structure. In particular, the lower step-averaged twist values reported in Table 2 indicated a slight unwinding of the RNA/PNA helices with respect to canonical A-RNA structures, in agreement with what was previously observed in other MD simulations of RNA/PNA duplexes [43, 49]. The lower roll and tilt values observed in the MD run pointed at an expansion of the major groove. Finally, the analysis of torsion angles reported in Table 2 highlighted the strong similarity between the two duplexes. Taken together, the MD results indicated that both heteroduplexes assumed a conformation resembling the canonical A-type RNA helix rather than the experimentally determined NMR structure. Moreover, the torsion angles of RNA segments in miR-509-3p/PNA2 and miR-509-3p/PNA1 duplexes showed values very similar to those adopted by miR20a in the 4F3T crystal structure [42] suggesting that PNA2 and PNA1 could easily interact with the AGO-miRNA complex, not requiring any conformational adaptations. On the basis of the positive indications coming from the MD studies, we synthesised the PNA2 molecule and studied its ability to recognize the 2-OMe mimic of miR-509-3p by CD, UV, and EMSA studies and evaluated its ability to restore the expression of the luciferase gene containing the 3 UTR of the CFTR gene in the presence of miR-509-3p.

3.2. Synthesis of PNA2 and PNA3. PNA2 and PNA3, chosen as the negative control and bearing the same functionalization of PNA2, were synthesized using the standard Fmoc-solid-phase strategy on the Rink-amide resin following the

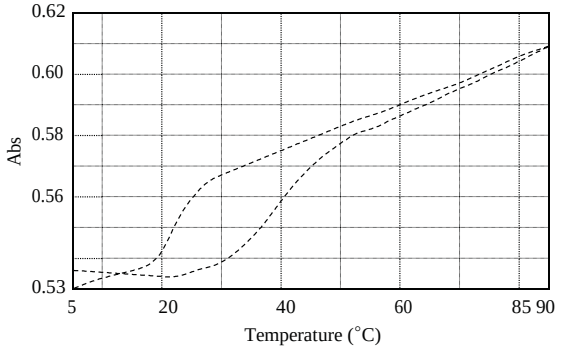

Figure 4: UV melting profile of miR-509-3p alone (dashed line) and miR-509-3p/PNA2 mixture (1 : 1.5 dotted line).

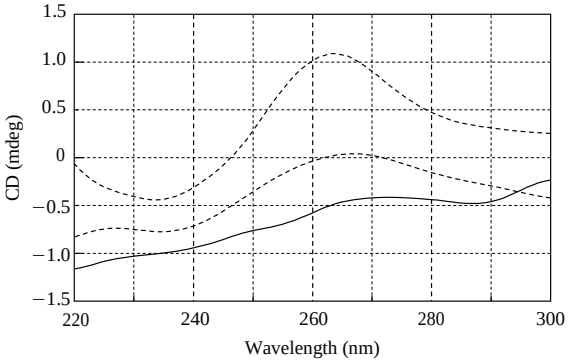

Figure 5: CD spectra of miR-509-3p alone (dashed line), PNA2 alone (solid line), and miR-509-3p/PNA2 mixture (1 : 1.5) (dotted line).

previously reported synthetic approach [37]. The sequences and the complete structures of PNA2 and PNA3 are shown in Table 1.

UV and UV Melting Studies. The miR-509-3p/PNA2 complex, prepared as described in Materials and Methods, was analysed by UV spectroscopy in the temperature range of 25–90°C. The data showed for the miR-509-3p/PNA2 complex a lower value of absorbance than the arithmetic sum of each component alone (Figure 3), thus evidencing that heteroduplex stacking interactions between the miRNA strand and the PNA2 had occurred. The UV melting experiments performed on the miR-509-3p/PNA2 mixture (1 : 1.5 ratio) showed a sigmoidal profile, which was indicative for the heteroduplex/single strands transition (Figure 4). The calculated apparent melting temperature of the miRNA/PNA2 heteroduplex was 40° C. The UV melting profile of the sole PNA2 did not show any significant variation in the A_{260} value in 10–70°C (data not shown), whereas, the UV melting of the sole miR-509-3p, in the same experimental conditions, showed a sigmoidal profile with an apparent melting temperature of 26°C, which could be attributed to the melting of poorly stable secondary structures of the miRNA. This data suggests that PNA2 is able to form a complex with miR-509-3p provided with the thermal stability required for *in vivo* experiments.

Circular Dichroism Spectra Analyses. To further confirm the formation of the miR-509-3p/PNA2 heteroduplex complex, circular dichroism (CD) spectra were registered for the miR-509-3p, PNA2, and their 1 : 1.5 mixture after the annealing procedure (Figure 5). In particular, the miR-509-3p/PNA2 mixture showed the typical CD profile of antiparallel RNA/PNA heteroduplexes, characterized by maxima at around 260 and 220 nm and minima at around 235 and 196 nm, thus confirming the capability of the PNA2 to form a heteroduplex with the miR-509-3p miRNA.

EMSA Results. The recognition phenomena between the miR-509-3p and the FITC-labelled PNA2 were also studied by electrophoretic mobility shift assay (Figure 6(a)). To allow the visualization of miR-509-3p alone, the gel was also visualized after the EtBr staining (Figure 6(b)). The superimposition of FITC and EtBr stained gels is shown in Figure 6(c). The electrophoretic mobility of PNA2 alone (lanes 1) was slower than that of miR-509-3p alone (lane 2). When miR-509-3p and PNA2 were mixed in the molar ratios of 1 : 1.5 and 1 : 5 (lanes 3 and 4, resp.) we observed the appearance of a new band, corresponding to the miR-509-3p/PNA2 complex, which was upshifted relative to the bands of the two components alone. The formation of the miR-509-3p/PNA2 complex was further confirmed by the disappearance of the band of the free miR-509-3p in the miRNA/PNA2 1 : 5 complex (lane 4, Figures 6(b) and 6(c)). The EMSA data further corroborated the CD evidence about the ability of PNA2 to form a stable complex in the presence of miR-509-3p miRNA.

Biological Activity. Once the ability of PNA2 to form a stable heteroduplex with miR-509-3p was demonstrated, we examined its potential of being a miR-509-3p inhibitor in a biological context. For this purpose we tested the ability of PNA2 to revert the reduction of luciferase activity induced by the transfection of the 2-OMe mimic of miR-509-3p in A549 cells. As shown in Figure 7 the transfection of PNA2, but not of PNA3, was able to rescue the luciferase activity in a dose-dependent manner. In this experiment A549 cells were first transfected with the pLuc-CFTR-3UTR plasmid (a reporter luciferase construct sensitive to the miR-509-3p mimic action due to the presence of the 3 UTR of the CFTR gene) and with miR-509-3p miRNA. As expected, the transfection of the miR-509-3p reduced the luciferase activity down to 40%. The luciferase activity was rescued after the transfection of the PNA2 in a dose-depended manner. In these experiments the commercially available Attractene cationic lipid transfection reagent was used. The fluorescent microscopy image of the A549 cells taken 24 h after the transfection with PNA2 (Figure 8) confirmed the PNA2 uptake by the cells.

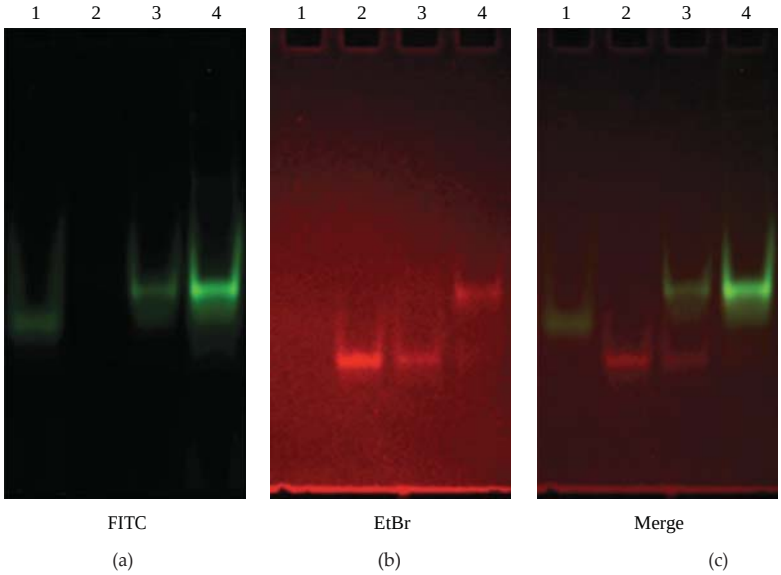

Figure 6: EMSA of PNA2 alone (lanes 1), miR-509-3p alone (lanes 2), miR-509-3p/PNA2 1 : 1.5 (lanes 3), and miR-509-3p/PNA2 1 : 5 (lanes 4) visualized by FITC (a) or EtBr (b) staining. The superimposition of FITC and EtBr stained gels is shown in (c).

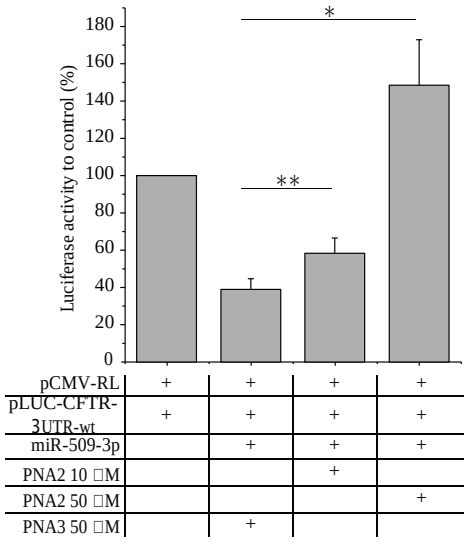

Figure 7: Inhibition of miR-509-3p effect by PNA2. Different doses of PNA2 were transfected in A549 cells. A significant inhibition of miR-509-3p was observed using PNA2 in a dose-dependent manner. *□ values < 0.02, **□ values < 0.002. The 7-mer poly-thymine PNA3 had no effect on miR-509-3p.

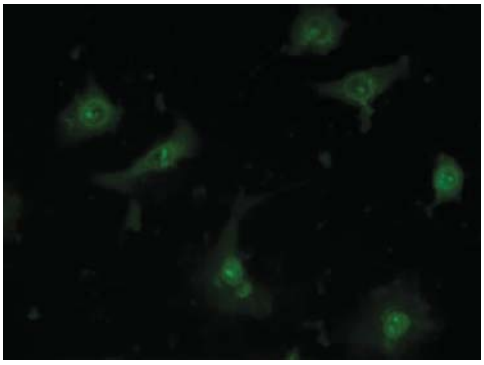

Figure 8: Representative uptake of FITC-labelled PNA2 by A549 cells.

4. Conclusions

Previously, we showed that the activity of the miR-509-3p miRNA, one of miRNAs involved in the posttranscriptional regulation of CFTR gene of CF and CF-RD, could be inhibited through the use of the 14-mer PNA1 fully complementary to the first fourteen bases of miR-509-3p [37]. With this study, we demonstrate that the activity of miR-509-3p can be inhibited even with the use of a PNA as short as seven bases long targeting exclusively the seed region of the miRNA. This finding, probably due to the higher affinity of PNAs over RNAs towards the complementary RNA strand, further widens the interest towards the use of peptide nucleic acids as effective anti-miRNA agents, considering the number of advantages in terms of cost and time saving in the synthesis of the PNAs or for what attains their cellular uptake.

Conflict of Interests

The authors declare that there is no conflict of interests regarding the publication of this paper.

Acknowledgments

This work was financially supported by "Progetto FARO 2011" (Finanziamento per l'Avvio di Ricerche Originali) and PRIN Grant 2009 from the Italian Ministero dell'Università e della Ricerca. The authors are grateful to Dr. Luisa Cuorvo for her technical assistance.

References

[1] L. He and G. J. Hannon, "MicroRNAs: small RNAs with a big role in gene regulation," *Nature Reviews Genetics*, vol. 5, no. 7, pp. 522–531, 2004.

[2] S. Griffiths-Jones, H. K. Saini, S. van Dongen, and A. J. Enright, "miRBase: tools for microRNA genomics," *Nucleic Acids Research*, vol. 36, no. 1, pp. D154–D158, 2008.

[3] M. Selbach, B. Schwanhäusser, N. Thierfelder, Z. Fang, R. Khanin, and N. Rajewsky, "Widespread changes in protein synthesis induced by microRNAs," *Nature*, vol. 455, no. 7209, pp. 58–63, 2008.

[4] Q. Jing, S. Huang, S. Guth et al., "Involvement of microRNA in AU-rich element-mediated mRNA instability," *Cell*, vol. 120, no. 5, pp. 623–634, 2005.

[5] J. Brennecke, A. Stark, R. B. Russell, and S. M. Cohen, "Silencing of microRNA families by seed-targeting tiny LNAs," *Nature Genetics*, vol. 43, pp. 371–378, 2011.

[6] G. Castaldo, F. Lembo, and R. Tomaiuolo, "Molecular diagnostics: between chips and customized medicine," *Clinical Chemistry and Laboratory Medicine*, vol. 48, no. 7, pp. 973–982, 2010.

[7] A. G. Bader, D. Brown, and M. Winkler, "The promise of microRNA replacement therapy," *Cancer Research*, vol. 70, no. 18, pp. 7027–7030, 2010.

[8] S. Costinean, N. Zanesi, Y. Pekarsky et al., "Pre-B cell proliferation and lymphoblastic leukemia/high-grade lymphoma in E□- miR155 transgenic mice," *Proceedings of the National Academy of Sciences of the United States of America*, vol. 103, no. 18, pp. 7024–7029, 2006.

[9] A. Rodriguez, E. Vigorito, S. Clare et al., "Requirement of bic/microRNA-155 for normal immune function," *Science*, vol. 316, no. 5824, pp. 608–611, 2007.

[10] P. N. Brown and H. Yin, "PNA-based microRNA inhibitors elicit anti-inflammatory effects in microglia cells," *Chemical Communications*, vol. 49, pp. 4415–4417, 2013.

[11] S. Ullah, P. John, and A. Bhatti, "MicroRNAs with a role in gene regulation and in human diseases," *Molecular Biology Reports*, 2013.

[12] Y. Li and K. V. Kowdley, "MicroRNAs in common human diseases," *Genomics Proteomics Bioinformatics*, vol. 10, pp. 246–253, 2012.

[13] I. McIntosh and G. R. Cutting, "Cystic fibrosis transmembrane conductance regulator and the etiology and pathogenesis of cystic fibrosis," *FASEB Journal*, vol. 6, no. 10, pp. 2775–2782, 1992.

[14] A. E. Gillen, N. Gosalia, S.-H. Leir, and A. Harris, "microRNA regulation of expression of the cystic fibrosis transmembrane conductance regulator gene," *Biochemical Journal*, vol. 438, no. 1, pp. 25–32, 2011.

[15] F. Amato, M. Seia, S. Giordano et al., "Gene mutation in microRNA target sites of CFTR gene: a novel pathogenetic mechanism in cystic fibrosis?" *PLoS ONE*, vol. 8, Article ID e60448, 2013.

[16] E. van Rooij, A. L. Purcell, and A. A. Levin, "Developing MicroRNA therapeutics," *Circulation Research*, vol. 110, no. 3, pp. 496–507, 2012.

[17] E. van Rooij and E. N. Olson, "MicroRNA therapeutics for cardiovascular disease: opportunities and obstacles," *Nature Reviews Drug Discovery*, vol. 11, pp. 860–872, 2012.

[18] K. J. Rayner, C. C. Esau, F. N. Hussain et al., "Inhibition of miR-33a/b in non-human primates raises plasma HDL and lowers VLDL triglycerides," *Nature*, vol. 478, no. 7369, pp. 404–407, 2011.

[19] C. Esau, S. Davis, S. F. Murray et al., "miR-122 regulation of lipid metabolism revealed by in vivo antisense targeting," *Cell Metabolism*, vol. 3, no. 2, pp. 87–98, 2006.

[20] J. Elmén, M. Lindow, S. Schütz et al., "LNA-mediated microRNA silencing in non-human primates," *Nature*, vol. 452, no. 7189, pp. 896–899, 2008.

[21] R. E. Lanford, E. S. Hildebrandt-Eriksen, A. Petri et al., "Therapeutic silencing of microRNA-122 in primates with chronic hepatitis C virus infection," *Science*, vol. 327, no. 5962, pp. 198–201, 2010.

[22] E. Brognara, E. Fabbri, F. Aimi et al., "Peptide nucleic acids targeting miR-221 modulate p27Kip1 expression in breast cancer MDA-MB-231 cells," *International Journal of Oncology*, vol. 41, pp. 2119–2127, 2012.

[23] A. G. Torres, M. M. Fabani, E. Vigorito et al., "Chemical structure requirements and cellular targeting of microRNA-122 by peptide nucleic acids anti-miRs," *Nucleic Acids Research*, vol. 40, no. 5, pp. 2152–2167, 2012.

[24] M. M. Fabani, C. Abreu-Goodger, D. Williams et al., "Efficient inhibition of miR-155 function in vivo by peptide nucleic acids," *Nucleic Acids Research*, vol. 38, no. 13, pp. 4466–4475, 2010.

[25] P. E. Nielsen, M. Egholm, R. H. Berg, and O. Buchardt, "Sequence-selective recognition of DNA by strand displacement with thymine-substituted polyamide," *Science*, vol. 254, no. 5037, pp. 1497–1500, 1991.

[26] M. Pooga, T. Land, T. Bartfai, and Ü. Langel, "PNA oligomers as tools for specific modulation of gene expression," *Biomolecular Engineering*, vol. 17, no. 6, pp. 183–192, 2001.

[27] X. Zhang, T. Ishihara, and D. R. Corey, "Strand invasion by mixed base PNAs and a PNA-peptide chimera," *Nucleic Acids Research*, vol. 28, no. 17, pp. 3332–3338, 2000.

[28] S. A. Kushon, J. P. Jordan, J. L. Seifert, H. Nielsen, P. E. Nielsen, and B. A. Armitage, "Effect of secondary structure on the thermodynamics and kinetics of PNA hybridization to DNA hairpins," *Journal of the American Chemical Society*, vol. 123, no. 44, pp. 10805–10813, 2001.

[29] R. Besch, C. Giovannangeli, T. Schuh, C. Kammerbauer, and K. Degitz, "Characterization and quantification of triple helix formation in chromosomal DNA," *Journal of Molecular Biology*, vol. 341, no. 4, pp. 979–989, 2004.

[30] P. E. Nielsen, "Peptide Nucleic Acids (PNA) in chemical biology and drug discovery," *Chemistry and Biodiversity*, vol. 7, no. 4, pp. 786–804, 2010.

[31] J. Amato, M. I. Stellato, E. Pizzo et al., "PNA as a potential modulator of COL7A1 gene expression in dominant dystrophic

epidermolysis bullosa: a physico-chemical study," *Molecular BioSystems*, 2013.

[32] J. Amato, G. Oliviero, E. de Pauw, and V. Gabelica, "Hybridization of short complementary PNAs to G-quadruplex forming oligonucleotides: an electrospray mass spectrometry study," *Biopolymers*, vol. 91, no. 4, pp. 244–255, 2009.

[33] J. Amato, B. Pagano, N. Borbone et al., "Targeting G-Quadruplex structure in the human c-Kit promoter with short PNA sequences," *Bioconjugate Chemistry*, vol. 22, no. 4, pp. 654–663, 2011.

[34] M. Gaglione, G. Milano, A. Chambery, L. Moggio, A. Romanelli, and A. Messere, "PNA-based artificial nucleases as antisense and anti-miRNA oligonucleotide agents," *Molecular BioSystems*, vol. 7, no. 8, pp. 2490–2499, 2011.

[35] A. Manicardi, E. Fabbri, T. Tedeschi et al., "Cellular uptakes, biostabilities and anti-miR-210 activities of chiral arginine-PNAs in leukaemic K562 cells," *ChemBioChem*, vol. 13, pp. 1327–1337, 2012.

[36] M. Egholm, O. Buchardt, L. Christensen et al., "PNA hybridizes to complementary oligonucleotides obeying the Watson-Crick hydrogen-bonding rules," *Nature*, vol. 365, no. 6446, pp. 566–568, 1993.

[37] F. Amato, R. Tomaiuolo, N. Borbone et al., "Design, synthesis and biochemical investigation, by in vitro luciferase reporter system, of peptide nucleic acids as new inhibitors of miR-509-3p involved in the regulation of cystic fibrosis disease-gene expression," *MedChemComm*, 2013.

[38] S. Obad, C. O. dos Santos, A. Petri et al., "Silencing of microRNA families by seed-targeting tiny LNAs," *Nature Genetics*, vol. 43, no. 4, pp. 371–380, 2011.

[39] D. M. Patrick, R. L. Montgomery, X. Qi et al., "Stress-dependent cardiac remodeling occurs in the absence of microRNA-21 in mice," *Journal of Clinical Investigation*, vol. 120, no. 11, pp. 3912–3916, 2010.

[40] R. Lavery, M. Moakher, J. H. Maddocks, D. Petkeviciute, and K. Zakrzewska, "Conformational analysis of nucleic acids revisited: curves+," *Nucleic Acids Research*, vol. 37, no. 17, Article ID gkp608, pp. 5917–5929, 2009.

[41] W. Humphrey, A. Dalke, and K. Schulten, "VMD: visual molecular dynamics," *Journal of Molecular Graphics*, vol. 14, no. 1, pp. 33–38, 1996.

[42] E. Elkayam, C.-D. Kuhn, A. Tocilj et al., "The structure of human argonaute-2 in complex with miR-20a," *Cell*, vol. 150, pp. 100–110, 2012.

[43] S. C. Brown, S. A. Thomson, J. M. Veal, and D. G. Davis, "NMR solution structure of a peptide nucleic acid complexed with RNA," *Science*, vol. 265, no. 5173, pp. 777–780, 1994.

[44] V. Hornak, R. Abel, A. Okur, B. Strockbine, A. Roitberg, and C. Simmerling, "Comparison of multiple amber force fields and development of improved protein backbone parameters," *Proteins: Structure, Function and Genetics*, vol. 65, no. 3, pp. 712–725, 2006.

[45] D.A. Case, T.A. Darden, T.E. Cheatham III et al., "AMBER 12," University of California, 2012.

[46] J. M. Sanders, M. E. Wampole, C.-P. Chen et al., "Effects of hypoxanthine substitution in peptide nucleic acids targeting KRAS2 oncogenic mRNA molecules: theory and experiment," *The Journal of Physical Chemistry B*, 2013.

[47] F.-Y. Dupradeau, C. Cézard, R. Lelong et al., "R.E.DD.B.: a database for RESP and ESP atomic charges, and force field libraries," *Nucleic Acids Research*, vol. 36, no. 1, pp. D360–D367, 2008.

[48] J. W. Craft Jr. and G. B. Legge, "An AMBER/DYANA/MOLMOL phosphorylated amino acid library set and incorporation into NMR structure calculations," *Journal of Biomolecular NMR*, vol. 33, no. 1, pp. 15–24, 2005.

[49] R. Soliva, E. Sherer, F. J. Luque, C. A. Laughton, and M. Orozco, "Molecular dynamics simulations of PNA·DNA and PNA·RNA duplexes in aqueous solution," *Journal of the American Chemical Society*, vol. 122, no. 25, pp. 5997–6008, 2000.

[50] J. Panecka, C. Mura, and J. Trylska, "Molecular dynamics of potential rRNA binders: single-stranded nucleic acids and some analogues," *Journal of Physical Chemistry B*, vol. 115, no. 3, pp. 532–546, 2011.